

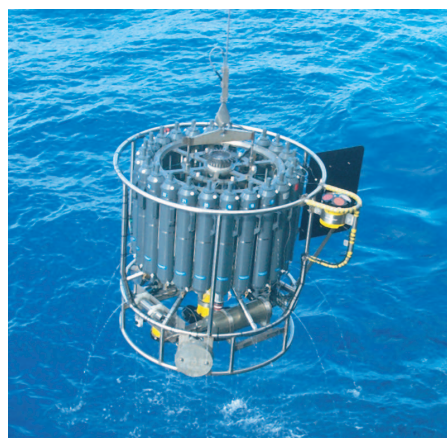


5th INTERNATIONAL PRECIPITATION WORKING GROUP WORKSHOP

WORKSHOP PROGRAM AND PROCEEDINGS

11-15 October 2010, Hamburg, Germany

Edited by C. Klepp and G. Huffman



Hinweis

Die Berichte zur Erdsystemforschung werden vom Max-Planck-Institut für Meteorologie in Hamburg in unregelmäßiger Abfolge herausgegeben.

Sie enthalten wissenschaftliche und technische Beiträge, inklusive Dissertationen.

Die Beiträge geben nicht notwendigerweise die Auffassung des Instituts wieder.

Die "Berichte zur Erdsystemforschung" führen die vorherigen Reihen "Reports" und "Examensarbeiten" weiter.



Notice

The Reports on Earth System Science are published by the Max Planck Institute for Meteorology in Hamburg. They appear in irregular intervals.

They contain scientific and technical contributions, including Ph. D. theses.

The Reports do not necessarily reflect the opinion of the Institute.

The "Reports on Earth System Science" continue the former "Reports" and "Examensarbeiten" of the Max Planck Institute.

Anschrift / Address

Max-Planck-Institut für Meteorologie
Bundesstrasse 53
20146 Hamburg
Deutschland

Tel.: +49-(0)40-4 11 73-0
Fax: +49-(0)40-4 11 73-298
Web: www.mpimet.mpg.de

Layout:

Bettina Diallo, PR & Grafik

Titelfotos:

vorne:

Christian Klepp - Jochem Marotzke - Christian Klepp

hinten:

Clotilde Dubois - Christian Klepp - Katsumasa Tanaka

5th INTERNATIONAL PRECIPITATION WORKING GROUP WORKSHOP
WORKSHOP PROGRAM AND PROCEEDINGS

11-15 October 2010, Hamburg, Germany

Edited by C. Klepp and G. Huffman

Hamburg 2011

The 5th INTERNATIONAL PRECIPITATION WORKING GROUP WORKSHOP

was hosted, funded and sponsored by





5th INTERNATIONAL PRECIPITATION WORKING GROUP WORKSHOP

WORKSHOP PROGRAM AND PROCEEDINGS

11-15 October 2010, Hamburg, Germany



KlimaCampus



Max-Planck-Institut
für Meteorologie

Program Committee

George Huffman, SSAI and GSFC, USA
Christian Klepp, KlimaCampus, MPI-M
Ralph Ferraro, NOAA/NESDIS, USA
Chris Kidd, Univ. of Birmingham, UK (now ESSIC and GSFC, USA)

Local Organizing Committee

Christian Klepp, KlimaCampus, MPI-M, Germany
Axel Andersson, MPI-M, Germany
Stephan Bakan, MPI-M, Germany
Barbara Zinecker, MPI-M, Germany
Hanna Stadelhofer, MPI-M, Germany

EUMETSAT Training Event Organizing Committee

Jose Prieto, EUMETSAT, Germany
Regina Hoefenmayer, EUMETSAT, Germany
Volker Gärtner, EUMETSAT, Germany
Christian Klepp, KlimaCampus, MPI-M, Germany

IPWG Co-Chairs

George Huffman
NASA GSFC
Code 613.1
Greenbelt, MD 20771
USA

Christian Klepp
KlimaCampus, Univ. Hamburg
Max Planck Institute f. M.
Bundesstr. 55, 20146 Hamburg
Germany

george.j.huffman@nasa.gov

christian.klepp@zmaw.de

FOREWORD

The Fifth Workshop of the International Precipitation Working Group (IPWG5) was held 11-15 October 2010 at the KlimaCampus, University of Hamburg, and the Max Planck Institute for Meteorology, Hamburg, Germany. IPWG5 was attended by about 85 scientists from 25 countries. There was a mix of oral presentations (42), posters (30), and working groups covering international projects and satellite programs, IPWG programmatic activities, algorithms, applications, validation, modeling, and new technology. A Hydrology and Precipitation Training Workshop was arranged with EUMETSAT to coincide with IPWG5 making this meeting the largest IPWG workshop to date.

One dominant theme in IPWG5 was the availability of precipitation-relevant satellite data. Issues included the need to maintain existing missions and extend the record with additional generations of precipitation-relevant sensors, particularly conically scanning passive microwave imagers, space-based precipitation radars, new passive microwave high-frequency channels, and satellites not specifically targeted at precipitation. Data-related issues included radiometric inter-calibration and the need to reprocess full data archives as new algorithms are put into operation. One session was devoted to the Special Sensor Microwave Imager/Sounder (SSMIS) data.

Algorithm development is focused on “challenging” situations – falling snow, snowy/frozen surfaces, complex terrain, and cloud development between satellite snapshots. Validation is considered key to progress, and an intercomparison campaign is planned with parallel validation for observational and model-based products.

Another important theme was reducing barriers to the use of precipitation datasets. The IPWG’s Web presence will be improved, providing more data-user-oriented information, and IPWG will work more closely with existing international training organizations.

The purpose of the IPWG is, in the area of quantitative precipitation measurement is to foster the development of better measurements, and improvement of their utilization; improvement of scientific understanding, and development of international partnerships. In following these goals, three successful bi-annual workshops have been held beginning with Madrid, Spain (2002), followed by Monterey, California, USA (2004), Melbourne, Australia (2006), and Beijing, China (2008). Additionally, specialty workshops have been held on snowfall measurement and modelling (2005, 2008, and 2010) and the evaluation on high resolution precipitation products (2007).

The goals of this fifth workshop include:

- To learn about the status of current and future satellite missions focused on precipitation retrieval.
- To update the current status of operational and quasi-operational satellite-based estimates of precipitation for weather, hydrometeorological and climate applications.
- To analyze the open issues underlying precipitation retrievals, such as retrievals over complex terrain, light precipitation, and snowfall.
- To analyze the statistical performance of current satellite techniques over various seasons, rainfall regimes, and space-time scales.

- To develop strategies within IPWG in the areas of community consensus algorithms, radiative transfer, and cloud resolving models, as well as satellite calibration and inter-calibration.
- To report on the current status of the SSMIS data issues and the development of the Unified Pre-Processor (UPP) applicable for the climate and precipitation community.
- To review the current status of the global water cycle issues and to link with the SEAFLUX and LANDFLUX communities.
- To develop key recommendations for short and long-term activities for the CGMS agencies and the IPWG.

The Wednesday afternoon and Thursday sessions were devoted to individual working groups to track action items established in Beijing and to develop key recommendations on future issues. The working group areas include research/new technology/techniques, applications, and validation.

We finally want to extend thanks to our hosts at the KlimaCampus, University of Hamburg, and the Max Planck Institute for Meteorology, Hamburg, Germany for their generosity and hospitality in addition to EUMETSAT for funding and carrying out the training event in parallel to IPWG5 and EUMETSAT and the World Meteorological Organization for scientific funding and in-kind support to make this workshop possible. We are extremely grateful for the generous funding made available by the company MABANAFT for the official conference dinner. Cordial thanks also go to the precipitation measurement companies METEK and EIGENBRODT for funding the icebreaker social event.

Goerge Huffman
Christian Klepp
Co-Chairs, IPWG

Schedule

Monday, October 11 to Friday, October 15

	Monday	Tuesday	Wednesday	Thursday	Friday
	8.30 – 9.30 Registration				
9.00-10.30	9.30 – 10.15 Welcome	Session C – oral	9.00 – 10.40 Session E – oral	Breakout Session 2	
	Welcome to IPWG 5 Introduction and Logistics	Algorithms	New Technologies and Future Activities		
10.30 – 12.30	Session A – oral	Session C – poster	11.00 – 12.30 Session E – discussion	10.30 – 11.00 Coffee	11.00 – 15.00 Outing
	The Big Picture Climatology Water cycle		SMMIS Update		
12.30 – 14.00	Lunch	Lunch	Lunch	Lunch	
14.00 – 15.30	Session B – oral	Session D – oral	Introduction to WGs 14.00 – 14.30	Breakout Session 3	
	Precipitation Data Sets	Validation	Breakout Session 1 14.30 – 17.30		
15.30 – 17.30	Session B – poster	Session D – poster		15.30 – 16.00 Coffee	
			15.45 – 16.15 Coffee	16.00 – 17.30 Closing Plenary	
	17.30 – 20.30 Ice-Breaker Reception ZMAW Building		18.45 – 23.15 Workshop Dinner Bus transfer from and back to conference venue		

Agenda Monday, October 11

Opening Session

Monday, 11 October, 8.30 – 9.30

Registration

ZMAW Building, Bundesstr. 53, Atrium/Hall 022/023

Monday, 11 October, 9.30 – 10.15

Oral Session /

Welcome:

Opening Remarks

Christian Klepp

**Welcome and introduction
to KlimaCampus and MPI-M**

Detlef Stammer (Inst. of Oceanog. ZMAW, Univ. of Hamburg)

IPWG summary/perspective

Christian Klepp/George Huffman

GEO summary/perspective

George Huffman (Point of Contact for GEO Precip Subtask)

Workshop goals

Christian Klepp/George Huffman

Logistics

Christian Klepp

Session A The Big Picture, Climatology, Water Cycle

Monday, 11 October, 10.30 – 12.30

Oral Session

- 10.30: Status and Overview on IPWG related Precipitation Data Sets**
C. Kidd (Univ. of Birmingham, UK)
- 10.50: SEAFLUX / Water Cycle**
C. Clayson (Florida State Univ., USA)
- 11.10: Global Ocean Freshwater Flux Components from Satellite, Re-analysis and In-Situ Climatologies**
A. Andersson (Max Planck Institute for Meteorology, Germany), C. Klepp, K. Fennig, S. Bakan, H. Graßl, J. Schulz
- 11.30: Quantifying Uncertainties in Satellite-based Global Precipitation Measurements**
Y. Tian (Univ. of Maryland College Park/ESSIC and NASA/GSFC, USA) and C.D. Peters-Lidard
- 11.50: The Global Precipitation Measurement (GPM) Mission: Overview and U.S. Status**
A.Y. Hou (NASA/GSFC, USA)
- 12.10: Global Flood and Landslide Nowcasts and Forecasts Using Multi-Satellite Precipitation Observations**
R. Adler (Univ. of Maryland, USA), H. Wu, Y. Hong, F. Policelli, Y. Tian, H. Pierce

Session B Precipitation Data Sets

Monday, 11 October, 14.00 – 15.30

Oral Session

- 14.00: The Global Precipitation Climatology Centre Serving the Hydro-Climatology Community**
A. Becker (DWD/GPCC, Germany), U. Schneider, A. Meyer-Christoffer, M. Ziese, P. Finger, B. Rudolf
- 14.20: The Status of NOAA/NESDIS Precipitation Algorithms and Products**
R. Ferraro (NOAA/NESDIS/STAR, USA), S. Boukabara, K. Gopalan, J. Janowiak, R. Kuligowski, H. Meng, M. Sapiano, H. Semunegus, T. Smith, D. Vila, N-Y. Wang, F. Weng, L. Zhao
- 14.40: EUMETSAT's Activities in Support of Precipitation Remote Sensing**
T. Heinemann (EUMETSAT, EU)
- 15.00: Status of Japanese Precipitation Measuring Missions and Global Rainfall Map in Near-Real-Time**
M. Kachi (JAXA/EORC, Japan), T. Kubota, R. Oki
- 15.20: Poster Introduction**

Monday, 11 October, 15.30 – 17.30

Poster Session

The HOAPS-3 Climatology

S. Bakan (ZMAW, Univ. of Hamburg), A. Andersson, C. Klepp, K. Fennig

Rain Drop Size Densities over Land and over Sea

K. Bumke (Leibniz-Inst. of Marine Sci. at the Christian-Albrechts Univ. zu Kiel, Germany)

Historical Time Series of Merged Raingauge-Satellite Rainfall Data for Climate Risk Management Applications in Ethiopia

T. Dinku (IRI and the Earth Inst. at Columbia Univ., USA), K. Hailemariam, D.F. Grimes

Release of CM-SAF HOAPS v3.2 Products Based on Improved Data Record of SSM/I Radiances

K. Fennig (DWD/SAF-Climate Monitoring, Germany), M. Schröder

Globally Gridded Satellite (GridSat) Observations for Climate Studies

K. Knapp (NOAA/NCDC, USA)

Global Precipitation Data Access, Value-added Services and Scientific Exploration Tools at NASA GES DISC

Z. Liu (NASA/GSFC DISC, USA), D. Ostrenga, G. Leptoukh, S. Kempler

Towards a Climate Data Record of Precipitation from Satellite Microwave Imager Data

M.R.P. Sapiano (Colorado State Univ., USA), W. Berg

Recent Development of GPCC's Data Base and Quality-Control in Preparation of New Gridded Global Precipitation Analyses

U. Schneider (DWD/GPCC, Germany), A. Meyer-Christoffer, M. Ziese, P. Finger, A. Becker, B. Rudolf

Implementation of a Methodology to Calibrate Ground Radars Using TRMM-PR over Argentina

L. Vidal (Dept. de Ciencias de la Atmósfera y los Océanos, Ciudad Univ., Brazil), P. Salio, C.A. Morales

A Climatology-Based Scheme for Special Sensor Microwave Imager (SSM/I) Quality Control: An Application to Monthly Rainfall Rates

D. Vila (Centro de Previsão de Tempo e Estudos Climáticos - Rodovia Presidente Dutra, Brazil, and Univ. of Maryland/ESSIC/CICS, USA), R. Ferraro, H. Semunegus

Gridded Data Products Provided and Interpolation Technique Utilized by the Global Precipitation Climate Centre (GPCC)

M. Ziese (DWD/GPCC, Germany), U. Schneider, A. Meyer-Christoffer, P. Finger, A. Becker, B. Rudolf

Ice-Breaker Reception

Monday, 11 October, 17.30 – 20.30

Hosted by KlimaCampus and MPI-M, sponsored by Eigenbrodt Umweltmesstechnik and METEK.



Agenda Tuesday, October 12

Session C Algorithms

Tuesday, 12 October, 9.00 – 10.30

Oral Session

- 9.00: Kalman-Filtered CMORPH using TRMM to Blend Satellite Rainfall**
R.J. Joyce (Wylie Information Sys. and NOAA/MWS/CPC, USA), P. Xie, S.-H. Yoo
- 9.20: New GSMaP Over-Land Precipitation Retrieval Algorithm**
K. Aonashi (Meteor. Res. Inst., Japan)
- 9.40: REFAME: A Combined Precipitation Estimation Technique using Adjusted-advection of Microwave Precipitation Estimates**
A. Behrangi (California Inst. of Technology/JPL and Univ. of California Irvine, USA), S. Sorooshian, K. Hsu, T.J. Bellerby, G.J. Huffman
- 10.00: A Physically-Based Rainfall Rate Algorithm for the Global Precipitation Mission**
S.-A. Boukabara (Joint Cent. for Sat. Data Assim. and NOAA/NESDIS/STAR) and K. Garrett
- 10.20: Poster Introduction**

Tuesday, 12 October, 10.30 – 12.30

Poster Session

Can Recently Observed Precipitation Trends over the Mediterranean Area Be Explained by Climate Change Projections?

A. Barkhordarian (GKSS Research Centre, Germany) and H. von Storch

Enhancements in the Version 7 TRMM Multi-satellite Precipitation Algorithm (TMPA)

G.J. Huffman (NASA/GSFC and Science Sys. and Appl., Inc., USA), D.T. Bolvin, E.J. Nelkin, R.F. Adler

Resolving Rainfall Rate Retrieval Ambiguities Associated with Cloud Types Using Multi-Satellite Passive Measurements

M. Itkin (Max Planck Inst. for Meteor., KlimaCampus, Germany), A. Loew

Characterization of Snow-Covered Terrains and Detection of Snowfall by Using the 183-WSL Retrieval Scheme

S. Laviola (ISAC-CNR, Italy), S. D'Aurizio, E. Cattani, V. Levizzani

Combining precipitation and soil moisture observations: a way for improved estimates of land surface water fluxes?

A. Löw (Max Planck Inst. for Meteor., CliSAP, Germany)

Improvement of GSMaP Passive Microwave Imager Rainfall Retrievals over the Mountainous Area in Japan

S. Shige (Kyoto Univ., Japan), H. Ashiwake, A. Taniguchi, S. Kida, T. Kubota

Precipitation Estimation for Typhoon Using Satellite Microwave Data

N.-C. Yeh (Chung Cheng Inst. of Technol., Nat. Defense Univ., Taiwan), W.-J. Chen, J.-L. Wang, J.-C. Hu, G.-R. Liu, M.-D. Tsai

Combining High-Resolution Satellite Estimates with Gauge Observations

S.-H. Yoo (Wyllie Inform. Systems and NOAA/NWS/CPC, USA) and P. Xie

Investigations of the Moisture Budget of the Tropical Atmosphere Using ERA Interim Data

M. Zahn (Univ. of Reading, UK), R.P. Allan

Session D Validation

Tuesday, 12 October, 14.00 – 15.30

Oral Session

14.00: Status of and Early Results from the IPWG/WGNE Model Precipitation Intercomparison

M.R.P. Sapiano (Colorado State Univ., USA)

14.20: Application of MET for the Verification of the NWP Cloud and Precipitation Products using A-Train Satellite Observations

P.A. Kucera (NCAR, USA), B. Brown, R. Bullock, C. Weeks

14.40: Performance of TRMM Level 2 and 3 Rainfall Retrievals in the Complex Terrain of South Asia

S.W. Nesbitt (Univ. of Illinois at Urbana-Champaign, USA) and K.A. Reed

15.00: Performance Evaluation of Precipitation Estimations over South-Eastern South America Considering Different Climatic Regions

P. Salio (FCEN- and CONICET-UBA, Argentina), D. Vila, Yanina G. Skabar, M. Paula Houbouchian, C. Matsudo

15.20: Poster Introduction

Tuesday, 12 October, 15.30 – 17.30

Poster Session

Uses of Satellite Precipitation Data in Nigeria

A.P. Adesi (Nigerian Meteorological Agency), T. Adelugba, T. Salami

Rain-gauge Validation of Satellite Rainfall Estimates over Argentina

D. Barrera (CONICET/Univ. of Buenos Aires, Argentina) and S. G. Gómez

Multi-Site and Multi-Objective Evaluation of High-Resolution Satellite-Rainfall Products

E. Habib (Univ. of Louisiana at Lafayette, USA), A.T. Haile, M. ElSadani, M. ElShamy, R. Kuligowski, Y. Tian

Rain Intensity Spectra Distribution Over Germany and Western Africa

M. Itkin (Max Planck Inst. for Meteorology, KlimaCampus, Germany), R. Athmer, A. Löw

Variability of Lightning Activity and Subsequent Convective Precipitation Derived from Satellite and Ground Based Sensors – Case Study

R. Iwanski (Inst. of Meteorology and Water Management/Sat. Remote Sensing Centre, Poland), B. Lapeta, D. Serafin

Three Studies: Can Models Replicate Tropical Precipitation Cycles Accurately? How Do Models and Satellite Estimates Perform in the North Atlantic? Do We Really Influence Precipitation?

C. Kidd (Univ. of Birmingham, UK)

Precipitation Validation over the Oceans

C. Klepp (KlimaCampus, Univ. of Hamburg, Germany)

Temporally Homogeneous Rainfall Time Series for Africa - Methodology and Validation

R. Maidment, E. Tranavsky, D. Grimes (Univ. of Reading, UK)

The Precipitation Product Validation Service Defined During the Development Phase of the Hydrological SAF

S. Puca (Italian Civil Protection Department), E. Labo, B. Lapeta, Ján Kanák, T. Maurer, A. Öztopal, F. Porcu, E. Roulin, I. Sonmez

Verification of NOAA CPC RFE at Various Temporal and Spatial Resolutions in the Hindu Kush - Himalayan Region

M.S. Shrestha, S.R. Bajracharya (Internat. Centre for Integrated Mountain Development, Nepal), P.K. Mool

Rainfall Retrieval Validation over the Americas: The STAR Precipitation Validation Center

D. Vila (CPTEC/INPE, Brazil, and Univ. of Maryland College Park/ESSIC, USA) and J. Janowiak

Agenda

Wednesday, October 13

Session E New Technologies and Future Activities

Wednesday, 13 October, 9.00 – 10.40

Oral Session

9.00: Current Status of Satellite Precipitation and GPM Activity at KMA

M.-L. Ou (KMA, Korea), J.-H. Kim

9.20: The GOES-R Rainfall Rate, Rainfall Potential, and Probability of Rainfall Algorithms

R.J. Kuligowski (NOAA/NESDIS/STAR, USA), Y. Li, Z. Zhang, R. Barnhill

- 9.40: Developing Winter Precipitation Algorithm over Land from Satellite Microwave and C3VP Field Campaign Observations**
N.-Y. Wang (Univ. of Maryland College Park/ESSIC and NOAA/NESDIS/STAR, USA),
K. Gopalan, R. Ferraro
- 10.00: Examination of CloudSat-Based Snowfall Profiles using C-band Ground Radar**
F.J. Turk (California Inst. of Technology/JPL, USA), K.-W. Park, Z. Haddad,
P. Rodriguez, D. Hudak
- 10.20: Megha-Tropiques: Mission and Algorithms Status**
N. Viltard (LATMOS-IPSL CNRS-UVSQ, France)

Wednesday, 13 October, 11.00 – 12.30

SSMIS Update

- 11.00: Introduction to the SSMIS and the UPP**
W. Bell (ECMWF, EU)
- 11.30: The UPP-CP**
F.J. Turk (NASA/JPL)
- 11.40: The NESDIS/STAR Corrected SSMIS Dataset**
D. Vila (Centro de Previsão de Tempo e Estudos Climáticos - Rodovia Presidente
Dutra, Brazil, and Univ. of Maryland/ESSIC/CICS, USA)
- 11.50: SSMIS Data Postings in NESDIS**
R. Ferraro (NESDIS/STAR, USA)
- 11.55: Developing CDRs for SSMIS**
M.R.P. Sapiano (Colorado State Univ., USA)
- 12.10: SSMIS at RSS**
K. Hilburn (Remote Sensing Sys., USA), presented by G. Huffman
- 12.15: Wrap-Up and Discussion**
G. Huffman

Working Group Activities

Wednesday, 13 October, 14.00 – 14.30

Introduction

- 14.00: CGMS summary/perspective**
V. Gärtner (CGMS Rapporteur for IPWG)
- 14.10: Introduction to WGs**
G. Huffman

Wednesday, 13 October, 14.30 – 17.30

Breakout 1

- New Technology** Room 1536B (Geomatikum)
- Operational Applications** Room 301

Research Activities Room 022/023
Validation Room 401

Workshop Dinner

Wednesday, 13 October, 18.45 – 23.15

Sponsored by MABANAFT. Buffet dinner in the HafenCity, Hamburg.



Agenda Thursday, October 14

Thursday, 14 October, 9.00 – 12.30

Breakout 2

New Technology Room 1536B (Geomatikum)
Operational Applications Room 002
Research Activities Room 022/023
Validation Room 401

Thursday, 14 October, 14.00 – 15.30

Breakout 3

New Technology Room 1536B (Geomatikum)
Operational Applications Room 002
Research Activities Room 022/023
Validation Room 401

Thursday, 14 October, 16.00 – 17.30

Closing Plenary

Reports by Working Groups and Discussion Working Group Chairs/Rapporteurs
Overall Recommendations C. Klepp, G. Huffman
Recommendations to CGMS V. Gärtner
Closing Statement G. Huffman, C. Klepp
Words of Thanks C. Klepp

Agenda
Friday, October 15

Outing

Friday, 15 October, 11.00 – 15.00

Bus and ship tour through the beautiful city of Hamburg enjoying the “Waterkant” from both sides.

- **with continued discussions on IPWG topics**
- **New co-chairs were selected:**

Paul Kucera, NCAR, Boulder, CO, USA

Bozena Łapeta, IMGW OKk, Kraków, Poland

Agenda EUMETSAT Trainingsevent Tuesday, October 12 to Thursday, October 14

Time/Day	Tuesday 12 th Oct	Wednesday 13 th Oct	Thursday 14 th Oct
9:00 - 11:00	Opening and introduction Prieto/ Klepp 5 min each Precip. Products, Generation and extraction Alessandro Galliani	Satellite precipitation datasets (9:00 - 10:00) George Huffman TOVAS System (TRMM) Zhong Liu (10:00-11:00)	H-SAF Product validation and applications Bozena Lapeta
11:00 - 11:30	Coffee	Coffee	Coffee
11:30 - 13:00	Soil moisture Barbara Zeiner	Soil moisture Barbara Zeiner	Applications: Precipitation related natural hazards: floods and landslides Bob Adler (11:30-13:00)
13:30 - 15:00	Lunch	Lunch	Lunch
15:00 - 17:30	Passive and Active Microwave sensors for precipitation research Joe Turk (15:00 - 16:30) Precipitation Algorithms (16:30-17:30) Ralph Ferraro	Calibration Activities Matt Sapiano(Wes Berg) (15:00-15:30) Calibration Methods Matt Sapiano (15:30-16:00) SCO Calibration Daniel Vila (16:00-16:30) Precipitation Validation Chris Kidd (16:30-17:30)	Participants' presentations Final discussion
	Visit and social event EUMETSAT Gröninger 19:00	Social Event Mabanaf Departure 18:45 in front of the venue, end 23:15 at venue	

EUMETSAT Training Event Participant List

Tuesday, October 12 to Thursday, October 14

22 participants from 18 countries

Name	Affiliation	Country	Email
Alao, Kamorudeen A.	NMA	Nigeria	talk2deputy@yahoo.com
Barrera, Daniel	Univ. Buenos Aires	Argentina	daniel.barrera@fibertel.com.ar
Bejenaru, Gherman	SHS	Moldova	intern@meteo.md
Calheiros, Alan	INPE	Brazil	alan.calheiros@cptec.inpe.br
Galliani, Alessandro	H-SAF	Italy	galliani@meteoam.it
Ganchev, Kiril	NIMH	Bulgaria	kiril.ganchev@meteo.bg
Hoefenmayer, Regina	EUMETSAT	Germany	regina.hoefenmayer@eumetsat.int
Kafi, Abdulla Hel	Inst. Water Modeling	Bangladesh	ahk@iwmbd.org
Kocsis, Zsofia	HMO	Hungary	kocsis.zs@met.hu
Komuscu, Ali Umran	H-SAF	Turkey	aukomuscu@dmi.gov.tr
Lapeta, Bozena	H-SAF	Poland	b.lapeta@gmail.com
Lukasevic, Justina	LHMS	Lithuania	j.juneviciute@meteo.lt
Mahesh, C.	ISRO	India	cmahesh@sac.isro.gov.in
Mala, Liudmila	UHC	Ukraine	myheat@gmail.com
Nadachowski, Jan	IMWM	Poland	jan.nadachowski@imgw.pl
Pogacnik, Nejc	EARS	Slovenia	nejc.pogacnik@gov.si
Prieto, Jose	EUMETSAT	Germany	jose.prieto@eumetsat.int
Ran, You	CMA	China	youran@cma.gov.cn
Sonmez, Ibrahim	H-SAF	Turkey	isonmez@dmi.gov.tr
Srdjan, Marjanovic	RHS	Serbia	srdjan.marjanovic@hidmet.gov.rs
Vidal, Luciano	CONICET	Argentina	lvidal@at.fcen.uba.ar
Zeiner, Barbara	ZAMG	Austria	barbara.zeiner@zamg.ac.at

Fifth Workshop of the
International Precipitation Working Group
11-15 October 2010, Hamburg, Germany



International Precipitation
Working Group

PHOTOGRAPHS



5th Workshop of the
International Precipitation Working Group
11 - 15 October 2010 • Hamburg, Germany



Workshop Summary and Conclusions

It is a tremendous challenge to estimate the global record of precipitation at the fine scales and long records that are needed. At present, precipitation estimates from satellite-based sensors constitute the key input for this vital information. In 2001 the Coordinating Group for Meteorological Satellites (CGMS) established the International Precipitation Working Group (IPWG) with co-sponsorship by the World Meteorological Organization (WMO) to provide a forum for the international precipitation research and operations communities to exchange information, establish common goals, and recommend future activities, primarily related to satellite-based precipitation work. Since that time the IPWG has pursued its goals by holding biennial workshops, organizing specialty workshops, and pursuing long-term cooperative projects among participants. IPWG5 is the latest in the series of biennial workshops, and builds on the results and recommendations of the fourth workshop (IPWG4), held in Beijing, China in October 2008 (Kidd et al. 2010). Two and a half days of presentations and posters set the stage for a day and a half of breakout sessions for three working groups: Applications, Research/New Technology, and Validation. All conference materials, presentations, posters, and proceedings papers as given herein including all training event lectures are available at <http://www.isac.cnr.it/~ipwg/hamburg-2010/Hamburg2010.html>.

To summarize, a few space-based radars are now taking data (on TRMM and CloudSat), but the best generally-available sensors are passive microwave (PMW) instruments, whose data have a relatively strong relation to hydrometeors (rain and snow). However, technological issues limit these sensors to low-earth-orbit (LEO) satellites, so their coverage is relatively sparse. Infrared (IR) sensors provide lower-quality information, but the data are available frequently because IR sensors are standard equipment on geosynchronous-earth-orbit (GEO) meteorological satellites. Algorithms have been developed to collect various combinations of these individual sensors to create multi-satellite products with uniform coverage at fine scales and reasonable quality that are not available from any single sensor type. Some multi-satellite products also include additional satellite sensors to address difficult situations and employ global analyses of precipitation gauge data to tie the satellite estimates more closely to “ground truth” data. One key development since the start of IPWG is that precipitation datasets are computed at a variety of delays (or “latencies”) from the time of observation. Short-latency data allow rapid use of the estimates, but at the price of less precise estimates. Long-latency datasets permit the use of additional data, including monthly analyses of precipitation gauge data.

Workshop Highlights

One key topic in the presentations and posters was the status and plans for the various operational and experimental precipitation products that are currently available or planned. A large number of precipitation datasets are freely available, and they are new enough that it is still challenging to enumerate them and track their status. As a result of IPWG5, it was agreed to establish a master list on the IPWG Web site (<http://www.isac.cnr.it/~ipwg>) to facilitate this process. Furthermore, it was a major concern at IPWG5 that these datasets must be properly maintained. Specifically, the

responsible agencies and research groups should seek to use the best calibration standards for the satellite radiances, and as new calibrations or algorithm versions are introduced for a particular dataset, it is imperative that the entire dataset be reprocessed with the new approach.

Several promising new approaches were discussed for retrievals from individual sensors, including one-dimensional variational retrievals and microwave-calibrated multi-channel GEO-data estimates using neural networks. Other algorithm research is focused on situations considered “difficult” in current PMW retrievals. One such problem situation is retrievals over complex terrain. Over land the useable PMW channels only sense the ice hydrometeors, yet a great deal of enhanced tropical and warm-season rainfall in complex terrain results from liquid-phase “warm rain” processes. As well, this enhancement tends to occur at scales smaller than the footprint of many PMW sensors. The solution being examined is to develop a simple model that incorporates ancillary data on atmospheric moisture profiles and the component of the wind blowing upslope against the local terrain. Another important “challenging” topic is quantitative detection of snowfall, or even liquid precipitation over icy surfaces. The current approach is to use PMW channels that do not “see” the surface, although research shows that there is a delicate balance between avoiding the surface and additionally missing the lowest layers of the atmosphere where the precipitation is located. In support of this work, IPWG is sponsoring the Third International Workshop on Space-based Snowfall Measurement, to be held 30 March – 2 April 2011 in Grainau, Germany. Turning to multi-satellite studies, two groups are working to use Kalman filtering to improve the time sequence of maps at fine scales, and one study showed promising results from a novel scheme for using daily precipitation gauge data to recalibrate the distribution of satellite precipitation estimates, as opposed to the monthly gauge analyses that are currently used.

The presentations covered new satellite systems, specifically the Global Precipitation Measurement (GPM) mission, which is a joint U.S.-Japan project that follows the highly successful Tropical Rainfall Measuring Mission (TRMM), another joint U.S.-Japan project that has marked 13 years of operation and features the first precipitation radar to fly in space. As well, the joint French-Indian Megha-Tropiques satellite will be launched in a very low-inclination orbit (20°, versus 35° for TRMM, 65° for GPM, and polar for most other PMW sensors) to maximize data collection in the deep tropics. The Japanese are preparing yet another LEO mission, the Global Change Observation Mission 1 – Water (GCOM-W1) satellite, which has a capable PMW sensor. Algorithm developers were urged to exploit the new generation of GEO sensors, which provides both numerous channels (10+) and lightning mappers.

More generally, IPWG5 strongly supported the continued launch and exploitation of multi-channel, dual-polarization, conically scanning PMW imagers with resolutions of 5-10 km, given their significant technical advantages for retrieving fine-scale precipitation estimates. As well, these sensors support numerous other retrievals, such as ocean surface winds and soil moisture, particularly when channels at 10 GHz or lower are included. IPWG5 also highlighted the significant contribution that the TRMM and CloudSat radars are making to research and calibration for precipitation, making it clear that agencies should be developing plans for on-going provision of space-based precipitation-capable radars.

Turning to a climate-scale perspective, for the first time at an IPWG meeting there were presentations on the concept of Climate Data Record (CDR) datasets. The CDR

concept is to provide carefully intercalibrated, long-term datasets that might omit recent innovations in order to preserve relative homogeneity over as long a period as possible. For satellite precipitation estimates, this starts with careful examination of each sensor's record, then extends to intercalibration at both the radiometric and precipitation algorithmic levels between satellites. One particular concern raised in the meeting is that the calibrations used in the CDR datasets should be carried over into the short- and medium-latency precipitation datasets, even while it is clear that residual differences are inevitable at the months-to-years range.

The calibration issues raised in CDR's were specifically focused in a special session on the Special Sensor Microwave Imager/Sounder (SSMIS). Although these sensors have flown on recent Defense Meteorological Satellite Program satellites, provided by the U.S. Department of Defense, they have suffered several calibration issues that have effectively prevented their use by the precipitation community. The data assimilation community developed the Universal Preprocessor code system to address these deficiencies from their own perspective, and this code is now being re-worked to address additional issues for precipitation estimation.

Another major topic at IPWG5 was validation of the various precipitation estimates. On the one hand, vigorous validation programs are being carried out at various institutions to support the choice and use of precipitation datasets for particular projects, as discussed above. On the other hand, IPWG has pursued a long-term project to provide large-region validation using precipitation gauge and radar analyses at the daily $0.25^\circ \times 0.25^\circ$ scale for routinely produced precipitation datasets. Multi-year results now include Australia, the continental U.S., Western Europe, parts of South America, and Japan. One exciting development, first proposed at IPWG4 and still being implemented, is to include estimates of precipitation from major numerical models in the IPWG validation exercises in cooperation with members of the Working Group on Numerical Experimentation (WGNE). Once the numerical model estimates are incorporated, it is planned to pursue an analysis phase, with a notional target of presentation-quality results by the time of the next IPWG meeting in 2012. It is considered key to refine the metrics used in the validation, compared to the wide-ranging list that is currently computed at the IPWG sites.

One on-going matter of concern to the IPWG is the lack of availability of quality-controlled precipitation gauge data sets in near real time for use by the precipitation research and operations communities. As noted above, such gauge data is critical to providing the best datasets for many applications. Another long-term issue on which IPWG is urging more attention is the provision of surface validation data in oceanic areas. Precipitation studies would benefit greatly from increased attention and systematic dataset preparation for collections of island stations, buoy-based gauges, and innovative ship-based instruments.

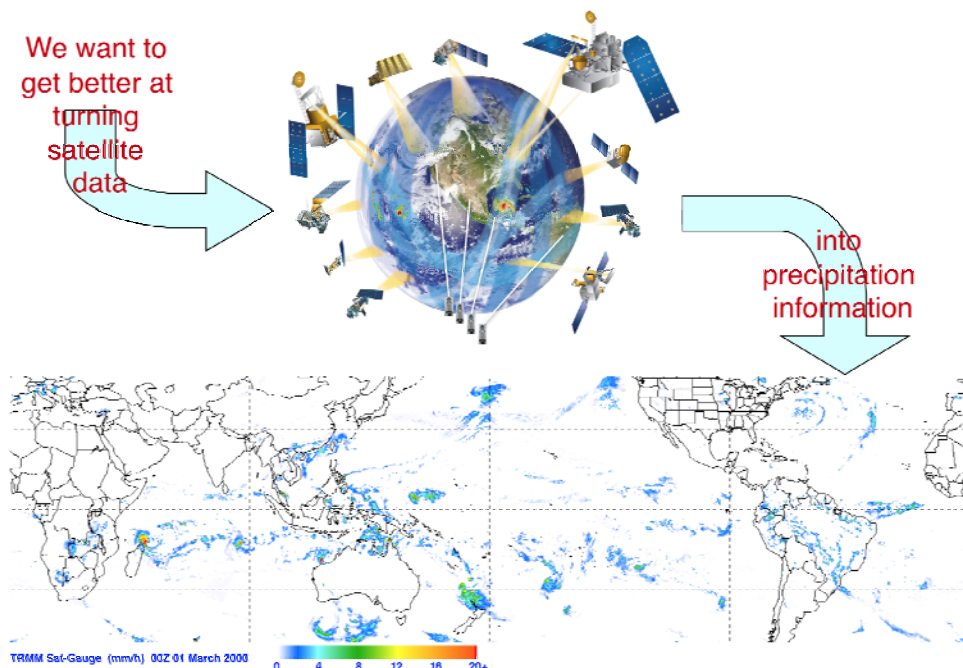
Interaction with data users was a point of emphasis at IPWG5. As the various precipitation datasets mature and become better known, there is an increasing need to inform users at all levels of scientific expertise about the various choices and their attributes. Some users are working toward application systems that turn precipitation estimates into guidance on crop growth, drought, flooding, or landslide probability. Such applications require a steady supply of short-latency precipitation estimates whose errors are characterized as well as possible. Other groups of "power users" are researchers seeking to close the global and regional water and energy budgets, or attempting to quantify global changes in precipitation. In addition, there is an increasing

need for tailored products that meet the needs of various researchers in related fields, many of whom do not have the extensive computer programming background that the power users have. In order to improve services to users, IPWG5 agreed to improvements in the IPWG web site, and planned to develop a summary of user needs for precipitation products.

The IPWG realizes that one important group of users is the personnel working in the hydrometeorological services in developing countries. Accordingly, IPWG partnered with EUMETSAT to develop a Hydrology and Precipitation Training Workshop that was held concurrently with IPWG5, 12-14 October 2010. The 16 attendees came from 15 different countries, and 11 of the 16 lecturers were scientists also attending IPWG5. Topics ranged from background on precipitation algorithms to exercises on accessing precipitation data across the Web. The IPWG will seek to hold such Training Workshops more frequently in the future.

OTHER NOTES

The IPWG serves as the leader of the Group for Earth Observations (GEO) precipitation sub-task (WA-08-01d in the current Work Plan). This activity is part of the Water Theme under the Integrated Products for Water Resource Management work plan task, and was reported during IPWG5. As well, the Co-Chairs serve two-year terms, and new Co-Chairs were nominated (and subsequently confirmed by CGMS): Paul Kucera (NCAR; USA) and Bozena Lapeta (IMWM/SRSC; Poland). Finally, the next workshop of the IPWG is planned for 2012, potentially in Brazil.



The international constellation of precipitation-relevant satellites has disparate platforms, sensors, orbits, and periods of record. It is a major challenge for satellite-based precipitation studies, such as the IPWG promotes, to best exploit these data, emphasizing the strengths and minimizing the weaknesses of the various resulting precipitation estimates. Most applications need merged estimates, illustrated at the bottom of the figure. [Upper images courtesy GPM project.]

REFERENCE

Kidd, C., R. Ferraro, and V. Levizzani, 2010: The Fourth International Precipitation Group Workshop. *Bull. Amer. Meteor. Soc.*, **91**, 1095-1099.

Huffman, G.J., C. Klepp, 2011: Meeting Summary: Fifth Workshop of the International Precipitation Working Group. *Bull. Amer. Meteor. Soc.*, in press.

HIGHLIGHTS OF THE CGMS-38 REPORT RELATED TO IPWG

Volker Gärtner

EUMETSAT

e-mail: Volker.gaertner@eumetsat.int

The CGMS-38 was very happy with the outcome and progress of IPWG-5. It was worthwhile to note that the ITWG meeting in 2010 echoed the IPWG recommendations to continue the conical scanning microwave imagers in the polar orbit, to provide microwave sensors in geostationary orbit, to optimize orbits, and to ensure the consistency of the SSMIS datasets. CGMS-38 was informed about the IPWG activities in 2010, including:

- IPWG Validation Activities began to include numerically generated precipitation estimates, in conjunction with the Working Group on Numerical Experimentation (WGNE).
- IPWG provided leadership in the GEO Precipitation Subtask, with Co-chair G. Huffman serving as the Point of Contact.
- Code and datasets were pushed toward completion for correcting errors in the SSMIS passive microwave satellite radiances, preparing to make them useful for the precipitation community.

CGMS took note and expressed its appreciation on the work done during the last months under the leadership of the outgoing co-chairs Dr. George Huffman (NASA, GSFC) and Dr. Christian Klepp from the Klima Campus, University of Hamburg (Germany). Especially the outcome of the IPWG-5 meeting held in Hamburg, October 2010, was considered an important contribution for the way forward in defining needs for future satellite instrumentation and optimised use of precipitation products. CGMS took note of the recommendations made by IPWG as listed below:

- Confirmation of the two new Co-chairs for the IPWG, Paul Kucera (NCAR) (USA) and Bozena Lapeta IMWM/SRSC (Poland), who CGMS-338 confirmed.
- Need for support of reprocessing activities for all available satellite precipitation product archives.
- SSMI/SSMIS dataset consistency has to be pursued.
- The need for coordination of satellite overpass times with a view to optimize temporal sampling, and taking advantage of backup satellites was emphasized.
- The continued availability of multi-channel, dual-polarization, conically scanning microwave imagers has to be ensured.
- Development of future geostationary microwave sensors has to be pursued.
- The continuity of cloud/precipitation space radars has to be ensured.
- The WMO was asked to develop an initiative, or task an existing initiative, to support the interface between providers and users to expand the use of precipitation products and opportunities for training.

- In particular, WMO is expected to facilitate access to rain gauge data in near real time, especially in data sparse regions.
- Consideration should be given to provide financial support for selected participants of IPWG-6, which is planned to be held in October 2012 (potentially in Brazil), together with a training event.

IPWG5 PARTICIPANT LIST

Name	Affiliation	Country	Email
Adesi, Adedayo Paul	NMA	Nigeria	adesiap@yahoo.com
Adler, Robert	Univ. Maryland	USA	radler@umd.edu
Alao, Kamorudeen A	NMA	Nigeria	talk2deputy@yahoo.com
Andersson, Axel	MPI-M	Germany	axel.andersson@zmaw.de
Aonashi, Kazumasa	MRI, Tsukuba	Japan	aonashi@mri-jma.go.jp
Arkin, Phil	Univ. Maryland	USA	parkin@essic.umd.edu
Bajracharya, Sagar	ICIMOD	Nepal	sagbajracharya@icimod.org
Bakan, Stephan	MPI-M	Germany	stephan.bakan@zmaw.de
Barkhordarian, Armineh	GKSS	Germany	armineh.barkhordarian@gkss.de
Barrera, Daniel	Univ. Buenos Aires	Argentina	daniel.barrera@fibertel.com.ar
Becker, Andreas	GPCC, DWD	Germany	andreas.becker@dwd.de
Behrangi, Ali	NASA JPL	USA	ali.behrangi@jpl.nasa.gov
Bejenaru, Gherman	SHS	Moldova	intern@meteo.md
Bell, William	ECMWF	UK	william.bell@ecmwf.int
Berg, Wesley	Colorado State Univ.	USA	berg@atmos.colostate.edu
Borsche, Michael	MPI-M	Germany	michael.borsche@zmaw.de
Boukabara, Sid	NOAA STAR	USA	sid.boukabara@noaa.gov
Bumke, Karl	Geomar, Kiel	Germany	kbumke@ifm-geomar.de
Calheiros, Alan	INPE	Brazil	alan.calheiros@cptec.inpe.br
Clayson, Carol Ann	Florida State Univ.	USA	cclayson@fsu.edu
Dinku, Tufa	IRI, Univ. Columbia	USA	tufa@iri.columbia.edu
Fennig, Karsten	DWD CMSAF	Germany	karsten.fennig@dwd.de
Ferraro, Ralph	NOAA	USA	ralph.r.ferraro@noaa.gov
Galliani, Alessandro	H-SAF	Italy	galliani@meteoam.it
Ganchev, Kiril	NIMH	Bulgaria	kiril.ganchev@meteo.bg
Garrett, Kevin	NOAA STAR	USA	kevin.garrett@noaa.gov
Gärtner, Volker	CGMS, EUMETSAT	Germany	volker.gaertner@eumetsat.int
Geppert, Gernot	MPI-M	Germany	gernot.geppert@zmaw.de
Grimes, David	Univ. Reading	UK	d.i.f.grimes@reading.ac.uk
Habib, Emad	Univ. Louisiana	USA	habib@louisiana.edu
Heinemann, Thomas	EUMETSAT	Germany	thomas.heinemann@eumetsat.int
Hoefenmayer, Regina	EUMETSAT	Germany	regina.hoefenmayer@eumetsat.int
Hou, Arthur	NASA GSFC	USA	arthur.y.hou@nasa.gov
Huffman, George	SSAI; NASA/GSFC	USA	george.j.huffman@nasa.gov
Itkin, Mikhail	MPI-M	Germany	mikhail.itkin@zmaw.de
Iwanski, Rafal	H-SAF	Poland	rafal.iwanski@imgw.pl
Joyce, Robert	NCP NWS NOAA	USA	robert.joyce@noaa.gov
Kachi, Misako	JAXA	Japan	kachi.misako@jaxa.jp
Kafi, Abdulla Hel	Inst. Water Modeling	Bangladesh	ahk@iwmbd.org
Kidd, Chris	Univ. Birmingham	UK	c.kidd@bham.ac.uk
Kim, Dongsoo	NOAA NESDIS	USA	dongsoo.kim@noaa.gov
Klepp, Christian	Univ. Hamburg	Germany	christian.klepp@zmaw.de
Knapp, Kenneth	NOAA/NCDC	USA	ken.knapp@noaa.gov
Kocsis, Zsolia	HMO	Hungary	kocsis.zs@met.hu
Komuscu, Ali Umran	H-SAF	Turkey	aukomuscu@dmi.gov.tr
Kucera, Paul	NCAR	USA	pkucera@ucar.edu
Kuligowski, Robert	NOAA STAR	USA	bob.kuligowski@noaa.gov
Lapeta, Bozena	H-SAF	Poland	b.lapeta@gmail.com
Levizzani, Vincenzo	ISAC-CNR	Italy	v.levizzani@isac.cnr.it
Liu, Zhong	NASA GSFC	USA	zhong.liu-1@nasa.gov
Löw, Alexander	MPI-M	Germany	alexander.loew@zmaw.de

Lukasevic, Justina	LHMS	Lithuania	j.juneviciute@meteo.lt
Mahesh, C.	ISRO	India	cmahesh@sac.isro.gov.in
Maidment, Ross	U. Reading	UK	ross.maidment@yahoo.co.uk
Mala, Liudmila	UHC	Ukraine	myheat@gmail.com
Mech, Mario	Univ. of Köln	Germany	mech@meteo.uni-koeln.de
Nadachowski, Jan	IMWM	Poland	jan.nadachowski@imgw.pl
Nesbitt, Steven	Univ. Illinois	USA	snesbitt@illinois.edu
Ou, Mi-Lim	KMA	Korea	milim@korea.kr
Pogacnik, Nejc	EARS	Slovenia	nejc.pogacnik@gov.si
Prieto, Jose	EUMETSAT	Germany	jose.prieto@eumetsat.int
Puca, Silvia	Italian Civil Protect. Dep.	Italy	silvia.puca@protezionecivile.it
Ran, You	CMA	China	youran@cma.gov.cn
Rudolf, Bruno	GPCC, Offenbach	Germany	bruno.rudolf@dwd.de
Salio, Paola	Univ. Buenos Aires	Argentina	salio@cima.fcen.uba.ar
Sapiano, Mathew	Colorado State Univ.	USA	msapiano@atmos.colostate.edu
Schneider, Udo	GPCC, DWD	Germany	udo.schneider@dwd.de
Semunegus, Hilawe	NOAA NESDIS	USA	hilawe.semunegus@noaa.gov
Shige, Shoichi	Univ. Kyoto	Japan	shige@kugi.kyoto-u.ac.jp
Sonam, Chedup	Gvmt Bhutan	Bhutan	shedup@moea.gov.bt
Sonmez, Ibrahim	H-SAF	Turkey	isonmez@dmi.gov.tr
Srdjan, Marjanovic	RHS	Serbia	srdjan.marjanovic@hidmet.gov.rs
Tarnavski, Elena	Univ. Reading	UK	e.tarnavsky@reading.ac.uk
Tian, Yudong	Univ. Maryland	USA	yudong.tian-1@nasa.gov
Turk, Joe	JPL NASA	USA	jturk@jpl.nasa.gov
Vidal, Luciano	CONICET	Argentina	lvidal@at.fcen.uba.ar
Vila, Daniel	CPTEC/INPE	Brazil	daniel.vila@cptec.inpe.br
Viltard, Nicholas	IPSL	France	nicolas.viltard@latmos.ipsl.fr
Wang, Nai-Yu	Univ. Maryland	USA	nai-yu.wang@noaa.gov
Yeh, Nan-Ching	National Defense Univ.	Taiwan	jim912104@gmail.com
Yoo, Soo-Hyun	CPC, NOAA	USA	soo-hyun.yoo@noaa.gov
Zahn, Mathias	Met Office	UK	maz@mail.nerc-essc.ac.uk
Zeiner, Barbara	ZAMG	Austria	barbara.zeiner@zamg.ac.at
Ziese, Markus	GPCC, DWD	Germany	markus.ziese@dwd.de

INDEX TO ABSTRACTS AND PAPERS

Lead Author	Title	Page
Adesi, Adedayo Paul	USES OF SATELLITE PRECIPITATION DATA IN NIGERIA	29
Adler, Robert	GLOBAL FLOOD AND LANDSLIDE NOWCASTS AND FORECASTS USING MULTI-SATELLITE PRECIPITATION OBSERVATIONS	44
Andersson, Axel	GLOBAL OCEAN FRESHWATER FLUX COMPONENTS FROM SATELLITE, RE-ANALYSIS AND IN-SITU CLIMATOLOGIES	45
Aonashi, Kazumasa	NEW GSMaP OVER-LAND PRECIPITATION RETRIEVAL ALGORITHM	56
Bajracharya, Sagar	VERIFICATION OF NOAA CPC RFE AT VARIOUS TEMPORAL AND SPATIAL RESOLUTIONS IN THE HINDU KUSH - HIMALAYAN REGION	57
Bakan, Stephan	THE HOAPS-3 CLIMATOLOGY	58
Barkhordarian, Armineh	CAN RECENTLY OBSERVED PRECIPITATION TRENDS OVER THE MEDITERRANIAN AREA BE EXPLAINED BY CLIMATE CHANGE PROJECTIONS?	67
Barrera, Daniel	RAIN-GAUGE VALIDATION OF SATELLITE RAINFALL ESTIMATES OVER ARGENTINA	68
Behrangi, Ali	REFAME, FORWARD-BACKWARD AND MULTI-SPECTRAL EXTENSION	69
Boukabara, Sid	A PHYSICALLY-BASED RAINFALL RATE ALGORITHM FOR THE GLOBAL PRECIPITATION MISSION	75
Bumke, Karl	RAIN DROP SIZE DENSITIES OVER LAND AND OVER SEA	76
Dinku, Tufa	BLENDING SATELLITE RAINFALL ESTIMATES AND NATIONAL RAINGAUGE OBSERVATIONS TO PRODUCE 30-YEAR RAINFALL TIME SERIES	77
Fennig, Karsten	RELEASE OF CM-SAF HOAPS v3.2 PRODUCTS BASED ON IMPROVED DATA RECORD OF SSM/I RADIANCES	86
Ferraro, Ralph	THE STATUS OF NOAA/NESDIS PRECIPITATION ALGORITHMS AND PRODUCTS	87
Habib, Emad	MULTI-SITE AND MULTI-OBJECTIVE EVALUATION OF HIGH-RESOLUTION SATELLITE-RAINFALL PRODUCTS	98
Heinemann, Thomas	EUMETSAT'S ACTIVITIES IN SUPPORT OF PRECIPITATION REMOTE SENSING	99
Hou, Arthur	THE GLOBAL PRECIPITATION MEASUREMENT (GPM) MISSION: OVERVIEW AND U.S. STATUS	108
Huffman, George	HIGHLIGHTS OF VERSION 7 TRMM MULTI-SATELLITE PRECIPITATION ANALYSIS (TMPA)	109
Itkin, Mikhail	RAIN INTENSITY SPECTRA DISTRIBUTION OVER GERMANY AND WESTERN AFRICA	111
Itkin, Mikhail	RESOLVING RAINFALL RATE RETRIEVAL AMBIGUITIES ASSOCIATED WITH CLOUD TYPES USING MULTI-SATELLITE PASSIVE MEASUREMENTS	112
Iwanski, Rafal	VARIABILITY OF LIGHTNING ACTIVITY AND SUBSEQUENT CONVECTIVE PRECIPITATION DERIVED FROM SATELLITE AND GROUND BASED SENSORS – CASE STUDY	113
Joyce, Robert	KALMAN-FILTERED CMORPH USING TRMM TO BLEND SATELLITE RAINFALL	124
Kachi, Misako	STATUS OF JAPANESE PRECIPITATION MEASURING MISSIONS AND GLOBAL RAINFALL MAP IN NEAR-REAL-TIME	125

Kidd, Chris	THREE STUDIES: CAN MODELS REPLICATE TROPICAL PRECIPITATION CYCLES ACCURATELY? HOW DO MODELS AND SATELLITE ESTIMATES PERFORM IN THE NORTH ATLANTIC? DO WE REALLY INFLUENCE PRECIPITATION?	134
Kim, Dongsoo	DIURNAL CHARACTERISTICS OF SATELLITE-DERIVED QUANTITATIVE PRECIPITATION ESTIMATE	135
Klepp, Christian	PRECIPITATION VALIDATION OVER THE OCEAN	136
Knapp, Kenneth	GLOBALLY GRIDDED SATELLITE (GRIDSAT) OBSERVATIONS FOR CLIMATE STUDIES	147
Kucera, Paul	APPLICATION OF MET FOR THE VERIFICATION OF THE NWP CLOUD AND PRECIPITATION PRODUCTS USING A-TRAIN SATELLITE OBSERVATIONS	148
Kuligowski, Robert	THE GOES-R RAINFALL RATE, RAINFALL POTENTIAL, AND PROBABILITY OF RAINFALL ALGORITHMS	157
Laviola, S.	CHARACTERIZATION OF SNOW-COVERED TERRAIN AND DETECTION OF SNOWFALL BY USING THE 183-WSL RETRIEVAL SCHEME	170
Liu, Zhong	GLOBAL PRECIPITATION DATA ACCESS, VALUE-ADDED SERVICES AND SCIENTIFIC EXPLORATION TOOLS AT NASA GES DISC	182
Löw, Alexander	COMBINING PRECIPITATION AND SOIL MOISTURE OBSERVATIONS: A WAY FOR IMPROVED ESTIMATES OF LAND SURFACE WATER FLUXES?	191
Maidment, Ross	TARCAT - TAMSAT AFRICAN RAINFALL CLIMATOLOGY AND TIME SERIES	192
Nesbitt, Steven	PERFORMANCE OF TRMM LEVEL 2 AND 3 RAINFALL RETRIEVALS IN THE COMPLEX TERRAIN OF SOUTH ASIA	199
Ou, Mi-Lim	ACTIVITY ON SATELLITE BASED PRECIPITATION IN KMA: CURRENT STATUS AND PLAN	200
Puca, Silvia	THE PRECIPITATION PRODUCT VALIDATION SERVICE DEFINED DURING THE DEVELOPMENT PHASE OF THE HYDROLOGICAL SAF	206
Rudolf, Bruno	THE GLOBAL PRECIPITATION CLIMATOLOGY CENTRE (GPCC) HAS RELEASED IN DECEMBER 2010 ITS FULL DATA REANALYSIS VERSION 5, SERVING THE HYDRO-CLIMATOLOGY COMMUNITY	207
Salio, Paola	PERFORMANCE EVALUATION OF PRECIPITATION ESTIMATIONS OVER SOUTH-EASTERN SOUTH AMERICA CONSIDERING DIFFERENT CLIMATIC REGIONS	215
Sapiano, Mathew	TOWARDS A CLIMATE DATA RECORD OF PRECIPITATION FROM SATELLITE MICROWAVE IMAGER DATA	216
Sapiano, Mathew	STATUS OF AND EARLY RESULTS FROM THE IPWG/WGNE MODEL PRECIPITATION INTERCOMPARISON	217
Shige, Shoichi	IMPROVEMENT OF GSMAP PASSIVE MICROWAVE IMAGER RAINFALL RETRIEVALS OVER THE MOUNTAINOUS AREA IN JAPAN	218
Tian, Yudong	QUANTIFYING UNCERTAINTIES IN SATELLITE-BASED GLOBAL PRECIPITATION MEASUREMENTS	219
Turk, Joe	VERTICAL PROFILING OF SNOW USING CLOUDSAT AND C-BAND GROUND RADAR	220
Vidal, Luciano	IMPLEMENTATION OF A METHODOLOGY TO CALIBRATE GROUND RADARS USING TRMM-PR OVER ARGENTINA	234
Vila, Daniel	SSM/I/S ASSESSMENT FOR RAINFALL RETRIEVAL: PRELIMINARY RESULTS	242
Viltard, Nicholas	MEGHA-TROPIQUES: MISSION AND ALGORITHMS STATUS	248

Wang, Nai-Yu	DEVELOPING WINTER PRECIPITATION ALGORITHM OVER LAND FROM SATELLITE MICROWAVE AND C3VP FIELD CAMPAIGN OBSERVATIONS	249
Yeh, Nan-Ching	PRECIPITATION ESTIMATION FOR TYPHOON USING SATELLITE MICROWAVE DATA	250
Yoo, Soo-Hyun	CORRECTING THE CMORPH BIAS USING A DAILY GAUGE ANALYSIS	257
Zahn, Mathias	INVESTIGATION OF TRENDS IN THE MOISTURE BUDGET OF THE TROPICAL ATMOSPHERE	265

INDEX TO WORKING GROUP REPORTS

Research / New Technology.....	271
Applications.....	276
Validation	279

USE OF SATELLITE PRECIPITATION DATA IN NIGERIA

A.P. Adesi¹, T. Adelugba² and T. Salami²

¹Nigerian Meteorological Agency, Nnamdi Azikiwe International Airport
Abuja. P.O. Box 11519, Garki, Abuja, Nigeria.

²Nigerian Meteorological Agency, Murtala Mohammed International Airport
Ikeja Lagos. P.M.B 1215, Oshodi Lagos, Nigeria.

e-mail: adesiap@yahoo.com

ABSTRACT

The use of satellite precipitation data for forecast in Nigeria is greatly advancing, this is due to the availability of satellite imagery and measured real time rainfall data that can be used to validating the estimated amount of rainfall been derived from imagery captured by satellite of an area.

Rainfall data from rain gauge measurements have been used to validate the data of the Tropical Rainfall Measuring Mission Precipitation Radar (TRMM PR) and the data of two other satellite algorithms namely 3B43 and TMP1 for 36 months (Jan1998-Dec2000) at 1.0°x1.0° latitude/longitude grid boxes over Nigeria.

Between 1998 and 2000 we studied the interconnection between precipitation imageries captured over Nigeria and the amount of Rainfall measured. We noted that there is critical connection between the Thermodynamic properties over the surface, the estimated amount of rainfall from a particular captured imagery and measured rainfall data. Therefore proper understanding of the satellite precipitation imagery will enable forecasters in Nigeria to forecast the amount of precipitation from a particular type of imagery for flood and disaster monitoring. More practical issues will be presented.

Flood disaster related event has claimed million of lives, make thousand homeless and devastated more million arable land in Africa.

1.0 INTRODUCTION AND HISTORY OF THE TROPICAL RAINFALL MEASUREMENT MISSION (TRMM)

Precipitation is the primary source of hydrological process on earth. Rainfall prediction has become so important because it controls the agricultural processes in the tropics. Hence the rainfall information can either improve food production or bring about drought. In environmental studies, it is imperative to have at the back of our minds that in the hydrological cycle the information on the spatial distribution of rainfall contribute to the knowledge on how rainfall influences global circulation and climate. In Nigeria, rainfall plays a prominent role on the social and economic aspect of the people. Therefore there is need for reliable rainfall data not only in the country but also globally.

The principal existing source of precision information on climate scale precipitation is rain gauge observations, which has advantages as well as shortcomings (Barrett and Martin, 1981; Ardanuy and Arkin, 1989). The advantage is enormous; however, rain gauges catch less precipitation than actually reaches the ground surface owing to turbulence around rainguage aperture. Difficulty also arises because its measurement networks are not so dense or regular (Adeyewa and Nakamura, 2003) and according to Arkin and Xie (1996), the observations suffer sampling error in representing area means, they are not available over most oceanic and underdeveloped land. Other problems associated with rainfall measurements in Nigeria are sparcity of data and lack of effective communication. Satellites have been thought as a means to circumvent some of these difficulties attendant on rain gauge measurement and other problems throughout the tropics. Nigeria is a component of this. Satellite remote sensing is probably the only way to provide reliable rainfall data.

Satellite – based precipitation products could provide very high temporal and spatial resolution (e.g. 3 – hourly / 0.50 x 0.50 lat – long. grid size). Nevertheless, they are subject to larger biases and stochastic errors and need to be adjusted to in –situ observation (Barrett et al., 1994; Rudolf et al., 1996). Satellite have biases and random errors which are caused by factors such as the sampling frequency, the diurnal cycle of rainfall, the non-uniform field of view of sensors and the uncertainties in the rain retrieval algorithms (Kousky, 1980; Bell et al., 1990; Chiu et al., 1990; Kummerow, 1998; Anagnostou et al., 1999). Huffman (1997) and Huffman et al. (1997) noted that often, the random error due mainly to sparsely sampled datasets is the dominant component. Accurate estimates of tropical precipitation are therefore desperately needed to validate satellite products. This can now give credibility to the use of satellite precipitation data. In this study, TRMM satellite algorithm used to validate rainfall from rain gauge are 3A25, 3B43 and TMP1. They are used so as to derive the geographical pattern of the distribution of rainfall over Nigeria.

1.1 OBJECTIVES OF THIS STUDY

The aims and objectives of this study are:

1. To validate the TRMM PR (3A25), 3B43 and TMP1 data with rainguage data over Nigeria.
2. To compare the mean seasonal rain gauge rainfall data in the country with those obtained by the satellite algorithms.
3. To estimate the bias and random errors of the satellite algorithms.

1.2 THE CORE TRMM INSTRUMENT

The core TRMM instruments include the TRMM PR (Tropical Rainfall Measuring Mission Precipitation Radar), TMI (TRMM Microwave Images), VIRS (Visible Infrared Scanner), CERES (Clouds and Earth's Energy System) and LIS (Lightning Imaging Sensor) but our interest will only be limited to TRMM PR in the course of this study.

1.2.1 TRMM PR

The TRMM PR is the first space borne precipitation radar developed by NASDA with the assistance of Communications Research Laboratory (CRL). The PR operating at 13.98 GHz, scans cross-track + 170; having 49 fields of view with a horizontal resolution of 4.3km at nadir and a vertical resolution of 250m (Kummerow et al., 1998). The sensitivity of the radar is 18 dbz which allows routine detection of rainfall intensities as low as 0.5mm/hr. It operates at a wavelength of 2.2cm with an observable range from the surface to a height of greater or equal to 15km and swath approximately 2.5km in width. It weighs 465kg having 250W power consumption.

Many researches revealed that TRMM PR has delivered incredible wealth of detailed rain structure information. Examples include the studies of propagating rainfall structures across land and ocean by Takayabu et al (1999) and also by Rosenfeld (2002). Gage et al. (1996) had earlier postulated that the PR functions somewhat as a global precipitation profiler without Doppler capabilities, providing information on the vertical structures of rain. However the primary importance of PR still remains the fact that it can provide 3-dimensional rainfall structure.

2. DATA SOURCE AND METHODS

2.1. Area of study

The area of study is Nigeria which is situated between latitude 3.50N-14.50N (longitude 2.50W-14.50W) and so the country lies within the tropical region. In general, two seasons characterize the climate conditions, namely, the winter and summer but locally called the dry season and rainy season. Closely associated with the seasons is the inter-tropical discontinuity (ITD): a zone separating the dry, dusty, cold at night and hot during the day, north-east trades (harmattan) from the moist, warm south-west trades (Hamilton and Archbold, 1945) and which roughly correspond respectively to the period when the continental Tropical (cT) and the maritime Tropical (mT) air masses and their associated wind influence most parts of the region.

With increase in the depth of the mT air, continuous rain occurs, hence rainy season set in from March. The duration of the season and intensity of the weather vary from the coastal areas (south), west to the East and to the extreme north. There is a principal rainy season in May, June and first of July in the southwestern part of the country while a secondary rainy season occupies the later half of September and October (Bi-modal rainfall). This gradually changes eastward to single rainy season from April to October. The northern part experience a single rainy season from June through September. Line squalls and thunderstorms, and deep convective systems, together contribute at least 80% of the annual rainfall (Eldridge, 1957; Obasi, 1975) has shown that at least 70% of the total annual precipitation over the coastal areas of Nigeria comes from these mesoscale phenomena. On the other hand, the dry season is characterized with airflow (cT) from the anticyclone over the Sahara.

Although in general, only two seasons are usually recognized but there are up to six seasons over the region, especially along the coast. Three of the seasons are associated with rainfall maxima and the other three with the rainfall minima. The first, primary maximum occurs between May-June and early July. The second occurs usually between February and April along the coastal areas since the mT air is deep enough in

these areas for convection to result in rainfall. The third maximum occurs between September and November also along the coastal areas.

The fourth season is the primary rainfall minimum associated with long dry season, when the ITD is located near the Guinea coast and most part is rainless. Towards the end of July and early August, a peculiar secondary rainfall minimum, the fifth possible season occurs when the ITD is farthest north. This season, known as the “Little Dry Season”, does not extend far inland (Ireland, 1962; Ojo, 1977). The sixth season, which may be distinguished as another secondary minimum, occurs between the early rainfall maximum late February to April) and the primary rainfall maximum which occurs between May and early July.

Satellite data finds its most useful application during the rainy season unlike the dry season where it has given no encouraging result (Adeyewa and Nakamura, 2003). Generally speaking, satellite observations (Infrared and passive microwave) can be used to observe estimates of large-scale precipitation over much of the globe, but these estimates are characterized by non negligible bias and random error associated with inadequate sampling, algorithm errors, and the indirect nature of the physical relationship between precipitation and the observations.

In order to quantitatively understand the capabilities of existing data sources and algorithms, Xie and Arkin (1995) conducted a comprehensive examination of several existing source of climate-scale precipitation.

2.2. Datasets

2.2.1 The gauge data

Rain gauge data utilized was obtained from the data section of the Nigerian Meteorological Agency, Oshodi under the Federal Ministry of Transport. The Agency is affiliated to World Meteorological Organization (WMO), a specialized agency of the United Nation.

For this study, monthly mean data for 36 months (Jan 1998-Dec 2000) have been used. It was well scrutinized, arranged in excel package, formatted and then spatialized into grid boxes at a resolution of 1° x 1° latitude/longitude in the Hierarchical Data format (HDF) using Transform software package. It is however important to note that 12 grid boxes are expressed in latitudinal and 13 grid boxes for longitudinal axes which implies that 156 grid boxes were used for the country (-99.99 was used to represent missing data). A macro was thereafter written in Noesys software package and used to analyses the datasets in order to conform and compare with the satellite precipitation data sets.

2.2.2. The Satellite data

Freely available Tropical Rainfall Measurement Mission data of 3A25, 3B43 and TMP1 were used in this study.

2.2.2.1. 3A25 (TRMM PR)

Product 3A25, denoting averages of precipitation is one of the primary sources of data for this study. Algorithm 3A25 gives the space-time averages of accumulations of 1C21, 2A21, 2A23 and 2A25 products (see Tropical Rainfall Measuring Mission Precipitation Radar Algorithm Instruction Manual Version 2.0 for details). The monthly product is

produced at two resolutions, a standard space scale, $5^\circ \times 5^\circ$ and $0.5^\circ \times 0.5^\circ$ latitude longitude grid cells at low and high horizontal resolutions respectively from level-2 product (Instantaneous PR Observation). However, the 3A25 product utilized were data over $0.5^\circ \times 0.5^\circ$ latitude-longitude grid cells, which corresponds to version 5 algorithms. They were derived from TRMM PR observation by TRMM science Team and were been regrided to $1.0^\circ \times 1.0^\circ$ latitude-longitude grid resolution in order to conform to the other rain gauge and satellite products used in this study. The data covers the whole tropical regions ($37^\circ\text{N} - 37^\circ\text{S}$) but the data of Nigeria ($3.5^\circ\text{N} - 14.5^\circ\text{N}$) were extracted from this.

2.2.2.2. 3B43

The 3B43 algorithm is tagged TRMM and other data (i.e. TRMM, calibrated IR and rain gauge products). It is a monthly temporal resolution and at $1^\circ \times 1^\circ$ latitude/longitude spatial resolution. The algorithm was developed by the TRMM Science Team and was processed by TRMM Science Data and Information system (TSDIS); a process which is based on the technique by Huffman et al (1997). The 3B43 dataset observation is primarily based on gauge measurements and satellite estimate of rainfall. The purpose of algorithm 3B43 is to produce the “Tropical Rainfall Measuring Mission (TRMM) and Other Data” best-estimate precipitation rate and root-mean-square (RMS) precipitation-error estimates. These two independent precipitation fields are the daily-average adjusted merged-infrared (IR) estimate (3B43) and the monthly accumulated Climate Assessment and Monitoring System (CAMS) or Global Precipitation Climatology Centre (GPCC) rain gauge analysis (3A25). A complete description of algorithm 3B43 is provided in the Algorithm 3B43 User’s Guide available from the TRMM Science Data and Information System (TSDIS).

2.2.2.3. TMPI

The Threshold Matched Precipitation Index (TMPI) was also used for this study. It is part of the Global Precipitation Climatology Project (GPCP) IDD (one-degree daily) precipitation project. The product is a gridded analysis based on estimates of a monthly analysis of satellite and gauge observations. The TMPI is a GOES Precipitation Index (GPI) – type algorithm of which the approximate instantaneous precipitation data covers 40° N/S latitudinal region and according to Huffman et al (1997 and 2001), the Advanced TIROS operational Vertical Sounder (ATOVS) dataset covers even outside this band. The dataset creators are G.J. Huffman, R.F. Adler, and D.T. Bolvin, working in the Laboratory for Atmospheres, NASA Goddard Space Flight.

2.3. Methodology

Generally, the data used covered 36-months (Jan 1998-Dec 2000) which were available for all the sources earlier specified. The analyses were carried out using rain gauge measurements as reference for the satellite algorithms (3A25, 3B43 and TMPI). A 3-year mean Bias Error (MBE, in mm) was computed for each algorithm using the formula:

$$MBE = \frac{\sum_{j=1}^N (Alg_j - Ref_j) / N}{N} \dots\dots\dots(1)$$

Where

- Alg. = Any of the algorithms (3A25, 3B43 or TMPI)
- j = a specific grid point
- Ref = reference or observed value i.e. Rain gauge data
- N = the number of grid points

The percentage or relative mean Bias Error (%MBE) was estimated as

$$MBE (\%) = \frac{\sum_{j=1}^N (Alg_j - Ref_j) / N}{\sum_{j=1}^N (Ref_j) / N} \times 100 \dots\dots\dots (2)$$

% MBE is used to ascertain the systematic component of the error in an algorithm in the present analysis. Also evaluated was the Root Mean square Error (RMSE, in mm).

$$RMSE = \sqrt{\frac{\sum_{j=1}^N (Alg_j - Ref_j)^2}{N}} \dots\dots\dots (3)$$

The percentage or relative RMSE (% RMSE) is given as

$$RMSE (\%) = \frac{\sqrt{\sum_{j=1}^N (Alg_j - Ref_j)^2 / N}}{\sum_{j=1}^N (Ref_j) / N} \times 100 \dots\dots\dots (4)$$

These parameters were used to assess the suitability of the satellite rainfall products.

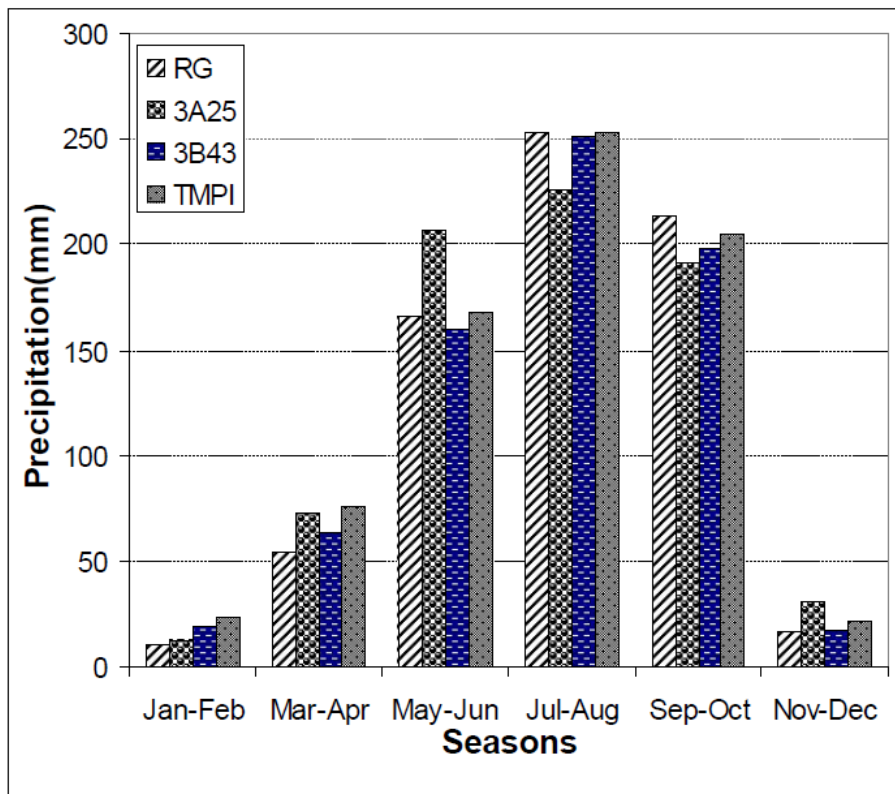


Fig 1. Mean seasonal plot of RG, 3A25, 3B43 and TMPI.

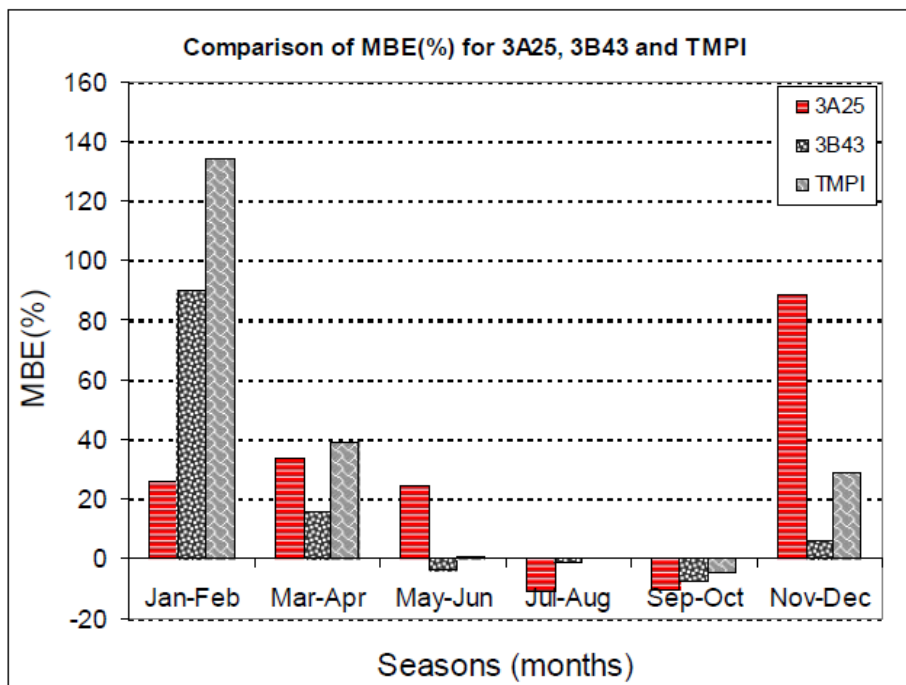


Fig 2(a). Comparison of MBE (%) for 3A25,3B43 and TMPI

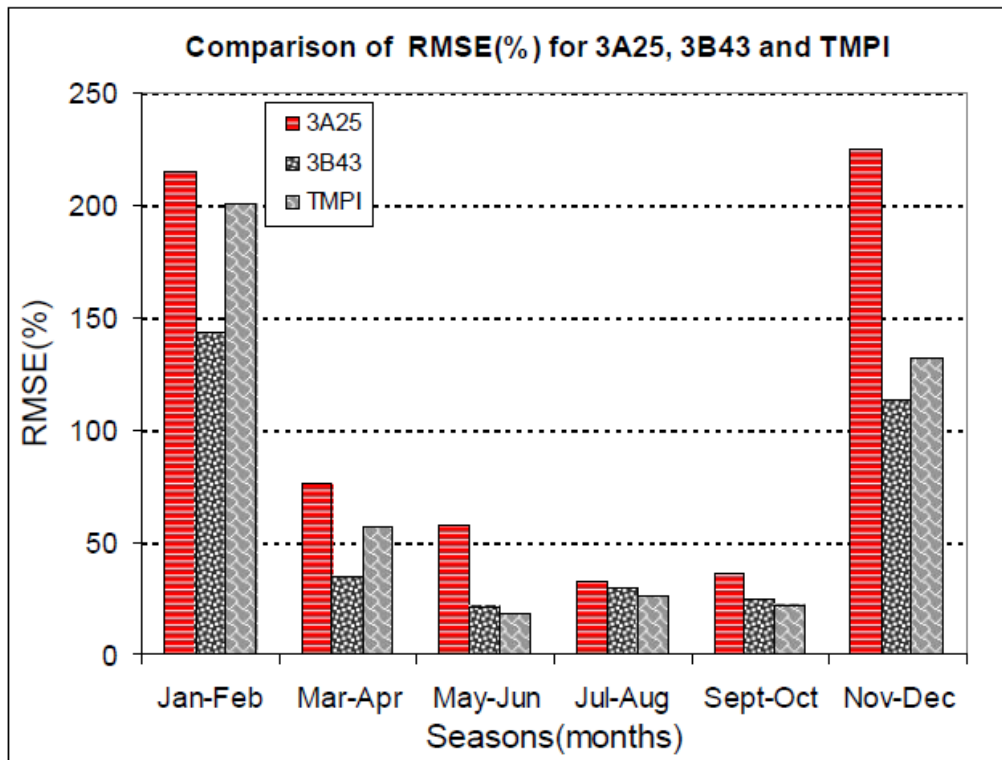


Fig. 2(b). Comparison of RMSE (%) for 3A25, 3B43 and TMPI

RG/ [3A25](#)

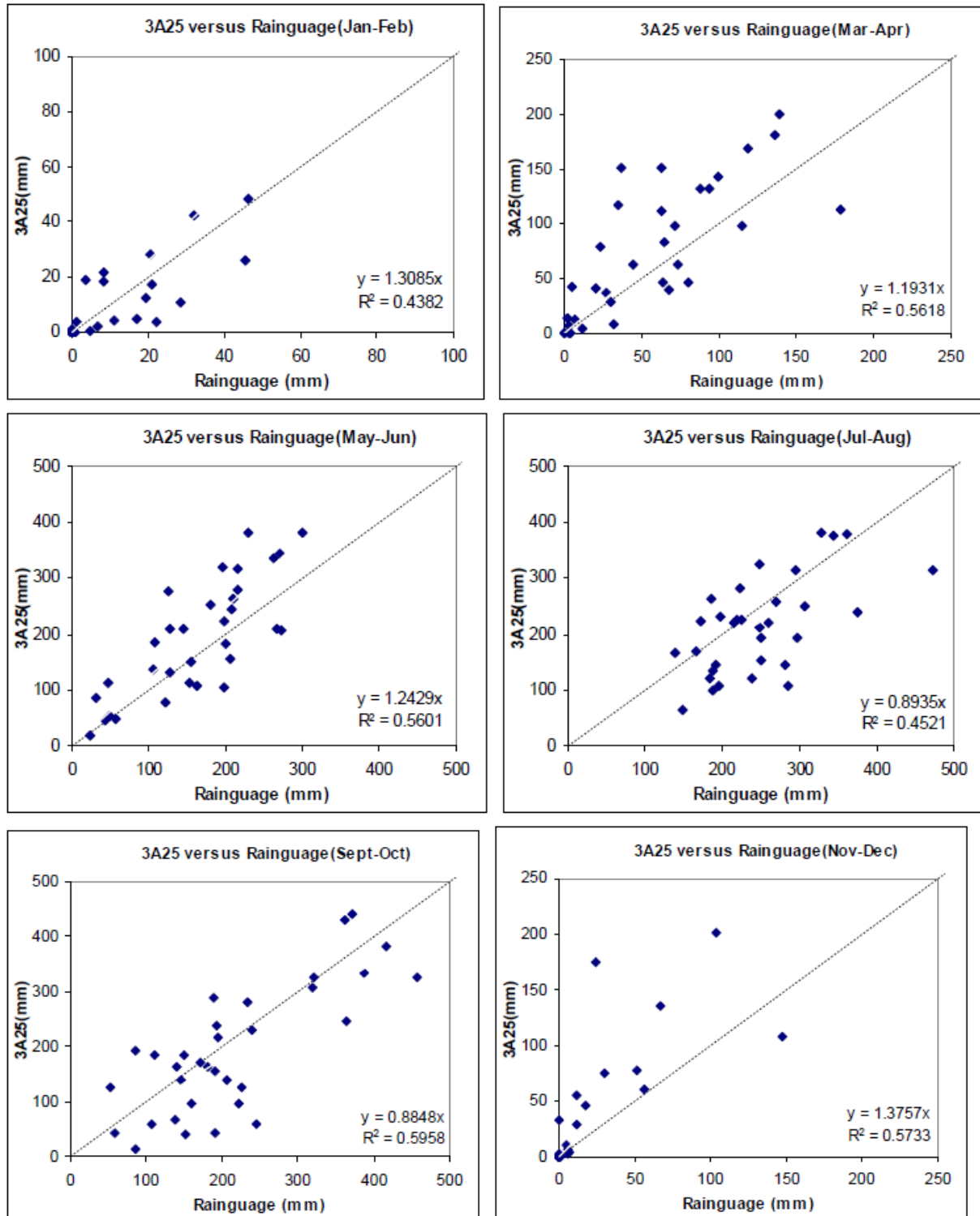


Fig. 3.(a): Scattergram of seasonal precipitation with 3A25

RG/ [3B43](#)

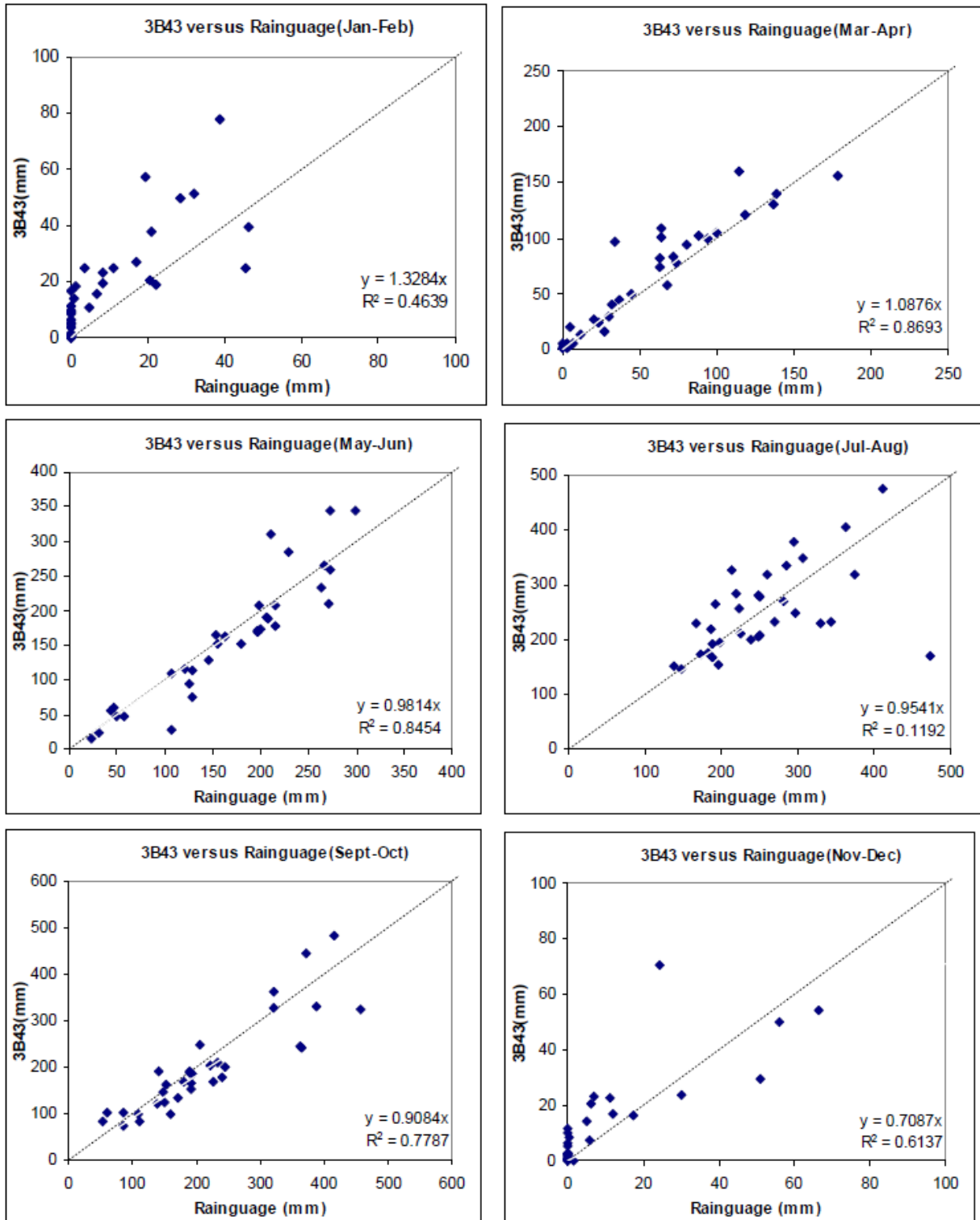


Fig. 3. (b): Scattergram of seasonal precipitation with 3B43.

RG/ [TMPI](#)

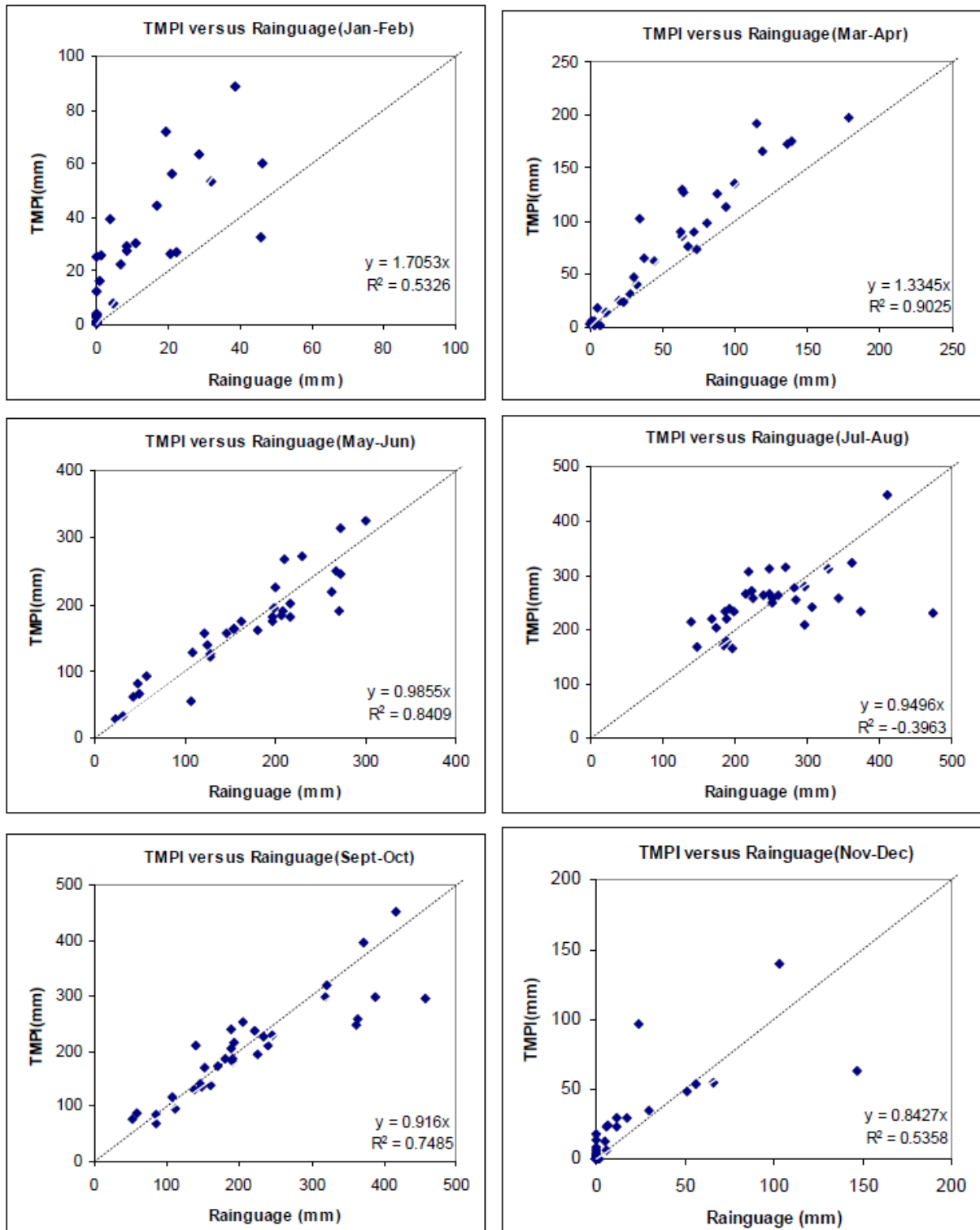


Fig. 3.(c): Scattergram of seasonal precipitation with TMPI.

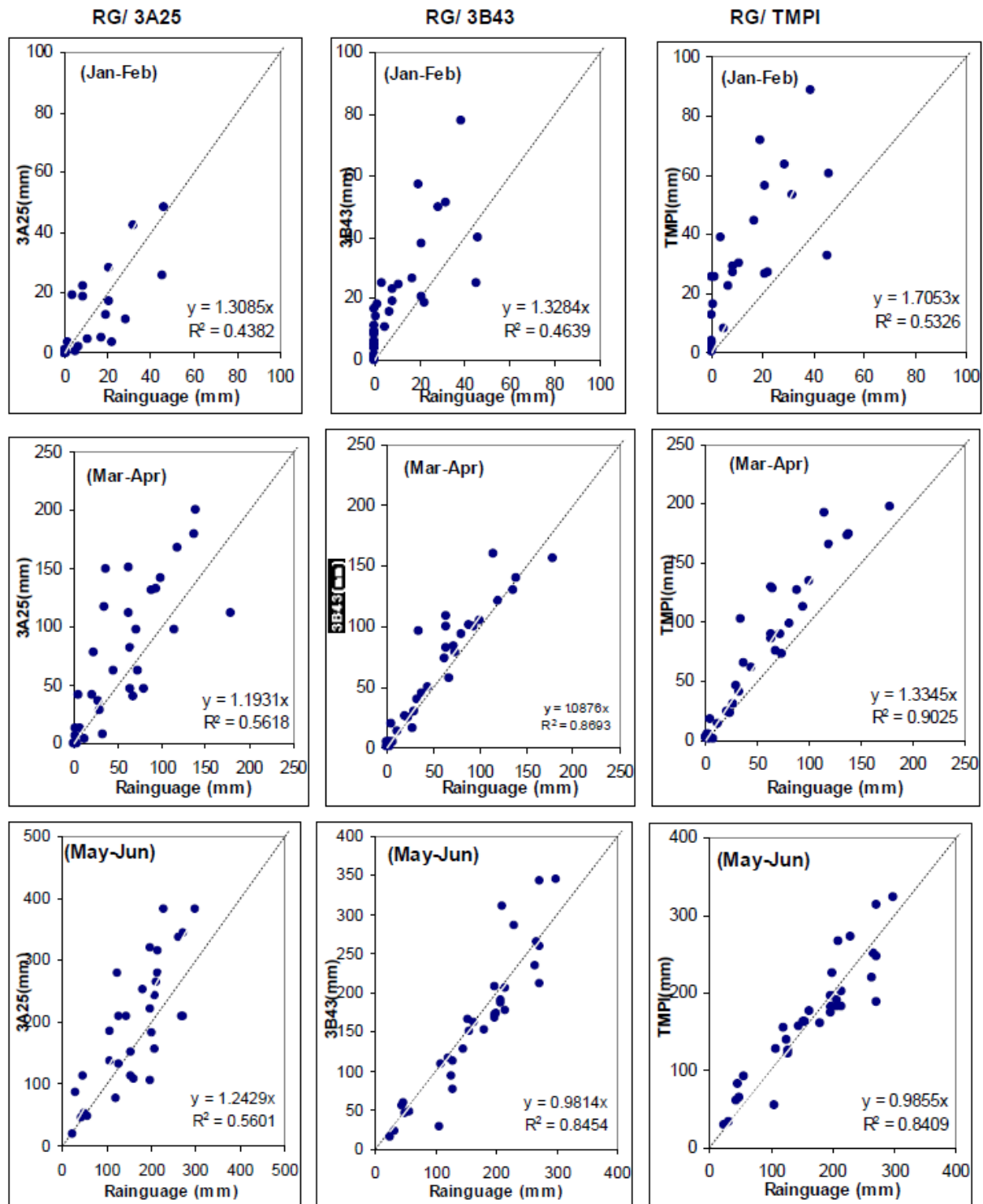


Fig. 3.2(a): Scattergram of seasonal precipitation with 3A25(Left), 3B43(middle) and TMPI(right) for Jan-Feb(above),Mar-Apr(middle) and May-Jun(below) respectively.

	3A25	3B43	TMPI
Jan-Feb	0.4382	0.4639	0.5326
Mar-Apr	0.5618	0.8693	0.9025
May-Jun	0.5601	0.8454	0.8409
Jul-Aug	0.4521	0.1192	-0.3963
Sep-Oct	0.5958	0.7784	0.7485
Nov-Dec	0.5733	0.6137	0.5358

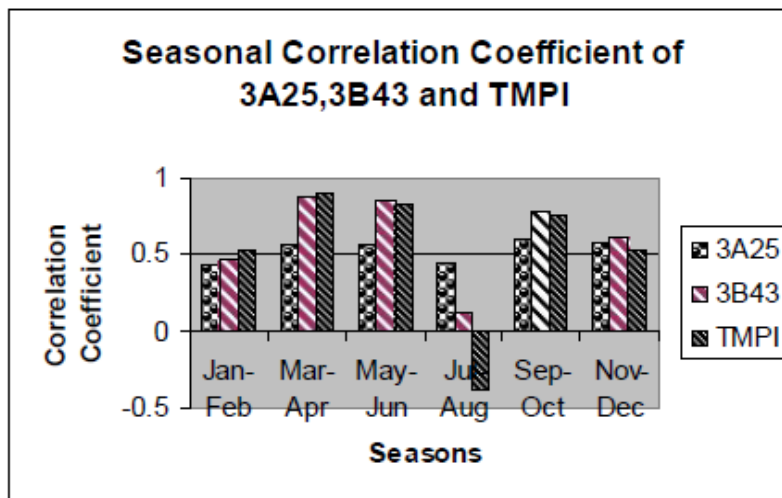


Fig. 3.3 Seasonal Correlation Coefficient of 3a25, 3B43 and TMPI

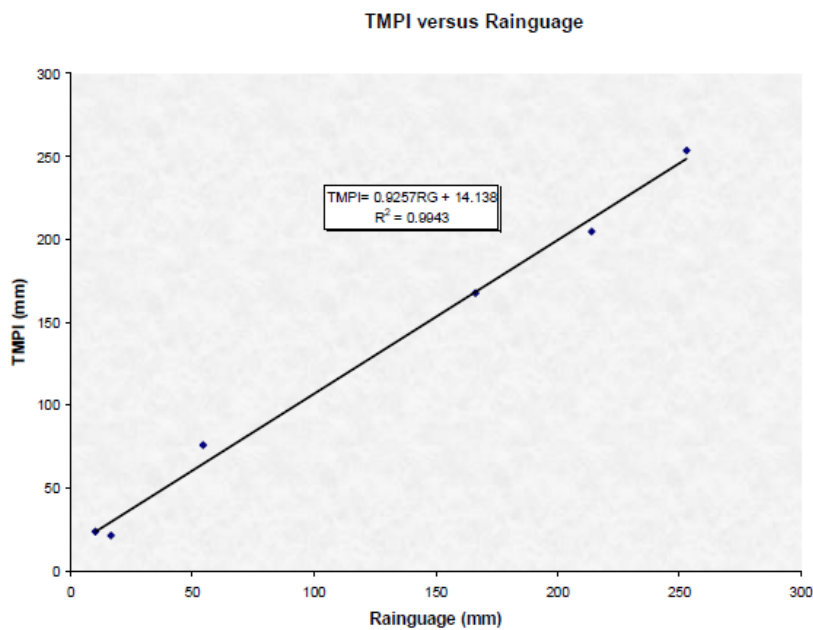


Fig. 3.4 Cumulative Scattergram of seasonal precipitation with TMPI.

4. CONCLUSIONS

From fig.1 above, from the mean seasonal plot for RG, 3A25, 3B43 and TMPI it can be seen that during the wet season i.e. May-October the TMPI algorithm is close to the RG measurements. Also it was deduced that during November – April the 3B43 is close to the RG measurements.

From Fig. 2a above, the percentage of Mean Bias Error MBE (%) is insignificant for TMPI during wet season i.e. May – October while it is significant in dry season (November - April). It was noticed that the bias is generally high for all the algorithms in dry seasons (November - April).

Also, as seen from the cumulative scattergram of seasonal precipitation versus rainguage measurements the graph of $y = ax+b$, ($y = 0.9257x + 14.138$ and $R^2 = 0.9943$).

Where $y = \text{TMPI}$

$a = 0.9257$

$x = \text{RG}$

$b = 14.138 = \text{intercept on } y\text{-axis}$

The study generally revealed that the TMPI algorithm is perfectly working for rainfall prediction over Nigeria especially during the wet season (May- October).

5. RECOMMENDATION

This study recommended that out of the three algorithms (**3A25**, **3B43** and **TMPI**) TMPI is the most suitable and can be used with less fear of failure over Nigeria especially in the wet season (May - October) while 3B43 algorithm can be used conveniently in the dry season (November - April) over Nigeria.

This study will go a long way helping in generating and estimating rainfall data for areas where rainfall are rarely available due to remoteness and jungle environments.

REFERENCES

Anagnostou E. N., W. F. Krajewski, and J. A. Smith, 1999: Uncertainty quantification of mean-areal radar-rainfall estimates. *J. Atmos. Oceanic Technol.*, **16**, 206-215.

Adeyewa, Z.D.; Nakamura, K. 2003 Validation of TRMM Radar Rainfall data Over Major Climatic Regions in Africa.

Arkin, P.A. and Ardanuy, P.E.: estimating Climatic-Scale Precipitation from Space: A Review.

Barrett, E.C. Doodge, M. Goodman, J Janowiak, E. Smith and C Kidd, 1994: The WetNet Precipitation Intercomparison Project (PIP-1). *Remote Sense. Rev.*, **11**, 49-60.

Bell T.L., A. Abdullah R.L. Martin, and G.R. North, 1990: Sampling errors for satellite derived tropical rainfall: Monte Carlo study using a space-time stochastic model. *J. Geophys Res.*, **95** 2195-2206.

Chiu L.S., D. Short, A. McConnel, and G. North, 1990: Rain estimation from satellites: Effect of finite field of view. *J. Geophys. Res.* **95**, 2177-2185.

Eldridge, R. H. 1957: A synoptic of West African disturbance lines.

Huffman G.J., Coauthors, 1997: The Global Precipitation Climatology Project (GPCP) combined precipitation dataset. *Bull. Amer. Meteor. Soc.*, **78**, 5-20.

Huffman G.J., M.M. Morrissey, S. Curtis, R. Joyce, B. McGavock, and J. Susskind, 2001: Global precipitation at one-degree daily resolution from multisatellite observations. *J. Hydrometeor.*, **2**, 36-50.

Kousky V.E., 1980: Diurnal rainfall variation in northeast Brazil. *Mon. Wea. Rev.* **108**, 488- 498.

Kummerow C., 1998: Beamfilling errors in passive microwave rainfall retrievals. *J. Appl. Meteor.*, **37**, 356-357.

Kummerow C., Coauthors, 2000: The status of the Tropical Rainfall Measuring Mission (TRMM) after two years in orbit. *J. Appl. Meteor.*, **39**, 1965-1982.

Obasi, G.O.P., 1975: Atmospheric, synoptic and climatological features of the West African Region. Nigerian Meteorological Services, Tech. Note No. 43pp

Rudolf B., T. Fuchs, W. Rueth, and U. Schneider, 1996: Comparison of rainguage analyses, satellite-based precipitation estimates and forecast model results. *Adv. Space Res.*, **18**(7), 53-62.

Xie P., and P. A.M. Arkin, 1995: An Intercomparison of gauge observations and satellite estimates of monthly precipitation. *J. Appl. Meteor.*, **34**, 1143-1160.

Xie P., and P. A.M. Arkin, 1996: Analyses of global monthly precipitation using gauge observations, satellite estimates, and numerical model predictions. *J. Climate*, **9**, 840-858.

GLOBAL FLOOD AND LANDSLIDE NOWCASTS AND FORECASTS USING MULTI-SATELLITE PRECIPITATION OBSERVATIONS

Robert Adler and H. Wu, Yang Hong, F. Policelli, Y. Tian, and H. Pierce

University of Maryland, USA

e-mail: radler@umd.edu

A global flood and landslide detection/prediction system is running in real-time using satellite multi-satellite rainfall analysis in combination with hydrological models and algorithms to estimate key flood parameters (<http://trmm.gsfc.nasa.gov>). The system also uses satellite-based land surface information such as digital elevation information from the NASA SRTM (Shuttle Radar Terrain Mission) and vegetation information from MODIS in the model and algorithm calculations. The flood and landslide determination algorithms consists of three major components: 1) multi-satellite precipitation estimation; 2) characterization of land surface including digital elevation information and other surface information, topography-derived hydrologic parameters such as flow direction, flow accumulation, basin, and river network etc.; 3) a hydrological model to infiltrate rainfall and route overland runoff and 4) a rainfall intensity/duration threshold scheme for landslides. Time-history of flood inundations are also calculated and displayed. Published validation results are summarized, indicating skill, but with general overforecasting of flood/landslide events.

Recent results with an improved global hydrological model running at 1/8th-degree resolution will be discussed that are shown to produce more realistic evolution of flooding events and more detailed information. Initial tests of using global numerical weather prediction rainfall forecasts to extend the period of utility of the flood information will also be presented.

GLOBAL OCEAN FRESHWATER FLUX COMPONENTS FROM SATELLITE, RE-ANALYSIS AND IN-SITU CLIMATOLOGIES

Axel Andersson¹, Christian Klepp², Stephan Bakan¹,
Karsten Fennig³, Jörg Schulz⁴

¹Max Planck Institute for Meteorology, Hamburg, Germany,

²University of Hamburg, Germany,

³Deutscher Wetterdienst, Offenbach, Germany

⁴Eumetsat, Darmstadt, Germany

e-mail: axel.andersson@zmaw.de

ABSTRACT

This paper presents a comparison of the evaporation, precipitation, and the resulting freshwater flux in HOAPS with recently available reference data sets from reanalysis and other satellite observation projects as well as in-situ ship measurements.

Results show, that the general climatological patterns are reproduced by all data sets. Global mean time series often agree within about 10% of the individual products, while locally larger deviations may be found for all parameters. HOAPS often agrees better with the other satellite derived data sets than with the in-situ or the reanalysis data. The agreement usually improves in regions of good in-situ sampling statistics. The biggest deviations of the evaporation parameter result from differences in the near surface humidity estimates. The precipitation data sets exhibit large differences in highly variable regimes with the largest absolute differences in the ITCZ and the largest relative biases in the extratropical storm track regions.

The resulting freshwater flux estimates exhibit distinct differences in terms of global averages as well as regional biases. Compared to long term mean global river runoff data, the ocean surface freshwater balance is not closed by any of the compared fields. The data sets exhibit a positive bias in E-P of 0.2 mm/d to 0.5 mm/d, which is in the order of 10% of the evaporation and precipitation estimates.

INTRODUCTION

The knowledge of the global water cycle is crucial for successful understanding and modeling of the climate system. An important component of the water cycle is the surface fresh water flux over global oceans and its components evaporation and precipitation. These quantities represent significant parts of the global energy transport in form of latent heat. Today, latent heat flux and precipitation over the global ocean surface can be determined from microwave satellite data as a basis for estimating the related fields of the ocean surface freshwater flux.

A prominent example of such a satellite data set is the HOAPS (“Hamburg Ocean Atmosphere Parameters and fluxes from Satellite data”) climatology. It is the only generally available satellite based data set with consistently derived fields of both evaporation and precipitation and hence of freshwater flux over the global ice-free ocean for the period 1987 to 2005. As these data fields are currently restricted to ocean only, since no long term global satellite based data sets for evapotranspiration over land exist, such water cycle quantities are mostly taken from reanalysis products. These ingest various available data sources, including satellite data, to create spatially consistent global fields by intelligent interpolation in accordance with the general meteorological development equations. An important question arises as to which extent these modern data sets reproduce the basic features of global ocean freshwater flux components realistically?

This paper presents a comparison of the evaporation, precipitation, and the resulting freshwater flux in HOAPS with recently available reference data sets from reanalysis and other satellite observation projects as well as in-situ ship measurements. Additionally, the humidity and wind speed input parameters for the evaporation are examined in order to identify sources for differences between the data sets.

INTER-COMPARISON OF GLOBAL MEAN TIME SERIES

2.1 Involved Data Sets

The following comparisons result from the endeavor to evaluate our most recent version 3 of the HOAPS (Hamburg Ocean Atmosphere Parameters and fluxes from Satellite data) climatology against other commonly available global climatologies. HOAPS-3 provides fields of turbulent heat fluxes, evaporation, precipitation, freshwater flux and related atmospheric variables over the global ice-free ocean for the time interval 1987-2005. All parameter values are derived from the passive microwave signal recorded by SSM/I (Special Sensor Microwave / Imager) radiometers on board the DMSP (Defense Meteorological Satellite Program) polar orbiting satellites with state of the art parameter retrieval procedures. Only the SST is taken from an external source, the AVHRR based Oceans Pathfinder V5 SST data set. Freely available monthly and pentad means, twice daily composites and scan-based data make HOAPS-3 a versatile data set for studying ocean-atmosphere interaction on different temporal and spatial scales (www.hoaps.org). More details can be found in the companion paper by Bakan et al. (2011) in this volume and in the publications by Andersson et al. (2010a) and Andersson et al. (2011).

No other commonly available purely satellite based data set provides both precipitation and evaporation estimates at the same time. For precipitation intercomparison we selected the TRMM product 3B43 (Huffman, 1997), CMAP enhanced (Xie and Arkin 1997), GPCP version 2 (Adler et al., 2003), and GsMap V484 (Kubota, 2007). The evaporation intercomparisons are based on the data sets J-Ofuro2 (Kubota, 2007), GSSTF2 (Chou, 2003), the blended fields of OAFUX V3 (Yu, 2007) and the IFREMER V3 product (Bentamy, 2003). For comparison with in situ observed near surface ship observations of evaporation we included version 2 of the NOCS data set (Berry and Kent 2009)

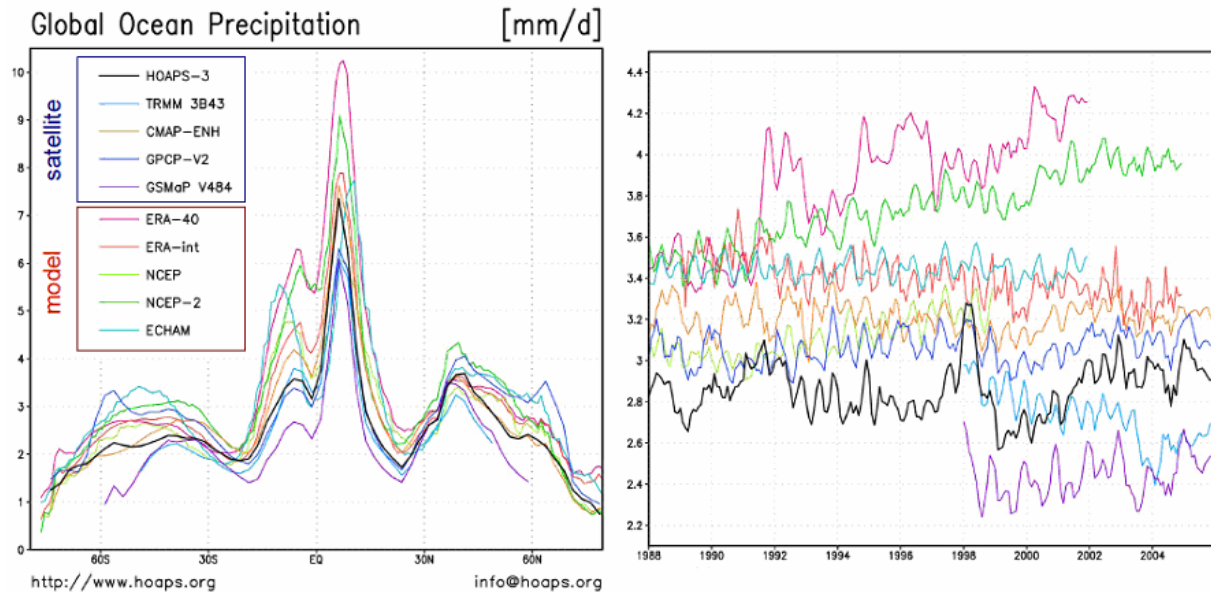


Figure 1. Comparison of zonal means (left) and monthly global means (right) of precipitation between several satellite and reanalysis products

Reanalysis data sets are widely used in the climate modeling community as benchmarks for the model results. Although these data sets are not independent of model assumptions, they are supposed to represent an optimal integration of all available data sources by skilful data assimilation. Therefore we included the NCEP reanalysis versions I and II (Kalnay et al. 1996; Kanamitsu et al., 2002) as well as ERA-40 (Uppala et al. 2005) and the recent ERA interim (ERA-Int; Simmons et al. 2007). In addition, we included an ensemble mean of 20th century climate model control runs from ECHAM-5 (Roeckner et al., 2003) in the comparisons.

2.2 Precipitation

Fig. 1 shows the zonal means and monthly global means of HOAPS over-ocean precipitation in comparison with several other satellite and reanalysis products. For zonal means, all products show the well known climatological large scale features as e.g. the ITCZ or the dry subtropical zones. Satellite products exhibit generally a similar behaviour with some exceptions in mid to high latitudes. Reanalysis products tend to provide comparatively high tropical precipitation and an intense southern ITCZ.

The temporal development of precipitation compares also fairly well among the satellite climatologies. While HOAPS average values are somewhat smaller but more variable than those of e.g. GPCP-V2 or CMAP, all of them exhibit insignificant temporal trends. GSMaP, which is based in parts on TRMM data, reveals considerably smaller average precipitation and the TRMM product itself sticks out by a considerable decrease with time which is likely to be caused by the introduction of the Advanced Microwave Sounding Unit-B (AMSU-B) data to the TRMM dataset in 2001–03 (GSFC 2007).

In comparison with reanalysis data we find, that both available NCEP reanalyses exhibit a substantial increase of precipitation over the global ocean after 1987. ERA-40 data

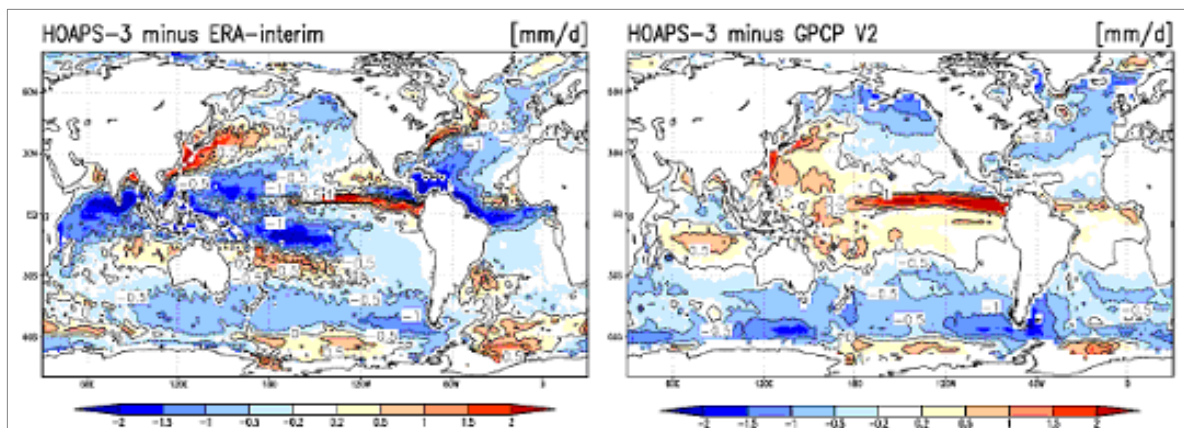


Figure 2. Difference of the 1992–2005 climate mean precipitation between HOAPS and ERA-Int (left) and GPCP V2 (right) (after Andersson et al., 2011)

show an even stronger increase, which has been known for some time to be erroneous. The recalculation in the ERA-Int project results in a slight temporal decrease of average precipitation rates over the global ocean.

ERA-Int precipitation is generally higher on global scale than all satellite-derived products as depicted in the difference plot of HOAPS and ERA-Int in Fig. 2. This bias originates mainly from the tropical belt, where ERA-Int exceeds HOAPS partly by more than 2 mm/d (up to 50%). The issue of excessive tropical precipitation is already known from the former ERA-40 reanalysis and has been considerably improved in ERA-Int.

Except for the large tropical biases, the deviations between HOAPS and ERA-Int are small and remain mostly below 1 mm/d. HOAPS precipitation is noticeably larger than ERA-Int over the Gulf Stream and the Kuroshio as well as over the ITCZ region of the central Pacific and the southeastern tip of the SPCZ.

The difference map between HOAPS and GPCP V2 precipitation shows in many regions good agreement. Regionally larger differences are found in regions of high variability over the western Pacific, the SPCZ, and the Indian Ocean. The maximum deviation of about 1.5 mm/d is found in the Pacific ITCZ. In the subtropical regions HOAPS precipitation is slightly larger than GPCP while the situation is different in the mid to high latitudes, where GPCP exhibits the highest values among the compared satellite based data sets.

Further validations for cold season snowfall over the ocean by co-locating ship based optical disdrometer and satellite data are presently ongoing. First measurement examples showed, in contrast to other satellite derived precipitation estimates, that the HOAPS retrieval was able to detect even light amounts of snowfall with an accuracy of 96% (Klepp et al., 2010).

2.3 Evaporation

The intercomparison for the zonally and globally averaged evaporation over ocean is displayed in Fig. 3. All data sets show fairly similar zonal mean evaporation. HOAPS exhibits a substantial increase during the study period, which results mainly from the

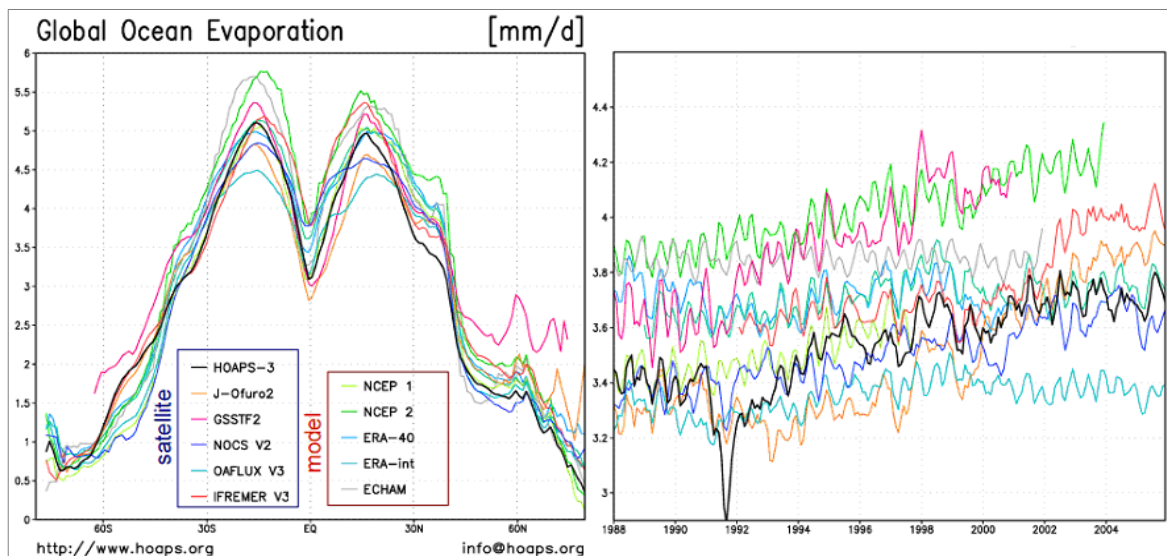


Figure 3. Comparison of zonal means (left) and monthly global means (right) of evaporation between several satellite and reanalysis products

increase in wind speed and in sea-air difference of specific humidity throughout the subtropics. Comparison with other satellite-derived evaporation products, among them e.g. the J-Ofuro V2 and the IFREMER V3 data sets, results in fairly similar average values, variability and trend behavior. Especially noticeable is the very similar temporal behavior of the NOCS V2 data set, which is estimated from a completely different data set, namely the ICOADS ship measurements. Only the recently published OAFLUX V3, which is a blending of satellite and reanalysis data, exhibits a substantially smaller increase with time.

Global evaporation in various reanalysis data sets shows strongly different temporal behavior. While globally averaged ocean evaporation from both NCEP reanalyses increases with time at approximately the same rate as in HOAPS, both ERA reanalyses exhibit insignificant long-term trends.

A conspicuous minimum in the HOAPS evaporation time series in 1991 is related to impaired accuracy of the SST data for several months after the eruption of Mt. Pinatubo.

The difference patterns between the data sets in Fig. 4, especially over the subtropics, exhibit higher difference values in regions of large evaporation and smaller values in regions with low evaporation. Furthermore, the differences appear to be determined to a large extent by the humidity fields, which is most distinct in the comparison of HOAPS with NOCS and ERA-Int (not shown here). Deviations are regionally largest in the comparison with NOCS, reaching more than 1.5 mm/d or 20% of the average value. In comparison with the satellite product IFREMER the relative differences are generally below 5%–10% (not shown here).

In a broad band from the Kuroshio over the North Pacific to the North American east coast ERA-Int and NOCS evaporation is systematically higher relative to HOAPS. This pattern continues southward along the Baja California. Over the cold tongue in the eastern equatorial Pacific and the Southeast Asian warm pool, HOAPS evaporation is

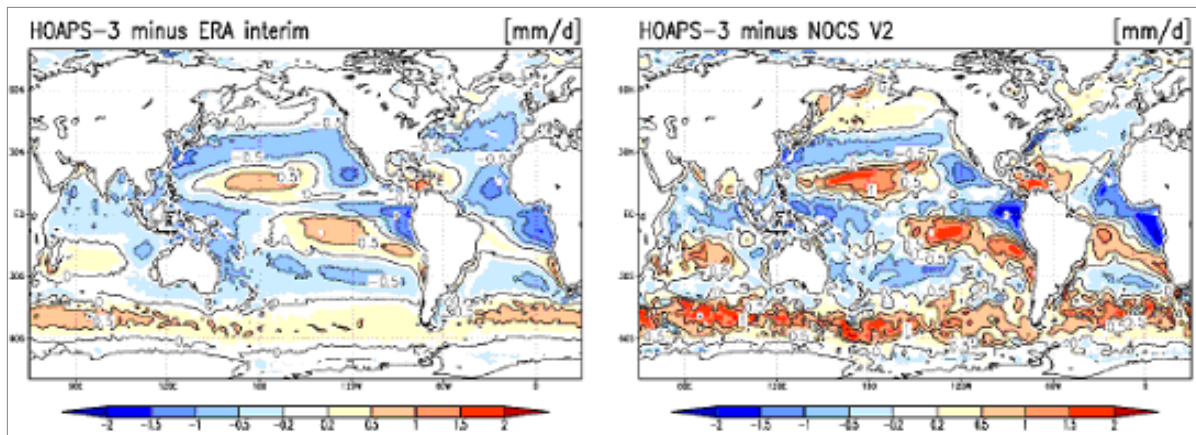


Figure 4. Difference of the 1992–2005 climate mean evaporation of HOAPS-3 and ERA-Int (left) and NOCS v2.0 (right) (after Andersson et al., 2011)

systematically lower relative to all other data sets. Because of the fairly small absolute values of evaporation, the relative error reaches more than 30% in these regions.

A low bias of HOAPS vs. NOCS is evident in the eastern tropical Atlantic with differences of more than 1 mm/d (up to 50%). This is most likely due to a combination of an overestimation of air humidity along the West African coast and an underestimation of sea surface temperature in the tropical and subtropical Atlantic.

Over the North Atlantic and North Pacific, the comparison between the data sets shows mixed results with fairly small differences. Over the storm tracks of the southern mid–high latitudes, NOCS and HOAPS exhibit the largest differences. This may mostly be attributed to the unsatisfactory coverage with ship data in this region. Relative to ERA-Int. The HOAPS evaporation is up to 0.75 mm/d (>30%) higher for the southern midlatitude storm tracks which results mostly from large differences between surface and atmospheric humidity.

2.4 Freshwater Flux

The difference between precipitation and evaporation yields the oceanic freshwater flux into the atmosphere. Over the global oceans, the dominant features of either precipitation or evaporation fields determine the resulting global distribution of the freshwater flux. The total precipitation is smaller than the total evaporation and the difference should be balanced mainly by continental runoff.

Only a very few of the considered data sets provide also fields of the ocean freshwater flux and its time development. While this is readily available from reanalyses and model data, among the satellite based data sets to day only HOAPS provides this ocean surface water balance quantity. Fig. 5 shows the globally averaged monthly mean values of freshwater flux (evaporation – precipitation) between 1988 and 2005 together with the seasonal range of continental runoff from NCEP. The data reflect generally the expected average preponderance of evaporation over precipitation over the global oceans. Only the ERA-40 data exhibit substantially negative freshwater fluxes due to the mentioned problems with the precipitation component. For a few months after the

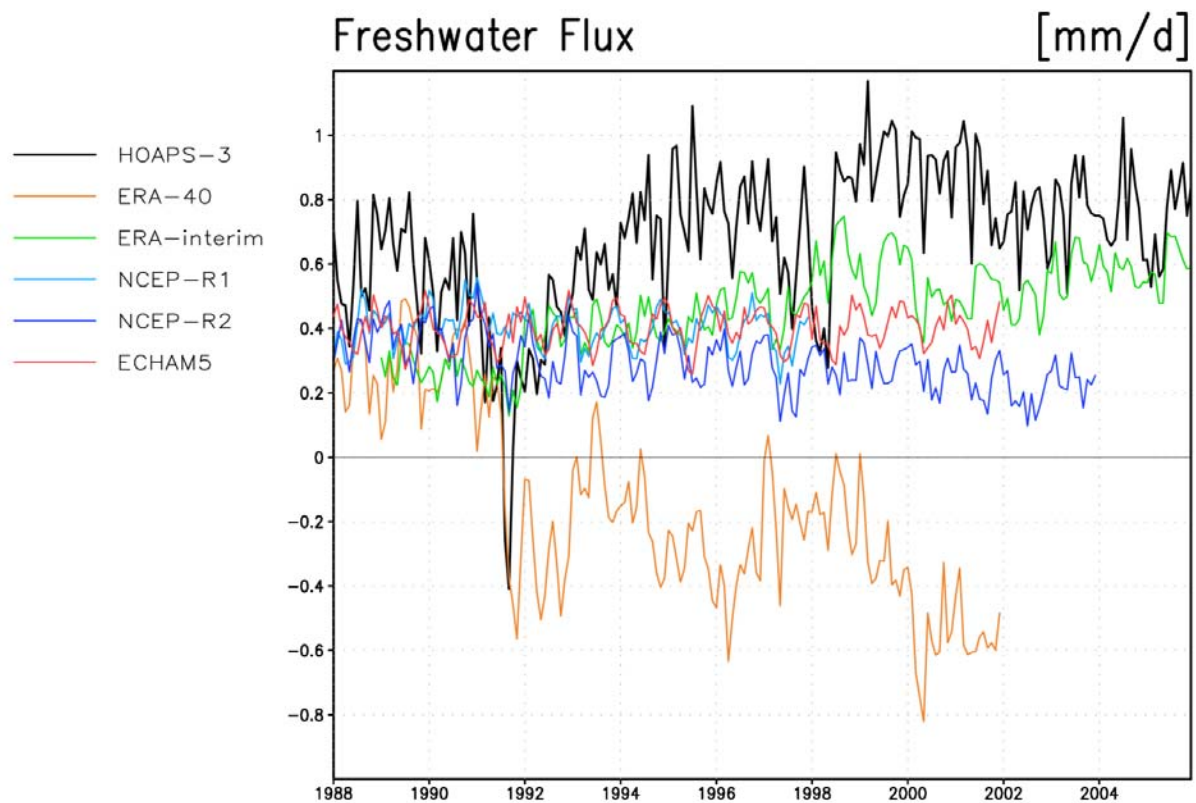


Figure 5. Comparison of monthly global means (right) of evaporation between HOAPS-3, several reanalysis products and the ECHAM-5 IPCC 20th century climate model run (mean of 3 ensemble members).

Pinatubo eruption in late 1991 also the HOAPS freshwater flux turns negative, which is mostly due to insufficiently corrected Pathfinder SST data during that time. Otherwise, all reanalysis products exhibit freshwater values in the early part of the comparison period that fit reasonably to the continental runoff distributed with the NCEP reanalysis data, but differ with time more and more. While the freshwater flux from both NCEP data sets remains fairly constant with time, ERA-Int increases at the same rate as HOAPS does. Both products seem to be substantially off the nominal continental runoff towards the end of the intercomparison period.

For completeness, Fig. 4 contains also the time development of the freshwater flux in the ECHAM-5 IPCC climate model run (mean of 3 ensemble members) for the 20th century (1988-2001). In this case none of the three quantities, average precipitation, evaporation and resulting freshwater flux over the global ocean, exhibits any obvious and significant trend during the 13 available model years.

Fig. 6 shows the climatological comparison of the HOAPS-3 freshwater flux with ERA-interim and a combination of GPCP and the IFREMER flux product. In the inner tropics the atmospheric freshwater deficit of ERA-Int exceeds HOAPS by up to 2 mm/d, while the deficit in HOAPS is larger in the eastern Pacific ITCZ and around 30° north and south. In the eastern Pacific as well as in the Atlantic the difference in the freshwater flux is mostly determined by the evaporation fields.

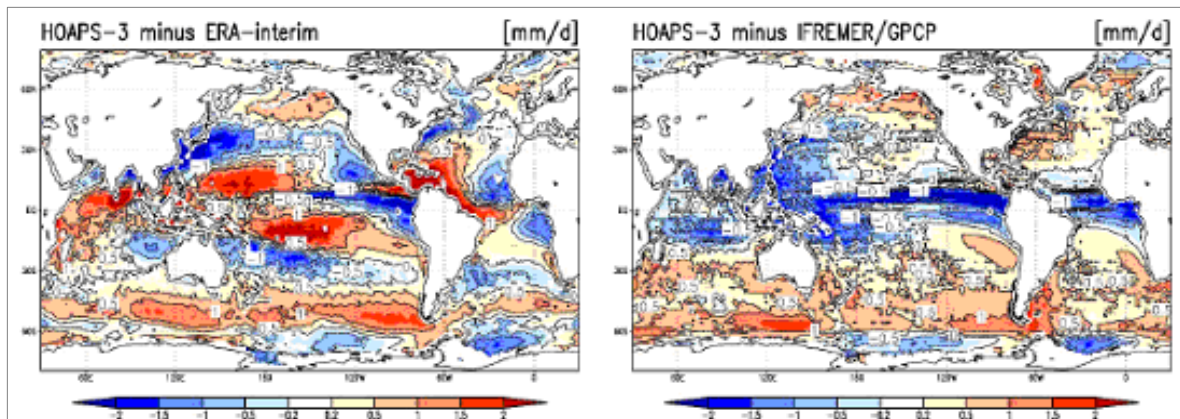


Figure 6. Difference of the 1992–2005 climate mean freshwater flux of HOAPS-3 and ERA-Int (left) and IFREMER/GPCP freshwater flux (right) (after Andersson et al., 2011)

The differences between HOAPS and the combination of the IFREMER evaporation and GPCP precipitation are less pronounced in the subtropical regions, except for the warm pool and the ITCZ. In the tropical warm pool region the deviations are dominated by the evaporation pattern, while differences in the ITCZ region are mainly due to the deviations of precipitation. At mid and high latitudes the positive bias in the GPCP precipitation leads to an enhanced freshwater flux into the ocean of IFREMER/GPCP compared to HOAPS.

Run-off balance:

The mean globally averaged HOAPS net ocean surface freshwater flux into the atmosphere for the 1992 to 2005 period is 0.73~mm/d (IFREMER/GPCP: 0.77~mm/d, ERA-Int: 0.50~mm/d). Furthermore, the time series of both satellite based data sets exhibit a larger variability with a standard deviation of 0.19~mm/d compared to 0.10~mm/d for ERA-interim reanalysis data.

However the estimated river runoff long term mean is about 40.000km³/a (0.32 mm/d), which is not matched by any of the compared data sets.

Particularly for the satellite based estimates the balance not closed, but the difference to the runoff data lies within 10-15% of the global mean values of the individual evaporation and precipitation retrievals.

Finally, the increase in freshwater flux from over the comparison period is larger than the expected increase in atmospheric storage by the C-C equation (7% per °C warming).

CONCLUSIONS

In this paper we compared recent data sets of global ocean precipitation and evaporation on the climatological scale.

These comparisons show, that the general climatological patterns are reproduced by all data sets. Global mean time series often agree within about 10% of the individual

products, while locally larger deviations may be found for all parameters. HOAPS often agrees better with the other satellite derived data sets than with the in-situ or the reanalysis data. The agreement usually improves in regions of good in-situ sampling statistics. The biggest deviations of the evaporation parameter result from differences in the near surface humidity estimates. The precipitation data sets exhibit large differences in highly variable regimes with the largest absolute differences in the ITCZ and the largest relative biases in the extratropical storm track regions.

The resulting freshwater flux estimates exhibit distinct differences in terms of global averages as well as regional biases. Compared to long term mean global river runoff data, the ocean surface freshwater balance is not closed by any of the compared fields. The data sets exhibit a positive bias in E-P of 0.2 mm/d to 0.5 mm/d, which is in the order of 10% of the evaporation and precipitation estimates.

HOAPS-3 is a well developed satellite climatology of water cycle components over the ice free global ocean, showing all the known global climatological features and regional details. Due to multi-satellite averages, use of all SSM/I operating at the same time, and careful inter-sensor calibration it provides consistent and homogeneous time series for the period 1987 through 2005. It provides a scan-based data set on pixel-level (HOAPS-S), from which pentad and monthly mean and daily composite gridded data sets (HOAPS-G, HOAPS-C) at 0.5° resolution are derived.

These make HOAPS-3 a versatile data set for studying ocean-atmosphere interaction on different temporal and spatial scales. HOAPS data are freely available from **www.hoaps.org** via the CERA database-system provided by the World Data Center for Climate, Hamburg (www.wdc-climate.de).

The HOAPS-3 data has been successfully used to study the variability of freshwater flux parameters and their dependence on the NAO (Andersson, 2010a). By the combination of HOAPS-3 over ocean satellite data and GPCP rain gauge based fields over the continents a nearly global precipitation data set is established. This combined data set from two independent data sources shows a coherent response to the NAO and allows a detailed view on the precipitation fields in relation to the atmospheric circulation. A strong connection of the precipitation and evaporation was found in this study.

In near future, some of the core HOAPS products will be routinely provided by the Eumetsat Climate Monitoring Satellite Application Facility (CM-SAF, www.cmsaf.eu) at the German Weather Service (DWD)

REFERENCES

- Adler, R.F. and Coauthors, 2003: The Version-2 Global Precipitation Climatology Project (GPCP) monthly precipitation analysis (1979–present). *J. Hydrometeor.*, 4, 1147–1167.
- Andersson, A., S. Bakan, H. Graßl, 2010: Satellite derived North Atlantic precipitation variability and its dependence on the NAO index, *Tellus A*, 62(4), 453-468, doi:10.1111/j.1600-0870.2010.00458.x.

Andersson, A., C. Klepp, K. Fennig, S. Bakan, H. Graßl, and J. Schulz, 2010a: The Hamburg Ocean Atmosphere Parameters and Fluxes from Satellite Data – HOAPS-3. *Earth Syst. Sci. Data*, 2, 215-234, doi:10.5194/essd-2-215-2010

Andersson, A., C. Klepp, K. Fennig, S. Bakan, H. Graßl, and J. Schulz, 2011: Evaluation of HOAPS-3 ocean surface freshwater flux components. *J. Appl. Meteor. Climatol.*, doi: 10.1175/2010JAMC2341.1, in print

Andersson, A., S. Bakan, H. Graßl, 2010b: Satellite derived North Atlantic precipitation and freshwater flux variability with special emphasis on the North Atlantic Oscillation. *Tellus A*, 62, 453-468.

Bakan, S., A. Andersson, K. Fennig, H. Graßl, C. Klepp, and J. Schulz, 2011: The HOAPS-3 climatology. *Proceedings of the 5th International Precipitation Working Group*, this volume, 58-66.

Bentamy, A., K. B. Katsaros, A. M. Mestas-Nunez, W. M. Drennan, E. B. Forde, and H. Roquet, 2003: Satellite estimates of wind speed and latent heat flux over the global oceans. *J. Climate*, 16, 637–656.

Berry, D. I., and E. C. Kent, 2009: A new air–sea interaction gridded dataset from ICOADS with uncertainty estimates. *Bull. Amer. Meteor. Soc.*, 90, 645–656.

Chou, S. H., E. Nelkin, J. Ardizzone, R. M. Atlas, and C. L. Shie, 2003: Surface turbulent heat and momentum fluxes over global oceans based on the Goddard satellite retrievals, version 2 (GSSTF2). *J. Climate*, 16, 3256–3273.

GSFC, cited 2011: Algorithm 3B43—TRMM and other data precipitation. Goddard Space Flight Center. [Available online at <http://trmm.gsfc.nasa.gov/3b43.html>.]

Huffman, G.J., 1997: "Estimates of Root-Mean-Square Random Error for Finite Samples of Estimated Precipitation," *J. Appl. Meteor.*, 1191-1201.

Huffman, G.J., R.F. Adler, B. Rudolph, U. Schneider, P. Keehn, 1995: "Global Precipitation Estimates Based on a Technique for Combining Satellite-Based Estimates, Rain Gauge Analysis, and NWP Model Precipitation Information", *J. Clim.*, 8, 1284-1295.

Kalnay, E., and Coauthors, 1996: The NCEP/NCAR 40-Year Reanalysis Project. *Bull. Amer. Meteor. Soc.*, 77, 437–471.

Kanamitsu, M., W. Ebisuzaki, J. Woollen, S.-K. Yang, J. J. Hnilo, M. Fiorino, and G. L. Potter, 2002: NCEP–DOE AMIP-II Reanalysis (R-2). *Bull. Amer. Meteor. Soc.*, 83, 1631–1643.

Klepp, C., K. Bumke, S. Bakan, P. Bauer, 2010: Ground Validation of Oceanic Snowfall in Satellite Climatologies during LOFZY. *Tellus A*, 62, 469-480.

Kubota, M., and H. Tomita, 2007: Introduction of J-OFURO latent heat flux version 2. *Proc. Joint 2007 EUMETSAT Meteorological Satellite Conf. and 15th Satellite Meteorology and Oceanography Conf.*, Amsterdam, Netherlands, EUMETSAT and Amer. Meteor. Soc., 5 pp. [Available online at http://www.eumetsat.int/home/Main/AboutEUMETSAT/Publications/ConferenceandWorkshopProceedings/2007/groups/cps/documents/document/pdf_conf_p50_s5_11_kubota_v.pdf.]

Kubota, T., and Coauthors, 2007: Global precipitation map using satellite-borne microwave radiometers by the GSMaP project: Production and validation. *IEEE Trans. Geosci. Remote Sens.*, 45, 2259–2275.

E. Roeckner, G. Bäuml, L. Bonaventura, R. Brokopf, M. Esch, M. Giorgetta, S. Hagemann, I. Kirchner, L. Kornblüeh, E. Manzini, A. Rhodin, U. Schlese, U. Schulzweida, A. Tompkins (2003): The atmospheric general circulation model ECHAM 5. PART I: Model description, MPI Report No. 349, Max-Planck-Institut für Meteorologie, Hamburg, Germany. [Available online at http://www.mpimet.mpg.de/fileadmin/publikationen/Reports/max_scirep_349.pdf]

Simmons, A., S. Uppala, D. Dee, and S. Kobayashi, 2007: ERA–Interim: New ECMWF reanalysis products from 1989 onwards. *ECMWF Newsletter*, No. 110, ECMWF, Reading, United Kingdom, 25–35.

Uppala, S. M., and Coauthors, 2005: The ERA-40 Re-Analysis. *Quart. J. Roy. Meteor. Soc.*, 131, 2961–3012.

Xie, P., and P. Arkin, 1997: Global precipitation: A 17-year monthly analysis based on gauge observations, satellite estimates, and numerical model outputs. *Bull. Amer. Meteor. Soc.*, 78, 2539–2558.

Yu, L.S., X. Jin, and R. A. Weller, 2008: Multidecade global flux datasets from the objectively analyzed air–sea fluxes (OAFlux) project: Latent and sensible heat fluxes, ocean evaporation, and related surface meteorological variables. Tech. Rep. OA-2008-01, Woods Hole Oceanographic Institution, OAFlux Project, 64 pp.

NEW GSMaP OVER-LAND PRECIPITATION RETRIEVAL ALGORITHM

Kazumasa Aonashi

Meteorological Research Institute
1-1 Nagamine, Tsukuba, 305-0052, JAPAN

e-mail: aonashi@mri-jma.go.jp

The GSMaP over-land algorithm estimates surface precipitation rates from depressions of brightness temperature (TB) at 37 GHz (TB37) and 85 GHz (TB85). One main problem of the conventional algorithm is that it does not consider variations in vertical precipitation profiles for different precipitation events with various precipitation top heights. The present study developed the new over-land algorithm that introduced the index of the precipitation top heights, and calibrated the conventional retrievals from TB depressions using the index.

As the index of the precipitation top heights, we introduced the ratio of TB85 depressions to TB 37 depressions (R8537). (We expressed R8537 in terms of ratio of precipitation retrieved from TB85 depression (rain85) to those from TB37 (rain37) using the conventional GSMaP algorithm.) This is based on the forward-calculation and observation results that TB85 was much sensitive to the frozen precipitation than TB37, and that the TB85 depression became larger than the TB37 depression for precipitation with higher top levels. In order to calibrate the conventional precipitation retrievals, first, we classified the TRMM data sets for 1998 by R8537 and the precipitation types. Then, we derived linear fitting coefficients between the conventional rain37 and PR surface precipitation rates. The new over-land algorithm used these fitting coefficients to calibrate rain37.

We validated the performance of the new over-land algorithm using TRMM data sets for 2004. The results show that the calibration using R8537 alleviated underestimation of the precipitation retrievals, in particular, for shallow precipitation.

VERIFICATION OF NOAA CPC RFE AT VARIOUS TEMPORAL AND SPATIAL RESOLUTIONS IN THE HINDU KUSH - HIMALAYAN REGION

Sagar R. Bajracharya, Mandira S. Shrestha, Pradeep K. Mool

International Centre for Integrated Mountain Development (ICIMOD), P.O.
Box 3226, Khumaltar, Kathmandu, Nepal

e-mail: sagbajracharya@icimod.org

The Hindu Kush - Himalaya (HKH) region includes the inner and south Asian mountains and high plateau and extends 3500 km west to east from Afghanistan to Myanmar. It contains the most extensive and rugged high altitude areas on Earth. The spatial distribution of the rain gauge in the HKH region is very sparse and not adequate to provide a detailed perspective for applied water resource modeling and also not sufficient to capture the highly varied nature of rainfall. The main aim of this work was to validate the Climatic Prediction Centre satellite – based rainfall estimate product version 2 (CPC_RFE2) developed by CPC of National Oceanic and Atmospheric Administration (NOAA) against the observed rain gauge in the HKH region as to determine their operational viability within the region. The validation was done on the basis of grid to grid analysis on a regional level with various temporal (24 hours, monthly, seasonal) and spatial resolutions (0.1°, 0.25°, 0.5° and 1°) by using visual, continuous and categorical rainfall verification statistical techniques. The results show that CPC RFE underestimates the rainfall in pre-monsoon, monsoon and post monsoon and overestimates the rainfall in dry season (winter). No significant decrease of the standard error was detected when the spatial resolution was increased from 0.1° to 1°. Results indicate that the CPC_RFE2.0 needs to be improved or modified before implementing in an operational application in the HKH region.

THE HOAPS-3 CLIMATOLOGY

Stephan Bakan¹, Axel Andersson¹, Karsten Fennig³, Hartmut Graßl², Christian Klepp² and Jörg Schulz⁴

¹Max Planck Institute for Meteorology, Hamburg, Germany,

²University of Hamburg, Germany,

³Deutscher Wetterdienst, Offenbach, Germany

⁴Eumetsat, Darmstadt, Germany

e-mail: stephan.bakan@zmaw.de

ABSTRACT

HOAPS-3, the latest version of the satellite climatology “Hamburg Ocean Atmosphere Parameters and fluxes from Satellite data” provides fields of turbulent heat fluxes, evaporation, precipitation, freshwater flux and related atmospheric variables over the global ice-free ocean. A sophisticated processing chain and careful inter-sensor calibration, ensures a homogeneous time-series with dense data sampling and hence detailed information of the underlying weather situations. The completely reprocessed data set with a continuous time series from 1987 to 2005 contains neural network based algorithms for precipitation and wind speed and Advanced Very High Resolution Radiometer (AVHRR) based SST fields. Freely available monthly and pentad means, twice daily composites and scan-based data make HOAPS-3 a versatile data set for studying ocean-atmosphere interaction on different temporal and spatial scales.

1. INTRODUCTION

The availability of microwave instruments on satellite platforms allows the retrieval of essential water cycle components at high quality for improved understanding and evaluation of water processes in climate modeling.

HOAPS-3, the latest version of the satellite climatology “Hamburg Ocean Atmosphere Parameters and fluxes from Satellite data”, is a climatology of freshwater flux over the global ocean derived from satellite data. It provides fields of turbulent heat fluxes, evaporation, precipitation, freshwater flux and related atmospheric variables over the global ice-free ocean.

A detailed description is given in Andersson et al. (2010a). An in depth evaluation of several parameters can be found in Andersson et al. (2010b), Klepp et al. (2010) and

Winterfeldt et al. (2010). Applications of the data set have been published, among others, by Andersson et al. (2010c), Blechschmidt et al. (2009), Romanou et al. (2010), and Romanova et al. (2010). The following is a short overview of the essential information on this exciting data set.

2. THE HOAPS CLIMATOLOGY

2.1 GENERAL

The HOAPS-3 data set contains fields of precipitation, evaporation and related surface and atmospheric parameters over the global ice free ocean for the time interval from 1987 through 2005. The parameter values are derived from the passive microwave signal recorded by SSM/I radiometers on board the DMSP (Defense Meteorological Satellite Program) polar orbiting satellites with state of the art parameter retrieval procedures. Only the SST is taken from an external source, the AVHRR based Oceans Pathfinder V5 SST data set (Casey, 2004). Table 1 provides an overview of parameters and algorithms in HOAPS-3.

Freely available monthly and pentad means, twice daily composites and scan-based data make HOAPS-3 a versatile data set for studying ocean-atmosphere interaction on different temporal and spatial scales.

Overview of HOAPS-3 parameters and algorithms.		
parameter	source	HOAPS-code
wind speed at 10m height	neural net algorithm	WIND
AVHRR Oceans Pathfinder SST	Casey (2004)	ASST
sea surf. satur. spec. humidity	Magnus formula	HSEA
near surf. spec. humidity	Bentamy et al. (2003)	HAIR
humidity difference	HSEA minus HAIR	DHUM
evaporation, latent heat flux	Fairall et al. (1996, 2003)	EVAP, LATE
latent heat transfer coefficient	Fairall et al. (1996, 2003)	TRCE
sensible heat flux at sea surface	Fairall et al. (1996, 2003)	HEAT
longwave net flux at sea surface	Schlüssel (1995)	FNET
vertically integrated liquid water	Bauer (1992)	LWPA
vertically integrated total water	Bauer and Schlüssel (1993)	TWPA
vertically integrated water vapor	Schlüssel and Emery (1990)	WVPA
precipitation	neural net algorithm	RAIN
freshwater flux	EVAP minus RAIN	BUDG

Table 1. Overview of HOAPS-3 parameters and algorithms (from Andersson et al., 2010a)

2.2 DATA PROCESSING

A sophisticated processing chain, including all available Special Sensor Microwave Imager (SSM/I) instruments aboard the satellites of the Defense Meteorological Satellites Program (DMSP) and careful inter-sensor calibration, has been implemented to ensure a homogeneous time-series with dense data sampling (Fig. 1).

Additionally, a new 85 GHz synthesis procedure for the defective SSM/I channels on DMSP F08 from 1989 on has been implemented.

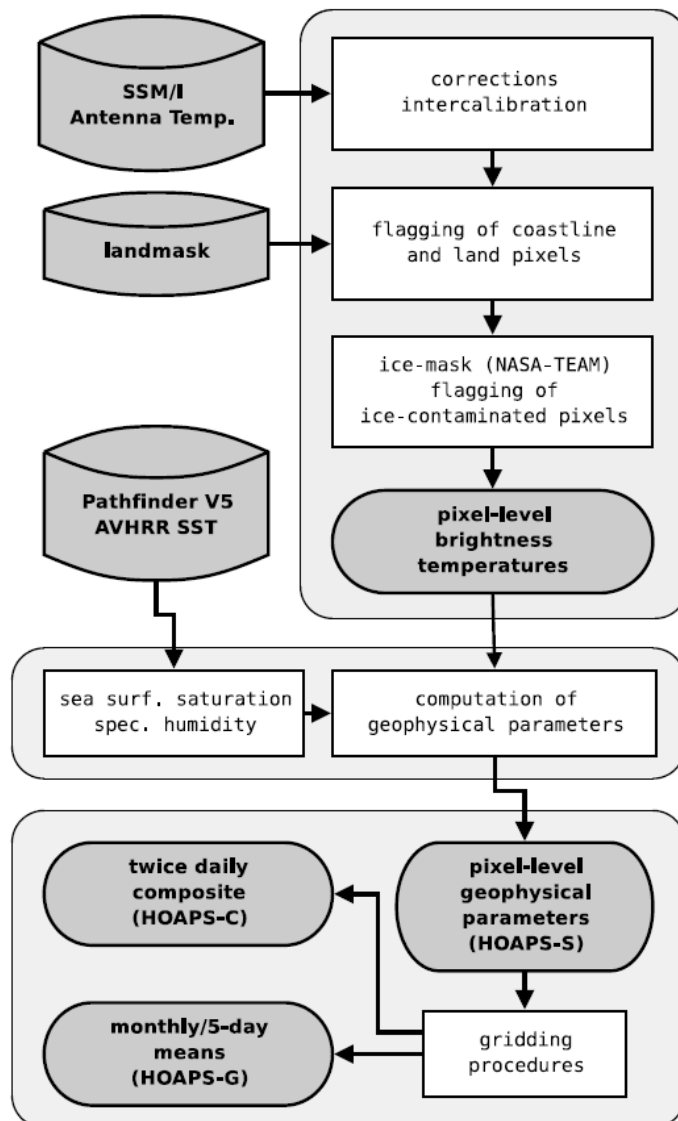


Figure 1. HOAPS-3 data processing scheme (from Andersson et al., 2010a)

The SSM/I inter-sensor calibration employs a statistical approach on a sophisticated selection of observed brightness temperatures. The data of DMSP F-11 have been selected as the calibration reference. For the inter-instrument comparisons, 10-day means of brightness temperatures of rain-free pixels have been averaged on a global $1^\circ \times 1^\circ$ grid. For each of the available 7 spectral channels match-ups have been collected between each available satellite and F-11 during one overlapping year. A histogram-equalization took care of the different observation densities for the various match-up pairs. Finally, a linear regression for TB calibration coefficients of each channel and satellite resulted. An example for the quality of the calibrated brightness temperature record for the vertically polarized 19 GHz channel is given in Fig. 2.

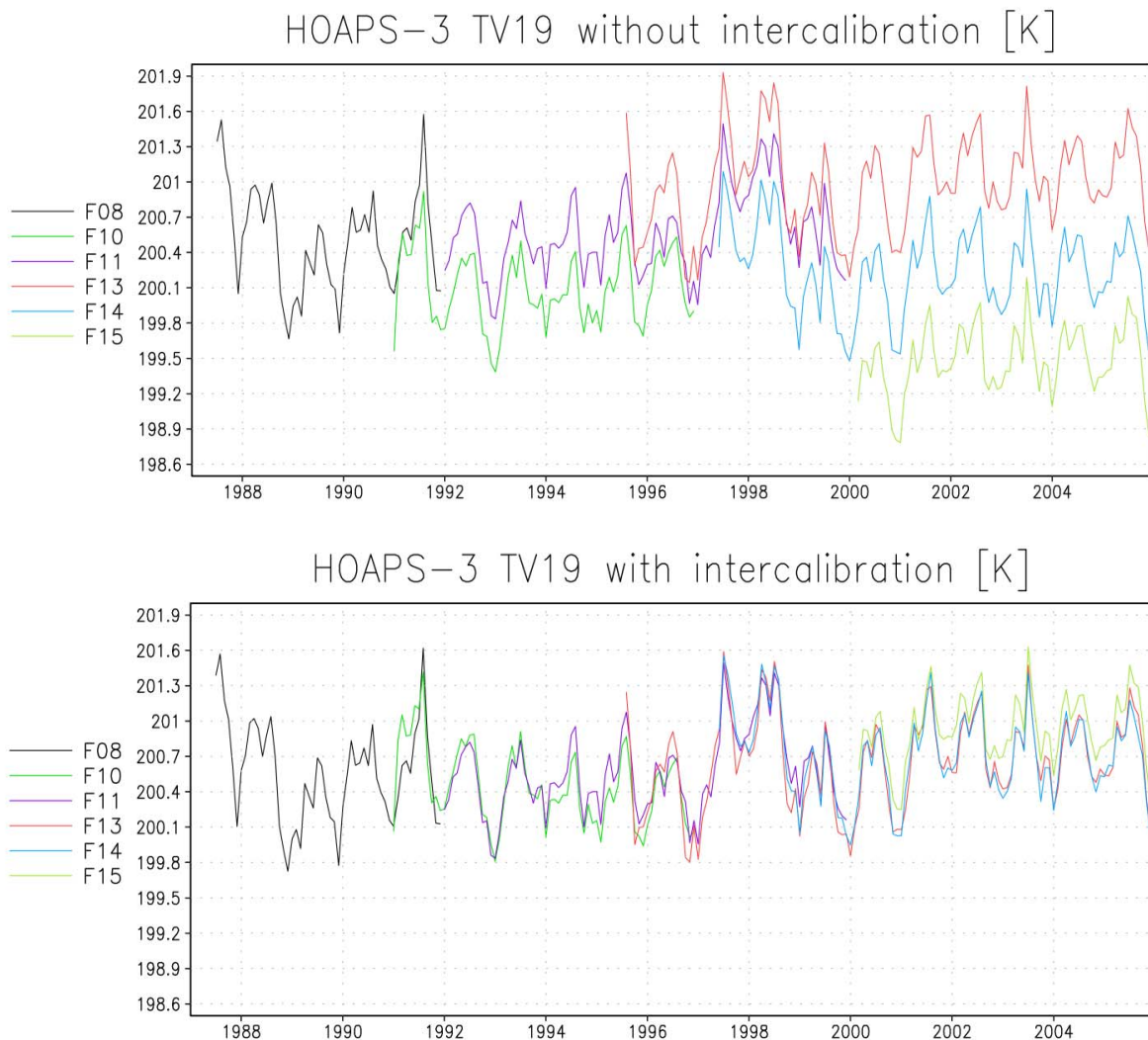


Figure 2. Result of SSM/I intercalibration for the vertically polarized 19 GHz channel (from Andersson et al., 2010a)

2.3 WATER FLUX PARAMETERS

Of the 15 parameters in HOAPS-3, most are related to the ocean-atmosphere water exchange. Among them are neural network based algorithms for precipitation and wind speed and Advanced Very High Resolution Radiometer (AVHRR) based SST fields. They allow in combination to calculate the ocean surface freshwater flux as the balance between evaporation and precipitation. Their calculation is explained in some more detail in the following (see also Andersson et al., 2010a).

Evaporation (E):

Evaporation is calculated according to the bulk formula suggested by Fairall et al. (1996, 2003):

$$E = (\rho_a/\rho_w) C_E U (q_s - q_a)$$

Here the wind speed (U) is calculated by a neural net procedure as explained in Andersson et al. (2010). The near surface specific humidity (q_a) is determined according to the formulation of Bentamy et al. (2003). The sea surface saturation specific humidity (q_s) is calculated with the help of the Magnus formula from SST-values. The latter are taken from the AVHRR Oceans Pathfinder V.5 SST data set (Casey, 2004). Finally, the latent heat transfer coefficient C_E is calculated with the COARE algorithm of Fairall et al., (1996, 2003).

Precipitation (P):

To determine the precipitation rate at the ocean surface more accurately than in the previous HOAPS version, a new neural net algorithm has been implemented recently. It was derived with the help of training data from radiative transfer calculations after Bauer et al. (2006a, b), provided kindly by the ECMWF.

Fig.13a shows the comparison of the neural network algorithm, the retrieval of Bauer and Schlüssel (1993) that has been used in HOAPS II, and the scattering algorithm of Ferraro (1997) with the verification data set of the neural network. While the Bauer algorithm exhibits a systematic underestimation of precipitation, the neural network performs significantly better. For rain rates exceeding 7 mm/h the neural network algorithm also exhibits an underestimation compared to the reference data set. The few cases with rain rates exceeding 12 mm/h in the reference data set are reproduced by the neural network and the Ferraro scattering algorithm with comparable values around 10 mm/h. The latter performs, however, not well for smaller rain rates, which should be due to the missing emission signal in the algorithm.

Fig.13 b shows accumulated histograms of the rain rates derived with the three different precipitation algorithms on a logarithmic scale. The histogram bins represent the accumulated fraction of the total reference precipitation from the verification data-set in

the range from 0.2 mm/h up to 30 mm/h. About 90% of the total ECMWF precipitation comes from rain rates up to 1 mm/h. The new neural network algorithm provides satisfactory coincidence with the nominal rain rates across all rain rates. The remaining deviations lead to a small underestimation of the total precipitation. Applying a lower threshold at 0.3 mm/h, as is necessary for the real HOAPS algorithm, results in a total bias of -0.166 mm/h.

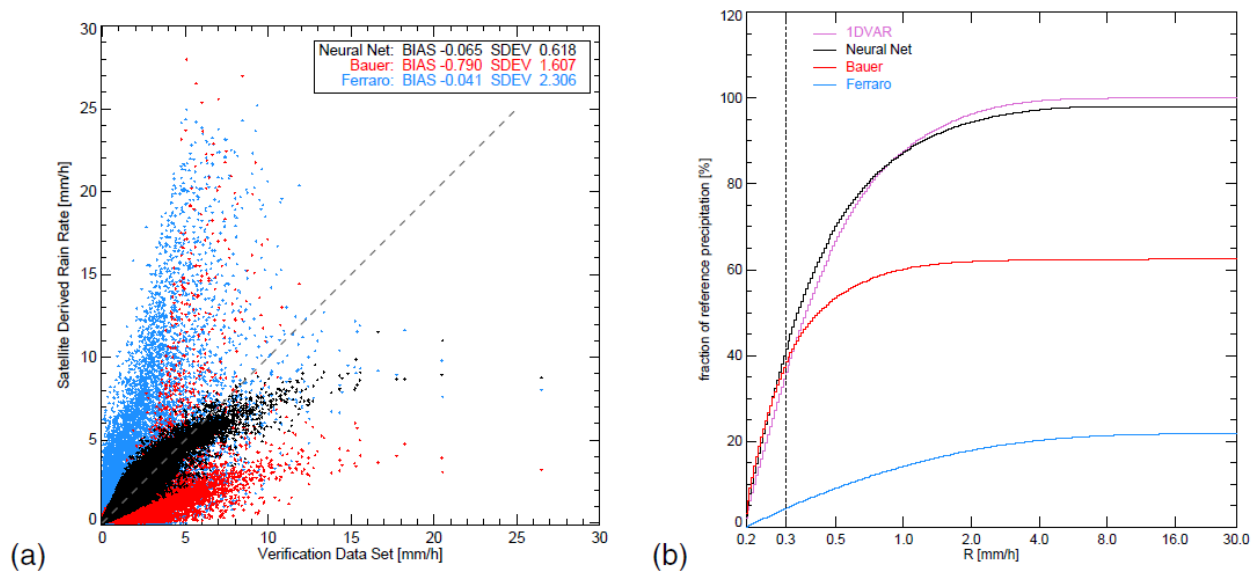


Figure 3. Evaluation of HOAPS precipitation algorithm. Panel a (left) shows retrieved precipitation rates of the HOAPS (black), the Bauer and Schlüssel (1993) and the Ferraro (1997) algorithm vs. the verification data set. Panel b (right) contains the accumulated precipitation for the different retrievals (from Andersson et al., 2010a)

Further validations for cold season snowfall over the ocean by co-locating ship based optical disdrometer and satellite data are presently ongoing. First measurement examples showed, in contrast to other satellite derived precipitation estimates, that the HOAPS retrieval was able to detect even light amounts of snowfall with an accuracy of 96% (Klepp et al., 2010).

2.4 APPLICATION EXAMPLE

The climatological fields and seasonal variation of evaporation, precipitation, and freshwater flux from the HOAPS-G monthly mean data set for the years 1988 to 2005 are shown in Fig. 4. Dominant features of either precipitation or evaporation fields determine the resulting global distribution of freshwater flux. A net flux into the ocean is mainly found in regions of precipitation maxima in the Intertropical Convergence Zone (ITCZ), the South Pacific Convergence Zone (SPCZ), the midlatitude storm tracks and at high latitudes. In contrast, subtropical regions generate the major part of the freshwater flux into the atmosphere.

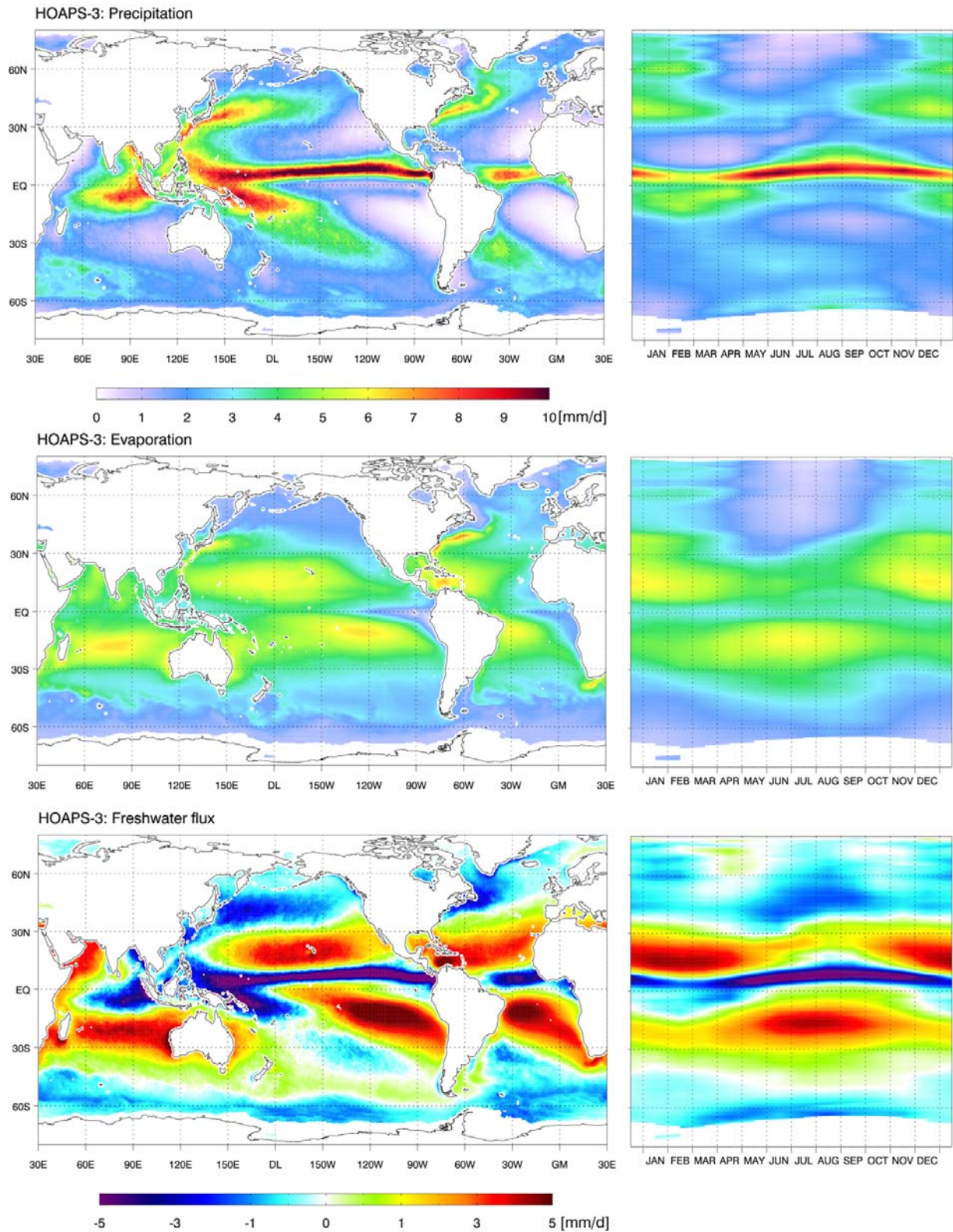


Figure 4. Climatological mean global fields (left) and annual cycle of zonal mean (right) of precipitation, evaporation and freshwater flux (from Andersson et al., 2010a)

2. CONCLUSIONS

HOAPS-3 is a well developed satellite climatology of water cycle components over the ice free global ocean, showing all the known global climatological features and regional details. Due to multi satellite averages, use of all SSM/I operating at the same time, and careful inter-sensor calibration it provides consistent and homogeneous time series for the period 1987 through 2005. It provides a scan-based dataset on pixel-level (HOAPS-S), from which pentad and monthly mean and daily composite gridded datasets (HOAPS-G, HOAPS-C) at 0.5° resolution are derived.

These make HOAPS-3 a versatile data set for studying ocean-atmosphere interaction on different temporal and spatial scales. HOAPS data are freely available from **www.hoaps.org** via the CERA database-system provided by the World Data Center for Climate, Hamburg (www.wdc-climate.de).

In near future, some of the core HOAPS products will be routinely provided by the Eumetsat Climate Monitoring Satellite Application Facility (CM-SAF, www.cmsaf.eu) at the German Weather Service (DWD)

3. REFERENCES

- Andersson, A., C. Klepp, K. Fennig, S. Bakan, H. Graßl, and J. Schulz, 2010a: The Hamburg Ocean Atmosphere Parameters and Fluxes from Satellite Data – HOAPS-3. *Earth Syst. Sci. Data*, 2, 215-234, doi:10.5194/essd-2-215-2010
- Andersson, A., C. Klepp, K. Fennig, S. Bakan, H. Graßl, and J. Schulz, 2010b: Evaluation of HOAPS-3 ocean surface freshwater flux components. *J. Appl. Meteor. Climatol.*, doi: 10.1175/2010JAMC2341.1, in print
- Andersson, A., S. Bakan, H. Graßl, 2010c: Satellite derived North Atlantic precipitation and freshwater flux variability with special emphasis on the North Atlantic Oscillation. *Tellus A*, 62, 453-468.
- Bauer, P., 1992: Wasserdampf, Gesamtwasser und Niederschlagsrate aus Daten passiver Mikrowellenradiometer über dem Ozean, Forschungsbericht, DLR, Köln, Germany, ISSN 0939-2963.
- Bauer, P. and P. Schlüssel, 1993: Rainfall, Total Water, Ice Water, and Water-vapor Over Sea from Polarized Microwave Simulations and Special Sensor Microwave Imager Data, *J. Geophys. Res.-Atmos.*, 98, 20 737–20 759.
- Bentamy, A., K. B. Katsaros, A. M. Mestas-Nunez, W. M. Drennan, E. B. Forde and H. Roquet, 2003: Satellite Estimates of Wind Speed and Latent Heat Flux Over the Global Oceans, *J. Climate*, 16, 637–656, 2003.
- Blechs Schmidt, A.-M., S. Bakan, H. Grassl, 2009: Large-scale atmospheric circulation patterns during polar low events over the Nordic seas, *J. Geophys. Res.*, 114, D06115, doi:10.1029/2008JD010865

Casey, K. S.: Global AVHRR 4 km SST for 1985-2001, Pathfinder V5.0, NODC/RSMAS, Tech. rep., NOAA National Oceanographic Data Center, Silver Spring, Maryland, NODC Accession Numbers 0001763-0001864: Pathfinder AVHRR Version 5.0, 2004.

Fairall, C. W., Bradley, E. F., Rogers, D. P., Edson, J. B., and Young, G. S.: Bulk Parameterization of Air-sea Fluxes for Tropical Ocean-Global Atmosphere Coupled-Ocean Atmosphere Response Experiment, *J. Geophys. Res.-Oceans*, 101, 3747–3764, 1996.

Fairall, C. W., Bradley, E. F., Hare, J. E., Grachev, A. A., and Edson, J. B.: Bulk parameterization of Air-sea Fluxes: Updates and Verification for the COARE Algorithm, *J. Climate*, 16, 571–591, 2003.

Ferraro, R., 1997: Special sensor microwave imager derived global rainfall estimates for climatological applications, *J. Geophys. Res.*, 102, 16 715–16 735.

Klepp, C., K. Bumke, S. Bakan, P. Bauer, 2010: Ground Validation of Oceanic Snowfall in Satellite Climatologies during LOFZY. *Tellus A*, 62, 469-480.

Romanou, A., G. Tselioudis, C. S. Zerefos, C.-A. Clayson, J. A. Curry and A. Andersson, 2010: Evaporation - Precipitation variability over the Mediterranean and the Black Seas from satellite and reanalysis estimates, *Journal of Climate*, in press, doi:10.1175/2010JCLI3525.1.

Romanova, V., A. Köhl, D. Stammer, C. Klepp, A. Andersson and S. Bakan, 2010: Sea Surface Freshwater Flux Estimates from GECCO, HOAPS and NCEP. *Tellus A*, 62, 435-452.

Schlüssel, P.: Passive Fernerkundung der unteren Atmosphäre und der Meeresoberfläche aus dem Weltraum, Vol. 20 of *Berichte aus dem Zentrum für Meeres- und Klimaforschung, Reihe A: Meteorologie*, Max Planck Institute for Meteorology, Bundesstr. 55, 20146 Hamburg, Germany, ISSN 0947-7128, 1995.

Schlüssel, P. and W. J. Emery, 1990: Atmospheric Water-vapor Over Oceans from SSM/I Measurements, *Int. J. Remote Sens.*, 11, 753–766.

Winterfeldt, J., A. Andersson, C. Klepp, S. Bakan and R. Weisse, 2010: Comparison of HOAPS, QuikSCAT and Buoy Wind Speed in the Eastern North Atlantic and the North Sea. *IEEE Transactions On Geoscience Remote Sensing* 48, 338-348

CAN RECENTLY OBSERVED PRECIPITATION TRENDS OVER THE MEDITERRANIAN AREA BE EXPLAINED BY CLIMATE CHANGE PROJECTIONS?

Armineh Barkhordarian¹ and Hans von Storch^{1,2}

¹Institute for Coastal Research, GKSS research centre

²Meteorological Institute, University of Hamburg

e-mail: armineh.barkhordarian@gkss.de

We examine the possibility that anthropogenic forcing (Greenhouse gases and sulfate aerosols, GS) is a plausible explanation for the recently observed precipitation trends over the Mediterranean area. For this purpose, we investigate the consistency of annual and seasonal observed trends in precipitation with the response to GS forcing estimated from 15 coupled atmosphere-ocean general circulation models derived from CMIP3 datasets and a set of regional climate models from CIRCE project. In summer we find that the projected changes in mean summer precipitation are consistent with the observed changes in recent decades. Consistency in summer suggests that the observed drying trend over the Mediterranean will continue in the future. Pattern similarity statistics used in this study indicates that, in winter and spring observed trends and variability are larger than climate change projections. In autumn we find an important difference, observations contradict the projections. Observations suggest that in autumn Mediterranean region has become wetter by about 2 mm/month per decade increase in amount of precipitation during last 30 years. In contrast to observed trends all global and regional scenarios give us a picture of increasingly drier and stable conditions. Inconsistency in annual cycle of precipitation over the Mediterranean can occur for two reasons: Either our expectation of future change is wrong, or the anthropogenic forcing is not dominant in recent years.

RAIN-GAUGE VALIDATION OF SATELLITE RAINFALL ESTIMATES OVER ARGENTINA

Daniel Barrera and Sebastián Gómez Gómez

CONICET / University of Buenos Aires, Argentina

e-mail: daniel.barrera@fibertel.com.ar

Over land areas, rain-gauge networks provide point measures which can be used to validate area-average rainfall estimates. In Argentina, rain-gauge observations are the only trustable source of data available to validate remote-sensing rainfall estimates. In the present project, statistical techniques already developed and used by the IPWG community are being implemented to run in an automated way.

These techniques include linear regressions and correlation coefficients in the bi-dimensional space given by “area-average estimates vs. point observed precipitation”, and binary statistical methods.

The present project deals with the issue of validation of current and future satellite operational and research precipitation estimates. It is planned to assess the performances of various satellite-derived products over continental Argentina, such as the NOAA/NESDIS Hydroestimator maps, the version of the Hydroestimator developed at the University of Buenos Aires, and the GSMaP daily rainfall maps in 0.250 spatial resolution.

A digital system is being developed for this purpose. The system will receive and ingest rain-gauge data from several sources. These sources include Governmental Agencies, Non Governmental Organizations, and private commercial institutions measuring rainfall –most of them related to agricultural businesses–.

The project will contribute to the assessment of performances of current satellite techniques over various seasons, rainfall regimes, and space-time scales.

REFAME, FORWARD-BACKWARD AND MULTI-SPECTRAL EXTENSION

Ali Behrangi^{1,2}, Soroosh Sorooshian², Kuolin Hsu²

¹ Jet Propulsion Laboratory, California Institute of Technology, Pasadena, CA, USA

² Center for Hydrometeorology and Remote Sensing (CHRS), Dept. of Civil &
Environmental Engineering, University of California, Irvine, Irvine, CA, USA

e-mail: ali.behrangi@jpl.nasa.gov

ABSTRACT

This paper provides a brief summary of a new multi-platform multi-sensor satellite precipitation estimation technique called Rain Estimation using Forward Adjusted-advection of Microwave Estimates (REFAME). The technique incorporates a cloud classification method to adjust microwave (MW) precipitation intensities as advected forward/backward in time. REFAME consists of three main steps: The first step uses successive IR images to calculate cloud motion streamlines from a 2D cloud tracking algorithm, explicitly incorporating the effect of cloud motion, growth, deformation and dispersal. The second step classifies cloudy pixels into a number of predefined clusters using several infrared-extracted cloud features representing radiative, textural and dynamic properties of clouds. By calculating the precipitation features in each class, the third step involves adjusting the MW precipitation intensities as advected between two consecutive microwave overpasses, which can be both forward and backward. The technique is developed and tested at 0.08-degree latitude/longitude resolution every 30 minutes and evaluated over the conterminous United States. The performance of the algorithm compared favorably with several existing products.

1. INTRODUCTION

Precipitation estimation at high temporal and spatial resolution is vital for many applications such as weather and climate studies, initialization of numerical models, disaster mitigation and flood monitoring and nowcasting. With the operation of the first Special Sensor Microwave Imager (SSM/I; Hollinger et al. 1987), microwave (MW) remote sensing of precipitation was recognized as the most effective tool for instantaneous estimate of precipitation intensity (Adler et al. 2001). However, MW-only precipitation data may not adequately address the growing demand of various scientific and operational communities for global/regional fine-scale precipitation estimates. Therefore, high-resolution precipitation products rely on combined information from MW and IR sensors to take advantage of the strengths that each sensor can offer. Among several combined precipitation products CMORPH (Joyce et al., 2004), for example,

has appeared successful in capturing high spatial and temporal variation of rainfall based on evaluation statistics reported during the Pilot Evaluation of High Resolution Precipitation Products (PEHRPP) initiative, the International Precipitation Working Group (IPWG) validation sites (Ebert et al. 2007), and few other studies (Dinku et al. 2008; Tian et al. 2009, Tian et al. 2007). There is one area which may limit the full potential of methods such as CMORPH, especially for near real time precipitation estimation which is useful for applications such as hydrologic flood forecasting. In specific, because the morphed precipitation product relies on the MW precipitation estimates at the two ends of a cloud advection path, the method may miss precipitation events forming or dissipating between two MW overpasses such as convective precipitation.

The proposed blending technique, REFAME, intends to adjust the advected MW precipitation estimates using frequent observation of cloud-top features and dynamics and through a multi-feature cloud classification technique developed by Behrangi et al. (2009). Note that for more complete discussion on the development of REFAME the readers are referred to Behrangi et al. (2010b).

2. METHODOLOGY

In a Lagrangian framework, REFAME employs a cloud motion vectors derived from successive high resolution (0.04 degree every 30 minutes) GEO-IR images using a 2D cloud tracking algorithm incorporating the effect of cloud motion, growth, deformation and dispersal (see Bellerby et al., 2006). The cloud features: cloud-top brightness temperature (T_b), mean and standard deviation of 3x3 neighboring grid-boxes and T_b gradient (calculated from successive T_b images) are used to classify clouds into 400 clusters following a filtering process to improve the classification skill. For each cluster mean precipitation rate (MPR) is calculated using ground radar precipitation estimates and used to derive an adjustment factor C_a : the ratio of MPRs for the current and previous clusters along the streamline. The adjustment factor C_a is calculated every 30 minutes and is applied to MW precipitation data as advected along the cloud motion stream, until the next MW overpass is reached. While the described technique (REFAME) is effective to capture the dynamics of precipitation as propagated forward in time, it cannot capture precipitation events that have not been observed in previous MW overpass. Therefore, an alternative method was developed, called REFAME-GEOmsa, which is based on weighted averaging of precipitation intensities obtained from REFAME and a previously-developed GEO-based precipitation estimation technique (PERSIANN-MSA; Behrangi et al., 2009). Note that REFAME and by extension REFAME-GEOmsa are designed to be flexible for incorporating diverse precipitation-relevant information, such as multi-spectral data. Note that REFAME was also implemented both forward and backward to benefit from the next MW overpass (REFAME-FwBw). While the forward-backward implementation of REFAME is expected to improve the overall results, its dependency to the next MW overpass (that may not be available up to more than few hours) can hamper its application for near-real time. In section 4, the performance of REFAME and REFAME-GEOmsa in both single (IR-only) and multi-spectral (IR 10.8 μ , WV6.7 μ , and VIS 0.65 μ) modes are evaluated and

compared with few other products. The results of implementing REFAME in forward-backward mode are also reported in the next section.

3. PRIMARY EVALUATION AND COMPARISON

While a more extensive evaluation and comparison of the algorithm is ongoing, in this section some early results are reported. Figure 1, compares the performance of REFAME-GEOmsa (Forward-only) with PERSIANN at 0.25 degree resolution for a five-day precipitation event during early June 2009 over the contiguous United States. Q2 precipitation is used as reference after calculating 30 minute precipitation maps from the original 5 minute dataset. Figure 1 suggests that with the REFAME-GEOmsa set up significant improvement for both precipitation detection (ETS, POD, FAR, BIASa) and precipitation estimation (COR, RMSE, BIASv) is obtained. The improvement in terms of COR and ETS is more than 30 % and 25%, respectively.

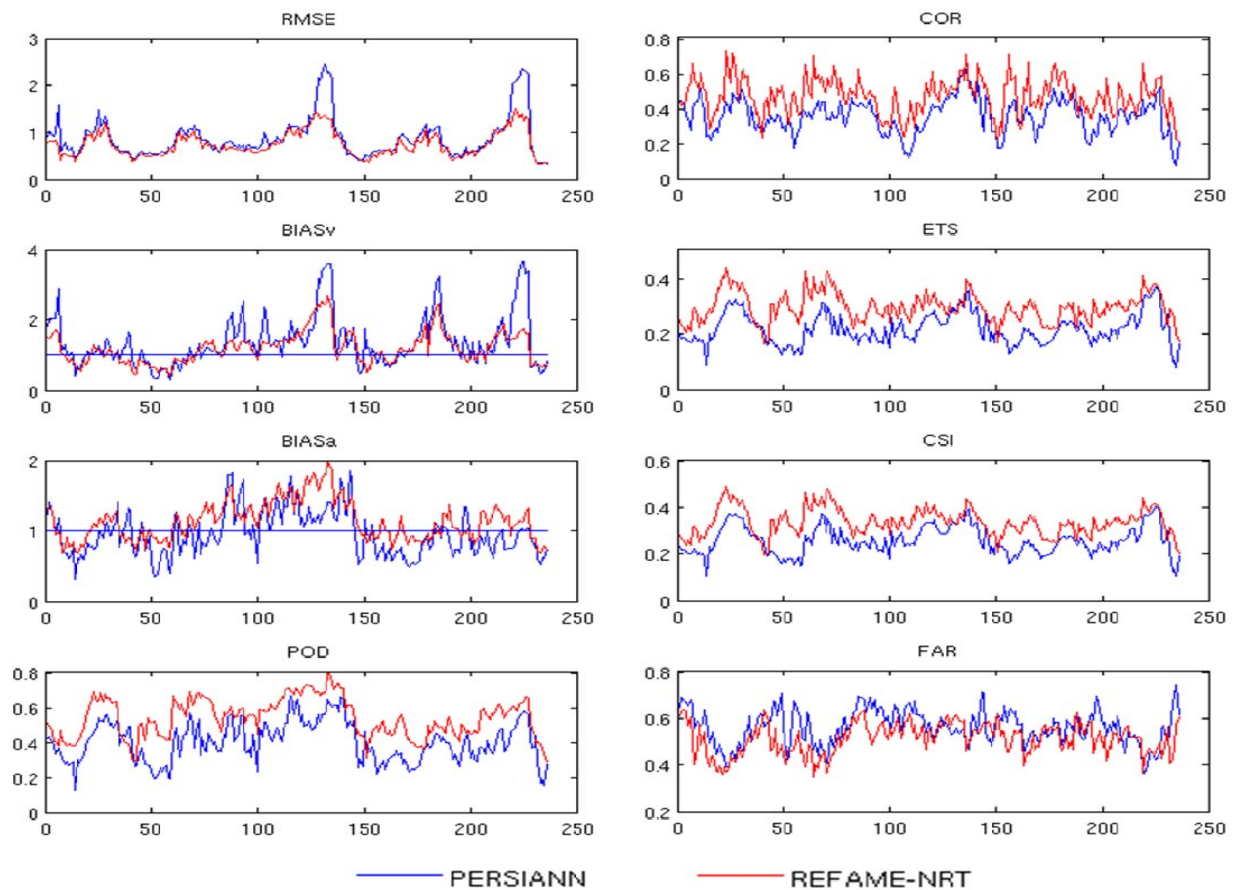


Figure 1. A selected five-day comparison of REFAME-GEOmsa with PERSIANN at 0.25 degree resolution every 30 minutes

Figure 2 demonstrates that by employing multi-spectral data (IR, WV, and VIS during daytime) the performance of REFAME is substantially improved, particularly in terms of precipitation detection capability (ETS, CSI, POD, FAR, and BIASa). Note that the observed cycles in the statistical scores suggest that VIS band can highly improve the performance of the algorithm for precipitation which is consistent with previous studies

such as Behrangi et al. (2010a) among several others. The original intention was to also conduct comparisons between REFAME and its other counterparts such as QMORPH and GSMaP-NRT. However, the comparisons could not be performed because of the following reasons. It was found that QMORPH is only temporary available and is replaced by new data every few months, therefore no QMORPH data was available for the period of study (summer 2009). In addition, GSMaP-NRT demonstrated a poor performance during summer 2009 because at the time the input MW precipitation to GSMaP-NRT was restricted to only TMI, AMSR-E, and SSM/I F13 and no AMSU precipitation estimates were being used in the product.

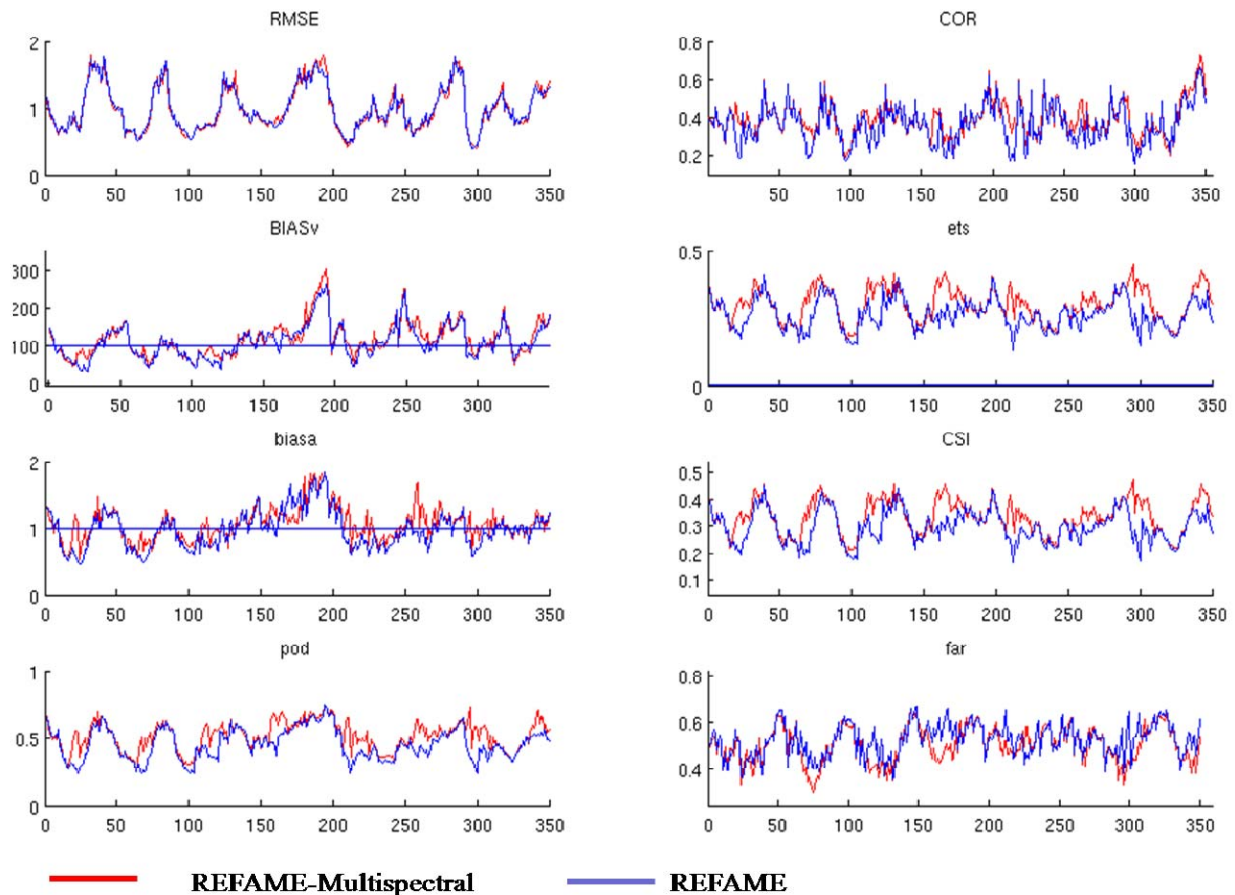


Figure 2. Comparison of REFAME using IR data (blue color) with REFAME using multi-spectral data (red color). As shown, by using multi-spectral data the skill of the algorithm for precipitation detection is significantly improved.

By applying REFAME in a forward-backward mode, Figure 3 compares REFAME-FwBw and REFAME-FwBw-multispectral with CMORPH during the first five days of June 2009. The results indicate that REFAME-FwBw can be effective to improve the statistics, particularly during those periods of time that the time distance from the previous or the next MW overpass is the farthest. However, the example shown in Figure 3 does not necessarily represent the performance of the products and more complete evaluations are needed.

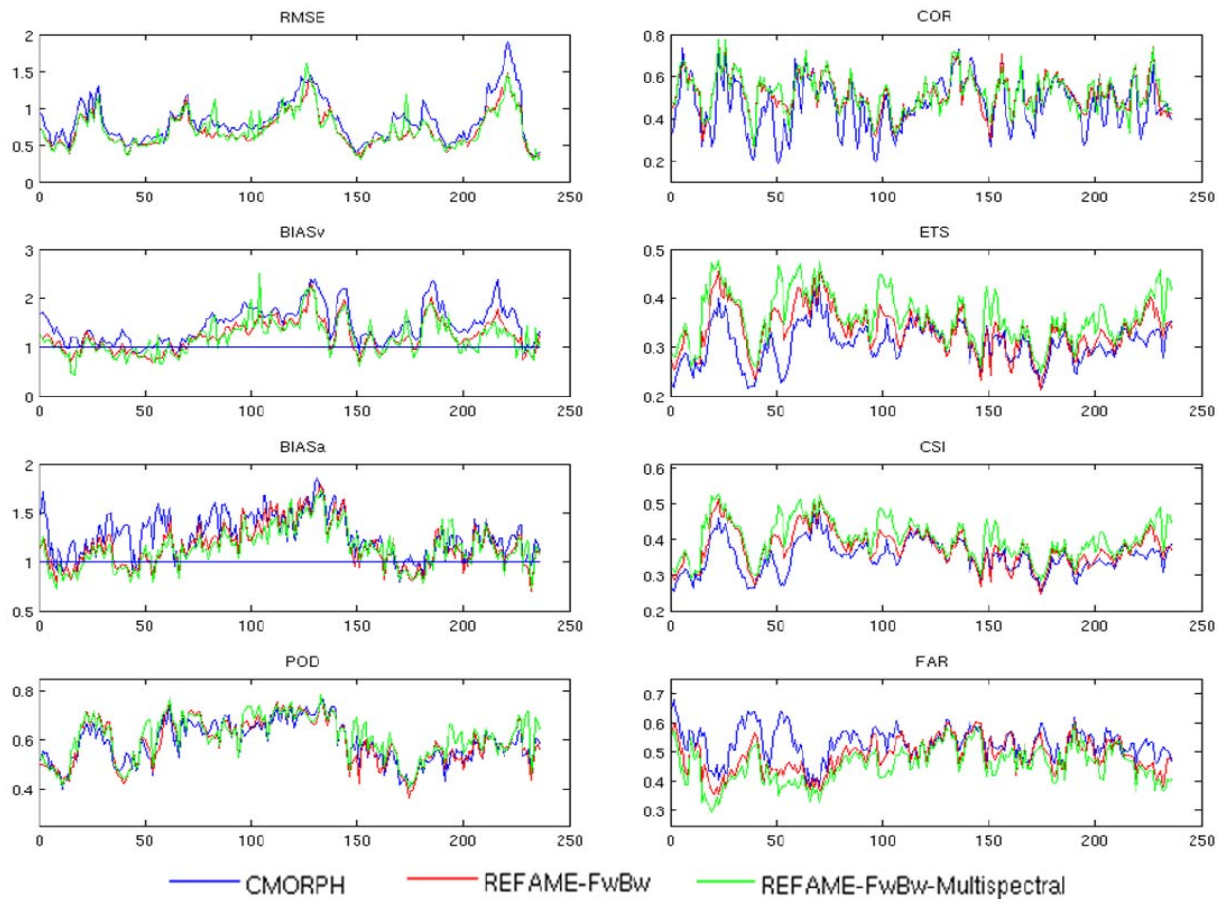


Figure 3. Comparison of REFAME-FwBw (single IR band), REFAME-FwBw-multispectral (multi-spectral bands), and CMORPH at 30min 0.25degree resolution

The use of multi-spectral data in conjunction with REFAME-FwBw was also found effective, particularly with respect to precipitation detection skill as shown in Figure 3.

4. SUMMARY

This paper provided a brief summary of the REFAME algorithm that is under development for operation at global scale. The algorithm uses a multi-feature cloud classification scheme to incorporate frequent observation of clouds from geostationary platform for adjustment of the MW precipitation intensities as propagated forward in time along cloud motion streamlines inferred from successive IR images. The algorithm is employed in both near real-time and in a forward-backward mode. In addition, it can include multi-spectral data. The results for both near real-time and Forward-backward implementations are found encouraging. More extensive evaluation and comparison of REFAME is ongoing and the results will be reported in near future.

5. ACKNOWLEDGMENTS

Partial financial support was provided by NASA Earth and Space Science Fellowship (NESSF award NNX08AU78H), and NASA NEWS (Grant NNX06AF934) programs.

Part of the research was carried out at the Jet Propulsion Laboratory, California Institute of Technology, under a contract with the National Aeronautics and Space Administration

6. REFERENCES

- Adler, R. F., C. Kidd, G. Petty, M. Morissey, and H. M. Goodman, 2001: Intercomparison of global precipitation products: The third Precipitation Intercomparison Project (PIP-3). *Bulletin of the American Meteorological Society*, **82**, 1377-1396.
- Behrangi, A., K. Hsu, B. Imam, S. Sorooshian, G. J. Huffman, and R. J. Kuligowski, 2009: PERSIANN-MSA: A Precipitation Estimation Method from Satellite-Based Multispectral Analysis. *Journal of Hydrometeorology*, **10**, 1414-1429.
- Behrangi, A., K. Hsu, B. Imam, S. Sorooshian, 2010a: Daytime Precipitation Estimation Using Bi-spectral Cloud Classification System. *Journal of Applied Meteorology and Climatology*, **49**, 1015-1031.
- Behrangi, A., B. Imam, K. Hsu, S. Sorooshian, T. J. Bellerby, and G. J. Huffman, 2010b: REFAME: Rain Estimation using Forward Adjusted-advection of Microwave Estimates. *Journal of Hydrometeorology*, doi: 10.1175/2010JHM1248.1.
- Dinku, T., S. Chidzambwa, P. Ceccato, S. J. Connor, and C. F. Ropelewski, 2008: Validation of high-resolution satellite rainfall products over complex terrain. *Int. J. Remote Sens.*, **29**, 4097-4110.
- Ebert, E. E., J. E. Janowiak, and C. Kidd (2007), Comparison of near-real-time precipitation estimates from satellite observations and numerical models, *Bulletin of the American Meteorological Society*, **88**(1), 47-64.
- Hollinger, J. P., R. C. Lo, G. A. Poe, R. Savage, and J. L. Peirce, 1987: Special Sensor Microwave/Imager User's Guide. *Washington, D.C.: Naval Research Laboratory*.
- Joyce, R. J., J. E. Janowiak, P. A. Arkin, and P. Xie, 2004: CMORPH: A method that produces global precipitation estimates from passive microwave and infrared data at high spatial and temporal resolution. *Journal of Hydrometeorology*, **5**, 487-503.
- Tian, Y., C. D. Peters-Lidard, B. J. Choudhury, and M. Garcia, 2007: Multitemporal analysis of TRMM-based satellite precipitation products for land data assimilation applications. *Journal of Hydrometeorology*, **8**, 1165-1183.
- Tian, Y., C. D. Peters-Lidard, J. B. Eylander, R. J. Joyce, G. J. Huffman, R. F. Adler, K. Hsu, F. J. Turk, M. Garcia, and J. Zeng (2009), Component analysis of errors in satellite-based precipitation estimates, *J. Geophys. Res.*, **114**, D24101, doi:10.1029/2009JD011949.

A PHYSICALLY-BASED RAINFALL RATE ALGORITHM FOR THE GLOBAL PRECIPITATION MISSION

Sid-Ahmed Boukabara^{1,2} and Kevin Garrett³

¹Joint Center for Satellite Data Assimilation, USA

²NOAA/NESDIS/STAR, USA

³I. M. Systems Group @ NOAA/NESDIS/STAR, USA

e-mail: sid.boukabara@noaa.gov

The Global Precipitation Mission (GPM) will be comprised of a constellation of satellites, from a variety of international organizations, with the primary purpose to better understand the global water cycle, including precipitation processes, occurrence, and measurement. Here we present a physical one-dimensional variational retrieval algorithm (1DVAR), developed at NOAA/NESDIS, which will be applied to GPM microwave observations for the retrieval of hydrometeor profiles and surface rainfall rate. The algorithm, known as the Microwave Integrated Retrieval System (MiRS), provides the ability to retrieve sounding, surface, and hydrometeor parameters simultaneously, that, if input to a forward model, results in reproducing the microwave observation. Currently MiRS is being applied routinely to passive microwave observations from the AMSU/MHS sensors onboard the NOAA-18, NOAA-19, and Metop-A satellites, the SSMI/S sensor on DMSP-F16 and DMSP-F18, proxy data for the upcoming NPP/NPOESS ATMS sensor, and also for Aqua AMSR-E. The GPM mission presents the opportunity to extend the MiRS algorithm to new sensors, including MADRAS and SAPHIR onboard Megha-Tropiques, as well as the GPM Microwave Imager (GMI) on NASA's GPM Core satellite. In this respect, the extension of MiRS to the current Tropical Rainfall Measuring Mission Microwave Imager (TMI) data as well as to GMI proxy data will be discussed.

RAIN DROP SIZE DENSITIES OVER LAND AND OVER SEA

Karl Bumke

Leibniz-Institute of Marine Sciences at the Christian-Albrechts Universität
zu Kiel

Düsternbrooker Weg 20, D-24105 Kiel, Germany

e-mail: kbumke@ifm-geomar.de

A detailed knowledge of rain drop size densities is an essential presumption with respect to remote sensing of precipitation. Since maritime and continental aerosol is significantly different yielding to differences in cloud drop size densities, maritime and continental rain drop size densities may be different, too. In fact only a little is known about differences in rain drop size densities between land and sea due to a lack of suitable data over the sea. To fill in this gap measurements were performed during the recent 10 years at different locations in Germany and on board of research vessels. Measurements were done by using an optical disdrometer (ODM 470, Großklaus et al., 1998). Measurements have been divided into four classes on the basis of prevailing continental or maritime influence: land measurements, coastal measurements, measurements in areas of semi-enclosed seas, and open sea measurements.

In general differences in drop size densities are small between different areas. A Kolmogoroff Smirnov test does not give any significant difference between drop size densities over land, coastal areas, semi-enclosed, and open seas at an error rate of 5%. The best fit of drop size densities is an exponential decay curve. The precipitation rate dependent factor in the exponential is similar to that given by Marshall and Palmer (1948). The intercept parameter, in the original Marshall Palmer formulation not depending on the rain rate, is also of the same order.

Further a number of recent publications have shown that drop size densities of convective and stratiform rain show significant differences, too. Several procedures have been developed in the past to decide, whether precipitation is of stratiform or convective character. Here two of them are used, temporal variability in rain rates and additional information by weather radar data for the South Western Baltic Sea. For integration times of 1 minute no significant differences can be detected at an error rate of 5%, while integration times of 10 minutes yield to significant differences between drop size densities of prevailing stratiform and convective rain.

BLENDING SATELLITE RAINFALL ESTIMATES AND NATIONAL RAINGAUGE OBSERVATIONS TO PRODUCE 30-YEAR RAINFALL TIME SERIES

**Tufa Dinku¹, Stephen Connor¹, David Grimes², Kinfe Hailemariam³, Ross
Maidement², and Elena Tarnavsky²**

1. International Research Institute for Climate and Society,
the Earth Institute at Columbia University
2. Department of Meteorology, University of Reading, UK
3. National Meteorological Agency, Addis Ababa, Ethiopia

e-mail: tufa@iri.columbia.edu

ABSTRACT

Long-term, temporally homogeneous time series of rainfall data are of great importance in a number of applications. The conventional source of climate data is weather stations. However, reliable climate information, particularly throughout rural Africa, is very limited. The available weather stations are unevenly distributed, with most of the stations located along the main roads in cities and towns. The alternative has been satellite rainfall estimates with the main advantage of excellent spatial coverage. But satellite rainfall estimates also suffer from a number of critical shortcomings that include heterogeneous time series, short time period, and poor accuracy particularly at higher temporal and spatial resolutions. Thus, it makes a lot of sense to combine the point accuracy of the raingauge measurements with the better spatial coverage of the satellite estimates. This paper describes the use of raingauges and satellite rainfall estimates to produce 30-year rainfall time series over Ethiopia at spatial resolution of 10km and ten-daily time scale.

1. INTRODUCTION

There is a growing understanding that climate variability and change pose serious challenges to development, particularly in Africa. The availability of decision-relevant climate information, at national and community level, is critical in integrating climate issues into development activities. Rainfall is the most important climate variable for many applications. Long-term, temporally homogeneous time series of rainfall data with good spatial coverage are therefore of great value. The conventional source of rainfall data has been raingauge measurements. However, reliable climate information, particularly throughout rural areas of Africa is very limited. An alternative to raingauge measurement has been satellite rainfall estimation. Different techniques exist to estimate rainfall from thermal infrared (TIR) and passive microwave (PMW) sensors and

combinations of the two. In terms of studying climate, currently available data sets suffer from either covering a very short time span (such as those based on from TRMM data) or being temporally inhomogeneous. Many of the most successful algorithms combine data from different sources with different weightings for each year depending on data availability. While this approach may provide the most accurate estimates in any one year, the interannual variations may be influenced as much by the different mix of inputs as by actual changes in rainfall amount so that trends and variability statistics will be inaccurately portrayed. However, a reliable and temporally homogeneous rainfall data set covering a 30-year time period can be generated from the archive of METEOSAT TIR imagery calibrated against local gauge data. Here we offer an example from Ethiopia where this approach can be further improved by optimal merging of the satellite estimates with observations from gauges. Many satellite products already include raingauge measurements for removing biases and merging the gauge observations with the satellite estimates. However, for most of Africa only the synoptic observations (or part of it) are internationally available for these adjustments. For instance, in Ethiopia only about 17 stations are accessible globally. However, as with many countries, Ethiopia has a much greater density of gauges available within the country. In this work, data from a network of over 600 gauges have been gridded and merged with the satellite estimates to generate an optimum rainfall product. The process involves rigorous quality checks of raingauge data, interpolating the gauge data to regular grids, and blending satellite estimates with the gauges. The final outputs are 30-year time series of homogenous ten-daily merged product at a spatial resolution of 10km, which optimize the use of satellite and gauge information.

2. DATA AND METHODOLOGY

2.1. Data

The two input datasets are raingauge observations and satellite TIR data. The raingauge data come from the National Meteorological Agency (NMA) of Ethiopia. Over 600 stations (Fig. 1) are used to calibrate the satellite algorithm, remove bias and merge with the satellite estimates. The raingauge data used covers the period from 1981 to 2008; but will soon be updated to 2010 to produce a 30-year time series. The use of this many raingauges was possible because all the work has been done at NMA by NMA personal. The International Research Institute for Climate and Society (IRI) and the TAMSAT group at the university of Reading in UK have provided onsite training and technical support.

The main requirement for the satellite data is homogenous estimates going back 30 years at spatial resolution of 10 km and ten-daily (dekadal) accumulations. There are many satellite estimates available with reasonable accuracy and very good temporal and spatial resolutions. TRMM TMPA (Huffman et al 2007), CMORPH (Joyce et al., 2004) and GSMAP (Okamoto et al., 2007) are good examples. However, these products do not go back thirty years and do not satisfy the homogeneity criteria as they use different amount of TIR and PMW inputs over the years. There are other satellite products that go back over thirty years (e.g. GPCP (Adler et al., 2003), CMAP (Xie and

Arkin, 1997)). But these also suffer from inhomogeneity in addition to coarse spatial and temporal resolutions. Thus, we had to produce the satellite estimates ourselves. This could only be done by using raw TIR data. Raw METEOSAT TIR data were obtained from EUMETSAT. This task, done by the TAMSAT group, was a very important and challenging one. In addition to the HUGE size of these data, there were missing images, and missing header files. These have been overcome and rainfall estimates have been produced over Ethiopia going back to 1983. Though the rainfall estimates are produced for Ethiopia, the processed TIR data covers the whole of METEOSAT disk. This will make scaling up the Ethiopian experience much easier.

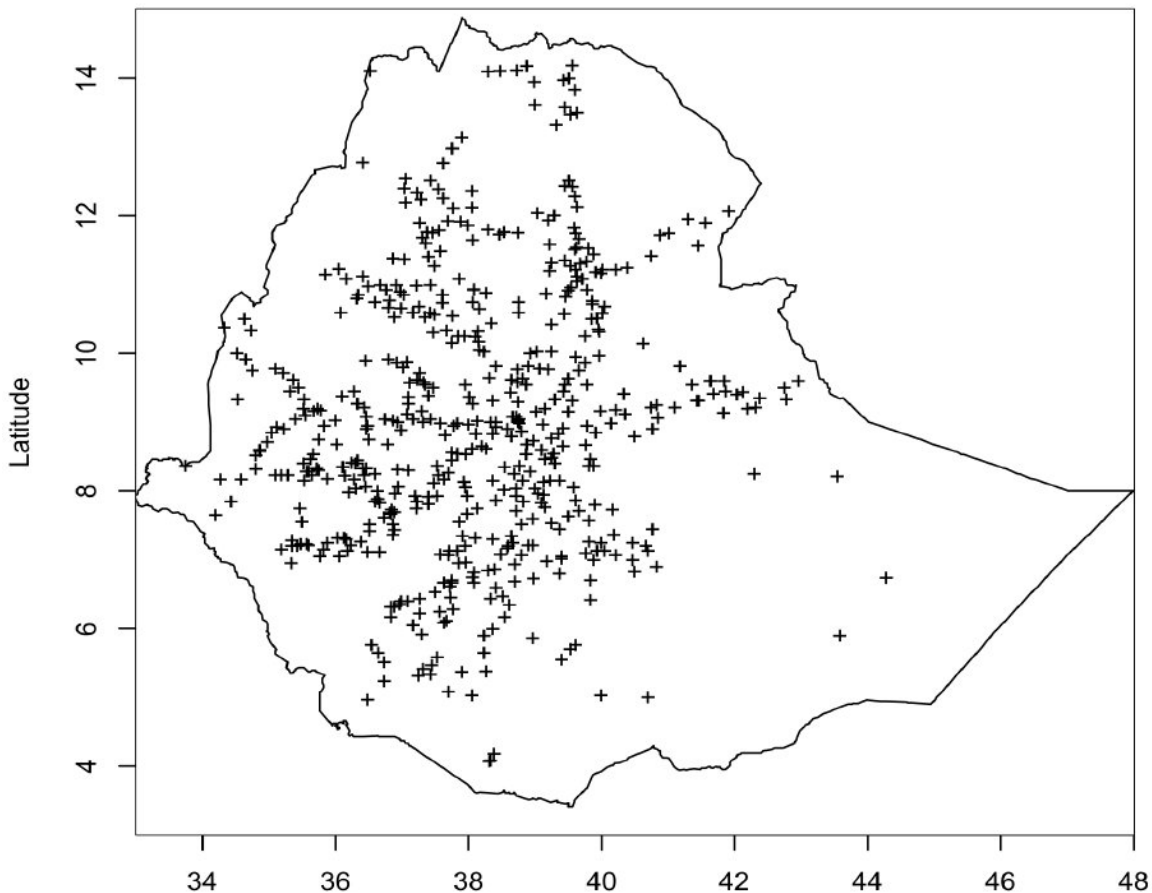


Figure1. Distribution of rain gauge stations used

2.2. Methodology

The overall process involves quality control and gridding of rain gauge data, calibration of satellite rainfall algorithm, removing bias from the satellite estimates and combining satellite estimates with rain gauge data.

2.2.1. Data organization and quality control

The data required by this project were organized and delivered by NMA. NMA performs routine quality checks on data in its archive. However, rigorous quality checks were performed to further improve the quality of the data. The quality control procedure includes temporal and spatial checks. The spatial quality check procedure compares values of a given station with corresponding values of the nearby stations, while the temporal check compares the values at a given station over time (Eischeid et al., 1995).

2.2.2. Interpolation of raingauge observations

The quality controlled gauge measurements are interpolated into regular grids of 0.1 X 0.1 deg lat/long using climatologically aided interpolation (Willmott and Robeson 1995). First the decadal mean values are interpolated with the mean satellite values as a background field. Then the interpolated mean values are used as a background to interpolate gauge values for each dekad using angular distance-weighted interpolation as in New et al. (2000).

2.2.3. Generation of satellite rainfall estimates

The TAMSAT method (Thorne et al., 2001) was used for the retrieval of satellite rainfall estimates. This algorithm is selected because it is simple to implement and has been shown to be as good as the more sophisticated methods when calibrated with local raingauge data (Dinku et al., 2007). This algorithm uses the Cold Cloud Duration (CCD) as an intermediate product between the raw TIR and the rainfall estimates. The CCD value for a given satellite pixel is defined as the length of time the pixel is colder than a specified threshold temperature T_c . The algorithm is calibrated over Ethiopia using over 600 stations. Calibration of the algorithm is carried out as a two-stage process. In Stage 1, the optimum T_c is found; in Stage 2 the best-fit parameters for the linear regression of CCD versus rainfall are determined. Temperature thresholds and calibration parameters are known to vary in space and time. To account for this, separate calibrations are carried out for each calendar month. Then, within a month calibration regions are determined on the basis of groupings of gauges with similar parameters (Fig. 2). The different calibration zones are possible because of the availability of a good number of gauges.

2.2.4. Blending gauge observations with satellite estimates

First raingauge data is used to remove bias from each satellite rainfall estimate (RFE) map. The difference between raingauge observations and RFE at raingauge locations are interpolated to RFE grids. Then the interpolated bias values are used to adjust the satellite estimates. Then satellite estimates are merged with raingauge data using optimal interpolation.

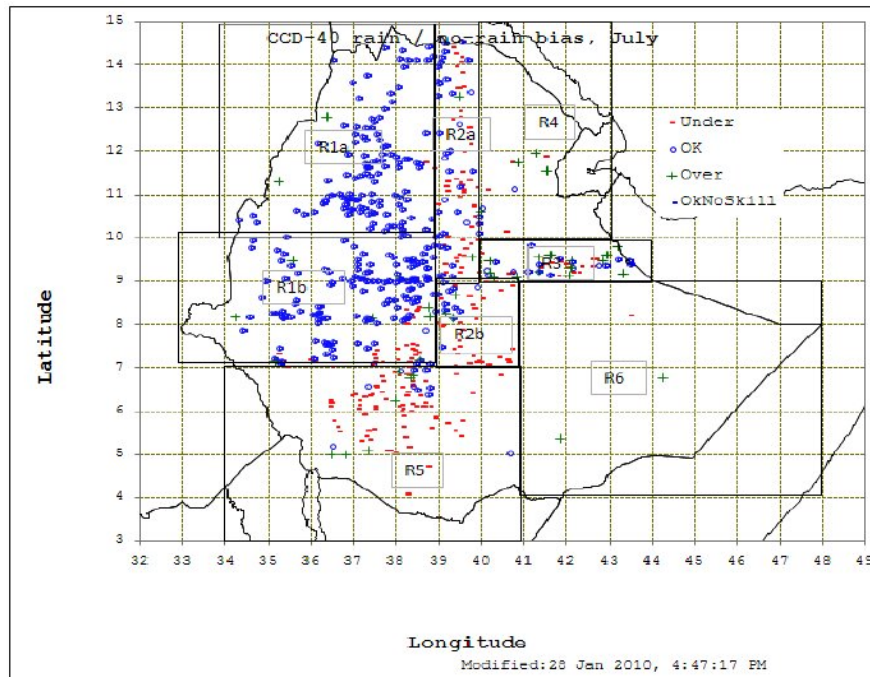


Figure 2. Sample output of the calibration process for the month of July. The different boxes represent different calibration zones, which is based on the difference between estimated and observed rainfall values

3. RESULTS

So far raingauge data from 19181 to 2008 have been gridded at NMA, and satellite estimates from 1983 to 2009 have been delivered to NMA. Satellite estimates suffer from missing data, particularly during the early 1980's. We are working on methodologies to fill the missing data. An example of the outputs is given in Fig. 3. The first panel (A) is mean (1981-2008) raingauge data for 2nd dekad of July. The points are station locations while the colors represent rainfall values per the color bar given for the images. Panel B is gridded gauge data. Panel C is also gridded raingauge data, but in this case satellite mean data are used as a background. The background is the bias-corrected RFE given in Panel D. The use of RFE as background improves the interpolation of the raingauge data significantly particularly over data sparse parts of the county. A good example is the northeastern part of the county with stations over the wetter highlands but not over the dry lowlands. As a result, the interpolation without RFE background makes the dry low land wetter that it actually is (panel B). This is corrected when RFE is used as background (panel C). Panel D is the satellite estimate, while panel E is the bias-corrected estimates. The satellite product consistently underestimates high rainfall values. This bias is removed in panel E. The effect of bias

correction is also shown in Fig. 4, which compares unadjusted and adjusted RFE time series from 1995 to 1999. Figure 4 also shows instances where RFE overestimates, but in most cases it underestimates heavy rainfall. The cause of this systematic underestimation of high rainfall values has been understood and steps are being taken to correct it.

4. SUMMARY

Efforts are being made to overcome the scarcity of climate data over Africa by the optimal combination of conventional station observations with satellite proxies. An example for Ethiopia has been provided where 30-year time series of combined satellite-gauge data are being generated. All available raingauge data have been quality controlled and used for the calibration of satellite rainfall retrieval algorithm. The raingauge data are also used to remove bias from the satellite estimates. Then the gauge data are combined with the satellite estimates using optimal interpolation. The gauge data are also gridded to provide a gauge-only product. A very active involvement by the National Meteorological Agency has made the use of large number gauges possible. The raw satellite data obtained and processed for this work covers the whole Africa. Thus, it is now easier to repeat this experience in other parts of Africa.

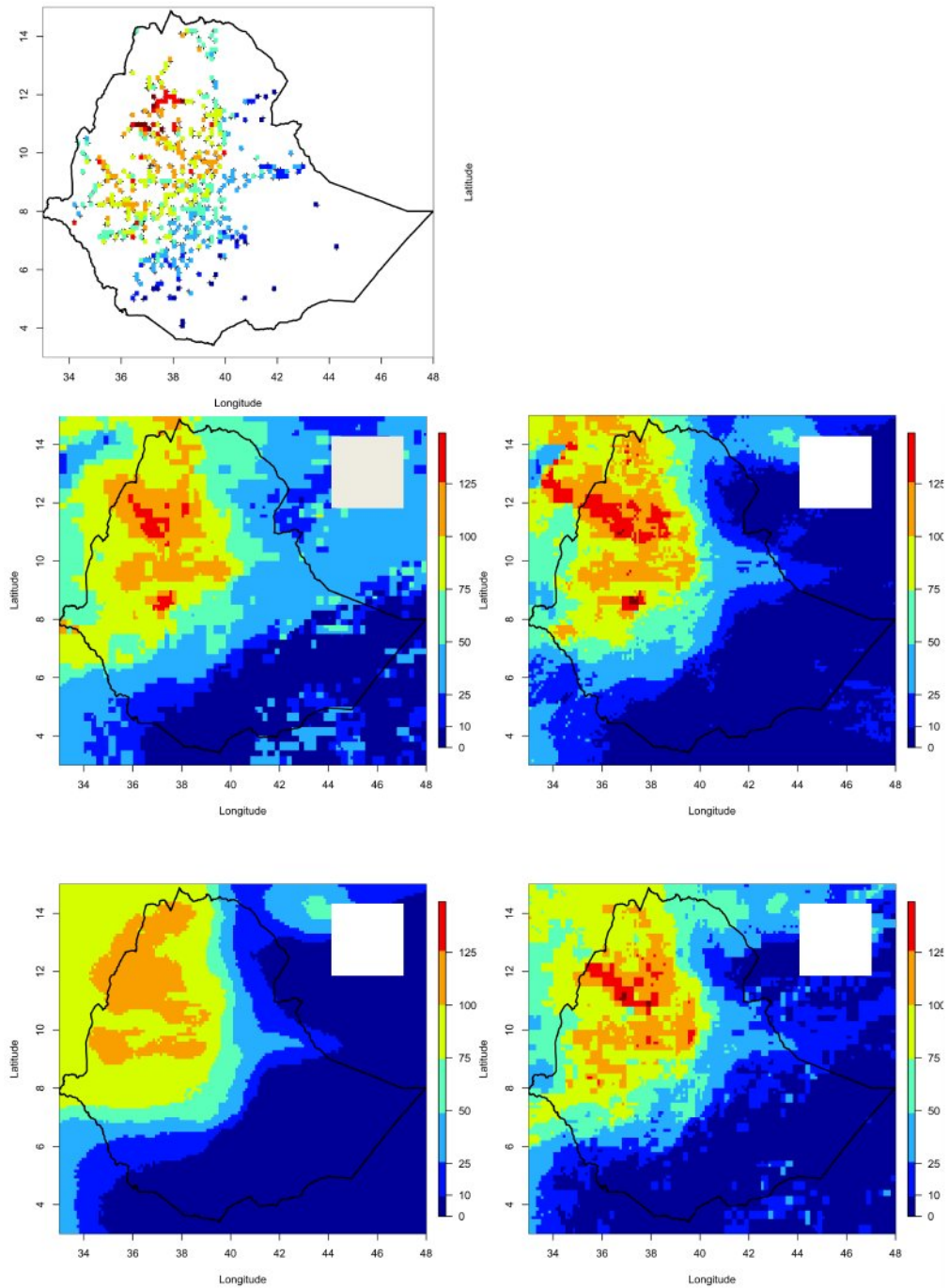


Figure 3. Sample outputs

- (A) Rain gauge data (mean 2nd dekad of July (1981-2008))
- (B) Interpolated gauge
- (C) As in (B) but bias-adjusted satellite data used as background
- (D) Satellite rainfall estimate
- (E) Bias-adjusted satellite rainfall estimate

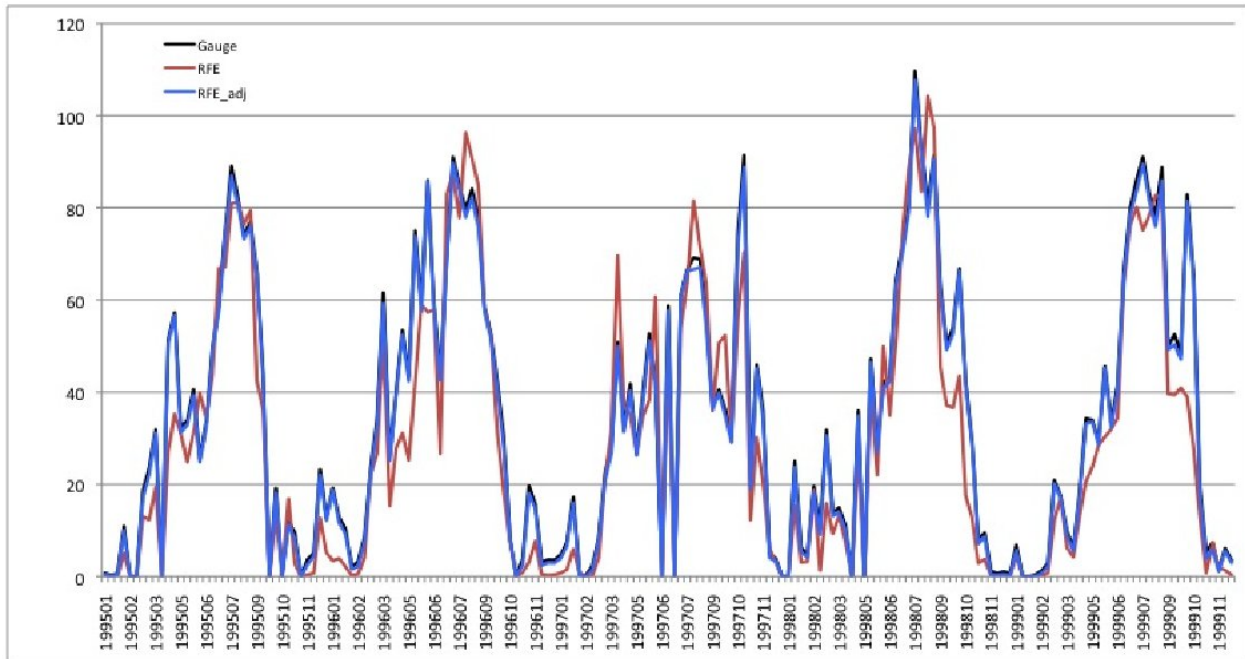


Figure 4. Comparison of unadjusted (red) and adjusted (blue) satellite rainfall estimates with the raingauge (black). These are averages over all gauges for each dekad.

ACKNOWLEDGMENTS

This work has been funded by Goog.org and a grant/cooperative agreement from the National Oceanic and Atmospheric Administration, NA050AR4311004. The views expressed herein are those of the author(s) and do not necessarily reflect the views of NOAA or any of its sub-agencies

REFERENCES

- Adler, R.F., Huffman, G.H., Chang, A., Ferraro, F., Xie, P., Janowiak, J., Rudolf, B., Schneider, U., Curtis, S., Bolvin, D., Gruber, A., Susskind, J., Arkin, P., and Nelkin, E. 2003, the version-2 Global Precipitation Climatology Project (GPCP) monthly precipitation analysis (1979–present). *J. Hydrometeorol.*, **4**, 1147–1167.
- Dinku, T., P. Ceccato, E. Grover-Kopec, M. Lemma, S. H. Connor, C. F. Ropelewski, 2007: Validation of satellite rainfall products over East Africa's complex topography. *International Journal of Remote Sensing*, **28(7)**, 1503-1526.
- Eischeid J K, Baker CB, Karl TR, Diaz HF. 1995. The quality control of long-term climatological data using objective data analysis. *Journal of Applied Meteorology* **34**: 2787-2795.
- Huffman, G.J., R. F. Adler, D. T. Bolvin, G. Gu, E. J. Nelkin, K. P. Bowman, Y. Hong, E. F. Stocker, and D. B. Wolf, 2007: The TRMM Multisatellite Precipitation Analysis (TMPA): Quasi-Global, Multiyear, Combined-Sensor Precipitation Estimates at Fine Scales. *Journal of Hydrometeorology*, **8**, 38-55.

- Joyce, R. J., Janowiak, J. E., Arkin, P. A., and Xie, P., 2004, CMORPH: A method that produces global precipitation estimates from passive microwave and infrared data at high spatial and temporal resolution.. *J. Hydromet.*, **5**, 487-503. New MG, Hulme M, Jones PD. 2000. Representing twentieth-century space-time climate variability. Part II: development of 1901–1996 monthly grids of terrestrial surface climate. *Journal of Climate* **13**: 2217-2238.
- Okamoto, K., T. Iguchi, N. Takahashi, T. Ushio, J. Awaka, S. Shige, and T. Kubota, 2007: High precision and high resolution global precipitation map from satellite data. Proceedings, *ISAP 2007*, 506-509
- Shepard D. 1968. two-dimensional interpolation function for irregularly spaced data. *23rd ACM National Conference. Brandon Syst. Press: Princeton, USA*, 517-524.
- Thorne V., Coakley, P., Grimes, D., and Dugdale, G., 2001, Comparison of TAMSAT and CPC rainfall estimates with raingauges, for southern Africa. *Int. J. Remote Sensing*, **22(10)**, 1951-1974.
- Willmott CJ, Robeson SM, Janis MJ. 1996. Comparison of approaches for estimating time-averaged precipitation using data from the USA. *International Journal of Climatology* **16**: 1103–1115.
- Xie, P., and Arkin, P. A., 1997, Global precipitation: A 17-year monthly analysis based on gauge observations, satellite estimates, and numerical model outputs. *Bull. Amer. Meteor. Soc.*, **78**, 2539–2558.

RELEASE OF CM-SAF HOAPS v3.2 PRODUCTS BASED ON IMPROVED DATA RECORD OF SSM/I RADIANCES

Karsten Fennig, Marc Schröder

Deutscher Wetterdienst, Satellite Application Facility on Climate Monitoring

e-mail: karsten.fennig@dwd.de

CM-SAF's expanding suite of products is tailored for applications focusing on key aspects of the Earth's atmospheric water and energy cycles and includes cloud and radiation budget parameters as well as temperature and water vapour.

As a part of the successful transition of HOAPS (Hamburg Ocean Atmosphere Parameters and Fluxes from Satellite data; <http://www.hoaps.org/>) into CM-SAF framework, an approximately 20-year Thematic Climate Data Record (TCDR) of total column integrated water vapour derived from the U.S. Defense Meteorological Satellite Program Special Sensor Microwave/Imager (SSM/I) covering ice free oceans has been released in 2009.

The next release of HOAPS parameters within the CM-SAF framework is planned for autumn 2010 and will include precipitation, evaporation, the resulting freshwater flux, near surface wind speed and near surface humidity. This new release extends the HOAPS time series to end of 2008 and is based on an improved data record of SSM/I radiances, with the main focus on a new inter-calibration of different SSM/I sensors to further improve the homogeneity of the SSM/I radiance record.

This presentation will give an overview of the SSM/I inter-calibration method and the planned generation of a CM-SAF Fundamental Climate Data Record (FCDR) of SSM/I radiances.

THE STATUS OF NOAA/NESDIS PRECIPITATION ALGORITHMS AND PRODUCTS

Ralph Ferraro^{1,2}

S. Boukabara³, K. Gopalan², J. Janowiak², R. Kuligowski³, H. Meng^{1,2}, M. Sapiano⁴,
H. Semunegus⁵, T. Smith^{1,2}, D. Vila², N-Y. Wang², F. Weng³, L. Zhao³

¹NOAA/NESDIS, College Park, MD USA

²Cooperative Institute for Climate and Satellites (CICS)
5825 University Research Court, Suite 4001
College Park, MD 20740-3823 USA

³NOAA/NESDIS, Camp Springs, MD USA

⁴Cooperative Institute for Research of the Atmosphere (CIRA), Ft. Collins, CO USA

⁵NOAA/NESDIS, Asheville, NC USA

e-mail: ralph.r.ferraro@noaa.gov

ABSTRACT

NOAA/NESDIS and its research partners at the University of Maryland's Cooperative Institute for Climate and Satellites (CICS) and Cooperative Institute for Research in the Atmosphere (CIRA) are actively involved in the development, operational transition, validation and application of satellite derived precipitation products, primarily from low-earth and geostationary orbiting satellites. The satellites include the current Geostationary Operational Environmental Satellites (GOES), Polar Orbiting Environmental Satellites (POES) and Defense Meteorological Satellite Program (DMSP) satellites; research missions such as Aqua, Cloudsat and the Tropical Rainfall Measurement Mission (TRMM); future satellites, including GOES-R, Joint Polar Satellite System (JPSS) and the Global Precipitation Measurement Mission (GPM). Additionally, climate scale products have been developed that utilize the satellite era data to develop long term precipitation reconstructions.

The precipitation data sets are used for a wide range of applications including short term forecasts and warnings (i.e., tropical rainfall potential, flash floods, etc.) and long-term climate studies (i.e., seasonal to interannual variability). It is the purpose of this overview paper to describe the current and future satellite precipitation activities at NOAA/NESDIS and set the stage for companion talks and posters on many of the specific products and data sets.

1. INTRODUCTION

NOAA/NESDIS and its research partners at its Cooperative Institutes are actively involved in the development, operational transition, validation and application of satellite derived precipitation products, primarily from low-earth and geostationary orbiting satellites. The satellites include the current GOES, DMSP and POES series; research missions such as Aqua, Cloudsat and TRMM; future satellites, including GOES-R, JPSS and GPM. Additionally, climate scale products have been developed that utilize the satellite era data to develop long term precipitation reconstructions.

The precipitation data sets are used for a wide range of applications including short term forecasts and warnings (i.e., tropical rainfall potential, flash floods, etc.) and long-term climate studies (i.e., seasonal to interannual variability). It is the purpose of this overview paper to describe the current and future satellite precipitation activities at NOAA/NESDIS and set the stage for companion papers on many of the specific products and data sets (e.g., see papers by R. Kuligowski; N-Y. Wang; D. Vila; S. Boukabara/K. Garrett; F. Weng; L. Zhao; M. Sapiano).

2. OPERATIONAL NOAA PRODUCTS

There are several NOAA/NESDIS products that are derived from operationally oriented satellites that are supported 24 hours a day/7 days a week. These are summarized in Figure 1. The color coding is such that those shaded in yellow are derived from polar orbiting satellites (e.g., POES, MetOp and DMSP); those shaded in pink are derived from NOAA geostationary satellites (e.g., GOES series); those shaded in green are “blended” products, using multiple satellite sources to develop enhanced precipitation products to users. Also in the Figure are the current capabilities and those envisioned to be implemented over the next five years. Each of these products is described further in this section of the paper.

Applications	Current Capability	Future Capability
MSPPS	AMSU Rain Rate, TPW, CLW, etc. (NOAA-15*, -16, -18, -19 and Metop-A)	Extended to include Metop-B MIRS will be the upgrade of MSPPS as NOAA enters to NPP, JPSS, and GPM era.
MIRS	AMSU Rain Rate, TPW, CLW, etc. (NOAA-18, -19, DMSP F16, Metop-A)	AMSU/MHS Rain Rate (DMSP F18, F19, Metop-B) ATMS Rain Rate (NPP, JPSS) GPM Rain Rate (M-T, GMI)
Hydro-Estimator	Instantaneous, 1-hr, 3-hr, 6-hr and 24-hr rainfall estimate over CONUS (GOES-11 and -13)	Extended to include multi-day rainfall estimate. Extended coverage from CONUS to global ScaMPR will be the upgrade of HE (GOES-R)
SCaMPR	Runs experimentally over CONUS and surrounding areas	1-hour, 6-hour and 24-hour rainfall total over Western Hemisphere (GOES-R)
Blended Hydro	Blended TPW and TPW percentage of normal products (NOAA-15, -16, -17, -18, -19, Metop-A, GPS, GOES, DMSP F13*, F14*, F15*) Blended RR products (NOAA-15, -16, -18, -19, Metop-A, DMSP F16, F17)	Blended TPW and TPW percentage of normal (Extended to include: DMSP F16, F17, F18 NPP, M-T, GCOM-W, JPSS, GOES-R) Blended RR products (Extended to include: DMSP F18, NPP, M-T, GCOM-W, GMI, JPSS)
eTRAP	Deterministic rain amount and probabilistic POP forecasts for each of four 6h time periods (e.g., 00-06h, 06-12h, 12-18h, 18-24h) as well as the 24 hour cumulative time period. (Rain Rate from NOAA-15, -16, -18, -19 and Metop-A, TRMM TMI, Aqua AMSR-E)	Extended to include: F16, F17, F18, HE, NPP, M-T, GCOM-W, JPSS, GMI

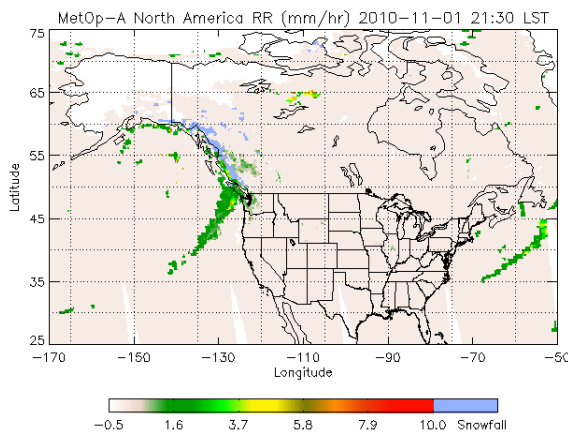
Figure 1 – Summary of operational NOAA/NESDIS precipitation products.

2.1 POES Based Products

The two primary POES based precipitation products are derived from the NOAA POES and EUMETSAT MetOp AMSU and MHS passive microwave sounders. The product systems are known as the Microwave Precipitation Products Systems (MSPPS) and the Microwave Integrated Retrieval System (MIRS). Figure 2 presents some examples of MSPPS and MIRS precipitation products.

MSPPS is NOAA's "legacy" AMSU retrieval system, with its roots dating back to NOAA-15 which was launched in 1998. The best summary of the MSPPS products can be found in Ferraro et al. (2005) whereas the most recent aspects of the precipitation retrieval are documented in Vila et al. (2007). Additionally, some recent applications of the MSPPS products are summarized in Ferraro et al. (2010). A snowfall rate addition to the current MSPPS snow identification algorithm (Kongoli et al. 2003) will be implemented in 2011. Further information on the MSPPS products as well as real-time imagery can be found at <http://www.star.nesdis.noaa.gov/corp/scsb/mspps/main.html> and <http://www.osdpd.noaa.gov/ml/mspps/index.html>. Data are readily available in near-real time from NOAA/NESDIS and are archived on the NESDIS CLASS system (<http://www.class.noaa.gov>).

MIRS was designed to take advantage of advanced physical models that can be ported to a wide array of microwave sensors, plus, take advantage of the sounding capabilities of the AMSU and MHS sensors (Boukabara et al. 2007). It also is highly desirable in an operational environment because the same physics package (e.g., 1DVAR scheme) is applied to multiple satellite data streams, thus, eliminating the so-called "stove pipe" systems that historically were needed for each individual satellite and sensor. The MIRS approach fully integrates the maximum information available for a particular sensor, thereby offering improved accuracy for individual products beyond MSPPS, plus, physical consistency between surface and atmospheric parameters. For example, the sounding information on AMSU improves the precipitation rates while the emissivity calculations improve retrievals along coastlines and sea-ice boundaries. MIRS will eventually replace MSPPS as the primary products system at NESDIS as we enter into the NPP and JPSS era. Further information on the MIRS products as well as real-time imagery can be found at <http://mirs.nesdis.noaa.gov/> and <http://www.osdpd.noaa.gov/ml/mirs/>. Data are readily available in near-real time from NOAA/NESDIS and are archived at NESDIS



CLA
SS.

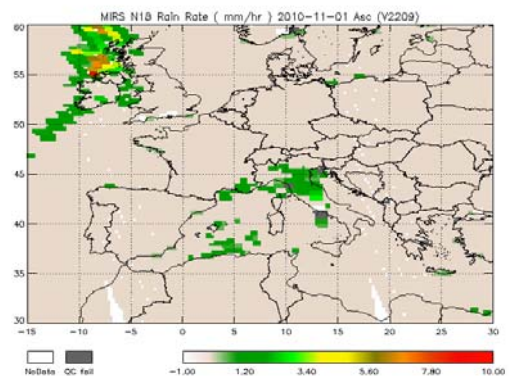


Figure 2– Example of MSPPS (left) and MIRS (right) precipitation rates for 1 November 2010.

2.2 GOES Based Products

Because of the demand for high time and space resolution precipitation products to support NOAA mission critical forecasts in flooding situations, NOAA/NESDIS has a legacy of innovative uses of GOES-based visible and infrared measurements to develop precipitation products. Perhaps the most widely used product is the HydroEstimator (HE; Vicente et al. 1998; Scofield and Kuligowski 2003), which is not only used at NOAA, but also by several other government agencies in other parts of the world to support flash flood forecasting (e.g., Brazil and South Africa). The HE relies on infrared estimates and NWP model information to adjust for precipitation efficiency and orography. More information as well as product imagery can be found at <http://www.star.nesdis.noaa.gov/smcd/emb/ff/HydroEst.php> and <http://www.ssd.noaa.gov/PS/PCPN/HE.html>.

To take advantage of additional information available in the near-IR spectrum as well as passive microwave information, an emerging technique known as the Self Calibrating Multivariate Precipitation Retrieval (SCaMPR; Kuligowski 2002) is being developed and will be the primary precipitation algorithm in the GOES-R era (2016 and beyond). GOES-R will also feature additional precipitation products such as 0-3 h rainfall potential and rainfall probability. Further information as well as product imagery for SCaMPR can be found at <http://www.star.nesdis.noaa.gov/smcd/emb/ff/SCaMPR.php>.

Figure 3 shows some examples of the HE and SCaMPR products.

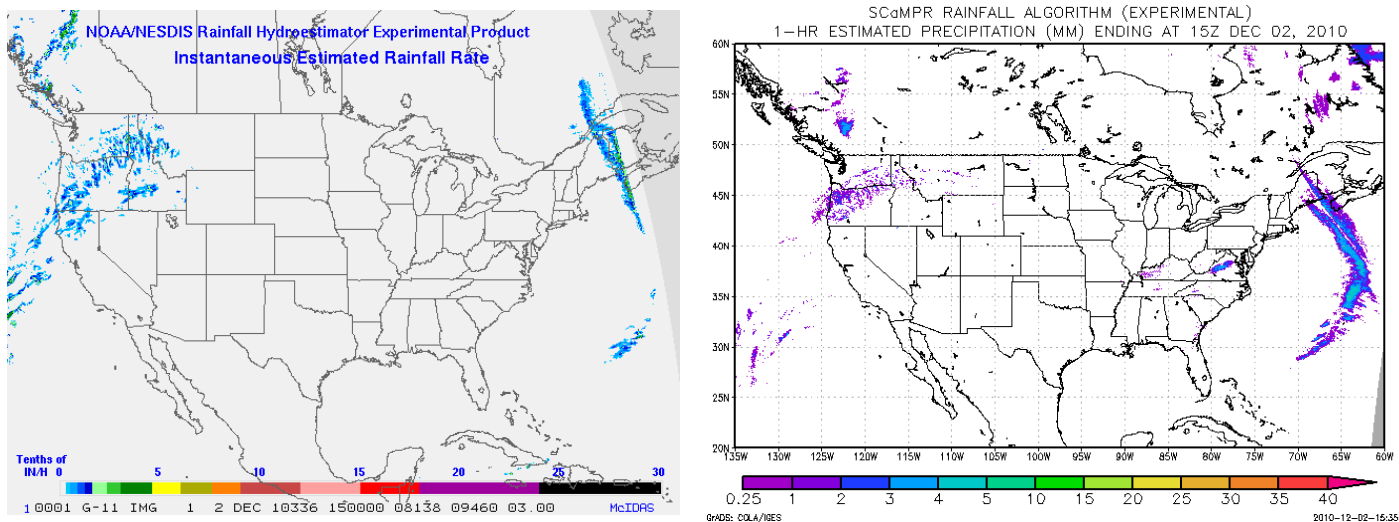


Figure 3– NESDIS HE (left) and SCaMPR (right) hourly precipitation for 1500 UTC 2 Dec 2010.

2.3 Blended Products

One disadvantage of polar orbiting satellites is their coarse temporal resolution: each satellite at best revisits a location on the Earth's surface every 12 hours. In the operational environment, the POES are configured such that their orbital overpass times

are spaced approximately 4 hours apart. In this three-satellite configuration, NOAA, the US Department of Defense and EUMETSAT, similar measurements of precipitation and total precipitable water (TPW) are available more frequently than if just one satellite is considered. In addition, with several backup satellites still in operation, global coverage every 3 hours is commonplace.

Rather than maintain separate product data streams for each satellite and product to support NOAA/NWS forecasters, NESDIS has recently developed product composites of the MW derived rainfall and TPW estimates from the full suite of sensors into a single image. The product is updated as soon as a new orbit of data is processed. Two such products are described below.

Perhaps the most widely used product is the blended TPW, which is extremely useful to forecasters to monitor “atmospheric rivers” that contribute to prolonged rainfall events and subsequent flooding (Ferraro et al. 2010). The NESDIS blended TPW, developed by researchers at CIRA (Kidder and Jones 2007) incorporates the TPW derived from AMSU, SSM/I and ground based GPS stations over the United States to form the composite. Special care must be taken to “normalize” the estimates to one of the sensor types to minimize biases and to make the product look “seamless”. Work is underway to bring in the MIRS TPW over land and TPW derived from other sensors like the SSMIS and AMSR-E. Figure 4 presents an example of the blended TPW product. More information on this product can be found at <http://www.osdpc.noaa.gov/bTPW/index.html>. Additionally, a companion blended rainfall rate product is being developed in much the same way. It is expected to become operational in 2011 or 2012.

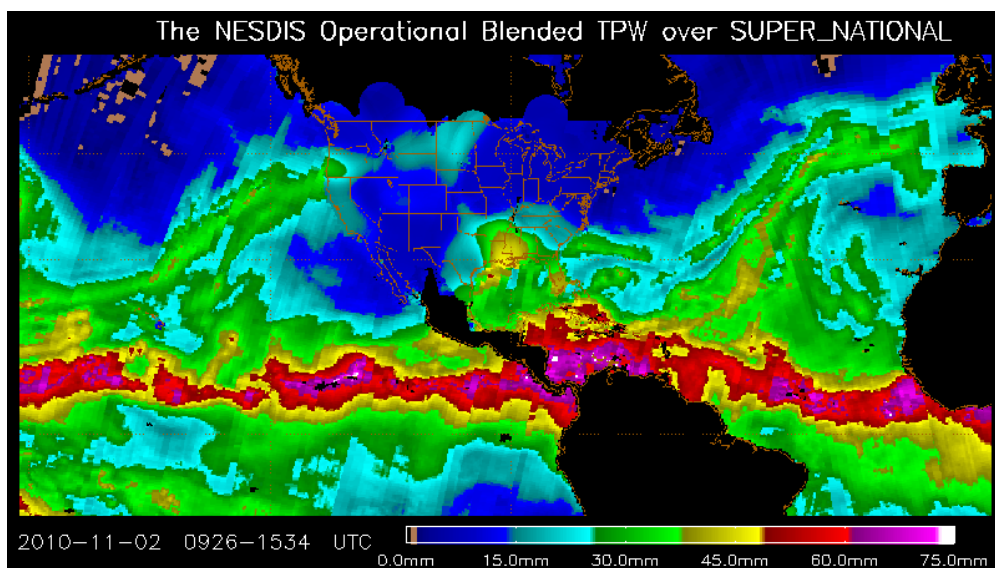


Figure 4– Example of the blended TPW product for 2 November 2010. In this example, the data has been composited for an approximate 6 hour period between 0926 and 1534 UTC.

Another blended rainfall product is the Ensemble Tropical Rainfall Potential (eTRaP) product (Ebert et al. 2010). eTRaP has its roots with the original TRaP product, which was a simple advection and accumulation of passive microwave rainfall fields along the predicted track of a tropical cyclone. This product was also developed at CIRA (Kidder

et al. 2005). Because of biases found within individual rainfall estimates for the various microwave products (AMSU, TMI, SSM/I, AMSR-E, etc.), the eTRaP combines these into a single product by weighting both the product accuracy and time latency from the forecast period. eTRaP also provides deterministic and probabilistic forecasts. The product is generated for all oceanic basins and is widely used by the international forecasting community. Figure 5 presents an example of the eTRaP for Hurricane Richard as it approached the Yucatan Peninsula in Mexico. The product and further information can be found at <http://www.ssd.noaa.gov/PS/TROP/etrap.html>.

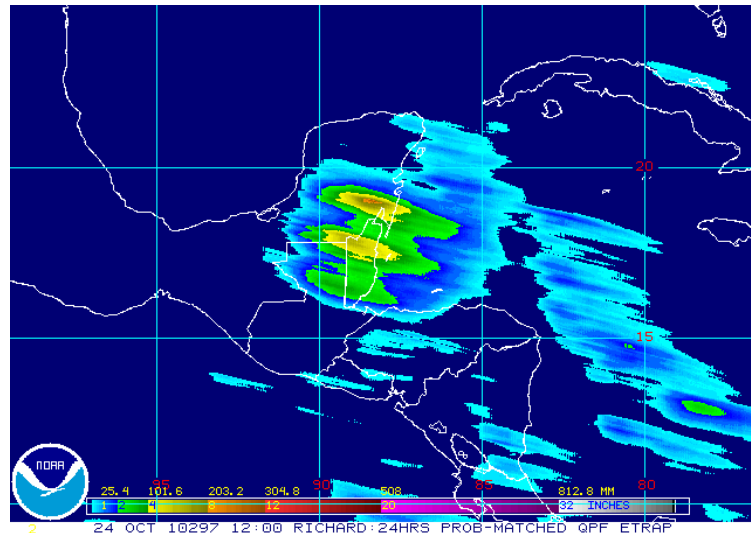


Figure 5– 24-hour eTRaP rainfall estimate for Hurricane Richard for the period ending 1200 UTC on 24 October 2010.

3. VALIDATION EFFORTS

A topic that is of major interest to IPWG--validation of precipitation products--is often difficult to perform and does not always accurately reflect the usefulness of the satellite estimates. Nonetheless, precipitation products, in particular, operational products, need to be routinely monitored and validated so that the user community (and the algorithm developers) can better understand the most effective way to utilize such products.

The IPWG has developed an effective method to validate the satellite products through the use of national radar and gauge networks, and through a “standard” package developed under the auspices of the IPWG validation working group (Ebert et al. 2007). At NESDIS, this process was taken one step further by establishing a “precipitation validation center” whose responsibility is not only to generate and maintain the validation processing system, but to evaluate them in detail and report on their performance to the NESDIS Precipitation Product Oversight Panel (PREPOP), who oversees the development and implementation of the NESDIS products. The validation center also can determine the impact of algorithm upgrades and intercompare emerging techniques. J. Janowiak and D. Vila, both CICS scientists, presently lead these activities in support of NESDIS.

During the past year, they have built off their IPWG activities over the U.S. and South America to perform swath validation for all of the POES and GOES products previously described in this paper. Figure 6 shows an example of some of their recent activities. More information and results can be found at http://cics.umd.edu/~johnj/STAR/html/MAIN_page.html.

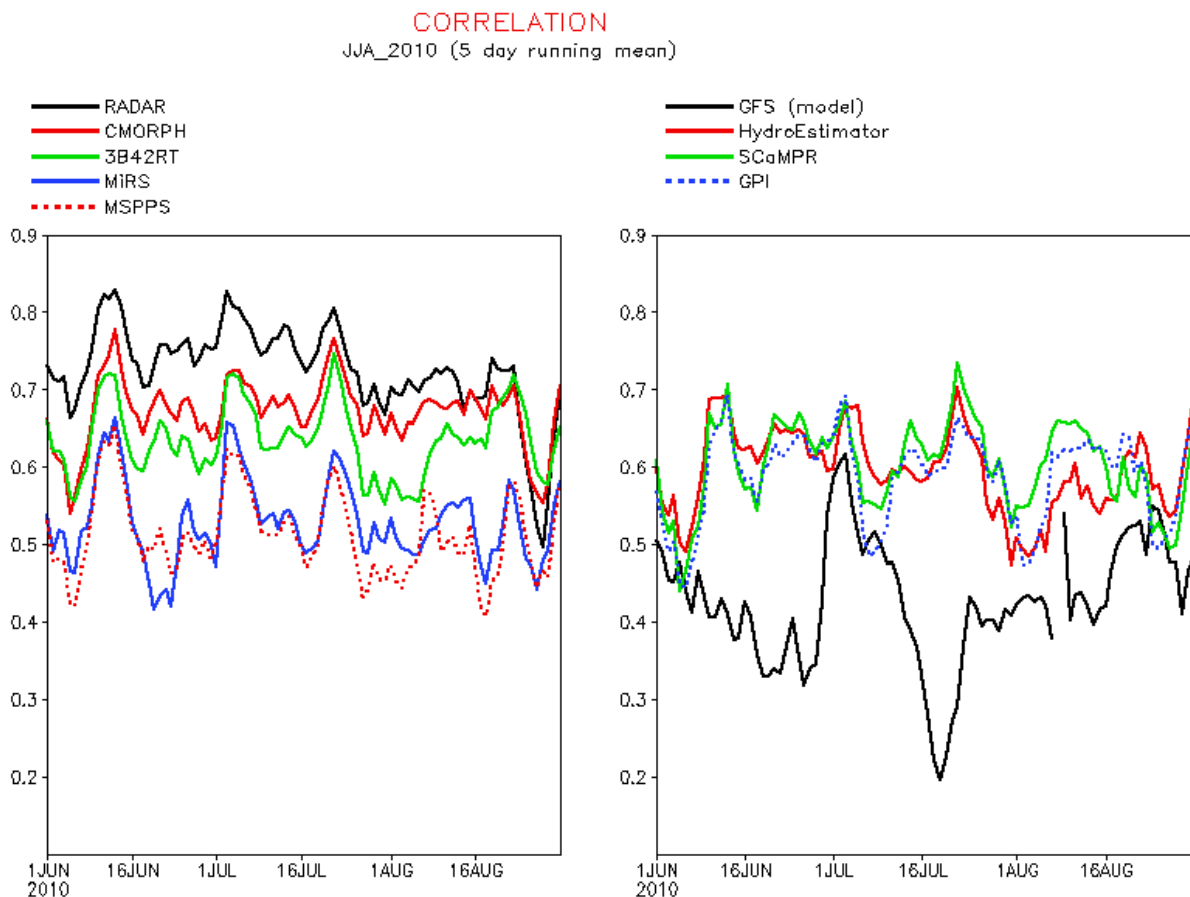


Figure 6— Correlation (5-day running mean) between satellite rainfall estimates with rain gauges over the United States for the period June 1 – August 31, 2010. Radar and NWP model data are included for comparison.

4. NON-NOAA SATELLITE PRODUCTS

Some of the earliest work performed at NOAA/NESDIS in the area of precipitation retrievals from passive microwave sensors was carried out through the use of DMSP Special Sensor Microwave/Imager (SSM/I). Many of these algorithms are still in use today (Ferraro et al. 1996; Ferraro 1997). This sensor, in operation for over 20 years on six different satellites, has been the cornerstone of much of the research, development and applications of passive microwave data that continues to evolve today.

Over the past decade, “research” satellite missions and their corresponding advanced precipitation retrievals have worked their way into supporting operational agencies like

NOAA, JMA, UKMET and ECMWF. NOAA has played an integral part in the development of algorithms for use with the TRMM and AMSR-E missions, in particular with the precipitation over land retrievals. Most recently, an upgrade to the TMI algorithm has been developed which substantially reduces a warm season bias that has been prevalent for a number of years (Wang et al. 2009; Gopalan et al. 2010). Figure 7 shows the improvement of the new algorithm compared to the current one, with the TRMM PR serving as the reference. Details are provided in Gopalan et al. (2010).

NOAA is also actively involved with the upcoming GPM mission, where the current precipitation algorithms will be enhanced to include falling snow and to utilize land surface emissivity information to allow for a more direct estimation of rainfall over land. NOAA is working with NASA to coordinate on a potential GPM follow on capability.

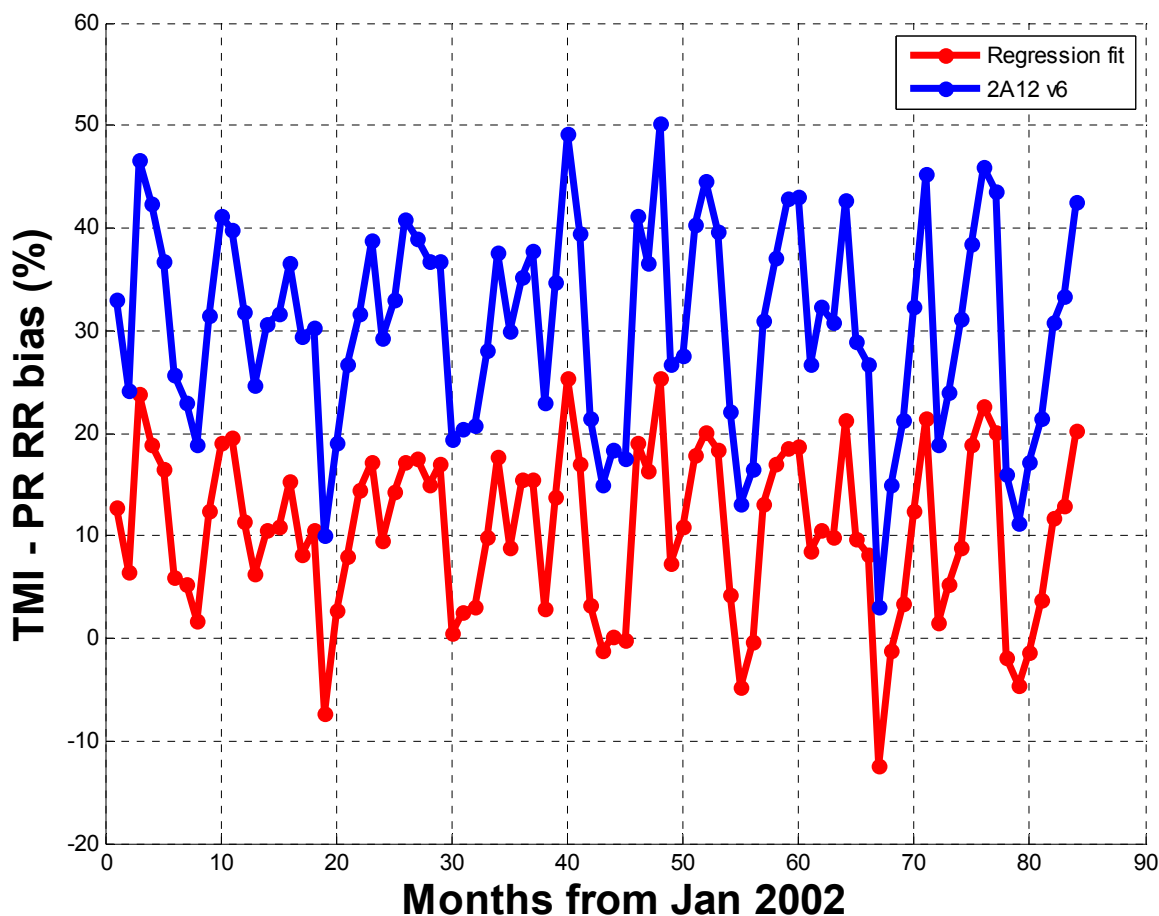


Figure 7– Monthly mean biases between the TRMM TMI 2A12 products and the PR 2A25 product for the current algorithm (blue) and the improved algorithm (red).

5. CLIMATE PRODUCTS

Developing stable, long term time series of precipitation information is a challenging problem. NOAA/NESDIS continues to be involved in several projects related to precipitation climatologies. The first and most mature is our contribution to the

GEWEX/Global Precipitation Climatology Project (GPCP), which has perhaps the most widely used global monthly climatology ever assembled to date. The GPCP monthly climatology is over 30 years in length. NESDIS is responsible for the delivery of SSM/I derived rainfall estimates over land; recent work has focused on the transition from SSM/I to SSMIS in the time series (Semunegus et al. 2010; Vila et al. 2010). Critical issues are the calibration of the SSMIS sensors and the shift from 85 to 91 GHz, which is the key frequency used to detect precipitation over land. NOAA/NCEP contributes the global IR information. CICS and our colleagues at NASA/GSFC are responsible for merging the satellite and gauges (provided by GPCC) into the final product. The GPCP data set can be obtained from <http://lwf.ncdc.noaa.gov/oa/wmo/wdcamet-ncdc.html>.

Emerging from NESDIS is NOAA's Climate Data Record (CDR) program, whose goal is to develop both Fundamental CDR's (FCDR – well calibrated and intersatellite calibrated radiances) and Thematic CDR's (TCDR – derived products such as precipitation). Two key projects are underway with passive microwave sensors: SSM/I CDR's and AMSU CDR's. NESDIS and it's CI partners, CICS and CIRA, are leading these efforts. Details on the CDR program can be found at <http://www.ncdc.noaa.gov/sds/index.html>. Other projects include the development of a high time/space scale microwave based rainfall time series (Joseph et al. 2009) and precipitation reconstructions using surface temperature (land and ocean) measurements to develop global climatologies back to 1900 (Smith et al. 2010). In the reconstruction work, the satellite rich era of data is used to develop the reconstruction tools for the pre-satellite era. More information and access to the data can be found at <http://www.atmos.umd.edu/~rjoseph/CHOMPS/CHOMPS.htm> and <http://cics.umd.edu/~tsmith/PR/PR.html>.

6. SUMMARY AND FUTURE

NOAA/NESDIS and its Cooperative Institute partners continue to be involved in several areas of precipitation product development, implementation and new applications using satellite measurements. NESDIS maintains a suite of operational POES and GOES based products, as well as emerging blended products such as ScaMPR, blended TPW and rain rates, and eTRaP. These products will continue with upcoming satellite series, including NPP, JPSS and GOES-R. Additionally, NESDIS is active with research related to non-NOAA missions such as DMSP, EOS, TRMM and GPM. Not only do these research missions serve as prototypes for future operational sensors, they are integral parts of NOAA operations; thus, they can have immediate impact to forecast accuracy if they are planned for well in advance. Such activities are ongoing with the upcoming GPM launch in 2013.

The views, opinions, and findings contained in this report are those of the author(s) and should not be construed as an official National Oceanic and Atmospheric Administration or U.S. Government position, policy, or decision.

7. REFERENCES

- Boukabara, S., F. Weng, and Q. Liu, 2007: Passive microwave remote sensing of extreme weather events using NOAA-18 AMSUA and MHS. *IEEE Trans. Geosci. Rem. Sens.*, **45**, 2228-2246.
- Ebert, E.E., J.E. Janowiak, and C. Kidd, 2007: Comparison of near real time precipitation estimates from satellite observations and numerical models. *Bull. Amer. Met. Soc.*, **88**, 47-64.
- Ebert, E., M. Turk, S. Kusselson, J. Yang, M. Seybold, P. Keehn and R. Kuligowski, 2010: Ensemble tropical rainfall potential (eTRap) forecasts. In press, *Weather and Forecasting*, doi: 10.1175/2010WAF2222443.1)
- Ferraro, R.R., F. Weng, N.C. Grody, and A. Basist, 1996: An eight year (1987-94) climatology of rainfall, clouds, water vapor, snowcover, and sea-ice derived from SSM/I measurements. *Bull. of Amer. Meteor. Soc.*, **77**, 894-905.
- Ferraro, R.R., 1997: SSM/I derived global rainfall estimates for climatological applications. *J. Geophys. Res.*, **102**, pp 16,715-16,735.
- Ferraro, R.R., F. Weng, N. Grody, L. Zhao, H. Meng, C. Kongoli, P. Pellegrino, S. Qiu and C. Dean, 2005: NOAA operational hydrological products derived from the AMSU. *IEEE Trans. Geo. Rem. Sens.*, **43**, 1036 – 1049.
- Ferraro, R., S. Kusselson, S. Kidder, L. Zhao and H. Meng, 2010: Application of AMSU-Based Products to Support NOAA's Mission Goals. *National Weather Digest.*, **34**, 1-14.
- Gopalan, K., N.Y. Wang, C. Liu and R. Ferraro, 2010: Version 7 of the TRMM 2A12 Land Precipitation Algorithm. In press, *J. Atmos. Oceanic Tech.*.
- Joseph, R., T.M. Smith, M.R.P. Sapiano, and R.R. Ferraro, 2009: A new high resolution satellite derived precipitation data set for climate studies. *J. Hydromet.*, **10**, 935-952.
- Kidder, S., J. Knaff, S. Kusselson, R. Ferraro, R. Kuligowski and M. Turk, 2005: The Tropical Rainfall Potential. Part 1: Description and Examples. *Weather and Forecasting*, **20**, 456 – 464.
- Kidder, S. and A. Jones, 2007: A blended satellite total precipitable water product for operational forecasting. *J. Atmos. Ocean. Tech.*, **24**, 74-81.
- Kongoli, C., P. Pellegrino and R. Ferraro, 2003: A new snowfall detection algorithm over land using measurements from the AMSU, *Geophys. Res. Let.*, **30**, 1756-1759.

Kuligowski, R. J., 2002: A self-calibrating real-time GOES rainfall algorithm for short-term rainfall estimates. *J. Hydrometeor.*, **3**, 112-130.

Semunegus, H., W. Berg, J. Bates, K. Knapp, C. Kummerow, 2010: An extended and improved Special Sensor Microwave Imager (SSM/I) period of record. *J. of Appl. Meteor. Clim.*, **49**, 424-436.

Scofield, R. A., and R. J. Kuligowski, 2003: Status and outlook of operational satellite precipitation algorithms for extreme-precipitation events. *Mon. Wea. Rev.*, **18**, 1037-1051.

T.M. Smith, P.A. Arkin, M.R.P. Sapiano, C.-Y. Chang, 2010: Merged statistical analyses of historical monthly precipitation anomalies beginning 1900. *J. Climate*, **23**, 5755 – 5770.

Vicente, G. A., R. A. Scofield, and W. P. Menzel, 1998: The operational GOES infrared rainfall estimation technique. *Bull. Amer. Meteor. Soc.*, **79**, 1883- 1898.

Vila, D., R. Ferraro, R. Joyce, 2007: Evaluation and Improvement of AMSU Precipitation Retrievals. *J. Geophys. Res.*, **112**, D20119, doi:10.1029/2007JD008617.

Vila, D. R. Ferraro and H. Semunegus, 2010: Improved global rainfall retrieval using the Special Sensor Microwave Imager (SSM/I). *J. Appl. Meteor. Clim.*, **49**, 1032 – 1043.

Wang, N., C. Liu, R. Ferraro, D. Wolff, E. Zipser and C. Kummerow, 2009: The TRMM 2A12 Land Precipitation Product – Status and Future Plans, *J. of Meteor. Soc. Of Japan.*, **87**, 237 – 253.

MULTI-SITE AND MULTI-OBJECTIVE EVALUATION OF HIGH-RESOLUTION SATELLITE-RAINFALL PRODUCTS

Emad Habib¹, Alemseged T. Haile¹, Mohamed EISadani¹, Mohamed ElShamy²,
Robert Kuligowski³, Yudong Tian⁴

¹Department of Civil Engineering, University of Louisiana at Lafayette, LA,
PO Box 70504 USA

²Nile Forecasting Center, Cairo, Egypt

³NOAA/NESDIS/Center for Satellite Applications and Research, USA

⁴NASA GSFC, Greenbelt, MD 20771 and ESSIC, Univ. Maryland, USA

e-mail: habib@louisiana.edu

We evaluated two satellite-rainfall products for hydrologic and climatologic purposes in different world regions. These products are the 'Tropical Rainfall Measuring Mission (TRMM) and other sources' (TRMM-3B42) product and the National Oceanographic and Atmospheric Administration Climate Prediction Center (NOAA-CPC) product which is based on the CPC morphing technique (CMORPH). First, we evaluated the rainfall products at an hourly and event time scales using gauge records from a dense network in the south Louisiana and a radar-based multi-sensor rainfall product. The CMORPH estimates successfully detected rainfall occurrences at least 30 % of the time and reported false detection only <4 % of the time. Specifying radar estimates instead of gauge records as a reference significantly changed the hit bias and the missed rain by the satellite estimates but it only slightly affected the total bias and the false rain. Next, we evaluated the satellite products for hydrologic as well climatologic purposes over the Nile basin in Africa. Over most parts of the Nile basin that are situated north of the equator, the CMORPH estimates show a wet bias while the TRMM-3B42 estimates show a dry bias. The estimates from both products were within the range of values of the climatologic records over parts of the basin around the equator. Both products reproduced the diurnal cycle of rain occurrence over the Lake Tana basin (the source of the Blue Nile) except over the mountains and the Lake shore. However, the TRMM-3B42 estimates underestimated the rainfall amounts in this basin. The satellite products captured the contrasting patterns of the diurnal cycles of rain occurrence and amount over the surroundings of Lake Victoria (the source of the White Nile). Finally, we showed that the performance of a basin-wide hydrologic model of the Nile river significantly improves when the CMORPH estimates serve as inputs instead of the IR-based estimates which are traditionally used by the Nile Forecasting Center in Egypt. In the Blue Nile basin, the relative volume error of the simulated flow decreased from -40 % when IR-based estimates served as the model input to -4 % when the CMORPH estimates served as the model input. However, merging the IR-based estimates with gauge data resulted in higher Nash-Sutcliffe model efficiency coefficient (0.86) than that of merging the CMORPH estimates with gauge data (0.8). The results suggest that the satellite estimates still can have an application in large-scale hydrologic modeling despite their significant error at finer scales.

EUMETSAT'S ACTIVITIES IN SUPPORT OF PRECIPITATION REMOTE SENSING

Thomas Heinemann

EUMETSAT, Meteorological Operations Division,
EUMETSAT Allee 1, Darmstadt, Germany

e-mail: Thomas.Heinemann@eumetsat.int

ABSTRACT

In recent years, the way in which operational satellite data providers support the meteorological and hydrological user communities in their precipitation related activities has developed significantly. Today, EUMETSAT provides not only relevant operational satellite data and products but covers also other important precipitation related aspects in the framework of its distributed ground segment.

The transfer of state-of-the-art algorithms to the operational stage is performed in the context of the EUMETSAT H-SAF and will supplement the list of EUMETSAT products for the users. At the same time, the long-term availability of the near-real time heritage-product MPE has been insured by adding SSMIS to the sources of microwave data for the blending algorithm.

In the next years it will become more and more important to find a reliable mechanism to make relevant satellite data also from non-operational satellites available to the users. For the timely provision of precipitation related data and products from current and future satellites, the satellite based NRT data distribution system EUMETCast is undergoing a continuous extension and improvement process. Meanwhile, EUMETCast distributes not only data from EUMETSAT satellites, but also satellite data and products from other sources (e.g. GOES, SSMIS, MODIS). In the future this list will be extended on the basis of user needs. EUMETSAT will also co-operate with the precipitation community in the form of a GPM partnership.

The future generation of EUMETSAT satellites, in the MTG as well as the EPS-SG program, will continue to deliver valuable data for precipitation remote sensing. In the planning process for those missions, the requirements from the meteorological, hydrological, and climate communities for precipitation retrieval are part of the considerations for the satellite and instrument design.

The training of the various groups of users in the evaluation and application of satellite based precipitation data in their daily work, is an important component in EUMETSAT's training activities, reaching out not only to EUMETSAT member states but also to Africa, the Middle East, and Eastern Europe.

1. INTRODUCTION

The connection between scientific development and operational application is a key factor for the success of new technologies. In satellite remote sensing, the high complexity of the systems requires a detailed analysis of the involved processes which connect satellite, instrument and algorithm development on the one side together with operational production and application on the other side.

The diagram in Fig. 1 illustrates the operational and scientific lifecycles which are involved in the generation of satellite data products. The yellow circle represents a typical operational development and production cycle. Based on user requirements a satellite and the instruments onboard of the satellite are build and the most appropriate algorithms for the required products are implemented in the data processing chain. Operational quality monitoring is applied and user support as well as training is provided to help the users in the application of the data. These tasks usually fall in the responsibility of satellite providers or associated operational organisations.

The red arrows are corresponding to processes and activities in the scientific environments. New instruments and algorithms are developed, tested and validated until they are considered to be mature enough to be used operationally.

The problems are occurring at the interfaces between the two worlds. The blue arrows represent the transitions from one to the other of the two cycles.

In this paper EUMETSAT's activities in support of precipitation remote sensing are sketched, with a special focus on the transition between scientific and operational environments.

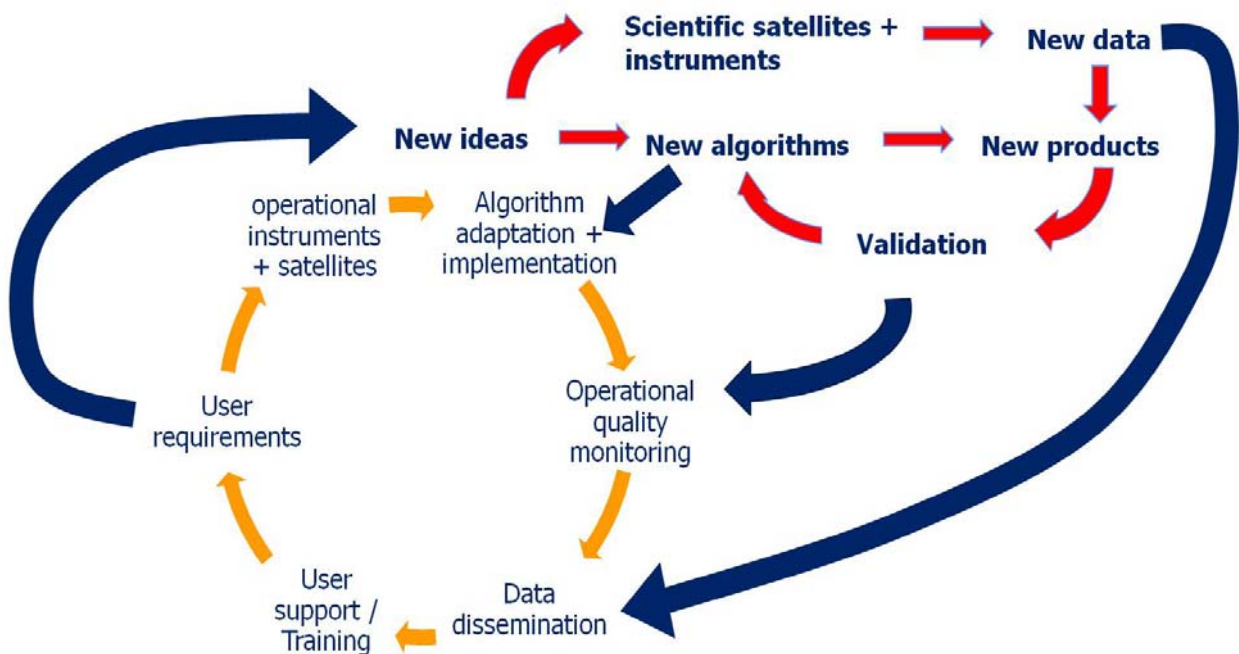


Figure 1. Schematic overview of scientific and operational lifecycles for the generation of satellite data products

2. H-SAF PRODUCT DEVELOPMENT

The most direct link between scientific and operational developments is the transfer of algorithms from experimental to operational application. For the precipitation remote sensing, the transfer and adaptation of enhanced scientific algorithms has been assigned as a major task to the SAF on Support to Operational Hydrology and Water Management (H-SAF).

In 1992 EUMETSAT adopted the concept of a Distributed Application Ground Segment including the EUMETSAT Central Facilities in Darmstadt and a network of elements known as Satellite Application Facilities (SAF), as specialised development and processing centres. SAFs utilise the specific expertise available in EUMETSAT's Member and Cooperating States. The SAF network complements the production of standard meteorological products derived from satellite data at the central facilities in Darmstadt and also distributes user software packages. SAFs are developed by consortia of organisations from the EUMETSAT Member States and Cooperating States, and are located at the National Meteorological Services in Member States.

The host institute of the H-SAF is the Italian Meteorological Service (USAM). Its products are covering four major thematic areas: precipitation, soil moisture, snow parameters and the utilisation of these parameters in hydrological models and NWP (validation programme). The H-SAF started the Development Phase in September 2005 and entered its Continuous Development and Operations Phase (CDOP) in September 2010.

The following precipitation products have been developed by the H-SAF and will become available operationally:

PR-OBS-1 and PR-OBS-2, Instantaneous precipitation rate at ground from MW, with indication of the phase (liquid or solid): These products are based on measurements from imaging and sounding passive microwave instruments onboard of polar orbiting satellites, such as SSMIS, AMSU and MHS. Products will be delivered with a timeliness of less than 3 hours. The PR-OBS-1 and PR-OBS-2 products are also input for the combined algorithms PR-OBS-3 and PR-OBS-4.

PR-OBS-3, Instantaneous precipitation rate at ground observed in MW+IR, with indication of the phase (liquid or solid): For this product data from the geo-stationary MSG satellites are combined with the PR-OBS-1 products from the polar orbiting satellites by the application of a blending approach. The product is produced and disseminated in near-real-time for each MSG repeat cycle. Fig. 2 shows an example of the product.

PR-OBS-4: Instantaneous precipitation rate at ground, from MW morphed by IR: This product will provide instantaneous rain rates from MW data propagated between the satellite overpasses by motion vectors derived from geo-stationary imagery.

PR-OBS-5, Cumulated precipitation over 3, 6, 12 and 24 hours, observed in MW + IR: The cumulated products are based on the PR-OBS-2 products and contain the corresponding accumulated precipitation.

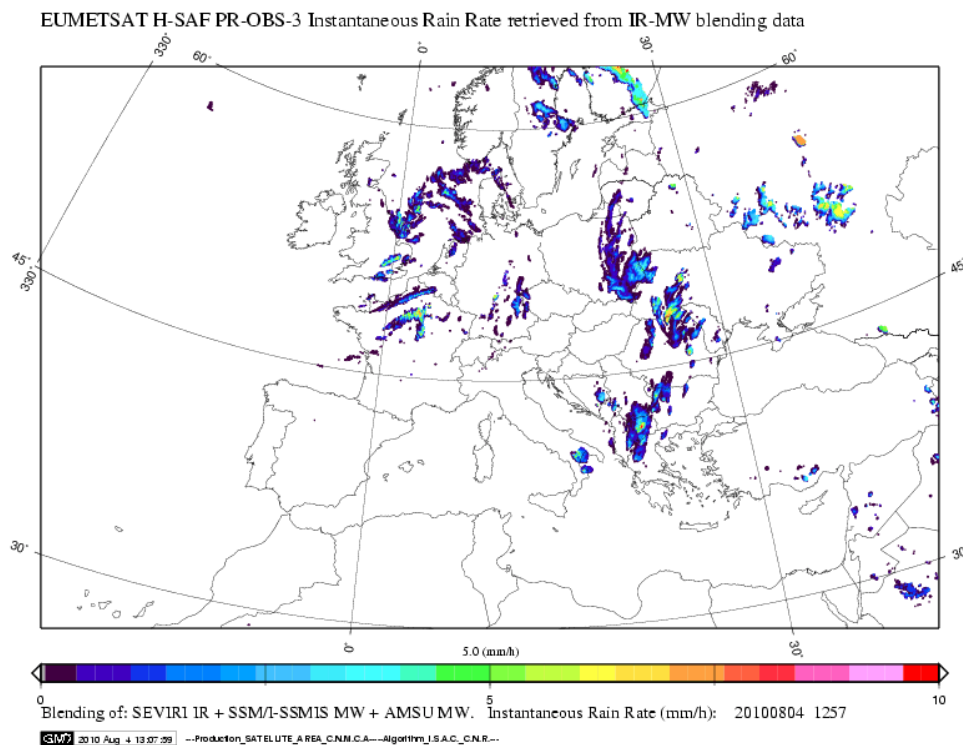


Figure 2. H-SAF PR-OBS-3 instantaneous rain rate product derived by blending of METEOSAT-9 IR data with rain rates derived from SSM/I, SSMIS and AMSU.

3. PRECIPITATION PRODUCT QUALITY MONITORING

The highly complex task of satellite precipitation product validation has been approached by various groups around the world. The range spans from regional validations against rain-gauges to continental validations against ground-based radar data. A special role in this context plays the validation by the application of precipitation data in hydrological models as it is done for example by the H-SAF.

Many of the tools developed for the validation of precipitation products can be adapted for the application in the operational product quality monitoring. This transfer is symbolised by the blue arrow in the middle-right of Fig. 1.

Automated product quality monitoring is essential for an operational processing chain, because the timely delivery of the products requires an on-line check of the product and cannot wait for the regular product validation. By these checks sudden changes as well as long-term trends in the product quality can be observed. Making the results of the quality monitoring available to the users, e.g. with the product as quality indicators, can give the user more confidence in the application of the product.

A prerequisite for the quality monitoring is the scientific validation of the algorithm and the regular validation of the product. Depending on the requirements and the availability

of reference data, operational product quality monitoring can be performed on various levels of complexity:

1. Product statistics: The simplest method to track sudden changes and unexpected results in the product contents are statistical measures like maximum, minimum, total and regional averages or standard deviations. This method is usually only good enough to detect major errors in the processing. EUMETSAT has introduced product statistics for all L2-products.
2. Algorithm-internal quality information: Most algorithms produce information on the confidence which can be used to monitor the expected product quality. This information can be e.g. the distance from thresholds in threshold-based algorithms, the time from the last calibration data set in a morphing algorithm, or the cost-function in an OE-algorithms. Fig 3. shows one of the quality indicators of EUMETSAT's Multi-sensor Precipitation Estimate product as an example for this type of information. The MPE algorithm is based on the blending technique and this quality indicator describes the correlation between the passive microwave rain-rates which have been used to calibrate the IR-retrieval and the IR-retrieval itself. A detailed description MPE and the quality indicators can be found in Heinemann, 2002.

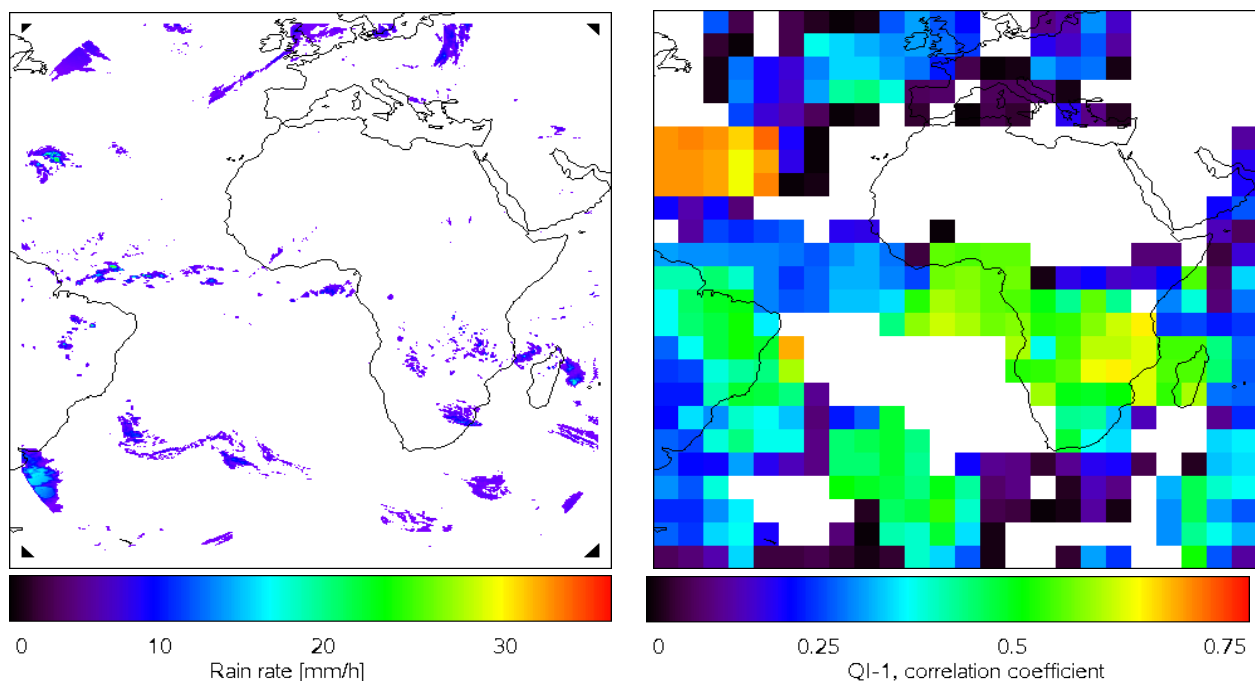


Figure 3: Rain retrieval with the EUMETSAT Multi Sensor Precipitation estimate (MPE).
Left image: Retrieved rain rate in mm/hr. Right image: Quality indicator based on the

correlation between rain-rates derived from SSM/I and the co-located rain-rates of the MPE algorithm.

3. Comparison with other satellite products: The operational comparison of two satellite precipitation-rate products can make sense if the algorithms are based on different approaches or if the products are derived from different satellites. The major problem with this method is that in case of a discrepancy between the two data sets, the problem can be with the any of the two products. Therefore, the inter-comparison should never be the only monitoring method.

4. Comparison with independent data-sets: The most sophisticated method is the routine comparison with independent data like ground-based radar, rain-gauge networks or model analysis or forecast data. For precipitation retrieval monitoring forecast data are not providing the required accuracy and the other external data sources are usually only available with a certain delay. Therefore this method is most suitable for the monitoring of products which are not delivered in NRT. The validations performed by several IPWG-participants, e.g. the inter-comparison activities by the University of Birmingham (Kidd et al 2008) could be used as monitoring methods. Since these services are usually not operational and the validation data sets can also be influenced by errors, also this method should always be applied in conjunction with method 1 and/or 2.

4. INTEGRATION OF NEW SATELLITE DATA INTO OPERATIONS

In the past there was a clear distinction between experimental and operational satellites. Satellites which were designed for scientific prove-of-concept studies hardly ever were used by operational users. This situation has changed with longer lifetime of satellites and instruments and easier availability of data from research organisations like NASA, ESA, ISRO or CNES. A good example is the TRMM mission which started as a research project and is today one of the most important sources of operational satellite based rainfall measurements in tropical regions.

Key for the application of new satellite data by operational users is the timely and reliable availability. Established dissemination routes of operational data providers are designed to fulfil these requirements. Adding new satellite data to these dissemination routes is therefore a very effective way to bring them into operations. The long blue arrow on the right in Fig.1 symbolises this process.

EUMETSAT is providing with the EUMETCast satellite dissemination system a scalable and reliable way to disseminate various meteorological data and products to Europe, Africa and South America. A detailed description of EUMETCast and its role in the world-wide GEONETCAST data exchange and dissemination system can be found on the EUMETSAT web-page (www.eumetsat.int).

Fig. 4 illustrates the role of EUMETSAT as a global provider of data from different originators. More and more data with origins other than EUMETSAT have been added to the EUMETCast dissemination baseline, during the last years. This ongoing process of the integration of third-party data covers also some precipitation related data sets:

- **Available** on EUMETCast:
 - AMSU-A/MHS N-19 (Global and EARS)
 - MODIS (European area)
 - TAMSAT (Univ. of Reading, accumulated rain over Africa)
- **Planned** for implementation:
 - SSMIS (full resolution in BUFR)
 - NPP (all instruments)
 - FY3 (sounders)
- **Potential:**
 - Megha-Tropiques
 - GPM (core)
 - GCOM-W (AMSR-2)

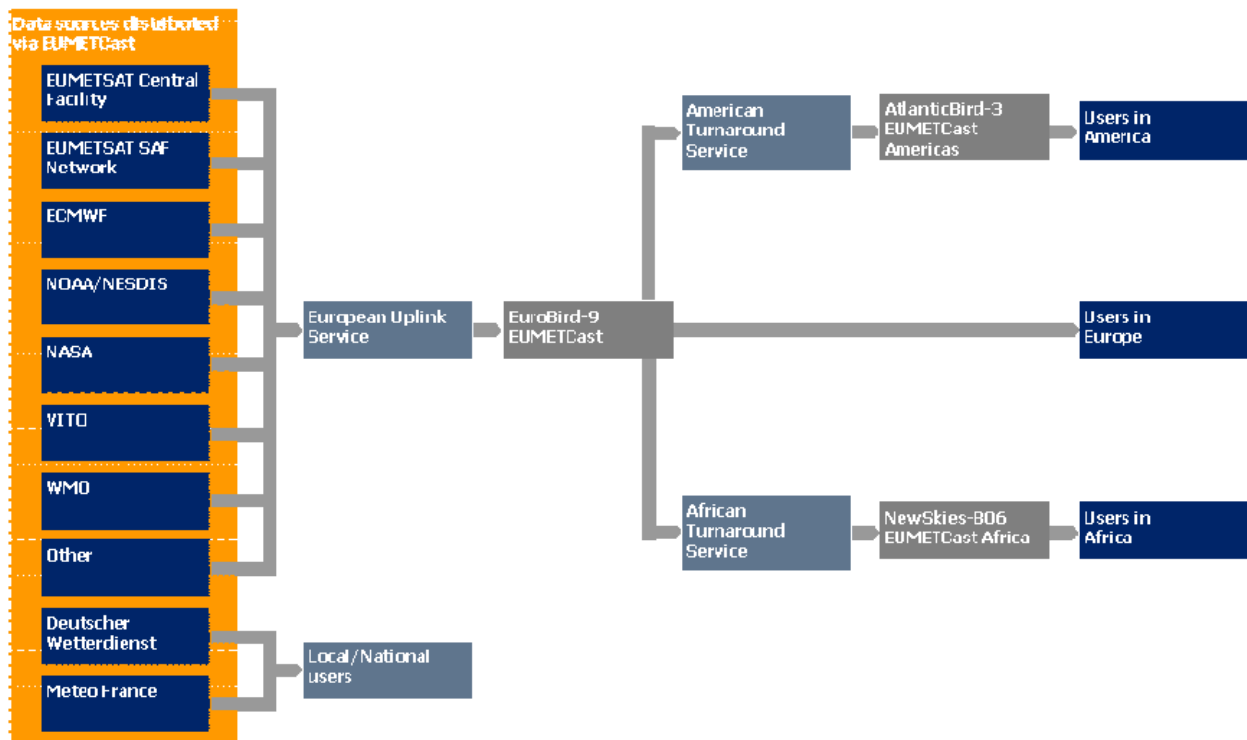


Figure 4: EUMETSAT as a global data provider

5. PRECIPITATION RELATED INSTRUMENT ON FUTURE EUMETSAT SATELLITES

While launches of the next geo-stationary MSG satellite and the next polar orbiting METOP satellite are foreseen for 2012, the planning for the next generation of EUMETSAT's operational satellite systems is ongoing.

Meteosat Third Generation (MTG), the new geo-stationary satellite program, is already in the approval process by the EUMETSAT member states. The current plans foresee a twin satellite configuration consisting of an imaging mission, MTG-I, and a sounding mission, MTG-S. The MTG-S is foreseen to carry an Infrared Sounder (IRS) and an Ultra-violet, Visible and Near Infrared Sounder (UVN). More interesting from the point of view of the precipitation community is the MTG-I, which will consist not only of 16 channel imager (Flexible Combined Imager, FCI) with high spatial resolution and repetition rate, but also the first geo-stationary Lightning Imager (LI). The potential exploitation of the data from the LI-instrument to improve precipitation retrievals will be an important area of research, in the coming years. The launch of the first MTG-I satellite is currently planned for 2016.

The planning for the next generation of polar orbiting satellites (Post-EPS) is in a much earlier stage. Through consultation with users and application experts, requirements have been defined for a range of candidate missions. Among the instruments which fulfil the requirements of the candidate missions are a microwave sounder (MWS) and a microwave imager (MWI). The decision on realisation depends on mission priority and gap-analysis. This process is ongoing. Earliest start date for a post-EPS satellite could be in 2019/2020.

6. USER SUPPORT AND TRAINING

EUMETSAT always considered the support and the training of users in the application of satellite data in their operational environments as a key activity for operational data providers. During the last years, the SAFs started to participate in EUMETSAT's various training activities.

EUMETSAT's training mainly addresses operational personnel from weather services in Europe, Africa and the Middle East. It focuses on web guides, the generation of interactive training modules, guides on the EUMETSAT web pages and courses. Many of those are integrated in EUMETCAL, the European Virtual Organisation for Meteorological Training with focus on courses (<http://www.eumetcal.org/>).

A new concept is a series of so-called blended courses, which consist of a mixture of distant learning and classroom phases. Usually they are covering a period of two to three months. Both learning phases of the courses are supported by new communication tools (Moodle, Centra Saba) which allow e.g. online presentations, discussions, forums, chat, quiz and other interactive participation of the trainees.

During the 5th IPWG meeting in Hamburg, a EUMETSAT training event was held in coordination with the Satellite Application Facilities (SAF). The invited audience consisted of Eastern Europe hydrologists from NMHS and scientists from all over the

world. Members of the H-SAF contributed as lecturers, planners, and training module providers.

7. CONCLUSION

The transfer of new ideas and technology from the scientific to the operational framework as well the transfer from experience and user contacts in the other direction is essential for the effective exploitation of precipitation remote sensing data and the associated future development.

EUMETSAT contributes by various activities in the SAFs and in the Central Facility in Darmstadt to these efforts.

8. REFERENCES

Heinemann, (2004): Integration of the EUMETSAT Multi-sensor Precipitation Estimate (MPE) in an operational real-time processing environment, International Precipitation Working Group (IPWG) meeting, Monterey, CA, USA, September 2004

Kidd C (2008), Heinemann T, Levizzani V, and Kniveton D.R: Inter-comparison of regional precipitation products, International Precipitation Working Group (IPWG) meeting, Beijing, China, October 2008

Heinemann T (2008): Quality indicators in an operational precipitation, International Precipitation Working Group (IPWG) meeting, Beijing, China, October 2008

THE GLOBAL PRECIPITATION MEASUREMENT (GPM) MISSION: OVERVIEW AND U.S. STATUS

Arthur Y. Hou

NASA Goddard Space Flight Center, Greenbelt, MD 20771 USA

Phone: 001-301-614-6150, Fax: 001-301-286-1626

e-mail: arthur.y.hou@nasa.gov

The Global Precipitation Measurement (GPM) Mission is an international satellite mission designed to unify and advance precipitation measurements from a constellation of research and operational microwave sensors. NASA and JAXA will deploy the GPM Core Observatory carrying an advanced radar-radiometer system to serve as a physics observatory and a transfer standard for inter-calibration of constellation radiometers. The GPM Core Observatory is scheduled for launch in July 2013. NASA will provide a second radiometer to be flown on a partner-provided GPM Low-Inclination Observatory to enhance the near real-time monitoring of hurricanes and mid-latitude storms. JAXA will also contribute data from the Global Change Observation Mission-Water (GCOM-W) satellite. Additional partnerships are under development to include microwave radiometers on the French-Indian Megha-Tropiques satellite and U.S. Defense Meteorological Satellite Program (DMSP) satellites, as well as cross-track scanning humidity sounders on operational satellites such as the NPP, POES, JPSS, and MetOp satellites, which are used to improve the precipitation sampling over land. Brazil has in its national space plan for a GPM low-inclination radiometer, and data from Chinese and Russian microwave radiometers could potentially become available through international collaboration under the auspices of the Committee on Earth Observation Satellites (CEOS) and Group on Earth Observations (GEO).

The current generation of global rainfall products combines observations from a network of uncoordinated satellite missions using a variety of merging techniques. GPM will provide "next-generation" precipitation data products characterized by: (1) more accurate instantaneous precipitation measurement (especially for light rain and cold-season solid precipitation), (2) more frequent sampling by an expanded constellation of microwave radiometers including operational humidity sounders over land, (3) inter-calibrated microwave brightness temperatures from constellation radiometers within a unified framework, and (4) physical-based precipitation retrievals from constellation radiometers using a common a priori cloud/hydrometeor database constructed from GPM Core sensor measurements.

As a science mission with integrated application goals, GPM will (1) provide new measurement standards for precipitation estimation from space, (2) improve understanding of precipitation physics, the global water cycle variability, and freshwater availability, and (3) advance weather/climate/hydrological prediction capabilities to directly benefit the society. An overview of the GPM mission concept, NASA program status, science activities in the United States, as well as a wide range of international scientific collaborations in radiometer inter-calibration, retrieval algorithm development, and ground validation will be presented.

HIGHLIGHTS OF VERSION 7 TRMM MULTI-SATELLITE PRECIPITATION ANALYSIS (TMPA)

George J. Huffman^{1,2}, David T. Bolvin^{1,2}, Eric J. Nelkin^{1,2}, Robert F. Adler³

¹ NASA/GSFC Laboratory for Atmospheres, Greenbelt, MD, USA

² Science Systems and Applications, Inc., Lanham, MD, USA

³ University of Maryland College Park/ESSIC, College Park, MD, USA

e-mail: george.j.huffman@nasa.gov

ABSTRACT

Version 7 of the TRMM Multi-satellite Precipitation Analysis (TMPA) provides a number of scientific and processing enhancements over the previous Version 6 algorithm. The TMPA now includes important additional sources of passive microwave satellite precipitation, including NOAA-18 MHS, NOAA-19 MHS, Metop-A MHS, and F16 and F17 SSMIS. These are in addition to the Version 6 suite that already included TRMM, SSMI, AMSU-B, and AMSR-E. Furthermore, Version 7 now includes the 0.07° Grsat-B1 infrared data during the period 1998-1999 and represents a significant improvement in resolution and areal coverage over the 1° 24-Class histogram infrared data used in Version 6. In addition to new satellite sources, Version 7 TMPA now uses the new GPCP "Full" gauge analysis, when available, and the GPCP "Monitoring" gauge analysis elsewhere. At the request of users, the number of output product data fields increased from two to six in the 3-hourly product and from two to three in the monthly product. The new 3-hourly data fields include the satellite precipitation source, the passive microwave-only precipitation estimates, the infrared-only estimates, and the satellite observation time. The new monthly field consists of the gauge relative weighting. These new parameters allow the user much more flexibility in analyzing and understanding the "background" information used to compute the final estimates. Finally, Version 7 includes a new automated QA algorithm designed to detect data anomalies prior to dissemination.

1. INTRODUCTION TO THE POSTER

The poster presented at the meeting has fairly complete text covering all of the major points, so it seems unnecessary to reproduce those words here in detail. The basic concept is that the production code that computes the various TRMM products in the Precipitation Processing System (PPS) is frozen between versions. The current Version 6 was instituted in early 2005, and a number of input dataset changes have occurred, as well as additional analysis of the dataset choices made in creating Version 6. Accordingly, Version 7 is a chance to refresh and improve the consistency of the

input dataset records. At the same time, both users and developers have discovered the need to preserve more intermediate information about the final output products and to apply lessons learned in Version 6, such as strengthening the quality assurance of those products.

The poster does not state the timing for the release of Version 7, and since IPWG5 it again slipped anyway. At the time of this publication (September 2011), the TRMM microwave, precipitation radar, and combined microwave-radar algorithms had been shifted to Version 7 at the start of July 2011, with reprocessing completed by mid-August. The SSMI, SSMIS, and AMSR inputs to the TMPA are just now being finalized, after which additional calibration work must be done to finalize the Version 7 TMPA. Given these tasks, Version 7 TMPA might be fully processed around February 2012. During the reprocessing the existing Version 6 archive will be maintained, but all newly arriving data will be processed using the Version 7 code.

RAIN INTENSITY SPECTRA DISTRIBUTION OVER GERMANY AND WESTERN AFRICA

Mikhail Itkin, Rabea Athmer, Alexander Loew

Max Planck Institute for Meteorology, KlimaCampus, Hamburg, Germany

e-mail: mikhail.itkin@zmaw.de

Long-term precipitation climatologies built from records made by passive microwave instruments onboard polar-orbiting satellites might be prone to regional biases due to differences in temporal sampling in different areas of the globe. Another possible source of errors lies in low sensitivity to light rain events that might contribute significantly to the total rain volume in some regions. To analyze these possible biases it is necessary to know how well can we resolve the precipitation diurnal cycle and what is the fraction of rain volume that is missed due to weak rainfall signatures.

In this work we analyze long-term rain gauge measurements from Germany and Western Africa to estimate diurnal variations of statistics of rain occurrence and rain volume with respect to different rainfall intensity classes. We also discuss regional and seasonal diurnal cycle variations.

Time series are made of 15 years of measurements across Germany and 3 years of measurements in several catchment areas in Western Africa. Observation networks have spatial resolution between 10 and 40 kilometers.

Our results show that in total in Germany drizzle and light rain events (less than 1 mm/h) contribute up to 36% of total rain volume occupying 78% of the total rain occurrence. Moderate rain events (1-5 mm/h) contribute almost as much as light rain events (49%) however they happen less frequently (in 20% of all cases). Strong and heavy rain events (over 5 mm/h) produce more than 18% of the total rainfall volume while they occur only in 1.4% of all cases. As expected, rain gauge records from Donga catchment basin in Western Africa show different behavior: light rain events (less than 1 mm/h) contribute only up to 10% of total rainfall volume and occupy about 60% of all rain occurrence, while the largest contribution comes from the heavy rain events (over 5 mm/h) which make more than 70% of total rainfall volume and occur in about 15% of total number of rain events.

RESOLVING RAINFALL RATE RETRIEVAL AMBIGUITIES ASSOCIATED WITH CLOUD TYPES USING MULTI-SATELLITE PASSIVE MEASUREMENTS

Mikhail Itkin, Alexander Loew

Max Planck Institute for Meteorology, KlimaCampus, Hamburg, Germany

e-mail: mikhail.itkin@zmaw.de

In this study we propose a rain rate retrieval correction method based on merging multi-spectral multisatellite passive measurements. It's main purpose is to minimize ambiguities associated with the effect of clouds with similar image properties but different physical structure.

It is difficult to discriminate precipitating clouds from non-precipitating ones and easy to misinterpret thin ice clouds from thick convective anvils as well as to miss high convective cloud masked by thin ice cloud, which can cause biases in rainfall estimates. While modern spaceborn radar systems can solve this problem well we still need an approach for minimizing this effect in long-term datasets based on historical satellite records.

Our approach is based on using microwave information from sensors like SSM/I and AMSU, though information from newer AMSR/E or TRMM instruments can be utilized as well. Rain rate estimates from passive microwave sensors are merged with cloud types and cloud physical properties retrieved from IR sensors like SEVIRI and AVHRR. By combining these data types spatial resolution of 10 km is achieved.

The performance of approach is analyzed through a case study for the year 2006, where corrected rain rate retrievals were compared with hourly accumulated precipitation records from German meteorological stations. For this study cloud properties information was obtained from EUMETSAT Satellite Application Facility on Climate Monitoring (CM-SAF) and combined with rain intensity retrievals based on SSM/I records.

VARIABILITY OF LIGHTNING ACTIVITY AND SUBSEQUENT CONVECTIVE PRECIPITATION DERIVED FROM SATELLITE AND GROUND BASED SENSORS – CASE STUDY

Rafał Iwański, Bożena Łapeta and Danuta Serafin-Rek

Satellite Remote Sensing Centre,
Institute of Meteorology and Water Management - Krakow, Poland

e-mail: rafal.iwanski@imgw.pl

ABSTRACT

In the paper, the ability of the H-SAF products to reproduce the precipitation patterns will be discussed on the base of quantitative and temporal relations between lightning activity and heavy precipitation information derived from ground based sensors within chosen convective storm cell of 11th of May 2009. Also the ability of atmospheric electrical activity information to present temporal evolution of storm cell will be introduced. Finally, the quality of the satellite products in estimation of precipitation intensity will be presented.

1. INTRODUCTION

Extreme convective precipitation events resulting in flood danger are more and more common in Central Europe as we are facing progressing climate changes. Recognition and understanding of relations between meteorological events within storm cells are crucial for correct interpretation of satellite and ground-based real-time operational monitoring systems data and their proper applications. Polish lightning detection network PERUN (Vaisala SAFIR 3000 system) provides high accuracy real time information on atmosphere electrical activity in Poland and neighboring countries. Network of over a thousand automatic telemetric posts collects precipitation information from all over the country in the near-real-time mode. Both systems provide quality spatial and temporal distribution of meteorological information for purposes of scientific studies as well as validation of satellite precipitation products.

The main goal of EUMETSAT Satellite Application Facility in Support to Operational Hydrology and Water Management (H-SAF) is to provide satellite products in near real time mode to be useful for operational hydrology. Among them, the pre-operational precipitation products based on both passive microwave sensors (conical and cross track scanning) and IR sensors calibrated by MW have been available since 2009 for cooperating teams for detailed validation before release of operational products.

The objective of this study is to investigate the relation between liquid precipitation fields calculated from ground and satellite sensors datasets and lightning activity within chosen convective storm recorded in Poland.

2. DATA SOURCES

2.1 ATS

ATS – network of Automatic Telemetric Stations consists of 430 precipitation posts. Each post is equipped with two gauges: heated and non-heated, what enables some quality control of data. For study purposes, readings from both gauges were compared in order to eliminate the cases of clogged instruments. If both gauges worked properly, higher values were taken (automatic rain gauges are known to underestimate the real precipitation). Telemetric posts are allocated all over the country. The network density increases in the mountainous regions of Poland, where the flood danger is higher (see Fig.4). The measurements time resolution was set up in time step of 10 minutes, what allows estimating the rain rate with reasonable quality. To increase that quality rain gauge data from SYNOP stations were combined with ATS data and used as well.

2.2 PERUN

PERUN – PERUN lightning detection, localization and registration system bases on a Vaisala SAFIR 3000 VHF/VLF system (Surveillance et d'Alerte Foudre par Interferometrie Radioelectrique). The ground based network of 9 detection stations collects information on atmospheric electric activity. The system works on the basis of the interferometry technique using measurements of the phase shifts of electromagnetic impulses produced by lightning discharges and received by the system's antennas (Bodzak 2007). An impulse is received by some antennas (stations) and the data is sent to the central unit where the localization of a discharge is determined using the triangulation method.

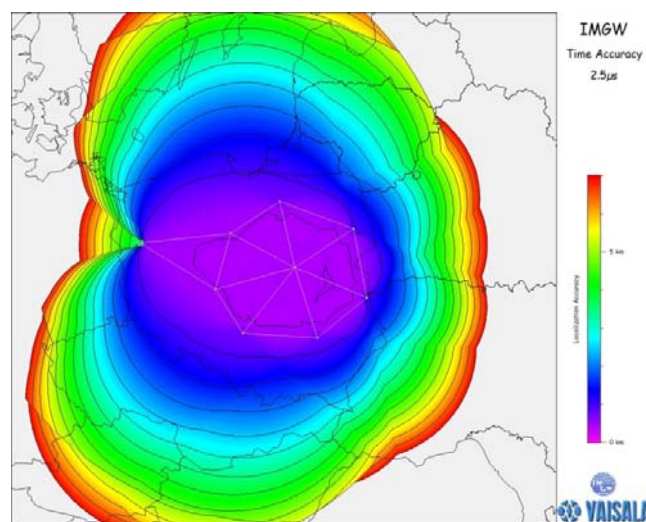


Figure 1. Map of location accuracy for PERUN system in Poland (courtesy of J.Y. Lojou).

The detection of the signal by each of the five dipole receiving antennas working in the group is carried out in the very high frequency (VHF) range of 110-118 MHz, and at the same time in the low frequency (LF) range (300 Hz – 3 MHz) by a flat antenna. The mean distance between receiving antennas is 200 km which is thought to guarantee a detection effectiveness at 95% and accuracy of localization below 1 km over central Poland (see Fig.1).

The PERUN system detects and localizes both cloud-to-ground (CG), inter-cloud and intra-cloud (CC and IC) discharges. Rudimentary information received for each atmospheric discharge is: date and time (GPS-based), localization, electromagnetic field amplitude, the time-scale of the increase and decrease of the current impulse (for CG discharges), and the number of stations receiving the signal.

2.3 H-SAF PR-OBS-3 (H-03)

H-SAF PR-OBS-3 - precipitation rate at ground by GEO/IR supported by LEO/MW product is based on the IR data from the SEVIRI instrument onboard Meteosat satellites. The equivalent blackbody temperatures are converted to precipitation rate by lookup tables updated at intervals by precipitation rate generated from MW instruments (in this case: AMSU and SSMI). The product is generated at the 15 minute imaging rate of SEVIRI, and the spatial resolution is consistent with the SEVIRI pixel – 8 km (ATDD 2010). The processing method is called “Rapid Update”.

3. METHOD

Relations between precipitation derived from ground and satellite instruments and lightning activity were investigated in a single case study using 1h cumulated precipitation and lightning activity maps.

3.1 Precipitation maps.

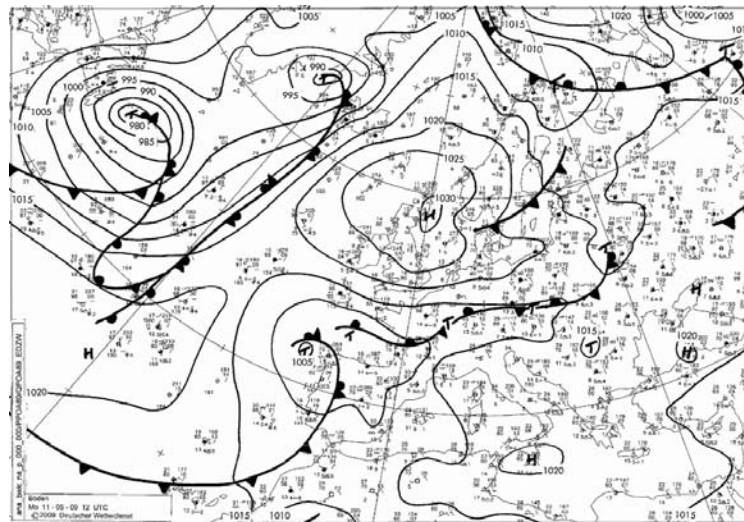
On the basis of 10 minute ATS rain cumulated values the hourly sums were calculated for each precipitation post. The similar method was also applied to H-03 15 minute rain rate dataset for each H-03 grid. Obtained values were used to draw 1h time pace precipitation maps with Natural Neighbour spatialisation algorithm. The Natural Neighbour interpolation algorithm uses a weighted average of the neighbouring observations, where the weights are proportional to the Thiessen polygon. This method does not extrapolate contours beyond the convex hull of the data locations (Sibson 1981).

3.2 Lightning activity maps.

All lightning density and localization maps were drawn using PERUN secondary ASCII output data and centered at 51°56'32" N 20°10'44" E using Vaisala SAFIR Post Processing software - DAM. The lightning density maps present amount of total lightning (IC + CG) per 1km² in 1h successive periods. The localization maps reflect spatial and temporal evolution of storm cells in six delimited periods.

4. CASE STUDY

On the 11th of May 2009 the dominant frontline moved from Poland to Ukraine and Belarus leaving ground for new group of clouds translocating to Poland from Germany (see Fig.2).



<http://www.wetter3.de/fax>

Figure 2. Surface synoptic map at 1200 UTC on 11th of May 2009.

Low and medium clouds moved over S Poland bringing convective precipitation. This rainfall was magnified by small low pressure centre moving from Austria over Slovakia. The main wind direction over Middle Europe was N but clouds moving from Germany to Poland were directed by SW circulation. Ground frosts were possible in Poland due to N cold flow.

The meteorological situation resulted in heavy convective precipitation that occurred in the afternoon, at the South of Poland. The 6 hour cumulated precipitation measured at the SYNOP stations exceeded 60 mm. The precipitation was accompanied by strong lightning activity within clouds convective cores.

5. RESULTS AND DISCUSSION

Precipitation and lightning activity maps were created for each hour on the hour from the period of 1300-2300 UTC when the convective storm was active in terms of rainfall and lightning. The information gained was completed by appropriate Meteosat SEVIRI HRV imagery (see Fig.3). In addition 11h cumulated precipitation maps as well as appropriate lightning localization map were drawn to investigate mutual dependency between recorded phenomena.

In general, high precipitation values report better correlation between ATS and H-03 datasets than low ones. Peak values are more pronounced in ATS precipitation maps than in H-03 where derived precipitation field is more diffused (but also homogenous)

and covers larger area (see Fig.4). Because of precipitation retrieval method, H-03 field reassembles related cloud structures, which explains similarities between HRV imagery and satellite derived precipitation distribution. It seems that in some cases H-03 algorithm allows for rain rate miscalculation from ice clouds of cirrus type (see Fig.3 1300 UTC H-03 and ATS maps). Ground data source tends to focus precipitation field around ATS posts leaving surrounding area blank which is also matter of interpolation method.

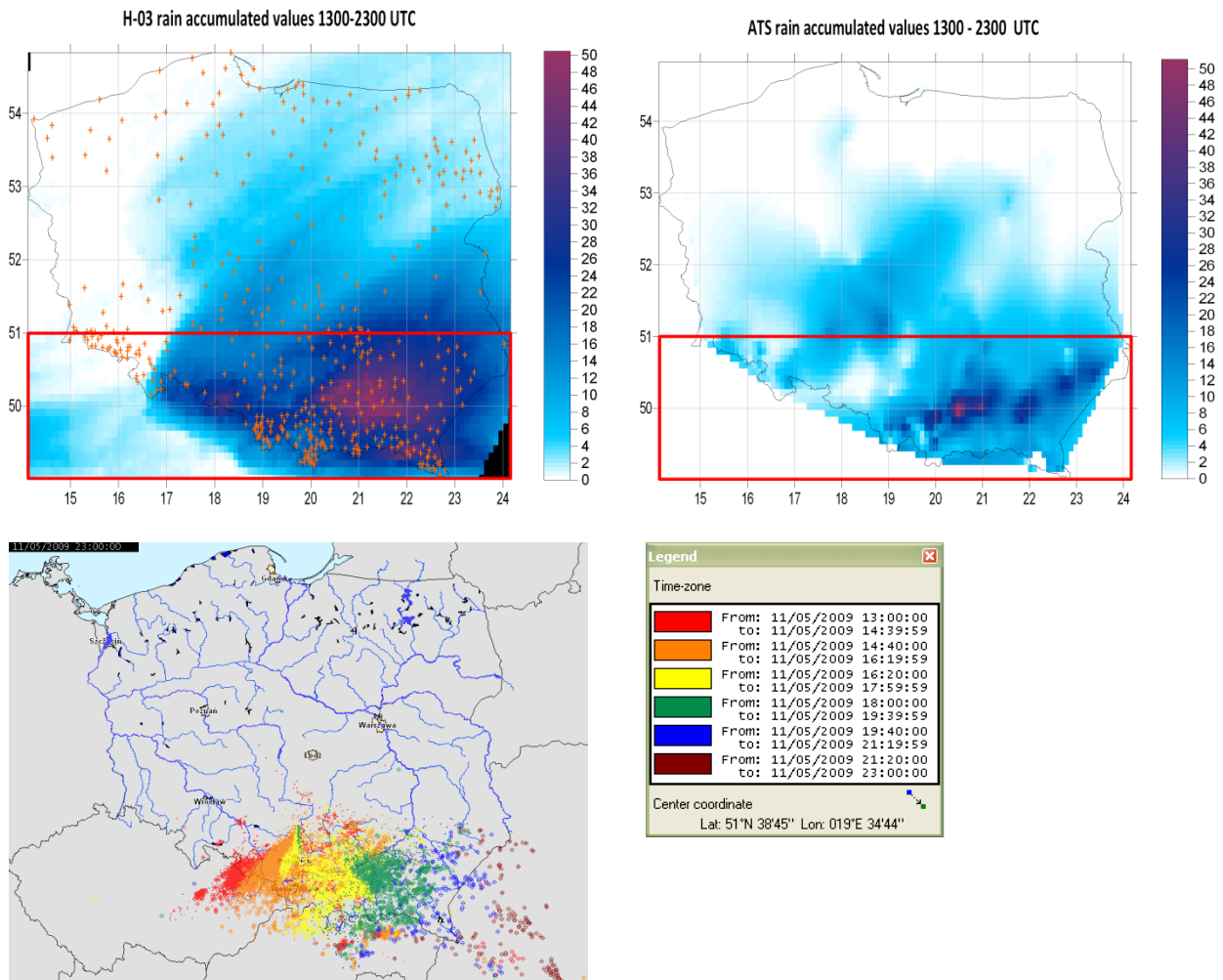
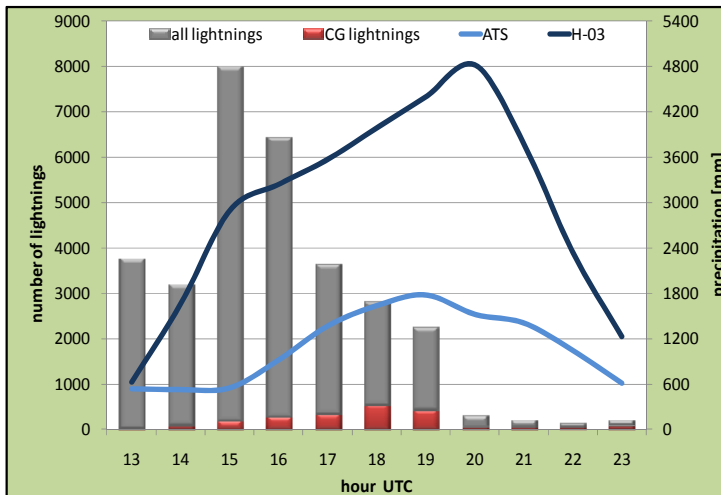


Figure 4. 11h cumulated precipitation fields maps obtained from satellite and ground sensors (upper panel) and lightning localization map for defined period of 11th of May 2009. The red rectangle defines the area where convective precipitation connected with T-storm occurred.

Despite that high precipitation values are underestimated - low precipitation values are magnified by H-03 and in result satellite 1h cumulated precipitation estimates present significantly higher values than ATS ones. As it was stated above differences between H-03 and ATS precipitation fields might be related to nature of relevant measurement techniques.

It should be also stressed that maximum H-03 precipitation values at early stage of storm development are in good correlation with subsequent lightning activity max values (see Fig.3 1500 UTC H-03 and lightning maps). Detailed analysis of this dependency was conducted on the basis of subsequent precipitation and lightning activity data sets. Rainfall records from red rectangle area (see Fig.4) were taken to calculate accumulated precipitation from period of 1300-2300 UTC and then used in comparison with derived lightning activity values. Results obtained are presented in Table 1. and Fig.5. below.



	11.05.2009 1300-2300 UTC			
	IC	CG -	CG+	total
1200-1300 UTC	2623	110	4	2737
1300-1400 UTC	2800	242	15	3057
1400-1500 UTC	4477	280	21	4778
1500-1600 UTC	5268	661	36	5965
1600-1700 UTC	3756	681	44	4481
1700-1800 UTC	1521	751	33	2305
1800-1900 UTC	1422	626	21	2069
1900-2000 UTC	290	213	33	536
2000-2100 UTC	70	71	29	170
2100-2200 UTC	22	84	16	122
2200-2300 UTC	3	76	19	98
Case in total	22252	3795	271	26318

Figure 5. Temporal variability of 1h ATS and H-03 cumulated precipitation and discriminated lightning activity totaled for the area occupied by the studied T-storm on 11th of May 2009.

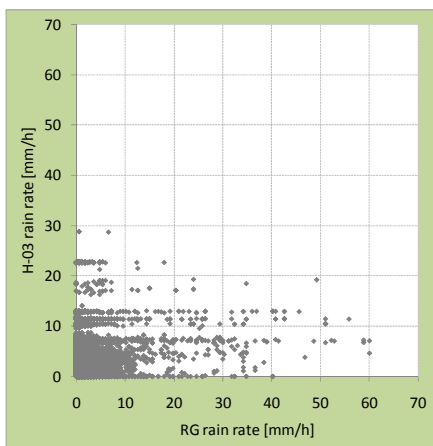
Table 1. Lightning production discrimination and time variability.

There is a strong correlation between CG (both CG- and CG+) lightning activity and ATS rainfall seen in presented case. Precipitation curve follows increase and subsequent decrease of CG lightning numbers (this confirms conclusions of earlier observations over the world). H-03 curve can be also correlated with total lightning activity but it is characterized by 5h time lag. This behavior needs further analysis on bigger number of cases. One can notice huge difference between ATS and H-03 11h cumulated values calculated over defined previously red rectangle area. To investigate that difference H-03 values were validated against ATS values (see Fig.6 and also Table 2 and 3 below). On average H-03 underestimates precipitation values (ME negative score – see Tab. 2). Yet light rainfall is overestimated while the high values are underestimated (see Fig.6). High FAR score (see Tab. 3) bigger than POD value points to H-03 difficulties in proper rainfall recognition. It may explain why differences between ATS and H-03 curves in Fig. 5 are so huge.

To conclude one can say that:

- There is a strong correlation between CG (both CG- and CG+) lightning activity and ATS rainfall while maximum H-03 precipitation values at early stage of storm development are in good correlation with subsequent lightning activity maximum values;
- Differences between H-03 and ATS precipitation fields might be related to nature of relevant measurement techniques;
- Because of precipitation retrieval method, H-03 field reassembles related cloud structures. It seems that in some cases H-03 algorithm allows for rain rate miscalculation from ice clouds of cirrus type (see 1300 UTC H-03 and ATS maps);

Finally it should also be mentioned that lightning activity data derived forthwith and presented instantly on operational basis at the synoptic office could be valuable information in process of convective precipitation time determination.



Parameter	[mm/h]
Max RG	60.0
Max SAT	28.9
Mean RG	3.2
Mean SAT	3.0
ME	-1.5
St. Dev	5.9
RMSE	6.0

Parameter	
POD	0.57
FAR	0.62
ACC	0.81
CSI	0.29

Figure 6. H-03 and ATS comparison results for 11th of May 2009 (left panel). Table 2 and Table 3 – continuous and categorical statistics respectively.

6. REFERENCES

Bodzak, P., 2007: Detection and Localization of Atmospheric Discharges. *Series: Instrukcje i podręczniki*, Wydawnictwo IMGW, Warszawa (in Polish);

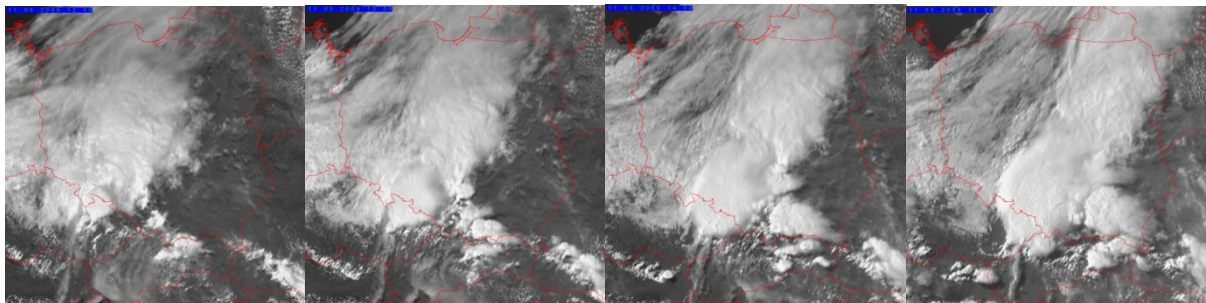
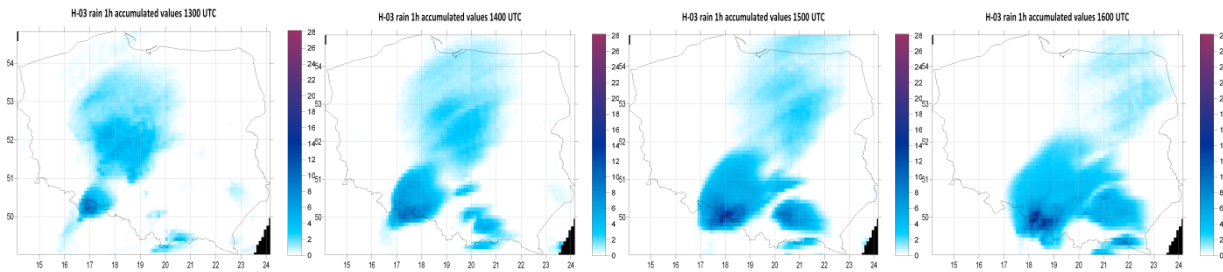
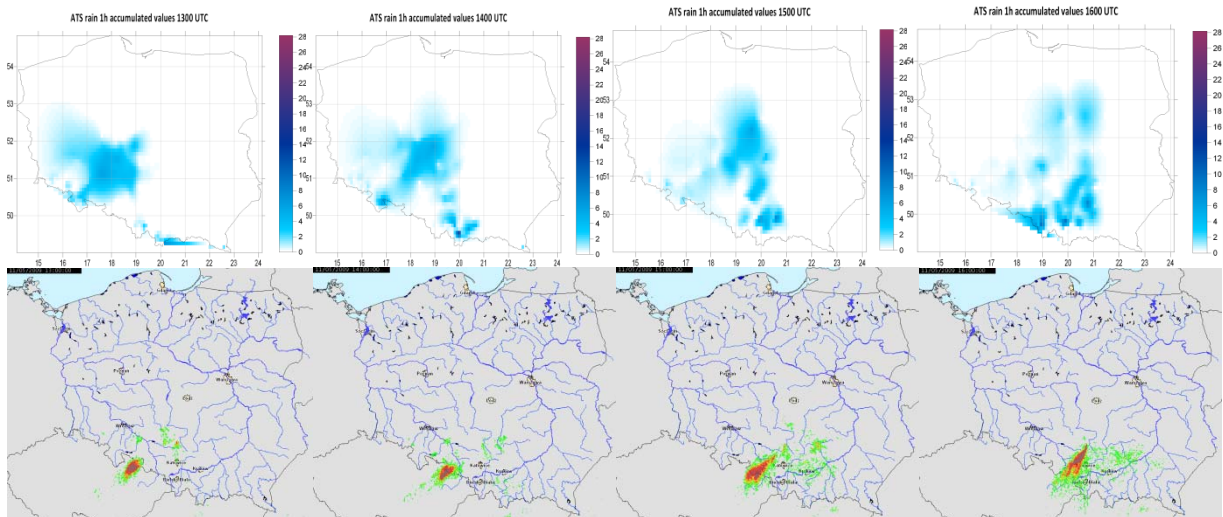
Satellite Application Facility on Support to Operational Hydrology and Water Management (H-SAF), 2010: PR-OBS-3 - Precipitation rate at ground by GEO/IR supported by LEO/MW. *Algorithms for precipitation products generation*, August 2010. <http://hsaf.meteoam.it/documents/ATDD/ATDD-03.pdf>;

Sibson, R., 1981: *A Brief Description of Natural Neighbor Interpolation, Interpreting Multivariate Data*. V. Barnett editor, John Wiley and Sons, New York, p. 21-36;

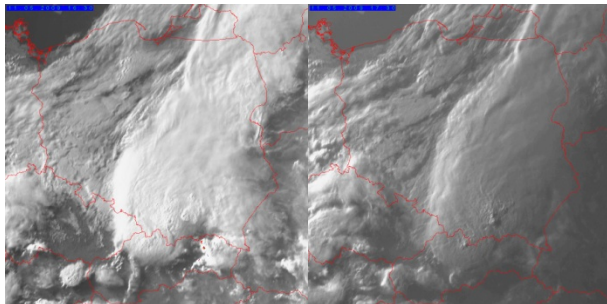
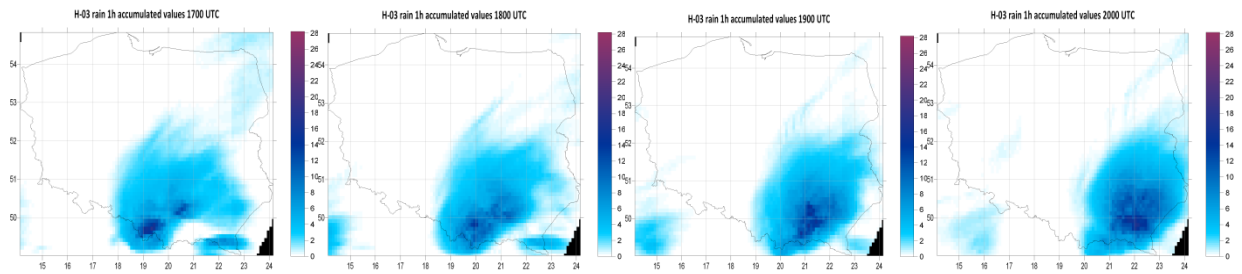
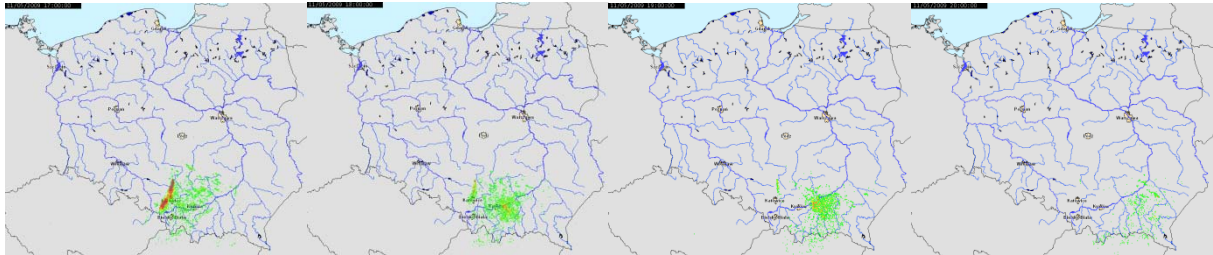
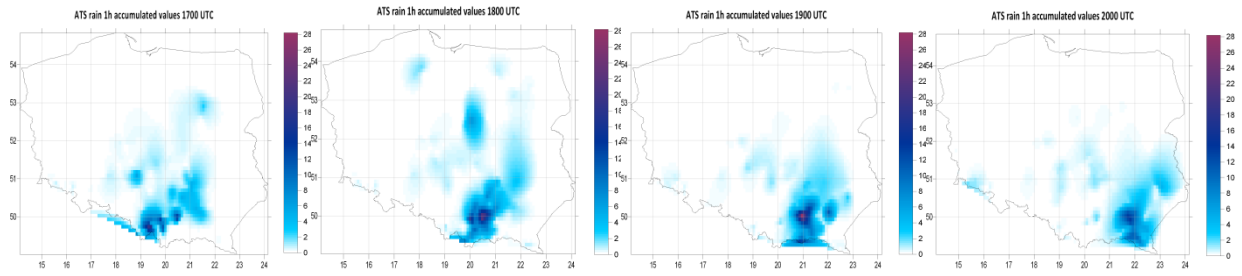
Acknowledgements

The work was partially financed by EUMETSAT H-SAF Project (Satellite Application Facility on Support to Operational Hydrology and Water Management). The Vaisala SAFIR Post Processing software – Data Analysis Module used in this study is licensed to the Institute of Meteorology and Water Management Ground Based Remote Sensing Centre.

**Fifth Workshop of the
International Precipitation Working Group
11-15 October 2010, Hamburg, Germany**



**Fifth Workshop of the
International Precipitation Working Group
11-15 October 2010, Hamburg, Germany**



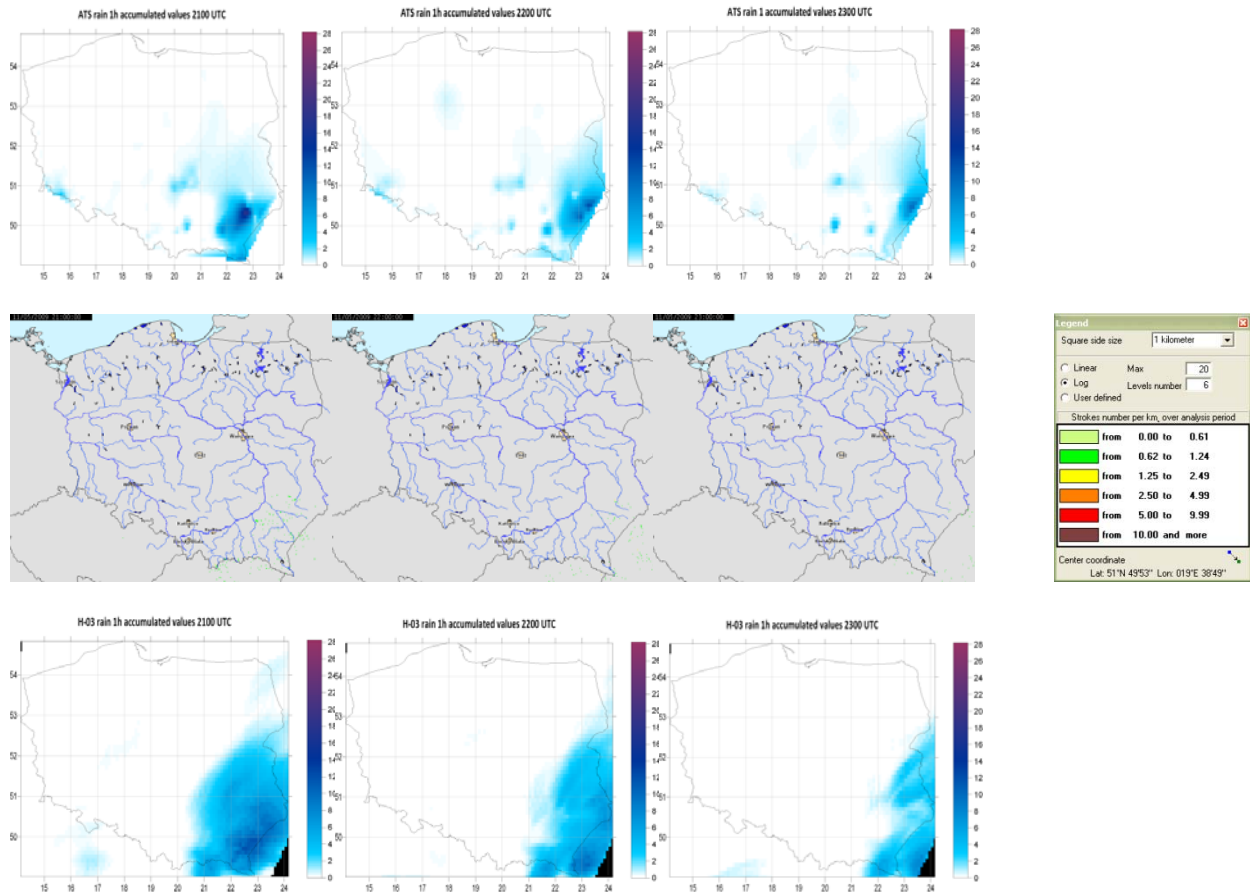


Figure 3. Variability of electric activity on the 11th of May 2009 from period 1300-2300 UTC (total lightning density maps) and subsequent convective precipitation on the basis of ATS data and H-03 data completed by Meteosat SEVIRI HRV imagery (daytime only).

KALMAN-FILTERED CMORPH USING TRMM TO BLEND SATELLITE RAINFALL

Robert. J. Joyce¹, Pingping Xie², and Soo-Hyun Yoo³

¹Wyle Information Systems and Climate Prediction
Center/NCP/NWS/NOAA, USA

²Climate Prediction Center/NCP/NWS/NOAA, USA

³Wyle Information Systems and Climate Prediction
Center/NCP/NWS/NOAA, USA

e-mail: robert.joyce@noaa.gov

The CPC Morphing (CMORPH) blended satellite rainfall product ingests various sources of satellite passive microwave (PMW) rainfall estimation as input. PMW rainfall retrievals differ in: microwave channel availability/selection, retrieval earth coverage, sampling frequency, and Equator-crossing time. The current operational CMORPH algorithm uses a simple Kalman filter in which the weights for combining both “past” and “future” propagations of PMW rainfall estimates are the inverses of the temporal distance from estimation to observation. Geostationary satellite IR data are used to determine the propagation vectors for the PMW rainfall, however until now, IR information has not been used for the calculation of the actual rainfall estimate. Using withheld TRMM TMI rainfall, regional, seasonal, and surface type dependent weights are derived from 30-minute 0.25-degree collocations with forward/backward propagated PMW rainfall as well as IR-based estimates. The CMORPH rainfall estimates are reconstructed from various satellite sources using a Kalman filter whose statistical parameters are determined from these weights. A year of Kalman filter CMORPH (July 2009–June 2010) is developed and compared with high temporal and spatial resolution National Severe Storms Laboratory (NSSL) Q2 rainfall, and the global CPC daily 0.25-degree rainfall gauge analyses. The Q2 rainfall allows a determination of the skill and error of this new version CMORPH, stratified in 30 minute intervals from the nearest PMW observation, as well as an evaluation of the improvement in locations of the diurnal cycle that sun-synchronous PMW estimation currently under-samples.

STATUS OF JAPANESE PRECIPITATION MEASURING MISSIONS AND GLOBAL RAINFALL MAP IN NEAR-REAL-TIME

Misako Kachi, Takuji Kubota and Riko Oki

Earth Observation Research Center, Japan Aerospace Exploration Agency (JAXA),
Tsukuba, Japan

e-mail: kachi.misako @jaxa.jp

ABSTRACT

The Global Precipitation Measurement (GPM) started as an international mission and scheduled for launch in 2013. GPM is follow-on and expand mission of the Tropical Rainfall Measuring Mission (TRMM), which continues observation from orbit since 1997, and its core satellite carries the Dual-Frequency Precipitation Radar (DPR) developed by Japan.

The first generation of the Global Change Observation Mission (GCOM) Water (GCOM-W1) will carry the Advanced Microwave Scanning Radiometer-2 (AMSR2). AMSR2 is a successor of AMSR for EOS (AMSR-E) on NASA's Aqua satellite, which also continues observation since 2002.

Global rainfall map products were developed before the TRMM's launch, but they were intended mainly to obtain global "climatology" of precipitation. As the accuracy of satellite precipitation estimates improves and number of satellite and instruments increases, there are strong requirements from user community to generate high-frequency and fine resolution global precipitation map in near-real-time. JAXA has developed and operates global rainfall map production system, a prototype for GPM era, in near-real-time since October 2008, and hourly and 0.1-degree resolution binary data and images available via internet (<http://sharaku.eorc.jaxa.jp/GSMaP/>). The algorithms are based on outcomes from the Global Satellite Mapping for Precipitation (GSMaP) project, and data from Special Sensor Microwave-Imager/Sounder (SSMIS) is newly introduced to the system recently. Near-real-time version of GSMaP data is distributed via internet and utilized by end users. Processing of reanalysis version of GSMaP (GSMaP_MVK) by latest algorithms to produce more accurate and continuous products, which can be applied to climate studies, is underway.

1. THE GLOBAL PRECIPITATION MEASUREMENT (GPM) MISSION

1.1. OVERVIEW

Global Precipitation Measurement (GPM) started as an international mission and follow-on and expand mission of the TRMM satellite to measure the global distribution of precipitation accurately in a sufficient frequency so that the information provided by this

program can drastically improve weather predictions, climate modeling, and understanding of water cycles. As shown in Figure 1, an important goal for the GPM mission is the frequent measurement of global precipitation using a GPM core satellite, which is jointly developed by U.S. and Japan, and a constellation of multiple satellites, which are developed by each international partner that will carry passive microwave radiometers and/or microwave sounders. The accurate measurement of precipitation will be achieved by two sensors onboard the GPM Core satellite which will be launched in JFY 2013; the Dual-frequency Precipitation Radar (DPR) developed by Japan Aerospace Exploration Agency (JAXA) and National Institute of Information and Communications Technology (NICT), and the GPM Microwave Imager (GMI) developed by NASA. The roles of the GPM core satellite are to collect as much microphysical information as possible for accurate rain estimation by performing synchronous observation with the GMI and the DPR and to provide calibration standards for the other microwave radiometers on the constellation satellites.

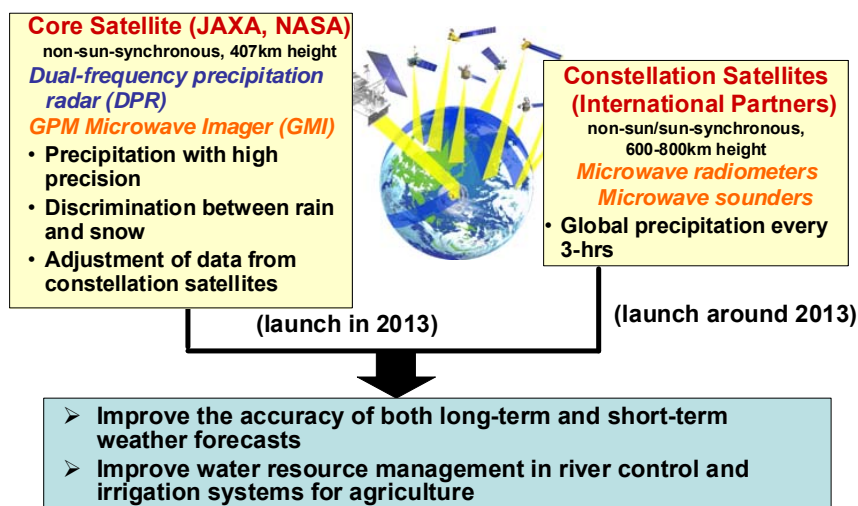


Figure 1. Overview of the Global Precipitation Measurement (GPM) mission.

The configuration of precipitation measurement using active radar and passive microwave imager is similar to the Tropical Rainfall Measuring Mission (TRMM), which has been flown since November 1997. The major difference is that DPR is used for the GPM core satellite instead of PR for the TRMM satellite. The inclination angle of the core satellite is 65 degrees where TRMM is 35 degree, and the flight altitude is about 407 km. The non-sun-synchronous circular orbit is necessary for measuring the diurnal change of rainfall similarly to TRMM.

1.2. DUAL-FREQUENCY PRECIPITATION RADAR (DPR)

The DPR consists of two radars, which are Ku-band (13.6 GHz) precipitation radar (KuPR) and Ka-band (35.55 GHz) precipitation radar (KaPR). There are three major objectives of the DPR observation; 1) to provide three-dimensional precipitation structure including snowfall over both ocean and land; 2) to improve the sensitivity and accuracy of precipitation measurement; and 3) to calibrate, with GMI on the GPM core satellite, the estimated precipitation amount by microwave imagers and/or sounders on the constellation satellites.

DPR interface Critical Design Review (CDR) and the GPM/DPR total system review was completed in July 2009. DPR CDR was completed in October 2009. Peer review of the GPM core spacecraft DPR interface and the NASA GPM core total system was held in October, 2009. GPM core observatory mission CDR was completed in December 2009. NASA ground system interface peer review was held in August 2010. In November 2010, DPR Pre Environmental-test peer review is planned.

For DPR development, all engineering unit tests were completed and GMI-DPR interference test using KaPR and GMI engineering test unit was done in December 2009 in Japan. Through the development test, DPR designs are satisfies requirements and are confirmed the readiness to manufacture proto-flight model. Currently, all of the DPR components PFM have been manufactured. DPR system integration will start in September, and initial far field antenna pattern test will start in October.

1.3. GROUND VALIDATION FOR DPR

JAXA put two new field-portable Ka-band Ground Validation (GV) radars for validation purpose to, and they have started observation experiments since autumn 2010. Each component, such as antennas, T/R unit, and signal processing, was constructed in JFY 2010. To use the two GV radars in two-way measurement, it is possible to calculate radar attenuation characteristics of precipitation particles in Ka-band bi-directionally. If the radar is placed to face an upper direction, it can observe a detailed vertical structure of precipitation systems, especially for the melting layer where precipitation particles change from solid to liquid. It is also possible to observe simultaneously with the DPR on-orbit to make direct comparison with DPR observation. Several observation topics for “Algorithm Validation”, such as precipitation profiles, snowfalls, and melting layers, are currently proposed and planned using JAXA Ka-band GV radars and other ground-based instruments. Figure 2 indicates five GPM GV sites in Japan, and list of observation targets of each site and current schedule of campaign experiments.

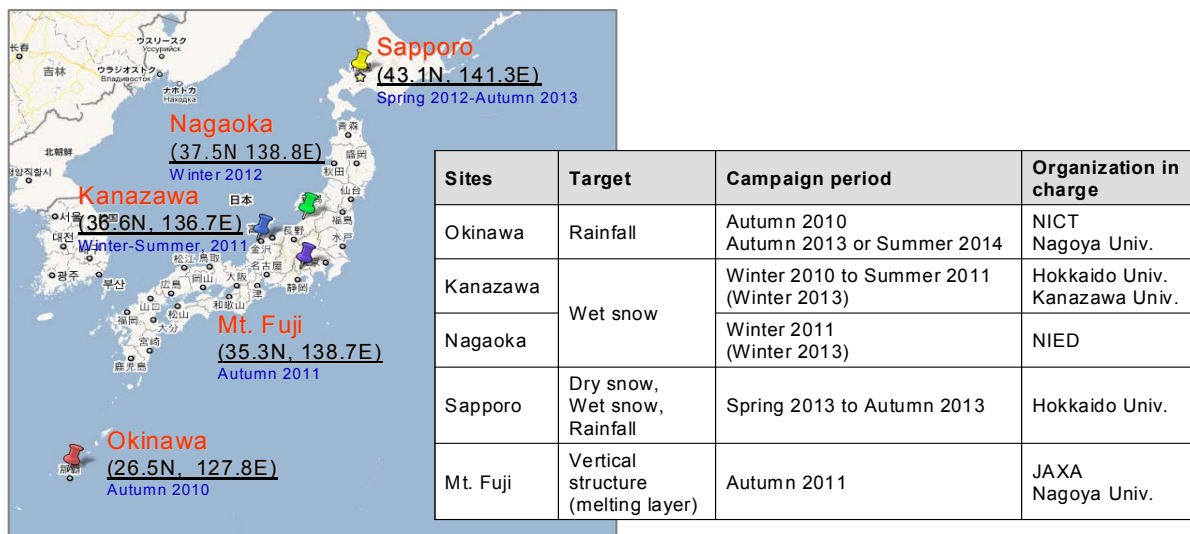


Figure 2. Japanese GPM ground validation sites and campaign experiments.
(as of October 2010)

2. THE GLOBAL CHANGE OBSERVATION MISSION (GCOM)

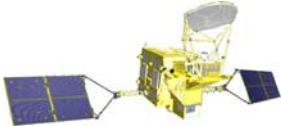
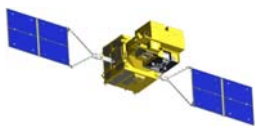
2.1. OVERVIEW OF GCOM

The Global Change Observation Mission (GCOM) is planned by the Japan Aerospace Exploration Agency (JAXA) for long-term continuous observation of the Earth's environment. GCOM is a successor mission of the Advanced Earth Observing Satellite-II (ADEOS-II), launched on December 2002 but stopped its operation due to the satellite malfunction in 2003. JAXA developed two core sensors for ADEOS-II, the Advanced Microwave Scanning Radiometer (AMSR) and the Global Imager (GLI). AMSR for the EOS (called AMSR-E) was also provided to NASA's Aqua satellite launched on May 2002, and is still continuing its operation for more than 7 years.

"GCOM" is not a name of single satellite mission, but consists of two medium-sized satellites, GCOM-W (water) and GCOM-C (climate), and three generations with one year overlap to ensure 10-15 years stable data records. Table 1 is overview of their first generation satellites. The GCOM-W1 will carry the Advanced Microwave Scanning Radiometer-2 (AMSR2), follow-on sensor of AMSR-E, and contribute to the observations related to global water and energy circulation, while GCOM-C1 will carry the Second-Generation Global Imager (SGLI), which is follow-on sensor of GLI, and contribute to the surface and atmospheric measurements related to the carbon cycle and radiation budget.

GCOM-W1 will participate to the A-Train satellite constellation, and GCOM-W1 position in the A-Train will be in front of the Aqua satellite. This will provide a perfect opportunity for cross-calibrating between AMSR-E and AMSR2. Since the AMSR-E instrument is recently exhibiting an increase of motor rotation torque, which could be considered as an aging sign, the prompt handover process including inter-calibration will be necessary. Also, since AMSR2 will be a single instrument onboard, participating in the A-Train will enhance the synchronous measurement capability with other satellite instruments available in the constellation, such as MODIS/AIRS/AMSU on Aqua, CloudSat, and CALIPSO.

Table 1. Overview of GCOM-W1 and GCOM-C1 satellites.

	GCOM-W1	GCOM-C1
Orbit	Type : Sun-synchronous orbit Altitude : 699.6 km Inclination : 98.2 degrees Local sun time : 13:30±15min	Type : Sun-synchronous orbit Altitude : 798 km Inclination : 98.6 degrees Local sun time : 10:30±15min
Satellite overview		
Mission life	5 years	
Launch vehicle	H2A launch vehicle	
Instrument	AMSR 2 (Advanced Microwave Scanning Radiometer-2)	SGLI (Second Generation Global Imager)
Launch	JFY 2011	JFY 2014

2.2. GCOM-W1 AND ADVANCED MICROWAVE SCANNING RADIOMETER-2 (AMSR2)

Through AMSR-E and AMSR2 on board three generation of GCOM-W, we can make continuous and homogeneous observation of water cycle variables more than 20 years. Furthermore, integration of those data with past microwave imager data will enable us to evaluate trends of water cycle variables for nearly 50-year, such as changes in sea ice extent. It is needless to say that such information provides us substantial information to understand long-term climate variation.

Targets of the GCOM-W satellite are water-energy cycle, and will carry the AMSR2. AMSR2 will continue AMSR-E observations of water vapor, cloud liquid water, precipitation, SST, sea surface wind speed, sea ice concentration, snow depth, and soil moisture. Following improvements of AMSR2 instrument are planned based on experience in the AMSR-E mission; a) Deployable main reflector system with 2.0m diameter; b) Frequency channel set is identical to that of AMSR-E except additional 7.3GHz channel for radio frequency interference mitigation; and c) Two-point external calibration with the improved High Temperature Source (HTS). In addition, deep-space maneuver will be considered to check the consistency between main reflector and Cold Sky Mirror (CSM).

GCOM-W1 standard products, which are brightness temperature, integrated water vapor, integrated cloud liquid water, precipitation, sea surface temperature, sea surface wind speed, sea ice concentration, snow depth, and soil moisture, will be disseminated via JAXA online system. Currently JAXA plans data distribution schedule as follows; 1) to research and development or operational organizations under the cooperative agreement with JAXA, data will be distributed after the satellite commissioning (launch + 3 months) for calibration and validation purposes; and 2) to public researchers, data will be distributed after calibration and validation phase (launch + about 1 year).

3. GLOBAL SATELLITE MAPPING OF PRECIPITATION (GSMaP)

3.1. GSMaP NEAR-REAL-TIME VERSION (GSMaP_NRT)

Global rainfall map products were developed before the TRMM's launch, but they were intended mainly to obtain global "climatology" of precipitation. As the accuracy of satellite precipitation estimates improves and number of satellite and instruments increases, there are strong requirements from user community to generate high-frequency and fine resolution global precipitation map in near-real-time.

The Global Satellite Mapping for Precipitation (GSMaP) project was sponsored by the Japan Science and Technology Agency (JST) under the Core Research for Evolutional Science and Technology (CREST) framework between 2002 and 2007 (Okamoto *et al.*, 2005). Rainfall retrievals, referring statistical information from the TRMM Precipitation Radar, from several microwave imagers are merged (Aonashi *et al.*, 2009), and moving vector information from five geostationary satellite IR data with Kalman filtering techniques is combined to fill temporal gaps (Ushio *et al.*, 2009).

Near-real-time processing system of GSMaP product (GSMaP_NRT) has been in operation since October 2008. Binary data and browse images in 0.1 degree

latitude/longitude grid box and hourly resolution, are available at JAXA's GSMaP web site (<http://sharaku.eorc.jaxa.jp/GSMaP/>) 4-hours after observation (Ushio and Kachi, 2009). Since 14 June 2010, two Special Sensor Microwave-Imager/Sounder (SSMIS) instruments onboard DMSP F16 and F17 has been introduced to the GSMaP_NRT system in response to decrease of number of available passive microwave imagers, and microwave sounders are in preparation.

The GSMaP algorithm for SSMIS is developed based on GSMaP microwave imager algorithm for SSM/I. Due to calibration problem of SSMIS instruments, current algorithm uses only imager channels of SSMIS. We, however, expect to use sounder channels when SSMIS calibration completed.

3.2. GSMaP REANALYSIS VERSION (GSMaP_MVK)

Processing of reanalysis version of GSMaP products (hereafter referred as GSMaP_MVK) for meteorological and climate studies is currently underway. GSMaP_MVK applies latest retrieval algorithms (same as GSMaP_NRT) for entire period from 2002 to present. Table 2 shows differences in data sources used in original GSMaP (JST/CREST GSMaP), GSMaP_NRT, and GSMaP_MVK. Major characteristics of GSMaP_MVK compared to GSMaP_NRT products are; 1) to use "nearest" Global Analysis (GANAL) data provided by Japan Meteorological Agency (JMA) for 00Z, 06Z, 12Z, and 18Z to calculate look up table used in microwave imager retrieval algorithms for precise estimation of freezing level; 2) to use all available microwave imagers, including SSMIS, AMSU, and MHS; 3) to use NOAA Climate Prediction Center (CPC) full-resolution IR data for MVK to reduce missing area over the South-East Pacific; and 4) to combine forward and backward processing in MVK for precise rainfall estimation by using morphing technique from both "past" and "future" microwave observation.

Table 2. Data sources for GSMaP products.

Category	Instrument	JST/CREST GSMaP (2002-2006)	JAXA/EORC GSMaP_NRT	JAXA/EORC GSMaP_MVK (online)
Passive Microwave Imager & Sounder	TRMM TMI	NASA/GSFC Standard	NASA/GSFC Realtime	NASA/GSFC Realtime
	Aqua AMSR-E	JAXA/EORC	JAXA/EORC	JAXA/EORC
	DMSP SSM/I (F13, 14, 15)	Remote Sensing Systems	NOAA/DDS	NOAA/DDS
	DMSP SSMIS (F16, 17)	<i>Not used</i>	NOAA/DDS (2010.6~)	NOAA/DDS
	NOAA AMSU-A (N15-19), AMSU-B (N15~18), MHS (N19)	NOAA/NESDIS MSPPS Precipitation	<i>In preparation</i> NOAA/DDS (ocean) MSPPS Precipitation (land)	NOAA/DDS (ocean) MSPPS Precipitation (land)
	MetOp-A AMSU-A, MHS	<i>Not used</i>	<i>In preparation</i> NOAA/DDS (ocean) MSPPS Precipitation (land)	NOAA/DDS (ocean) MSPPS Precipitation (land)
IR imager on geostationary satellite	MTSAT, METEOSAT-7/8, GOES-11/12	NOAA/CPC Full-resolution IR data	Pixel TB of each geostationary satellite (MICOS JWA)	NOAA/CPC Full-resolution IR data
Atmos. Info.	---	JMA GANAL	JMA GANAL	JMA GANAL
SST	---	JMA MGDSST	JMA MGDSST	JMA MGDSST

The GSMaP microwave sounder algorithm to retrieve rainfall over the ocean is developed by Shige *et al.* (2009), based on the GSMaP microwave imager algorithm. The algorithm combines an emission-based estimate from Tbs at 23 GHz and a scattering-based estimate from Tbs at 89 GHz, depending on a scattering index computed from Tbs at both 89 and 150 GHz. Precipitation inhomogeneities are also taken into account.

Development of the GSMaP algorithm for AMSU over land is underway. Currently, the Microwave Surface and Precipitation Products System (MSPPS) Day-2 rainfall products, which are provided by NOAA, are also used as input rainfall over the land.

Figures 3 and 4 show impact of addition of SSMIS and AMSU instruments into GSMaP_MVK. Figure 3 show differences of coverage of hourly microwave radiometer observation area from 00Z to 03Z January 1, 2007, for MVK using only microwave imagers (left column), and for MVK using all available microwave imagers/sounders (right column). Observation areas by microwave imagers/sounders at 1-hour time frame are indicated in yellow in each image.

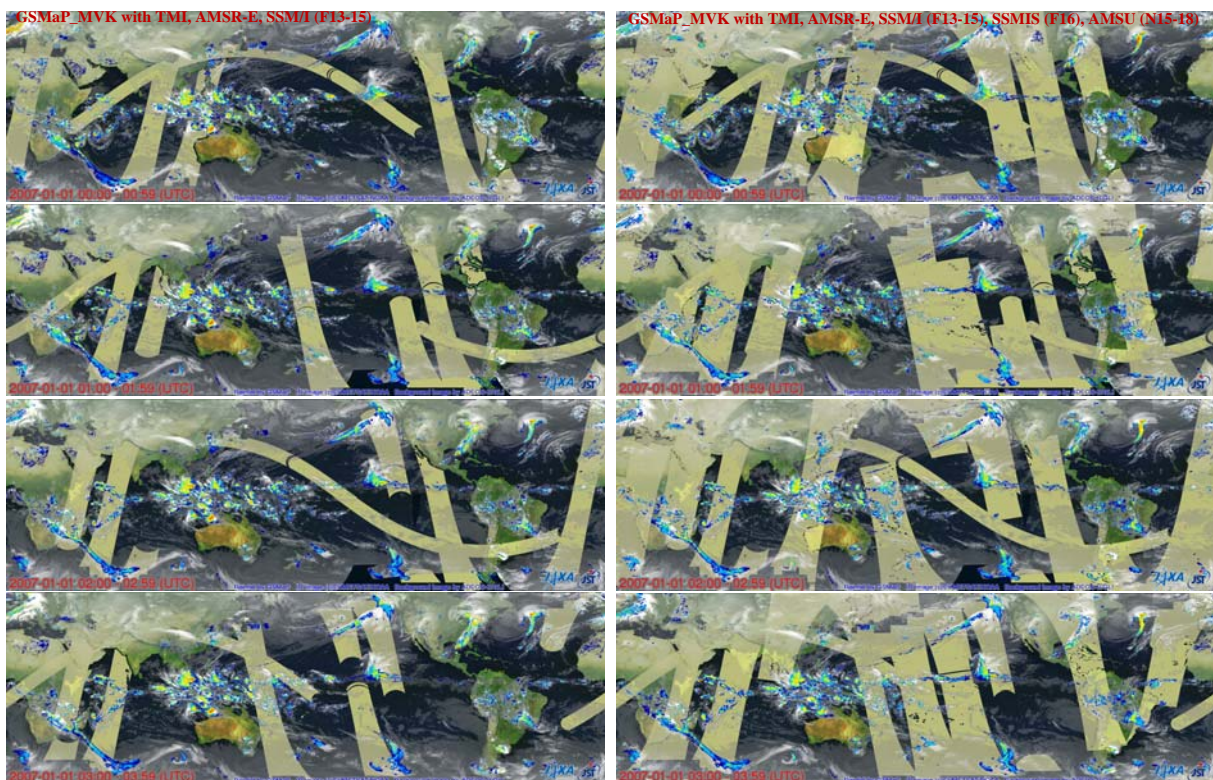


Figure 3. Effect of addition of SSMIS and AMSU to GSMaP_MVK.

Left: using only microwave imagers. Right: using all microwave radiometers.

Figure 4 shows monthly zonal average of rainfall in January 2007, for ocean (right figure) and land (left figure), comparing MWR (no temporal interpolation by IR) and MVK. Large amount of rainfall at mid and high latitude of Northern Hemisphere over land observed by MWR and MVK using only microwave imagers (TMI, AMSR-E, and SSM/I) is not shown in those using all available microwave imagers/sounders (TMI, AMSR-E,

SSM/I, SSMIS, and AMSU). Those differences will be caused by more frequent microwave imager/sounder observation.

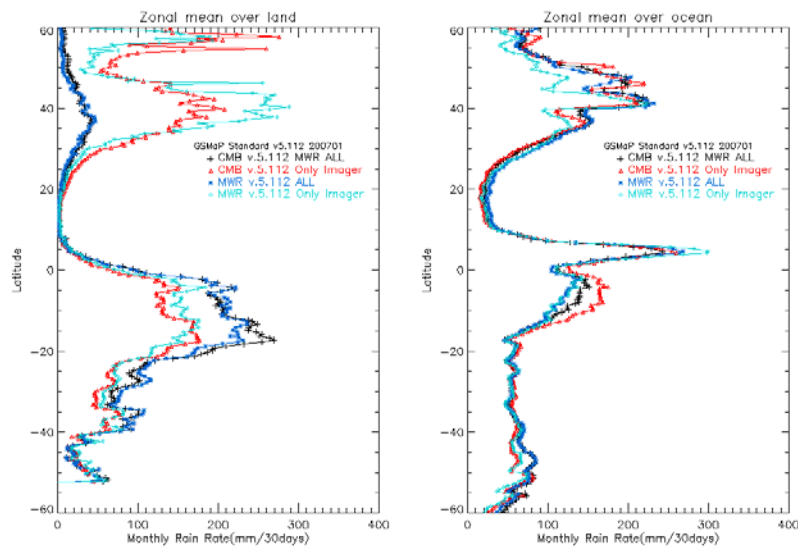


Figure 4. Monthly zonal mean average of GSMaP_MVK in January 2007. Black line (MVK using all microwave radiometers), red line (MVK using only microwave imagers), blue line (MWR using all microwave radiometers), and light blue line (MWR using only microwave imager), for over land (left) and over ocean (right).

4. SUMMARY

JAXA's precipitation missions, GPM and GCOM-W1, are introduced in this paper.

DPR, which is a successor of PR on the TRMM satellite, will be carried by the GPM core satellite, and is being developed by JAXA and NICT. The allocated requirements of each component and the performance of DPR system are verified through the development test, and the DPR system has currently been manufactured. Ground validation activities using newly manufactured Ka-band GV radars are planned in five GV sites in Japan from 2010 to 2013/2014, targeting to observe rainfall, wet snowfall, dry snowfall, and melting layers. Observation data by those radars expected to contribute to DPR algorithm development and its calibration/validation.

GCOM-W1 satellite and its core instrument AMSR2, which is a successor of AMSR-E on NASA's Aqua satellite, is being developed by JAXA for scheduled launch of JFY 2011. To keep continuous observation records from AMSR-E to AMSR2, and perform inter-calibration between AMSR-E and AMSR2, the GCOM-W1 satellite will join the A-train constellation and fly just in front of Aqua satellite. The GCOM-W1 satellite system test has started after delivery of AMSR2 flight model to the satellite system.

Global Rainfall Map in Near-Real-Time based on GSMaP algorithms (GSMaP_NRT) has been in operation at JAXA since October 2008, and we distribute 0.1 degree grid box and hourly global rainfall data four hours after observation. Processing of reanalysis version, GSMaP_MVK, by latest algorithms from 2002 to present is underway, and will

be distributed via GSMaP web site at JAXA. SSMIS and AMSU data are introduced to GSMaP_MVK and number of available microwave radiometers are largely increased compared to current status. Results for 2007 data show that impact of increase of number of microwave imagers/sounders are quite effective.

5. REFERENCES

- Aonashi, K., Awaka, J., Hirose, M., Koza, T., Kubota, T., Liu, G., Shige, S., Kida, S., Seto, S., Takahashi, N., and Y. N. Takayabu, 2009: GSMaP passive, microwave precipitation retrieval algorithm: Algorithm description and validation. *J. Meteor. Soc. Japan*, **87A**, 119-136.
- Okamoto, K., Iguchi, T., Takahashi, N., Iwanami K., and T. Ushio, 2005: The global satellite mapping of precipitation (GSMaP) project. *Proc. 25th IGARSS*, 3414-3416.
- S. Shige, T. Yamamoto, T. Tsukiyama, S. Kida, H. Ashiwake, T. Kubota, S. Seto, K. Aonashi and K. Okamoto, 2009: The GSMaP precipitation retrieval algorithm for microwave sounders. Part I: Over-ocean algorithm. *IEEE Trans. Geosci. Remote Sens.*, **47**, 3084-3097.
- Ushio, T., Kubota, T., Shige, S., Okamoto, K., Aonashi, K., Inoue, T., Takahashi, N., Iguchi, T., Kachi, M., Oki, R., Morimoto, T., and Z. Kawasaki, 2009: A Kalman filter approach to the Global Satellite Mapping of Precipitation (GSMaP) from combined passive microwave and infrared radiometric data. *J. Meteor. Soc. Japan*, **87A**, 137-151.
- Ushio, T., and M. Kachi, 2009: Kalman filtering application for the Global Satellite Mapping of Precipitation (GSMaP). *Satellite Rainfall Applications for Surface Hydrology*, M. Gebremichael and F. Hossain, Ed., Springer, 105-123.

THREE STUDIES: CAN MODELS REPLICATE TROPICAL PRECIPITATION CYCLES ACCURATELY? HOW DO MODELS AND SATELLITE ESTIMATES PERFORM IN THE NORTH ATLANTIC? DO WE REALLY INFLUENCE PRECIPITATION?

Chris Kidd

University of Birmingham, United Kingdom

e-mail: c.kidd@bham.ac.uk

The paper presents work from three of my MSc students on precipitation studies carried out this summer. The first compares a year of 3-hourly, 0.25-degree resolution data derived from the 3B42 product and the operational 25 km ECMWF model. The main aim of the project was to evaluate the ability of the ECMWF model to capture the diurnal cycle when compared with the 3B42 satellite product. Harmonic analysis of the data shows that the model products a relatively smooth diurnal field, particularly over the oceans that follows the solar heating. In comparison, the 3B42 product shows more variation, and no identifiable solar-heating effect.

Over the North Atlantic previous studies have shown that there are significant discrepancies between different precipitation products derived from satellites and models. Deficiencies in the model precipitation fields have been attributed to the model not resolving the post-frontal/secondary low pressure systems. This study has reinforced this: a year of ECMWF, HOAPS and GPCP (1 degree/daily) precipitation products were compared. Analysis of the precipitation fields showed that the occurrences of model underestimation increased during the cold season when compared with the HOAPS data sets, commensurate with the increased occurrence of post-frontal low pressure systems in this region.

The final study looked at the precipitation accumulation and occurrence around Birmingham (UK) using radar data. Previous studies, primarily in the US, have shown that urban areas have some effect on the local climatology, including precipitation. A factor that has greatly hindered these studies has been the availability of a dense gauge network to evaluate the precipitation fields in any detail. This study therefore used 1-km/5-minute radar data to provide the spatial distribution of precipitation up to 100 km from the urban area of Birmingham. Results of the study have proved inconclusive however: this may be attributed partly to the radar data itself (due to clutter, range effects etc) and partly to the nature of the urban area, which is 'greener' and less dense than many of the cities used in the US studies.

DIURNAL CHARACTERISTICS OF SATELLITE-DERIVED QUANTITATIVE PRECIPITATION ESTIMATE

Dongsoo Kim

NOAA/NESDIS National Climatic Data Center (NCDC), 151 Patton Avenue
Asheville, North Carolina, USA

e-mail: dongsoo.kim@noaa.gov

Recently, several satellite-derived high spatial and temporal resolution quantitative precipitation estimates (QPEs) have been produced and made available for use in longer-term hydro-climate studies. The inter-comparison and validation work of Sapiano and Arkin (2009) motivated this work to examine the diurnal cycle of hydro-climate variables against ground based radar and in-situ hourly gauge data. We selected two satellite QPE products, CMORPH (Joyce et al. 2004) and TMPA (Huffman et al. 2007) as both have 0.25-deg and 3-hr resolution. They are compared with Stage 4 multisensory QPE and reprocessed Hydrometeorological Automated Data System (HADS) hourly precipitation data for 5 years (2003 – 2007) at selected locations of unique climate: one in Florida where the diurnal cycle is driven by convective activity, the other in the Midwestern U. S. where summer-time precipitation is dominated by transient convective systems. During the summer months (June – August), both diurnal cycles of Stage 4 and gauge observations are in phase, but the satellite-based QPEs are about 3 hours out-of-phase in the diurnal cycle.

PRECIPITATION VALIDATION OVER THE OCEAN

Christian Klepp¹, Karl Bumke², Olaf Dahl³, and Axel Andersson⁴

¹ Meteorologisches Institut, KlimaCampus, Universität Hamburg, Germany

² Leibniz-Institut für Meereswissenschaften (IFM-GEOMAR), Kiel, Germany

³ Eigenbrodt, Königsmoor, Germany

⁴ Max-Planck Institut für Meteorologie, Hamburg, Germany

e-mail: christian.klepp@zmaw.de

ABSTRACT

Recent evaluations of different state-of-the-art satellite derived and re-analysis based precipitation climatologies show remarkably large differences in detection, amount, variability and temporal behavior. The uncertainties are largest in the ITCZ and the cold season high-latitudes. Our HOAPS (Hamburg Ocean Atmosphere Parameters and Fluxes from Satellite data, www.hoaps.org) precipitation retrieval exhibits fairly high accuracy in such regions. However, the statistical basis for a conclusive validation over the ocean has to be significantly improved with comprehensive ground validation (GV) efforts. Conventional in-situ instruments are not designed for precipitation measurements under high wind speeds on moving ships; hence virtually no GV data exists over the ocean, especially for snow.

This changed with the development of the optical disdrometer ODM470 by our KlimaCampus cooperation partners at Geomar (Univ. Kiel) and the company Eigenbrodt (Hamburg). A prototype instrument for snow was tested during two field campaigns in 2005 and 2008 in the cold season Norwegian Sea. Point to area validation shows a dichotomous detection accuracy of 0.98 for HOAPS precipitation. Quantitative collocation between the disdrometer and HOAPS shows a correlation up to 0.6.

However, as these collocated campaign data comprise only snowfall intensities below 1 mm/h a more systematic data collection effort with redesigned automated instruments on multiple ships in climate system hotspots and high impact weather events started in 2009 within a project at the KlimaCampus, Hamburg. The long-term in-situ data gathering period started in June 2010 with the permanent installation of the first automatic disdrometer on the German research icebreaker R/V Polarstern. Two other instruments were mounted both in early September 2010, permanently on R/V Akademik Ioffe (P.P.Shirshov Institute of Oceanology, RAS, Moscow, Russia) in western Greenland and temporarily on R/V Aranda (Finnish Meteorological Institute, Helsinki, Finland) in the context of the LPVEX (Light Precipitation Validation Experiment) campaign in the framework of GPM-GV. The core regions for these long-term precipitation measurements currently comprise the Arctic, Nordic Seas, Baffin Bay, ITCZ, the Southern Oceans, and the Antarctic. This paper gives an overview on the ODM470 instrument and the current status of the project.

1. INTRODUCTION

A thorough knowledge of the global water cycle components is an indispensable prerequisite for the understanding and successful modeling of the global climate system. While the majority of the global precipitation falls over the ocean its detection and quantification still remains a challenging task. Global ocean observations of precipitation fields with high spatio-temporal sampling can only be derived from passive microwave satellite data and are used for assimilation into re-analysis data sets. Although recent evaluations of different state-of-the-art satellite derived and re-analysis based precipitation climatologies show that the commonly known patterns are well represented, remarkably large differences still exist in terms of detection, amount, variability and temporal behavior among the products (Andersson et al., 2010b, Romanova et al., 2010). The uncertainties are largest in climate system hotspot areas like the ITCZ or the cold season high-latitudes. Evaluation studies indicate that our HOAPS (Hamburg Ocean Atmosphere Parameters and Fluxes from Satellite data (www.hoaps.org)) precipitation retrieval exhibits fairly high accuracy in these regions (Andersson et al., 2010a). However, the statistical basis for a sophisticated over ocean validation has to be significantly improved. To further increase the observing capability of global precipitation from space the Global Precipitation Measurement (GPM) Mission aims at 3-hourly 0.25° resolution fields using a multitude of sensors that need to be inter- and cross-calibrated into global climatologies. Retrieving high quality estimates of rain and especially snow calls for the need of comprehensive ground validation (GV) of precipitation. Over land several instruments capable of measuring precipitation are used in supersites and field campaigns to receive GV data. However, these distribution droplet meters (Disdrometers) and gauges are not designed for high wind speeds on moving ships, hence virtually no GV data exists over the ocean, especially for snow, but is urgently required.

This motivated the development of the optical disdrometer ODM470 by our Clisap co-operation partners at Geomar, Kiel and the company Eigenbrodt. Today the ODM470 is the only instrument capable of measuring rain and snow with high accuracy under high wind speeds on moving ships. The prototype instrument for snow was tested during two field campaigns in 2005 and 2008 in the cold season Norwegian Sea. Further analysis of the data within our KlimaCampus, Hamburg project "Objective Global Ocean Precipitation Climatology through Validation in Climate System Hotspots" shows a dichotomous detection accuracy of 0.98 when point to area validated against HOAPS precipitation data (Klepp et al., 2010). Quantitative collocation between the disdrometer and HOAPS shows a correlation of up to 0.6. However, the collocated campaign data comprises snowfall intensities below 1 mm/h only. Comparing case study data for intense snowfall up to 7 mm/h in both HOAPS and ODM470 data yields plausible results but also large spatio-temporal collocation mismatches (Brümmer et al., 2010). Hence, the systematic collection of GV data from 2010 until 2015 within our project over remote ocean areas on several ships in all climatic regions will lead to a data set capable of comprising all precipitation events from light to severe including liquid, mix-phase and solid precipitation for validation against satellite retrievals.

Section 2 gives a description of the optical disdrometer ODM 470 system and summarizes the algorithms used for the derivation of the disdrometer rain and snowfall rate. The LOFZY 2005 field campaign results using the prototype instrument are summarized in Section 3. A more detailed overview on this field campaign is given in

Klepp et al. (2010). Section 4 summarizes and concludes the recent technical developments that qualify the ODM470 as an automatic measurement system and gives an overview on recent ship operations and field campaigns and points at the need of point to area validation techniques.

2. THE ODM470 OPTICAL DISDROMETER

The optical disdrometer originally developed by Großklaus et al. (1998) is today called ODM470 (Fig. 1) and is commercially available from Eigenbrodt Environmental Measurement Systems near Hamburg, Germany. It was successfully validated to measure liquid and solid precipitation even under strong wind conditions (Großklaus, 1996; Bumke et al., 2004). Lempio et al. (2007) further developed the snowfall algorithm and applied the disdrometer measurements during an intercomparison field campaign in Uppsala, Sweden in winter 1999/2000. Comparison with gauge data and manual measurements showed reliable instrument performance.

The measurement principle of the ODM470 disdrometer is light extinction of an infrared light emitting diode at 880 nm wavelength caused by hydrometeors passing through a cylindrical sensitive volume of 120 mm length and 22 mm diameter, which is kept perpendicular to the local wind with the aid of a wind vane. The cylindrical form of the volume causes the measurement to be independent of the incident angle of the hydrometeors (Lempio et al., 2007). The relative wind speed is measured using an anemometer. The electronic signal caused by the hydrometeor is proportional to its cross-sectional area. The disdrometer measures the size of the cross-sectional area and the residence time of hydrometeors in the sensitive volume within a size range of 0.4–22 mm. Measurements are partitioned in 129 size bins with highest resolution for small particles and a logarithmic increase in size:

$$d_p(\text{bin}) = \frac{e^{\left(\frac{\text{bin}}{94} \cdot \ln 10\right)} - 1 + e^{\left(\frac{\text{bin}+1}{94} \cdot \ln 10\right)} - 1}{2}, \quad [\text{mm}]$$

Collector lenses and an optical blend are used for homogeneous illumination of the sensitive volume (Fig. 1). The averaging time interval is set to 60 s. Coincidence effects of multiple hydrometeors within the sensitive volume at the same time and edge effects of partly scanned hydrometeors are considered for liquid phase precipitation.

The precipitation rate in mm h⁻¹ is calculated using the size bins, terminal velocity, mass of the hydrometeors and the particle size distribution density which is calculated after Clemens (2002) by particle counting given the local wind speed along with the measuring time interval and the size of the optical volume. The determination of the rainfall rate through its liquid water content or mass $M_{tr}(\text{bin}) = \pi \cdot \left(\frac{4}{3}\right) \cdot 1000 \cdot \left(\frac{d_p(\text{bin})}{200}\right)^3$ and the fall velocity ($V_{fall}(\text{bin}) = 9.65 - 10.3 \cdot \text{EXP}(-1.2 \cdot (d_p(\text{bin})^{12}/2))$) is easily parameterized as rain drops have a nearly spherical shape and a constant density.

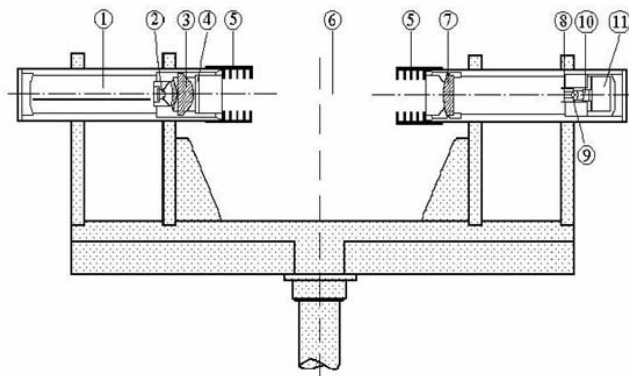


Figure 1. Cross-section of the optical disdrometer ODM 470 (left) and the measurement system onboard a ship (right). From left to right: electronics (1), light emitting diode (2), lens system (3), window (4), baffles (5), sensitive volume (6), achromatic collector lens (7), optical blend (8), ocular (9), photo diode (10), electronics compartment (11).

In contrast to rainfall, solid precipitation is characterized by a variety of complex shapes with different fall velocities and different equivalent liquid water content even if identical in maximum dimension. The measured cross-sectional area depends on size, shape and orientation of the solid particles hindering the development of a unique solid precipitation retrieval scheme. The relationship between mass or equivalent liquid water content and the terminal fall velocity for snow crystals is analysed by Hogan (1994) as a function of their maximum dimension. However, the disdrometer measures the size of the cross-sectional area instead of the maximum dimension of non-spherical particles. Assuming that the ice crystals fall randomly oriented through the sensitive volume (Brandes et al., 2007) and that a large sample of crystals of the same type has a repeatable mean cross-sectional area, the parametrization of Hogan (1994) can be used. This allows the derivation of a transformation function to derive the maximum dimension of the crystal type from the mean cross-sectional area and hence the equivalent liquid water content $M_{tr}(bin)=0.0000107*(dp(bin))^{**3.1}$ and terminal fall velocity $V_{fall}(bin)=7.33*(dp(bin))^{**0.78}$, resulting in the liquid water equivalent of the precipitation (rain and snow) rate in mm h⁻¹:

$$R = 3600 \cdot \sum_{bin=0}^{128} n(bin) \cdot V_{\infty}(bin) \cdot M_{tr}(bin).$$

given the size bins from 0 to 128 in logarithmic size, the terminal velocity of the hydrometeors $v_{\infty}(bin)$ and the mass of the hydrometeors $M_{tr}(bin)$ using the particle size distribution density by Clemens (2002) $n(bin)$ by particle counting $N(bin)$:

$$n(bin) = \frac{N(bin)}{L \cdot D \cdot T \cdot \sqrt{ff^2 + (v_{\infty}(bin))^2}}$$

using the measured local wind speed (ff), the measuring time interval (T) and the geometry of the sensitive volume length (L) and diameter (D).

However, the disdrometer cannot identify the type of a particle. Hence, Macke et al. (1998) developed a geometrical model to simulate different snow crystal types and a ray tracing model to determine the mean cross-sectional area out of 3000 randomly orientated projections for different sizes with regard to their maximum dimension. Lempio et al. (2007) found from theoretical experiments that the product of the terminal velocity and the equivalent liquid water content as a function of the cross-sectional area of different types of snow crystals are of the same order of magnitude and allow using one common parametrization for lump graupel. As lump graupel is nearly spherical in shape, it needs no transformation function from cross-sectional area to maximum dimension. The parametrization for lump graupel is applicable for particles with a size range of 0.4–9 mm. Single precipitation events showed larger cross-sectional areas up to 22 mm caused by giant snowflakes. Lump graupel was the most frequently observed precipitation type over the Nordic Seas during the LOFZY campaign. Current investigations in our group indicate that if no observations of the precipitation phase are available, the shape of the size spectra of the disdrometer calibrated for solid precipitation can be used to identify rain, snow or sleet from the data.

The ODM470, calibrated for solid precipitation measurements, was previously operated on R/V Knorr over the cold season Labrador Sea (Marshall et al., 1998) and successfully compared against other precipitation measuring devices and with manual measurements in a winter campaign 1999/2000 at the Meteorologisk Institut Uppsala in Sweden. High amounts of snowfall caused the disdrometer precipitation rates to be larger when compared to other instruments. This might result from flow distortion effects of the other instruments as the disdrometer is able to measure correctly even under high wind speeds. An opto-electronically infrared rain sensor (IRSS88), commercially available from Eigenbrodt Environmental Measurement System operationally measured precipitation frequency. The instrument houses two high-intensity infrared beams generating an active sensing area of about 120 mm × 25 mm. The system is able to detect even low density and small-sized hydrometeors that pass through the sensing area. The averaging time interval is set to 60 s.

Overall, the ODM470 in combination with the IRSS88 is a unique system based on a robust hardware with minimal maintenance requirements that enables a complex measurement task— the estimation of the rain and snow rate even under high wind speeds on a moving ship. This system, installed on the highest parts of the ship's mast, allows the generation of a vitally important ship-based precipitation data set for validation of remote sensing and model analysis data.

The satellite derived HOAPS climatology is the only generally available compilation of both precipitation and evaporation with the goal of estimating the net freshwater flux from one consistently derived global satellite data set. To achieve this goal, HOAPS utilizes multi-satellite averages, inter-sensor calibration, and an efficient sea ice detection procedure. All 15 HOAPS variables are derived using radiances of the Special Sensor Microwave/Imager (SSM/I) radiometers, except for the sea surface temperature, which is obtained from Advanced Very High Resolution Radiometer (AVHRR) measurements. Since 1987, six SSM/I instruments have been launched into space, which are considered to be temporally stable measuring instruments, thus providing a reliable basis for a climatological data set. Global ocean data between 1988 and 2005 of the recently released improved and extended version HOAPS-3 is publicly available via www.hoaps.org (Andersson et al., 2010a and Andersson et al., 2010b).

3. FIELD CAMPAIGN RESULTS

The optical disdrometer ODM470 demonstrated its potential by measuring liquid and solid precipitation during the LOFZY 2005 campaign on R/V Celtic Explorer in February and March 2005 over the cold season Nordic Seas offshore Norway. For monitoring and quality control of the disdrometer data a precipitation detector was operated accompanied by a detailed observer's log. During 15 d a total of 171 cases could be point-to-area collocated against SSM/I satellite data of the DMSP F-13, F-14 and F-15 spacecrafts. This includes 52 precipitation events and 119 correct negatives. The dichotomous verification of the precipitation frequency resulted in a perfect score between the disdrometer, the detector and the observer's log giving confidence in the collected ground validation data. The HOAPS precipitation is overall consistent with the disdrometer data with a detection accuracy of 96%, a bias score of 94%, a hit rate of 90%, a false alarm ratio of only 4% and a probability of false detection of only 2%. In contrast, GPCP 1DD and GPROF2004 data turn out to be not sensitive to solid precipitation at high-latitudes (Klepp, et al., 2010)

Some of the most interesting cases are the events shorter than 6 min duration, where the disdrometer values are close to zero while HOAPS detects precipitation between 0.3 and 0.6 mm h⁻¹. All these cases contained ice-virga observations of snowfall in scattered showers that only partially reached the ground. Such high latitudes ice-virga observations are also described by Hobbs et al. (2001) and Wang et al. (2004). The microwave radiation emitted from these evaporating hydrometeors correctly leads to a precipitation signal in the HOAPS climatology. This leads to the question how much virga precipitation is falling on Earth and how much it might contribute to the total amount in satellite climatologies. In five cases the disdrometer measured precipitation while the HOAPS values were zero. These were single events during the ± 45 min interval with durations shorter than 6 min. Such events cannot be detected in the HOAPS climatology as the precipitation is too weak or evolves too quickly to contribute significantly to the satellite signal of the 50 km pixel size, given that a lower threshold of 0.3 mm h⁻¹ needs to be reached.

The significantly better performance of the solid precipitation in the HOAPS precipitation retrieval compared to other satellite precipitation products points at a fundamental issue of precipitation retrievals, namely the importance of the a priori knowledge that constrains the retrieval. Passive microwave observations of precipitation over oceans are mainly sensitive to integrated contents of hydrometeors and exhibit, except for deep tropical convection, little sensitivity to frozen hydrometeors, in particular in cold environments and shallow convection. Most retrieval algorithms that are applied to global observations are trained with datasets that rarely represent high-latitude precipitation events so that the combined effect of weak radiometric sensitivity and insufficient statistical representativeness produces unrealistic precipitation retrievals. HOAPS is the only generally available product that has been trained with global NWP model output that is—within the limits of global model physics parametrizations—consistent in terms of cloud physics and radiative transfer. Since most global NWP models produce rather realistic liquid and frozen precipitation forecasts at the surface, the HOAPS training dataset can be expected to include a much better statistical representation of precipitation than other datasets. Hence, HOAPS precipitation can be expected to be better than other satellite based precipitation datasets at high- and mid-latitudes (Klepp et al., 2003 and 2005).

The encouraging results of HOAPS detecting solid precipitation over the cold season Nordic Sea will allow for a quantitative analysis between the point-to-area collocated precipitation rates of HOAPS and the ODM 470 disdrometer. As a first attempt a separation time of 6 min for splitting the data set containing 52 snowfall events is selected from the observer's log and the disdrometer data, as this length of time represents the typical duration of a single cell precipitation event. The correlation between the disdrometer and the HOAPS climatology is 0.6 for precipitation events longer than 6 min. However, this analysis needs to be investigated in more detail in terms of representativeness errors associated with the point to area comparisons along with sampling and instrument errors. The LOFZY campaign is described in detail in Klepp et al. (2010) and Brümmer et al. (2010).

The high accuracy for the collocated precipitation events during LOFZY 2005 indicates that HOAPS-3 is able to reliably detect solid precipitation at high latitudes during the cold season. Nevertheless, only precipitation events below 1 mm h⁻¹ could be point-to-area validated. Although two additional case studies indicate that the HOAPS precipitation values are also plausible for substantially higher snowfall rates, longer term measurements covering the entire precipitation spectrum including extreme values are required.

4. CURRENT STATUS AND OUTLOOK OF THE PROJECT

A first attempt to obtain more Nordic Sea cold season disdrometer measurements was carried out in March 2008. In close cooperation with the Bjerknes Centre for Climate Research (BCCR) and the Norwegian Coast Guard (Kystvakten) the ODM470 participated in the THORPEX field campaign within the International Polar Year and operated successfully onboard K/V Senja.

The main aim of the first phase of the newly established KlimaCampus, Hamburg project "Objective Global Ocean Precipitation Climatology through Validation in Climate System Hotspots" by the beginning of 2009 was to purchase three ODM470, and to convert these in close cooperation with Eigenbrodt to fully automatic measurement systems, followed by a rigorous testing phase and finally to begin the operational measurement phase onboard ships.

In terms of modification, the instrument design was changed to further reduce flow distortion caused by the instrument itself. The experience from operating the prototype ODM470 instrument and the IRSS88 precipitation detector along with the knowledge that the accuracy in detecting precipitation between both instruments was identical led to the idea of interposing the IRSS88 between the ODM470 and the data processing computer. This now causes the IRSS88 to shut down the ODM470 if no precipitation is measured after a time interval of one minute and hence prolongs life time of the expensive optical system of the ODM470. The ODM470 LED is expected to operate for continuous 7000 hours lifetime or 292 continuous days. Given that precipitation events are rare compared to no precipitation events the lifetime of the instrument is prolonged significantly. The internal electronic card of the prototype instrument is changed from Windows 3.1 to Windows XP operation. An updated software package accounts for coincidences of two or more drops in the optical volume at the same time, partial scanning of drops at volume margin and also corrects for artifacts in the optical volume, e.g. spider webs. Such artificial signals measured by the ODM470 become additionally

unlikely as the decision to collect precipitation information by switching on the ODM470 is on the IRSS88 detector.

The ODM470 using the logarithmical size binning is capable of measuring liquid and solid precipitation. The decision which algorithm to use is momentarily transferred to ancillary data delivered by the research vessel. All meteorological data that is automatically collected is used together with GPS coordinates and the present weather observing codes ww, W1 and W2. Together with air temperature data from the ship the discrimination of liquid and solid precipitation in the ODM470 data turns out to be easy. This led to a procedure of using the rainfall algorithm for the entire shipboard time series first. Applying thresholds on air temperature and rainfall intensities can lead to an automatic procedure based on these findings to identify where the snowfall algorithm needs to replace the rainfall data. Also number concentration values plotted against particle diameter for particle size distributions can be used to discriminate usually fewer and larger solid particles from abundant small rain drops. Investigations using such procedures are currently tested. For the usually few cases with mix-phase precipitation the snowfall algorithm is used, which may lead to a slight underestimation of the precipitation estimate.

The maintenance-free system uses an automatic data back-up written to the internal hard disk and on memory stick and the system is plugged to an Uninterruptible Power Supply (USV) that buffers power outages for up to 45 minutes. Experience showed that short time power outages on ships occur frequently making this precaution measure unavoidable. In case of an unexpected system shut down the system reboots automatically and the data logging software restarts automatically without personal assistance.

During winter 2009/2010 all three ODM470 underwent rigorous testing on the rooftop of the KlimaCampus building in Hamburg. Several hardware and software update needs were identified and applied. A comprehensive technical document was written for mounting onboard ships.

Initially it was planned to equip three Norwegian Coast Guard ships. However, these ships are long-term docked for heavy maintenance and rebuilding. Nevertheless, contact to national and international field campaign programs, institutes and corresponding ship operators allowed for starting the systematic data collection procedure with the automated instruments on multiple ships that operate in climate related system hotspots not circumventing high impact weather events by mid 2010.

The long-term measurement phase started on 8 June 2010 with the installation of one instrument on R/V Polarstern of the Alfred Wegener Institute (AWI). The ODM470 time series on R/V Polarstern now comprises one complete year from 10 June 2010 to 20 May 2011 and is given in Fig. 2 together with the relative wind speed and the air temperature. Air temperatures below 0°C indicate the phases of solid precipitation. The ships cruise comprised 7 legs. In June 2010 ARK25/1 took place at the island of Svalbard in the inner Arctic. ARK25/2 was carried out in the Greenland Sea while ARK25/3 brought R/V Polarstern into the Labrador Sea. ANT27/1 comprised the transect of the entire Atlantic Ocean towards Antarctica. ANT27/2 and /3 were carried out in Antarctic waters by collecting data in the usually data-void Southern Oceans while ANT27/4 was the return transect to Bremerhaven (Fig. 2.). A total of 40176 minutes (equivalent to 670 hours or 28 days of continuous precipitation) of precipitation (rain and snow) were measured by the ODM470 without any data outage or noticeable problems. After minor maintenance of the instrument in June 2011 in Bremerhaven, Germany, R/V

Polarstern again left for the Arctic with our instrument onboard by the end of June 2011. On 02 September 2010 the second ODM470 was long-term mounted onboard R/V Akademik Ioffe in co-operation with the P.P.Shirshov Institute of Oceanology, RAS, Moscow, Russia (S. Gulev). The installation took place in Kangerlussuaq, Greenland. From there the ship cruised the Labrador Sea followed by several transects of the North Atlantic Ocean in the region of the storm track. After a stop in Kaliningrad, Russia, the ship transected the Atlantic Ocean towards Antarctica doing measurements in the Southern Oceans. This time series is also approaching a length of one year of continuous measurements and is awaiting analysis in the near future.

A third ODM470 was installed to R/V Aranda of the Finnish Meteorological Institute (FMI) from 13 September to mid October 2010 for measurements within the framework of the LPVEX (Light Precipitation Validation Experiment) campaign embedded in GPM-GV carried out in the Baltic Sea just South of Helsinki, Finland. The aim of this campaign was to measure light precipitation from a variety of measurement devices, both on land and over the sea carrying out point to area validation using the ship, coastal radar, aircraft data (Wyoming King Air) and several sources of satellite data (e.g. SSMIS and Cloudsat). Despite our ODM470 the ship was equipped with a Parsivel disdrometer and a micro rain radar from Metek. Several target cases were identified during this experiment and data analysis is currently being carried out. Joint validation effort will be coordinated at during a workshop in Helsinki in fall 2011.

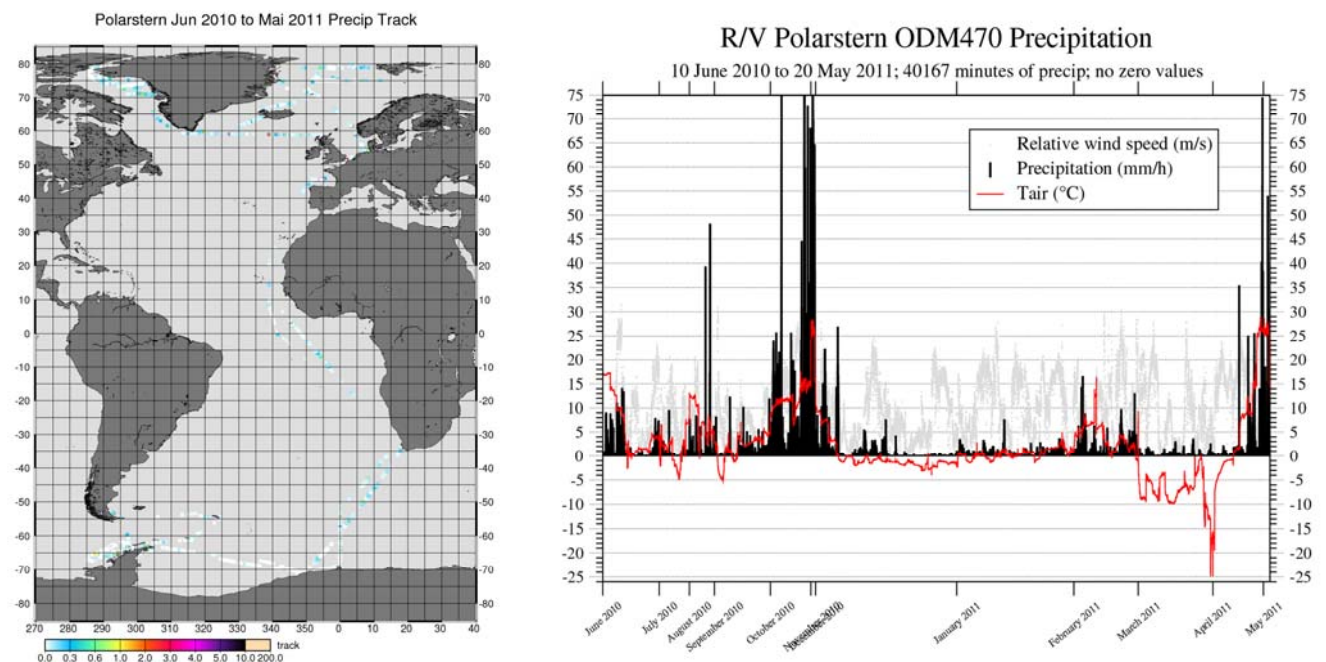


Figure 2. One complete year of ODM470 time series from 10 June 2010 to 20 May 2011 onboard R/V Polarstern showing the cruise track for precipitation events only in mm/h (left) and the entire time series for precipitation events only (rain and snow) in mm/h in black, relative wind speed in grey and air temperature in red.

The goals of our disdrometer measurements are to help constraining satellite retrievals for the upcoming GPM satellite generation in terms of liquid and solid precipitation over

the ocean by supplying GV data and to validate and improve the HOAPS precipitation retrieval for the upcoming SSMIS period. The project is hosted until 2015 through the KlimaCampus, Hamburg and funded through the MABANAFT, Initiative-Pro-Klima fellowship.

The intermittent nature of precipitation, its high variability in space and time and the indirect approaches for its measurement cause a very large range of estimates among available products, especially over the oceans. For all observational data, it is hence important to understand their accuracy and limitations. However, point measurements from gauges or optical disdrometers are likely to be unrepresentative of the aerial value estimated by the satellite of various different footprint sizes. Additionally the timescale can also be unrepresentative if accumulated rainfall of gauges is compared to instantaneous data from satellites. This requires the application of advanced statistical verification methods that filter out the representativeness of the measurements along with estimate sampling and instrument errors and decorrelation lengths for different precipitation types and regimes needed for point to area measurement intercomparisons. Such methods are currently in development for various specific applications and depend on how large and numerous the point samples are compared to the area averages. The exploitation of these statistical measures can additionally deliver some explicit definition of the input errors for numerical prediction models. Aerial data from radar, aircraft or satellites have different spatial scales and hence the precipitation variability within the field of view is scale dependant. Comparisons of scale dependant multisensor collocated precipitation data sets including ship based optical disdrometers, land based gauges, radar, and remote sensing data from aircraft and satellite data of varying resolution along with NWP model data needs to be used to assess the statistical characterization of multiscale precipitation variability.

5. REFERENCES

Andersson, A., K. Fennig, C. Klepp, S. Bakan, H. Graßl, and J. Schulz, 2010a: The Hamburg Ocean Atmosphere Parameters and Fluxes from Satellite Data—HOAPS-3. *Earth Syst. Sci. Data Discuss.*, 3, 143–194.

Andersson, A., Klepp, C., Fennig, K., Bakan, S., Graßl, H., and Schulz, J., 2010b: Evaluation of HOAPS-3 ocean surface freshwater flux components, *J. Appl. Meteor. Climatol.*, doi:10.1175/2010JAMC2341.1.

Brandes, E. A., Ikeda, K., Zhang, G., Schönhuber, M. and Rasmussen, R. M. 2007. A statistical and physical description of hydrometeor distributions in Colorado snowstorms using a video disdrometer. *J. Appl. Met. Clim.* **46**(5), 634–650.

Brümmer, B., Müller, G., Klepp, C., Spreen, G., Romeiser, R. and coauthors. 2010. Characteristics and impact of a gale-force storm field over the Norwegian Sea. *Tellus* **62A**, 481-496.

Bumke, K., Clemens, M., Grassl, H., Pang, S., Peters, G. and co-authors. 2004. Accurate areal precipitation measurements over the land and sea (APOLAS), *BALTEX Newslett.* **6**, 9–13.

Clemens, M. and Bumke, K. 2002. Precipitation fields over the Baltic Sea derived from ship rain gauge measurements on merchant ships. *Boreal Environ. Res.* **7**, ISSN 1239–6095, 425–436.

Großklaus, M. 1996. Niederschlagsmessung auf dem Ozean von fahrenden Schiffen. Dissertation, Institut für Meereskunde an der Christian- Albrechts-Universität Kiel.

Großklaus, M., Uhlig, K. and Hasse, L. 1998. An optical disdrometer for use in high wind speeds. *J. Atmos. Oceanic Technol.* **15**, 1051–1059.

Hobbs, P. V., Shupe, M. and Uttal, T. 2001. Airborne studies of cloud structures over the Arctic Ocean and comparisons with retrievals from ship-based remote sensing measurements. *J. Geophys. Res.* **106**, 15 029–15 044.

Hogan, A. 1994. Objective estimates of airborne snow properties. *J. Atmos. Oceanic Technol.* **11**, 432–444.

Klepp, C.-P., Bakan, S. and Graßl, H. 2003. Improvements of satellite derived cyclonic rainfall over the North Atlantic. *J. Climate* **16**, 657–669.

Klepp, C.-P., Bakan, S. and Graßl, H. 2005. Missing North Atlantic cyclonic precipitation in the ECMWF model and ERA-40 data detected through the satellite climatology HOAPS II. *Met. Z.* **14**, 809–821.

Klepp, C., K. Bumke, S. Bakan, and P. Bauer, 2010: Ground validation of oceanic snowfall detection in satellite climatologies during LOFZY. *Tellus*, 62, 469–480.

Lempio, G., Bumke, K. and Macke, A. 2007. Measurement of solid precipitation with an optical disdrometer. *Adv. Geosci.* **10**, 91–97.

Macke, A., Francis, P. N., Mc Farquhar, G. M. and Kinne, S. 1998. The role of ice particle shapes and size distributions in the single scattering properties of cirrus clouds, *J. Atmos. Sci.* **55**(17), 2874–2883.

Marshall, J., Dobson, F., Moore, K., Rhines, P., Visbeck, M. and coauthors. 1998. The labrador sea deep convection experiment. *Bull. Amer. Meteor. Soc.* **79**, 2033–2058.

Marshall, J., Dobson, F., Moore, K., Rhines, P., Visbeck, M. and coauthors. 1998. The labrador sea deep convection experiment. *Bull. Amer. Meteor. Soc.* **79**, 2033–2058.

Romanova, V., Köhl, A., Stammer, D., Klepp, C., Andersson, A., and Bakan, S., 2010: Intercomparison of GECCO, HOAPS and NCEP net Sea Surface Freshwater Flux Fields, *Tellus A*, 62, 435–452, doi:10.1111/j.1600-0870.2010.00447.x.

GLOBALY GRIDDED SATELLITE (GRIDSAT) OBSERVATIONS FOR CLIMATE STUDIES

Kenneth Knapp

NOAA National Climatic Data Center, Asheville, NC, USA

e-mail: ken.knapp@noaa.gov

Geostationary satellites have provided routine, high temporal resolution Earth observations since the 1970s. Despite the long period of record, use of these data in climate studies has been limited for numerous reasons, among them: there is no central archive of geostationary data for all international satellites, full temporal and spatial resolution data are voluminous, and diverse calibration and navigation formats encumber the uniform processing needed for multi-satellite climate studies. The International Satellite Cloud Climatology Project set the stage for overcoming these issues by archiving a subset of the full resolution geostationary data at ~10 km resolution at 3 hourly intervals since 1983. Recent efforts at NOAA's National Climatic Data Center to provide convenient access to these data include remapping the data to a standard map projection, recalibrating the data to optimize temporal homogeneity, extending the record of observations back to 1980, and reformatting the data for broad public distribution. The Gridded Satellite (GridSat) dataset includes observations from the visible, infrared window, and infrared water vapor channels. Data are stored in the netCDF format using standards that permit a wide variety of tools and libraries to quickly and easily process the data. A novel data layering approach, together with appropriate satellite and file metadata, allows users to access GridSat data at varying levels of complexity based on their needs. The result is a climate data record already in use by the meteorological community. Examples include reanalysis of tropical cyclones, studies of global precipitation, and detection and tracking of the intertropical convergence zone.

APPLICATION OF MET FOR THE VERIFICATION OF THE NWP CLOUD AND PRECIPITATION PRODUCTS USING A-TRAIN SATELLITE OBSERVATIONS

Paul A. Kucera¹, Barbara Brown¹, Randy Bullock¹, and Courtney Weeks¹

¹National Center for Atmospheric Research, Boulder, Colorado, USA

e-mail: pkucera@ucar.edu

ABSTRACT

This study demonstrates the usefulness of the NCAR Model Evaluation Tools (MET) applied to the verification of NWP cloud and precipitation products using high-resolution A-Train satellite observations. MET has been developed with support of the Developmental Testbed Center (DTC) at NCAR and has been integrated into community release of the Weather Research and Forecasting (WRF) system. The primary objective of MET is to provide users tools for forecast verification. MET provides grid-to-point, grid-to-grid, and advanced spatial verification techniques in one unified, modular toolkit that can be applied to a variety of spatial fields (e.g., comparison of NWP precipitation estimates with satellite observations). For advanced spatial verification, NCAR has been developing a spatial verification tool that has been incorporated into MET called Method for Object-based Diagnostic Evaluation (MODE). We have been developing additional capabilities of MET/MODE to evaluate NWP products in the vertical using swath or curtain data from A-Train satellite observations such as CloudSat, MODIS, and TRMM. The enhancements being developed match fields from NWP products with satellite observations and compare similar attributes such as vertical structure, cloud top height, and cloud base height. A summary of this effort is provided in this paper.

1. INTRODUCTION

The Model Evaluation Tools (MET) was originally developed for verification of the Weather Research and Forecasting (WRF) modeling system. This effort is supported by the Developmental Testbed Center (DTC: A joint collaboration between NCAR and NOAA; <http://www.dtcenter.org>) to provide a state-of-the-art verification package to the numerical weather prediction (NWP) community. By design, MET incorporates traditional statistical tools along with newly developed and advanced verification methodologies. These new methodologies include methods for diagnostic and spatial verification. The capabilities of other NWP verification systems (e.g., NCEP verification capabilities) are also included in the development of MET. These capabilities include input/output, methods, statistics, and data types. Besides the traditional verification

approaches (e.g., critical success index, root mean squared error), estimation of confidence intervals for verification measures and spatial forecast verification methods are included in MET. The goal of this study is to demonstrate the usefulness of MET applied to model cloud fields and A-Train satellite observations of clouds.

Originally, MET was designed with the primary focus of verifying NWP forecasts using surface measurements for reference. The same functionality lends itself to verification of cloud fields being produced in NWP models using satellite observations (e.g., CloudSat) as the reference. In this study, we show the usefulness of MET for the verification of cloud properties generated by the Rapid Update Cycle (RUC) using CloudSat observations as the verification reference. As a demonstration in this study, the verification methodology was applied to a large scale synoptic event observed over the continental United States. The remaining paper is organized as follows. The next section provides an overview of MET. Section 3 describes the datasets used in the study. In Section 4, we present the results of the example comparison. The final section provides a summary of the study.

2. OVERVIEW OF MET

The MET package has been designed to be modular and adaptable. For example, individual statistical tools can be used without running the entire analysis tools. The user can easily add new analysis tools that fit the needs of the required analysis. The MET software package runs on a Linux system that can easily be applied by any user on their local computer system. In addition, the MET tools can readily be incorporated into a larger “system” that may include a database as well as more sophisticated input/output and user interfaces. A more detailed description along with access to the MET software package can be obtained from the DTC website: <http://www.dtcenter.org/met/users/>.

The MET computes a variety of traditional statistics continuous and categorical variables, many of are described in detail in the text by Wilks (2006). For example, statistics such as bias, root-mean squared error (RMSE), correlation coefficient, and mean absolute error (MAE) are computed for continuous variables. For categorical measures, statistics such as Probability of Detection (POD), Probability of False Detection (POFD), False Alarm Ratio (FAR), and Critical Success Index (CSI) are computed in MET. In addition to providing traditional forecast verification scores for both continuous and categorical variables, confidence intervals are also produced using parametric and non-parametric methods. Confidence intervals take into account the uncertainty associated with verification statistics due to sampling variability and limitations in sample size. They are a valuable tool for obtaining more meaningful information about the uncertainty of the verification statistics.

MET provides tools that can be applied to spatial fields for various comparisons. A standard tool within MET is Point-Stat, which calculates statistics for verification between a grid and a point. For example, this tool can be used for verification studies between a satellite rainfall grid and a point rain gauge measurement. A second tool that can be used for verification is the Grid-Stat tool in MET. This tool can be used to

compute traditional statistical measures for grid-to-grid verification such as the comparison between satellite cloud or precipitation observations and NWP forecasted cloud or precipitation products. The final tool within MET applies advanced spatial verification techniques. This additional feature provides users with information about the spatial features of the precipitation fields that traditional statistical measures do not provide. Example statistics that are computed include displacement in time and/or space, location, size, intensity, and orientation errors. Schematic examples of these errors between observations (e.g., radar or satellite) (O) and NWP forecasts of cloud fields (F) are shown in Fig. 1. The upper two panels show examples of small and large displacement errors between O and F. The middle left panel shows an extreme example of large errors in orientation, size, which could also be interpreted as intensity. The middle right panel shows an example of an orientation error. The bottom panel shows an example of large size/orientation errors. However, the two precipitation fields overlap. Of all the examples, if only traditional statistical measurements are used, one would conclude that the last example gave the best verification results. On the contrary, visual inspection would indicate that the upper left panel shows the “best” verification. The advanced spatial techniques attempt to quantify these errors that a human can observe visually.

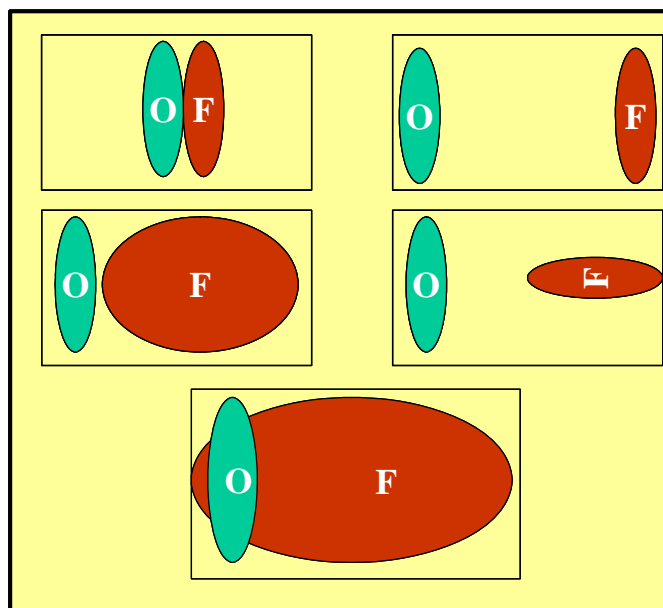


Figure 1. Examples of possible cases between satellite cloud or precipitation observations (O) and NWP cloud or precipitation forecasts (F).

To compute these spatial verification statistics, an object-based spatial verification tool called MODE (Method for Object-based Diagnostic Evaluation). A flow chart of how MODE works is shown in Fig. 2. MODE applies the object-based spatial verification technique described in Davis et al. (2006). This technique was developed in response to the “double penalty” problem shown schematically in Fig. 1. A verification comparison that is offset even a small distance is effectively penalized twice by standard categorical verification scores: once for missing the event and a second time for producing a false alarm of the event elsewhere. MODE defines objects in both surface observation (e.g. from radar) and from the satellite rainfall estimates. The objects in both fields are then

matched and compared to one another. Applying this technique also provides diagnostic verification information that is difficult or even impossible to obtain using traditional verification measures. Section 4 shows an example comparison of cloud fields using MODE.

Method for Object-based Diagnostic Evaluation (MODE): Object-based Approach

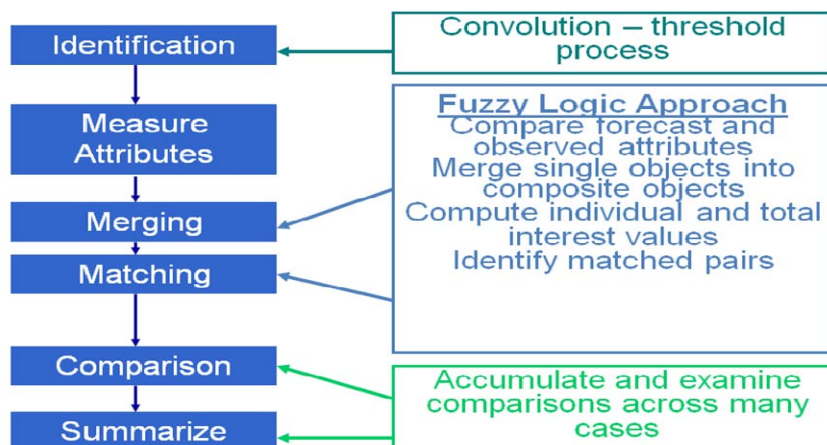


Figure 2. A flow chart outlining the components of MODE.

3. DATA

For this demonstration of the MET tools, we used the RUC (<http://ruc.noaa.gov/>) cloud top height and derived reflectivity products at a spatial resolution of 20 km over the continental US. The particular example presented in Section 4 was observed from a large-scale organized synoptic system located over the central region of the US. This reason that this system was selected was because it had a large scale, well organized cloud field. This provided a large sample of observed cloud that was used in the comparison.

For the A-train observations, we focused our analysis on the CloudSat GEOPROF product (<http://www.cloudsat.cira.colostate.edu/data/CDlist.php?go=list&path=/2B-GEOPROF>). In particular, we examined the vertical profile of radar reflectivity and cloud top height fields and compared those fields to RUC model derived and observed cloud top height field and vertical profile of radar reflectivity. We also evaluated cloud objects between RUC and the CloudSat observations. These comparisons will be presented in the next section.

4. EXAMPLE COMPARISONS

4.1 CloudSat/NWP Comparison: Traditional Statistics

For the first comparison, we used traditional statistical measures to evaluate the RUC cloud fields with CloudSat. In particular, we focused on cloud top height comparisons.

To match up the RUC grid and CloudSat observations, we only considered grid boxes with at least 6 CloudSat points (roughly half the maximum number of points that could be within one box) in a particular RUC grid box. The higher resolution CloudSat cloud top height observations were then averaged by various methods to create a matched pair of CloudSat and RUC observations. These pairs were then used to compute the traditional statistics to evaluate the RUC forecasts of cloud top heights. For this analysis, we only examined the cloud top height field at model initiation time (e.g., no lead time forecasts were evaluated).

The example case is shown in Fig. 3. The RUC cloud top height field with the CloudSat cloud top height field overlaid is shown in the plot. The image shows the well-organized synoptic system located in the eastern 1/3 of the United States and southern Canada. Cloud top heights ranged from about 5 to 12 km in the cloud field.

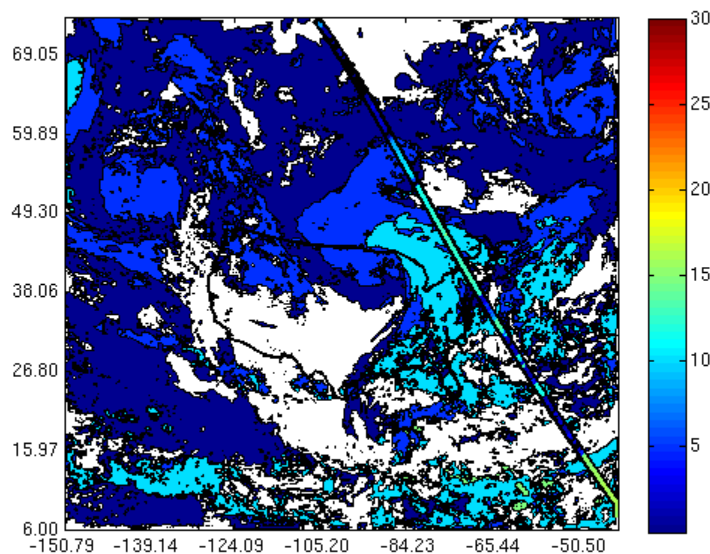


Figure 3. Contour of cloud top height (km) in the model (full figure) and CloudSat observations (thick black line).

Figure 4 shows a boxplot of the distribution of cloud top heights observed from CloudSat (left) and predicted by the RUC model (right). The lower and upper components of the box indicate the cloud top heights of the lower 25 and upper 75% of the distribution, respectively. The red line indicates the median value. The “whiskers” show the minimum and maximum observed cloud top heights. The results shown in Fig. 4 indicate that the distributions of cloud top heights are significantly different for this case. The observed median value is about 11.5 km where RUC has a median value of about 6 km. The inner quartile range (between 25-75%) was between 7.5 and 12.5 km for CloudSat observations and between 2 and 11.5 km for RUC. Clearly, RUC predicted a much broader range of cloud heights than what was observed by CloudSat.

The next set of results shown in Fig. 5 provide a summary of cloud top height comparison results using traditional statistics for various CloudSat averaging methods (nearest neighbor (blue), unweighted (red), and distance weighted (green)). The results show that there is little sensitivity to the weighting method. The plot indicates that the average cloud top heights differ by 2.5 km with CloudSat observing higher clouds on

average. As indicated in Fig. 4, the variability of cloud top heights with the RUC model is larger. The different correlations methods indicate the two fields are well correlated with values ranging between 0.7 and 0.8. The multiplicative bias is around 0.9. The ME is around 2.5 km, the RMSE is around 4.5 km and MAE error is around 3 km (see bottom panel in Fig. 5). These results are consistent with the distributions shown in Fig. 4 indicating the RUC cloud top heights are too low compared to CloudSat.

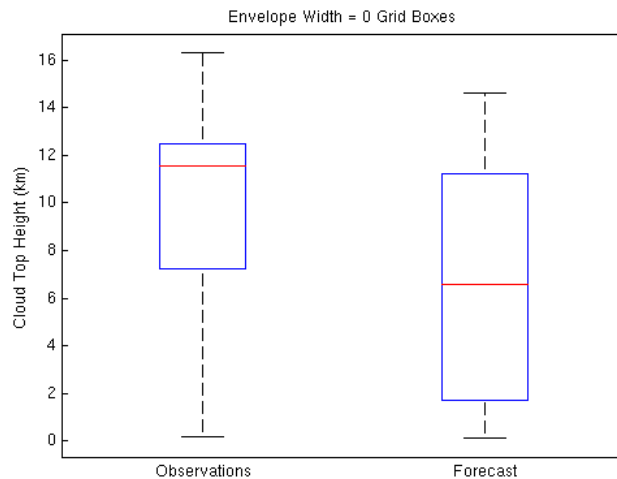


Figure 4. Boxplots of cloud top height for observations (left) and model (right) – model cross-section exactly along observation track.

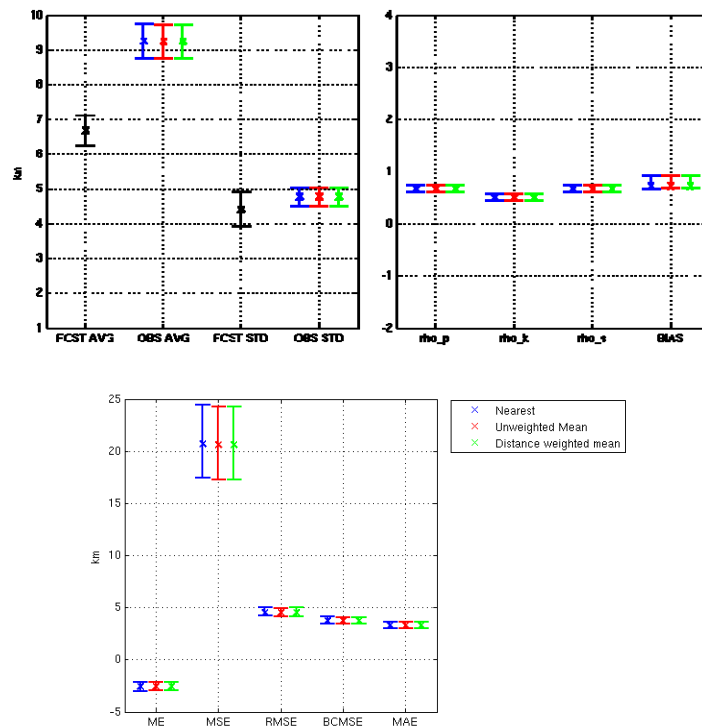


Figure 5. Traditional error metrics for cloud top height for the model cross-section exactly along the observation track. The mean (x symbol) and one standard deviation (vertical lines) are shown in the plot.

4.2 CloudSat/NWP Comparison: Object Based

This section provides a summary of using an object-based method to compare the cloud fields observed CloudSat and forecasted by the RUC model. For this comparison, we converted the model liquid and ice water content fields into derived radar reflectivity field using the method described by Haynes et al. (2007). This allowed for a more direct comparison between the fields. Figure 6 shows the model (top) and CloudSat (bottom) reflectivity fields. Visually, the RUC and CloudSat fields agree quite well in the horizontal plane. There are clouds and precipitation generally in the correct horizontal location. The object based feature retrieval shown in Fig. 7 confirms this result, which indicates 4 of the 5 objects match quite well in the horizontal. However, in the vertical, RUC is not predicting clouds in the correct location. It generally produces too much weak high cloud and too much low level convective cloud. Except for the convective system in the middle of the domain, most of the observed clouds are at mid-level. This is an example where the object based tool provides good diagnostic information to better understand the differences between the observed and forecast fields.

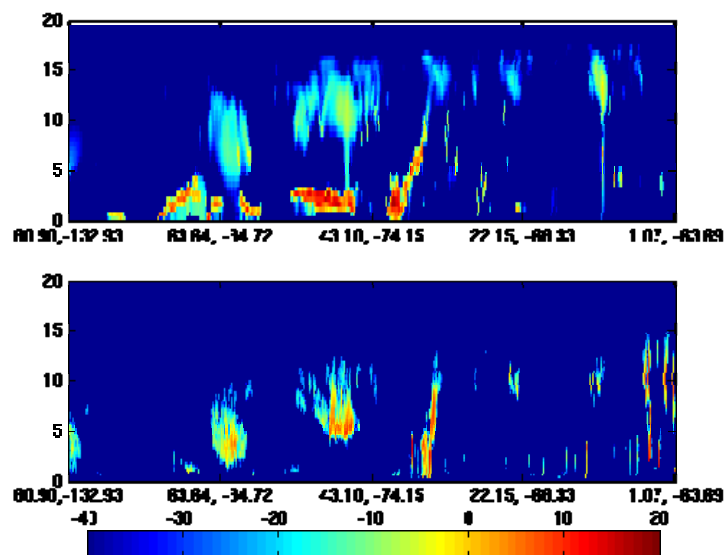


Figure 6. Reflectivity in the model (top) and observations (bottom).

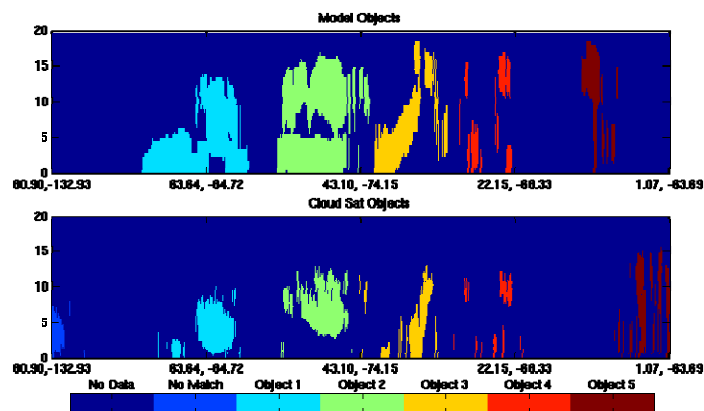


Figure 7. Resolved objects and matched pairs for model (top) and observations (bottom).

4.3 Comparison of modeled and observed reflectivity fields

The last comparison presented in this study evaluates the vertical profiles of reflectivity. Again, for this comparison, we use the case discussed earlier. Analysis of the same case is shown in Fig. 8; however the composite reflectivity field is being shown instead of cloud top heights. The plot shows that the composite reflectivity values generally ranged from 0 to 20 dBZ.

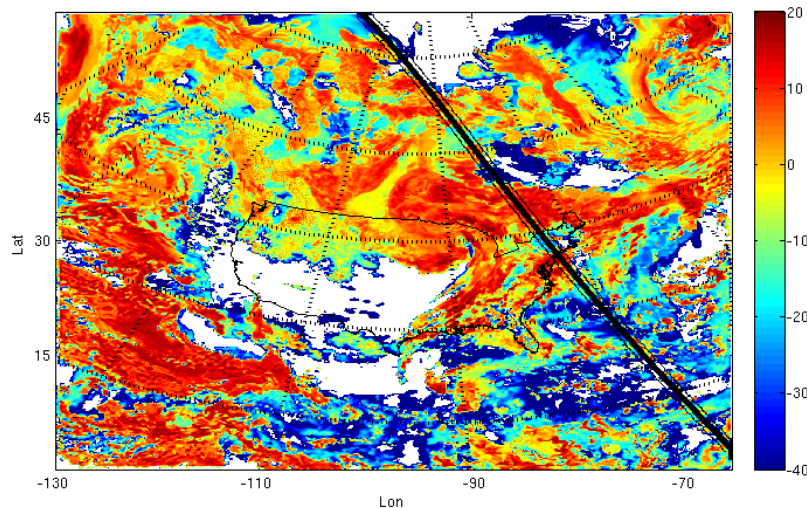


Figure 8. Composite reflectivity and location of observation track, with 5-grid box envelope shaded.

Figure 9 shows the results for the vertical profile comparisons. These plots show the contoured frequency by altitude diagrams (CFADs: Yuter and House (2005)), which indicates the frequency which a certain reflectivity value occurred with height. The panel on the right shows the difference between the RUC and CloudSat CFADs. The results show that the model cloud fields tended to be weaker in the vertical (higher frequency of weaker reflectivity values aloft). However, the model generated a relatively high frequency of low level clouds that were not observed with CloudSat. This provides a tool to examine the intensity and vertical structure of model forecasted clouds.

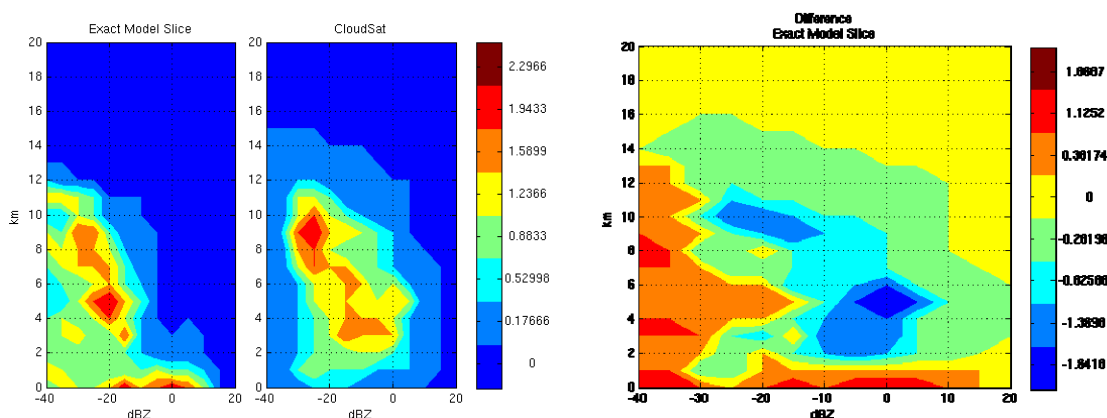


Figure 9. Contoured frequency by altitude diagrams (CFADs) for reflectivity along the observation track, and difference between observations and model (right).

5. SUMMARY

This paper presents the MET software package to demonstrate the potential use for verification studies of satellite cloud and precipitation observations compared to NWP cloud and precipitation fields. We demonstrated the usefulness of the tools for a CloudSat-RUC model comparison case located over the United States. We provided examples using the traditional MET statistical tools, object-based evaluation, and an evaluation method for comparing the vertical structure of clouds and precipitation.

Future updates to MET will include the completion of reading/remapping tools for A-Train products. We are also building our evaluation database for a variety of events (e.g., winter time precipitation, tropical storms, etc.) and geographical regions (e.g., complex terrain, ocean, flat regions, etc.). We are continuing to improve and refine our verification techniques of cloud and precipitation properties. We are designing a METViewer Database and Display system. Finally, we plan to extend the tools to other satellite datasets (HRPP, TRMM, GPM).

6. REFERENCES

Davis, C. A., B. G. Brown, and R. G. Bullock: 2006a: Object-based verification of precipitation forecasts, Part I: Methodology and application to mesoscale rain areas. *Mon. Wea. Rev.*, **134**, 1772-1784.

Haynes, J.M., R.T. Marchand, Z. Luo, A. Bodas-Salcedo, and G.L. Stephens, 2007: A multi-purpose radar simulation package: QuickBeam. *Bull. Amer. Meteor. Soc.*, **88**, 1723-1727.

Huffman, G. J., R. F. Adler, D. T. Bolvin, G. Gu, E. J. Nelkin, K. P. Bowman, Y. Hong, E. F. Stocker and D. B. Wolff, 2007: The TRMM Multisatellite Precipitation Analysis (TMPA): Quasi-Global, Multiyear, Combined-Sensor Precipitation Estimates at Fine Scales. *J Hydromet*, **8**, 38-55.

Wilks, D., 2006: *Statistical Methods in Atmospheric Sciences*, Elsevier, San Diego.

Yuter, S. E., and R. A. Houze, 1995: Three-Dimensional Kinematic and Microphysical Evolution of Florida Cumulonimbus. Part II: Frequency Distributions of Vertical Velocity, Reflectivity, and Differential Reflectivity. *Mon. Wea. Rev.*, **123**, 1941-1963.

THE GOES-R RAINFALL RATE, RAINFALL POTENTIAL, AND PROBABILITY OF RAINFALL ALGORITHMS

Robert J. Kuligowski¹, Yaping Li², Zhihua Zhang², and Richard Barnhill²

¹NOAA/NESDIS Center for Satellite Applications and Research (STAR)
Camp Springs, MD USA

²I. M. Systems Group, Lanham, MD USA

e-mail: bob.kuligowski@noaa.gov

ABSTRACT

GOES-R will be the first of the next generation of NOAA's operational geostationary meteorological satellites, and will include a 16-band Advanced Baseline Imager (ABI) with substantially enhanced spectral, spatial, and temporal capabilities compared to the current-generation Imager. The Hydrology Algorithm Team (AT) of the GOES-R Algorithm Working Group (AWG) has been tasked with providing recommended, demonstrated, and validated algorithms for retrieving the current instantaneous rainfall rate, predicted rainfall potential during the next 3 hours, and the probability of rainfall during the next 3 hours.

The first two of these algorithms were developed from existing algorithms after an intercomparison to select the best performers; the latter algorithm was developed from scratch. All three algorithms were evaluated using Spinning Enhanced Visible InfraRed Imager (SEVIRI) data as a proxy for ABI data and validated against available ground data from the Tropical Rainfall Measuring Mission (TRMM) Precipitation Radar and the Nimrod ground radar network over Western Europe. These three algorithms and their status and performance will be briefly outlined, followed by ongoing validation and development plans.

1. INTRODUCTION

The Geostationary Operational Environmental Satellites (GOES) series, which is operated by the National Oceanic and Atmospheric Administration (NOAA) National Environmental Satellite, Data, and Information Service (NESDIS) has monitored the Americas for over three decades, and instrument capabilities have improved significantly during that time. The next generation of GOES, starting with the satellite designated "R" and hence referred to as "GOES-R", is scheduled for launch in late 2015 (though followed by a check-out period of at least 12 months beyond that) and will feature an Advanced Baseline Imager (ABI; Schmit et al. 2005), a Geostationary Lightning Mapper (GLM), and improved space-weather monitoring instruments.

The ABI will improve significantly over current GOES Imager capabilities: additional spectral bands (increasing from 5 to 16), enhanced spatial resolution (footprint size reducing from 4 to 2 km at nadir in the IR and 1 to 0.5 km in the visible), and increased refresh rate (able to scan the full disk in 5 min instead of 30 min). The GLM will provide the first detection of lightning from geostationary orbit, using a single-channel near-IR optical detector to retrieve total lightning at roughly 10 km spatial resolution.

As part of the development of a ground processing system to generate products from GOES-R data, the GOES-R Algorithm Working Group (AWG) has been tasked with providing a recommended, demonstrated, and validated ground system which is being presented to Harris Corporation who will build the operational ground processing system. The AWG contains 17 Algorithm Teams (ATs) which are responsible for particular algorithm areas or for other functions critical to developing an integrated ground system.

One of these teams, the Hydrology Algorithm Team, is responsible for developing three products:

- Rainfall Rate—current instantaneous rain rate at the full ABI resolution;
- Rainfall Potential—predicted 0-3 h rainfall accumulation based on extrapolation of the current and recent Rainfall Rate products;
- Probability of Rainfall—probability of at least 1 mm of rainfall during the next 3 h at each ABI pixel.

GOES-R Rainfall Rate continues the legacy of rainfall rate products from GOES; the other two have not been produced operationally up to this time. The Hydrology AT is chaired by Robert J. Kuligowski of NOAA / NESDIS and the other members are Ralph Ferraro (NOAA / NESDIS), Kuo-lin Hsu (University of California at Irvine), George Huffman (contractor at NASA-Goddard Space Flight Center), Sheldon Kusselson (NOAA / NESDIS) and Mathew Sapiano (Colorado State University).

The development of the recommended ground system involves several steps by the ATs, including reviewing of the candidate algorithms and selection for intercomparison; comparing the performance of the algorithms; recommending an algorithm based on the results; and incorporating the recommended algorithm code into the prototype operational ground processing system. This conference paper describes the algorithms in brief and the results of their validation against requirements set forth by the GOES-R Program Office (GPO).

2. ALGORITHM DESCRIPTIONS AND EXAMPLES

2.1. Rainfall Rate Algorithm

The Rainfall Rate algorithm selected by the Hydrology AT is a modification of the Self-Calibrating Multivariate Precipitation Retrieval (SCaMPR; Kuligowski 2002) that uses some of the additional ABI bands not available on the current-generation GOES Imager to extract additional information about cloud-top properties in retrieving rainfall rate.

SCaMPR is a “combination” rainfall rate algorithm that uses data from both infrared (IR) and microwave (MW) portions of the spectrum. MW data are generally preferred for rainfall estimation because clouds are semi-transparent in the MW, allowing some information about the total-column cloud properties to be retrieved. Meanwhile, the opacity of raining clouds in the IR limits the information content to cloud-top properties; however, IR information is available from geostationary orbit which permits much more rapid refresh than from MW instruments in low-Earth orbit.

SCaMPR combines the two by using MW rain rates as a calibration standard for an IR-based algorithm. The calibration is based on a collection of matched MW rain rates and IR brightness temperatures (which have previously been aggregated to match the MW footprint) that is refreshed every time new IR data become available with the new data replacing the oldest.

To enhance the suitability of the fit, the data are divided into twelve different classes: three cloud types and four geographic regions (30-degree latitude bands covering 60 S to 60 N). The cloud types are based on selected brightness temperature differences (BTDs) with threshold values selected to maximize the difference between classes in terms of the relationship between rainfall rate and IR window brightness temperature. The cloud types are:

- “Water cloud”: $T_{7.34} < T_{11.2}$ and $T_{8.5} - T_{11.2} < -0.3$ K
- “Ice cloud” $T_{7.34} < T_{11.2}$ and $T_{8.5} - T_{11.2} \geq 0.3$ K
- “Cold-top convective cloud”: $T_{734} \geq T_{11.2}$

where the subscript indicates the central wavelength of the IR band.

The algorithm uses separate calibrations for rain / no rain discrimination and rain rate retrieval. The former is calibrated using discriminant analysis and the latter using stepwise forward multiple linear regression. The specific predictors used by the algorithm are indicated in Table 1. Since the relationship between IR brightness temperatures and rainfall rates is highly nonlinear (e.g., Figure 1 of Vicente et al. 1998), a supplemental set of transformed rainfall rate predictors is created by regressing each predictor in log-log space and thus creating a power function fit (i.e., $y = ax^b$).

$T_{6.19}$	$T_{8.5} - T_{7.34}$
$S = 0.568 - (T_{\min,11.2} - 217 \text{ K})$	$T_{11.2} - T_{7.34}$
$T_{\text{avg},11.2} - T_{\min,11.2} - S$	$T_{8.5} - T_{11.2}$
$T_{7.34} - T_{6.19}$	$T_{11.2} - T_{12.3}$

Table 1: Predictors used by the GOES-R Rainfall Rate algorithm.

In Table 1, T_{\min} refers to the minimum temperature in the surrounding 5x5-pixel region and T_{avg} refers to the average temperature of the four closest pixels in the scan line and the two closest pixels in the adjacent scan line—see Adler and Negri (1987) for details.

Initial results showed that the algorithm significantly underestimated heavy rainfall. This is believed to be caused by the strongly skewed distribution of rainfall rates—since the rainfall rate distribution is concentrated at very low rainfall rates, regression techniques will tend to optimize for these low rates. This problem was addressed by using a cumulative distribution function (CDF) matching technique similar to that used by other

IR-MW combination techniques (e.g., Turk and Miller 2005) except that in this case the MW rain rates are matched against the Rainfall Rate outputs rather than against IR brightness temperatures. This approach significantly improved the distribution of rainfall rates, particularly for higher rainfall rates, as illustrated by the comparison between the Rainfall Rates before and after the LUT correction to the TRMM PR (see Section 3.1 for additional details on the ground validation data set) in Figure 1.

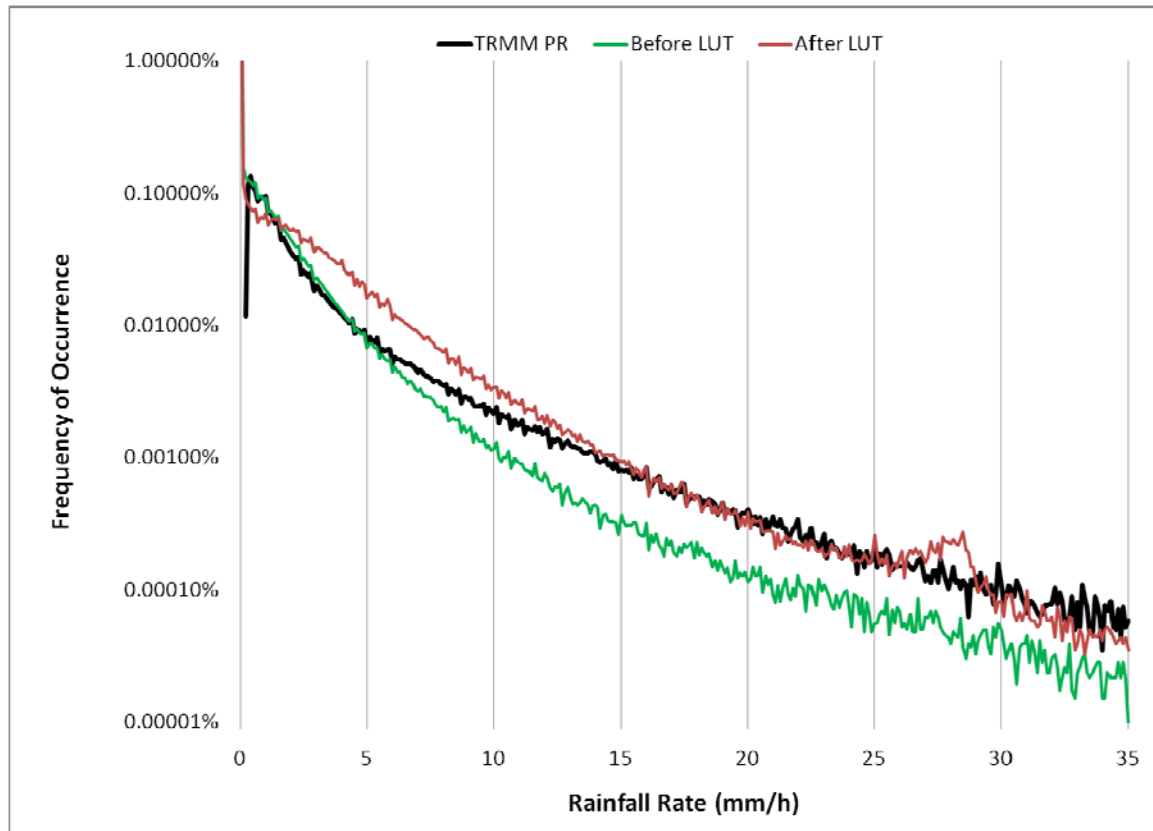


Figure 1. Probability Distribution Function (PDF) of rainfall rates from the Rainfall Rate algorithm before and after the distribution correction compared to corresponding TRMM PR values for 5-9 January, April, July, and October 2005.

A couple of randomly selected Rainfall Rate fields (actually 1-hour accumulations) are shown in Figure 2 along with corresponding Nimrod radar data (see Section 3.1 for description).

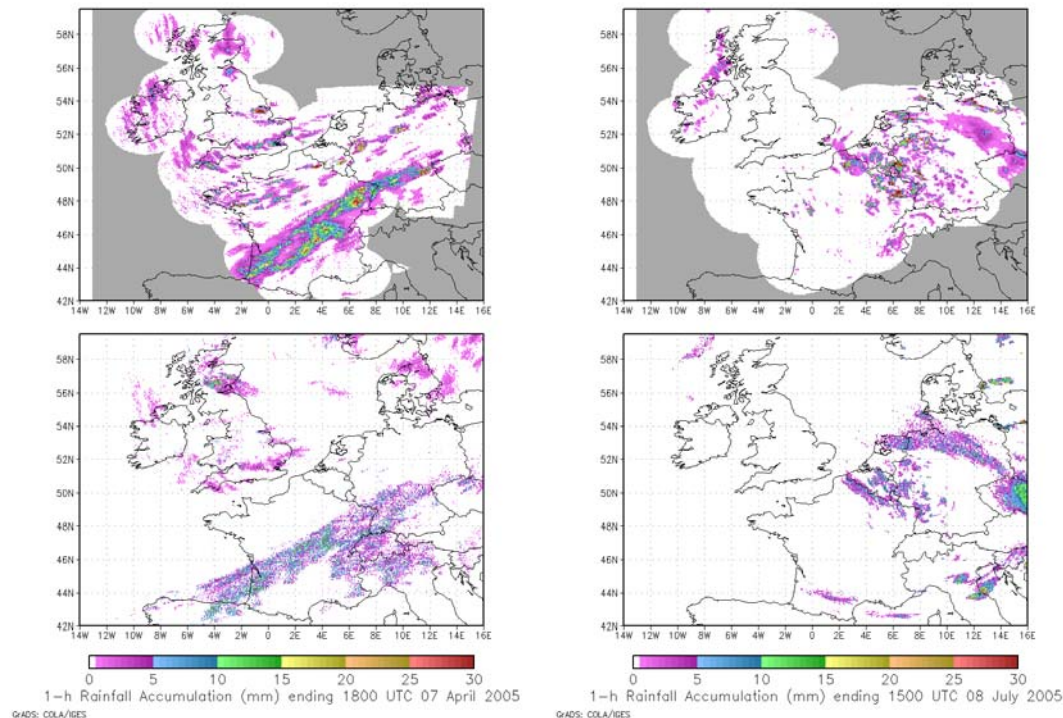


Figure 2. Comparison of GOES-R Rainfall Rate accumulation (bottom) derived from SEVIRI data with Nimrod radar composites (top) for the 1 hour ending 1800 UTC 7 April 2005 (left) and 1500 UTC 8 July 2005 (right).

2.2. Rainfall Potential Algorithm

The Rainfall Potential algorithm selected by the Hydrology AT was the K-Means algorithm (Lakshmanan et al. 2003, 2009a, 2009b) which uses current and previous Rainfall Rate fields as the basis for an extrapolation-based forecast of rainfall rates out to 3 hours. This is done by identifying features in the current Rainfall Rate image, determining the motion of these features via comparison with previous imagery, and then extrapolating forward in time.

The identification of features is performed using a K-Means image processing technique. After an initial filtering of the current Rainfall Rate image to reduce noise, the pixels in the image are organized using a cost minimization function $E_{xy}(k)$ for each cluster k :

$$E_{xy}(k) = \lambda d_{m,xy}(k) + (1 - \lambda) d_{c,xy}(k) \quad (1)$$

In this function, λ represents the weight of distance vs. disconguity in the cost function and has a value between 0 and 1. The distance in measurement space (i.e., similarity) $d_{m,xy}(k)$ is calculated as

$$d_{m,xy}(k) = \left\| \mu_k - I_{xy} \right\| \quad (2)$$

where μ_k is the mean intensity (magnitude) value for cluster k and I_{xy} is the intensity value for pixel xy , and the discontinuity (distance in physical space) $d_{c,xy}(k)$ is calculated as

$$d_{c,xy}(k) = \sum_{ij \in N_{xy}} (1 - \delta(S_{ij}^n - k)) \quad (3)$$

where S_{ij}^n is the cluster number for pixel ij and δ is the Dirac delta function, and thus the summation represents the number of pixels among the 8 neighbors that do not belong to cluster k .

In addition, smaller features are combined into larger ones such that the feature size exceeds a preset threshold. This is done because the lifetime of features is inversely related to their size and so smaller features have limited utility in nowcasting.

The motion vectors are derived by overlaying the pixels associated with each cluster over the previous Rainfall Rate image and determining the shift that minimizes the mean absolute error. (Actually, the centroid of the area with the lowest 20% of MAE values is used to reduce noise.) This approach was chosen in lieu of matching clusters in the two images because it was found to produce a more consistent result. One motion vector is thus derived for each cluster, and the resulting data field is then objectively analyzed to produce a smooth field of motion vectors. Finally, a Kalman filter is used to enhance consistency with previously derived motion vector fields.

The nowcasting step is performed by moving each cluster forward in time along the derived motion vectors in 15-minute steps. However, since it is clear that the motion vector fields cannot be expected to remain constant in time, the motion vector fields are used to advect themselves forward in time by 15 minutes, and these new motion vector fields are used in the next rainfall advection time step. These steps are repeated at 15-minute intervals out to 3 hours lead time, and the resulting intermediate rainfall rate fields are then aggregated to produce a 3-hour total. Some examples of the product are shown in Figure 3.

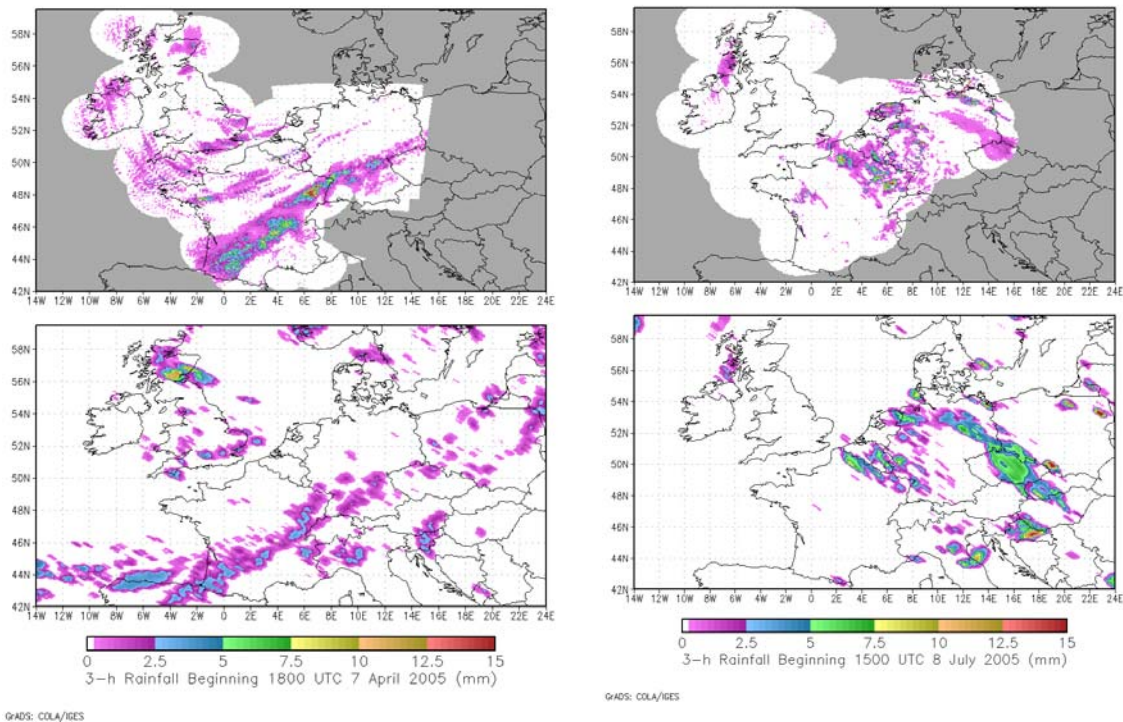


Figure 3. Comparison of GOES-R Rainfall Potential (bottom) derived from SEVIRI data with Nimrod radar composites (top) for the 3 hours ending 1800 UTC 7 April 2005 (left) and 1500 UTC 8 July 2005 (right).

2.3. Probability of Rainfall Algorithm

The Probability of Rainfall algorithm uses output from the Rainfall Potential algorithm as the basis for a probability of at least 1 mm of rainfall at each ABI pixel during the next 3 h. Specifically, the predictors for the Probability of Rainfall algorithm are derived from the 3-h Rainfall Potential total accumulation and the intermediate rain rate nowcasts produced by the algorithm every 15 min.

The probabilities are based on conditional probability tables calibrated against 3-hour rain / no rain (1-mm threshold) from the Rainfall Rate algorithm. For pixels where the 3-h Rainfall Potential value is at least 1 mm, the probability is based on the total number of 15-minute periods (up to 12) in which the rain rate is at least 1 mm/h. For pixels with a 3-h Rainfall Potential value below 1 mm, the probability is a function of the distance to the nearest pixel with a Rainfall Potential accumulation of at least 1 mm. It should be noted that this calibration was in the process of being modified when this paper went to press, and thus may be different from the final calibration.

Note that the calibration was performed against the Rainfall Rate algorithm rather than ground validation data primarily because of the scarcity of 3-hour ground validation data over the SEVIRI coverage area (discussed in additional detail below). This approach allowed calibration to be carried out over the entire SEVIRI full disk; however, it does result in a lost opportunity to account for any biases in the Rainfall Potential algorithm in

the calibration of the rainfall probabilities. Some examples of the product using the original calibration are shown in Figure 4.

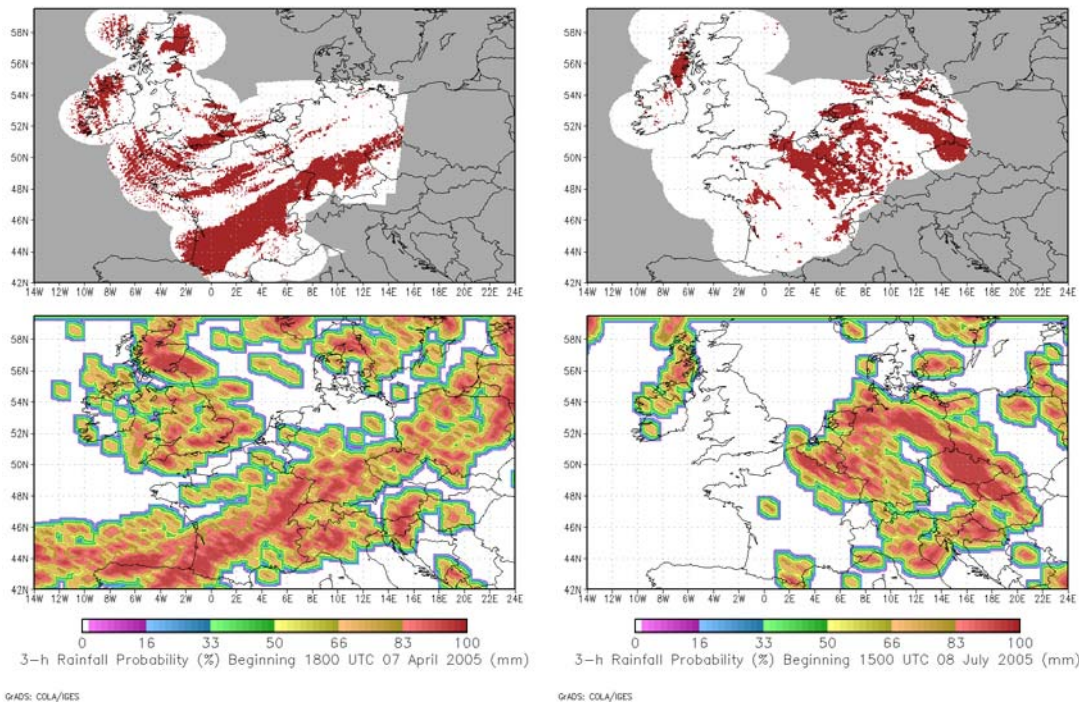


Figure 4. Comparison of GOES-R Probability of Rainfall (bottom) derived from SEVIRI data with Nimrod radar composites (top) for the 3 hours ending 1800 UTC 7 April 2005 (left) and 1500 UTC 8 July 2005 (right).

3. ALGORITHM VALIDATION

3.1. Ground Validation Data

The development of these algorithms using the SEVIRI as a proxy means that algorithm validation must be performed mainly over Europe, Africa and surrounding waters. This results in a significant challenge obtaining ground validation data, particularly when validation of the Rainfall Rate product requires instantaneous rainfall rates (generally available only from radar) and the Rainfall Potential and Probability of Rainfall products require rainfall accumulations of 3 hours (available from radar and a very limited fraction of the rain gauge data set).

The two data sets that were best suited for validating the algorithms are the Tropical Rainfall Measuring Mission (TRMM) Precipitation Radar (PR; Fig. 5a) and the Nimrod radar data set from the British Atmospheric Data Centre (BADC; Fig. 5b).

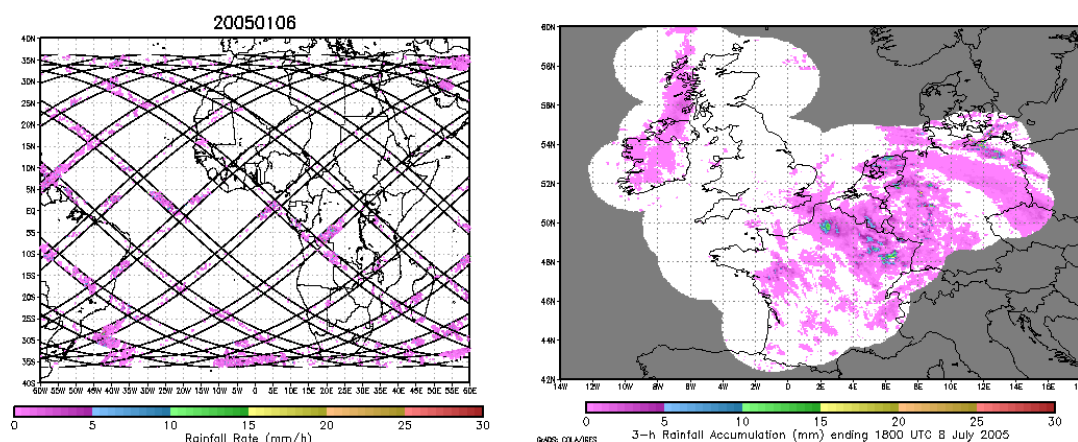


Figure 5. Examples of (a) TRMM Rainfall Rates for a 24-hour period on 6 January 2005 and (b) 3-hour rainfall accumulations from Nimrod from 8 July 2005.

The TRMM PR provides surface estimates of rainfall rate as part of the TRMM 2A12 product (Iguchi et al. 2000). It is suitable for evaluating the Rainfall Rate product but not for the Rainfall Potential and Probability of Rainfall products since it does not provide sufficient sampling for reliable 3-hour totals.

The Nimrod radar composite combines data from radars over the United Kingdom, France, and Germany. It is the only radar-based data set that is available for evaluating the Rainfall Potential and Probability of Rainfall algorithms, but unfortunately it covers only a very small fraction of the SEVIRI full disk (Fig. 5b).

3.2. Methodology

The primary purpose of algorithm validation is to determine whether the performance of the algorithm meets the Function and Performance Specifications (F&PS) set forth by the GPO. The two specific metrics addressed by algorithm validation are accuracy and precision.

Accuracy is simply the absolute difference between the mean values of the estimated and observed fields—in other words, it is the magnitude of the additive bias. Precision is the value of absolute error below which 68% of the error values fall—a basic measure of the degree of scatter between the estimates and observations.

The F&PS values for accuracy and precision for all three products are shown in Table 2.

Product	Accuracy	Precision
Rainfall Rate	6 mm/h	9 mm/h
Rainfall Potential	5 mm	5 mm
Probability of Rainfall	25%	40%

Table 2: F&PS accuracy and precision values for the three Hydrology GOES-R products.

As an example, then, for the Rainfall Potential algorithm the average 3-hour predicted rainfall accumulation should vary from the observed value by no more than 5 mm, and

at least 68% of the absolute errors in Rainfall Potential should be 5 mm or less. For Rainfall Rate, it is difficult for overall statistics to communicate the skill of the algorithm at high rain rates because they are so poorly represented in the statistical distribution. As a result, as per guidance from the GPO, the Rainfall Rate performance statistics are calculated only for pixels with a Rainfall Rate of 10 mm/h (actually 9.5-10.5 mm/h to ensure a significant sample) in order to provide a better measure of the performance of the algorithm for significant rainfall.

Another caveat is that regions of 10 mm/h of rainfall generally cover small regions compared to the footprint size, so even small spatial shifts can be strongly penalized in pixel-by-pixel statistics. To get more meaningful performance statistics, the philosophy of Ebert (2008) was followed where the validation comparisons for Rainfall Rate were not made exactly pixel-to-pixel, but the Rainfall Rate pixels were matched with the ground validation data values within a 10-km radius that had the closest value. This enables useful skill scores to be derived even when relatively small spatial shifts in the data would degrade a pixel-by-pixel comparison (see Fig. 6 for an example of a corresponding TRMM and Rainfall Rate fields where the spatial displacement would result in poor pixel-by-pixel comparisons even though the Rainfall Rate field contains useful information).

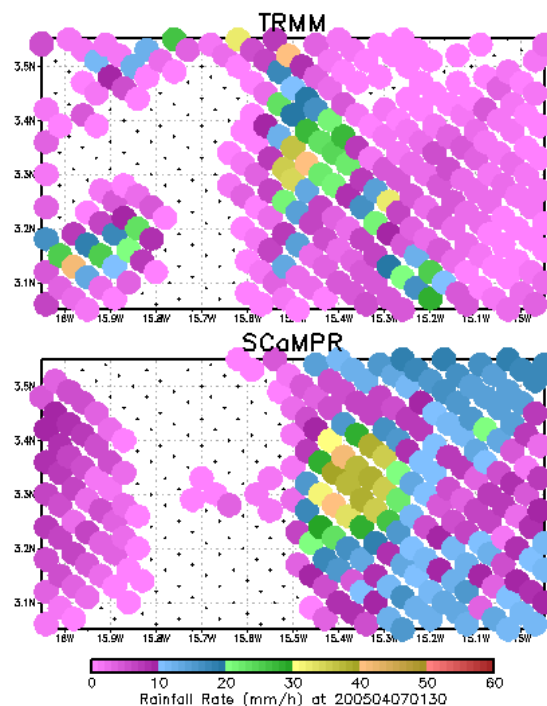


Figure 6. Comparison of TRMM PR and Rainfall Rate (SCaMPR) output at 0130 UTC 7 April 2005. The Rainfall Rate values have been aggregated onto the 5-km TRMM 2A12 pixels.

3.3. Results

Table 3 summarizes the performance of the Rainfall Rate algorithm against the F&PS values and indicates that the Rainfall Rate algorithm meets spec when validated against

the TRMM PR but not against NIMROD. This was found to be largely due to detection failure—IR algorithms typically have significant difficulty depicting stratiform precipitation due to the weak relationship between cloud-top properties and surface rainfall rates under those conditions. As a result of this, the F&PS was modified to be applied only to convective precipitation.

Ground Validation	Accuracy	Precision
TRMM PR	4.9 mm/h	8.9 mm/h
Nimrod	8.6 mm/h	9.7 mm/h
(F&PS)	6.0 mm/h	9.0 mm/h

Table 3. Validation of the Rainfall Rate algorithm versus TRMM PR data for 51 days of data (6-9 January, April, July, October 2005 and all of January 2008) and against Nimrod data (6-9 April, July, October 2005 only).

The scatterplot of Rainfall Rate versus TRMM (Fig. 7) shows a relatively good match between the two when the fuzzy validation is used, although a significant wet bias is also apparent. This wet bias is largely caused by the neighborhood validation—due to the highly skewed distribution of rainfall rates, most pixels with low estimated values and high observed values have their observations adjusted downward due to a low-value neighbor being available, but most pixels with high estimated values and low observed values are not sufficiently adjusted upward because neighboring pixels with sufficiently high values are not generally available.

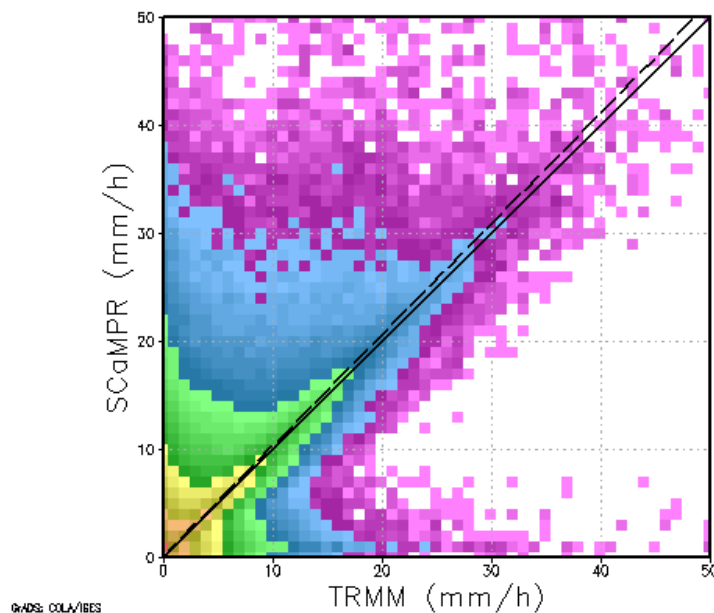


Figure 7. Comparison of Rainfall Rate values with collocated TRMM PR for 6-9 January, April, July, October 2005 and all of January 2008. Colors indicate frequency of values, with purple the lowest and red the highest.

Table 4 indicates that the Rainfall Potential algorithm meets spec by a significant margin, while Table 5 shows that the Probability of Rainfall algorithm meets spec for accuracy but not precision. The recalibration of the Probability of Rainfall algorithm should improve performance sufficiently to meet spec.

Ground Validation	Accuracy	Precision
Nimrod	8.6 mm/h	9.7 mm/h
(F&PS)	6.0 mm/h	9.0 mm/h

Table 4. Validation of the Rainfall Potential algorithm against Nimrod data for 6-9 April, July, and October 2005.

Ground Validation	Accuracy	Precision
Nimrod	8.6 mm/h	9.7 mm/h
(F&PS)	6.0 mm/h	9.0 mm/h

Table 5. Validation of the Probability of Rainfall algorithm against Nimrod data for 6-9 April, July, and October 2005.

Further insight into the skill of the Probability of Rainfall algorithm is given by a reliability diagram in which the frequency of observed rainfall of at least 1 mm is plotted as a function of Probability of Rainfall value. Figure 8 indicates that the low probabilities are generally underdone while the high probabilities are overdone, but there is still a skillful distinction between low- and high-probability events.

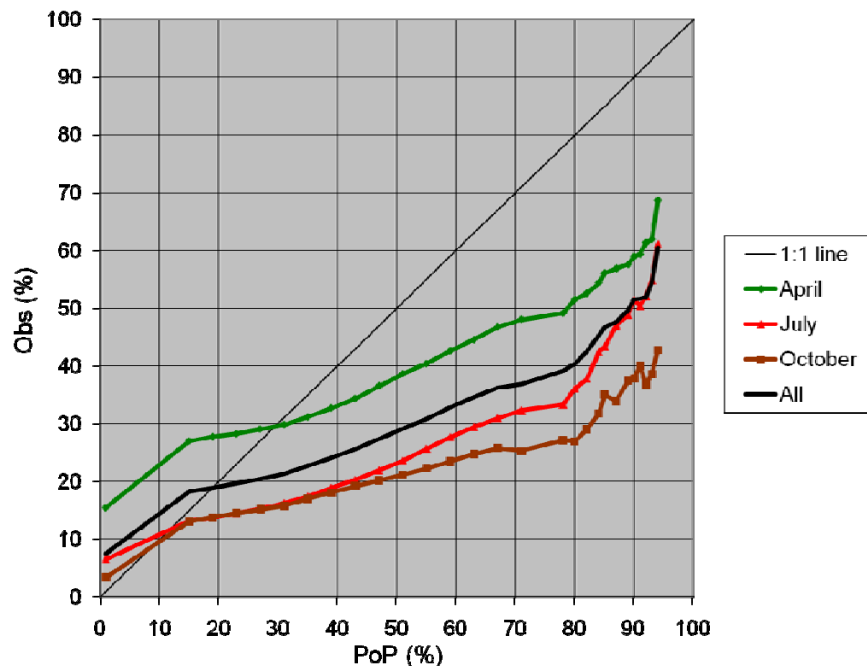


Figure 8. Reliability diagram for the Probability of Rainfall algorithm compared to Nimrod radar data for 5-9 April, July, and October 2005, with separate traces for each month and all data together.

4. STATUS AND FUTURE WORK

The final Rainfall Rate algorithm code was delivered to the GPO (and by them to Harris Corp.) on 30 September 2011, and the algorithm will be undergoing detailed validation during 2011 and 2012. Any potential adjustments identified during this detailed validation will be incorporated into a “maintenance” delivery of the code in late 2012.

The Rainfall Potential algorithm parameters are being optimized (e.g., determining the best combination of scales for each lead time) and the final algorithm code will be delivered to the GPO at the end of September 2011. The Probability of Rainfall algorithm is currently being recalibrated with a larger potential predictor set and delivery to the GPO is planned for the end of September 2011.

5. ACKNOWLEDGMENTS AND DISCLAIMER

This work is supported by the GOES-R Algorithm Working Group. The contents of this conference paper are solely the opinion of the author and do not constitute a statement of policy, decision, or position on behalf of the GOES-R Program Office, NOAA, or the U. S. Government.

7. REFERENCES

- Adler, R. A., and A. J. Negri, 1987: A satellite infrared technique to estimate tropical convective and stratiform rainfall. *J. Appl. Meteor.*, **27**, 30-51.
- Ebert, E. E., J. E. Janowiak, and C. Kidd, 2007: Comparison of near-real-time precipitation estimates from satellite observations and numerical models. *Bull. Amer. Meteor. Soc.*, **88**, 47-64.
- Iguchi, T., T. Kozu, R. Meneghini, J. Awaka, and K. Okamoto, 2000: Rain profiling algorithm for the TRMM Precipitation Radar. *J. Appl. Meteor.*, **39**, 2038-2052.
- Joyce, R. J., J. J. Janowiak, P. A. Arkin, and P. Xie, 2004a: CMORPH: A method that produces global precipitation estimates from passive microwave and infrared data at high spatial and temporal resolution. *J. Hydrometeorol.*, **5**, 487-503.
- Kuligowski, R. J., 2002: A self-calibrating GOES rainfall algorithm for short-term rainfall estimates. *J. Hydrometeorol.*, **3**, 112-130.
- Lakshmanan, V., K. Hondl, and R. Rabin. 2009a: An efficient, general-purpose technique for identifying storm cells in geospatial images. *J. Ocean. Atmos. Tech.*, **26**, 523-537.
- Lakshmanan, V., R. Rabin, and V. DeBruner, 2003: Multiscale storm identification and forecast. *Atmos. Res.*, **67-68**, 367-380.
- , and T. Smith, 2009b: Data mining storm attributes from spatial grids. *J. Ocean. Atmos. Tech.*, **26**, 2353-2365.
- Schmit, T. J., M. M. Gunshor, W. P. Menzel, J. J. Gurka, J. Li, and A. S. Bachmeier, 2005: Introducing the next-generation Advanced Baseline Imager on GOES-R. *Bull. Amer. Meteor. Soc.*, **86**, 1079-1096.
- Turk, F. J., and S. D. Miller, 2005: Toward improved characterization of remotely sensed precipitation regimes with MODIS/AMSR-E blended data techniques. *IEEE Trans. Geosci. Remote Sens.*, **43**, 1059-1069.
- Vicente, G. A., R. A. Scofield, and W. P. Menzel, 1998: The operational GOES infrared rainfall estimation technique. *Bull. Amer. Meteor. Soc.*, **79**, 1883-1898.

CHARACTERIZATION OF SNOW-COVERED TERRAIN AND DETECTION OF SNOWFALL BY USING THE 183-WSL RETRIEVAL SCHEME

S. Laviola, S. D'Aurizio, E. Cattani, and V. Levizzani

National Research Council of Italy, Institute of Atmospheric Sciences and Climate
(CNR-ISAC), Bologna, Italy,

e-mail: s.laviola@isac.cnr.it

ABSTRACT

A method for the characterization of snow-covered terrain and the detection of snowfall exploiting the frequencies between 90 and 190 GHz of the AMSU-B sensor is proposed. The study aims at enhancing the capabilities of the 183-WSL rain retrieval scheme (Laviola and Levizzani, 2011a). The discrimination of different ice hydrometeors is very difficult especially over frozen soils where the scattering signal from the terrain strongly masks the attenuation due to the hydrometeors. Snowflakes and snow-covered terrain scatter the upwelling radiation so that the snowfall appears to the satellite sensor almost undistinguishable from other strong scattering areas. The new module introduced in the 183-WSL retrieval design allows for a classification of ice-covered soils prior to the application of the precipitation retrieval modules. Then rainy pixels are categorized in convective, stratiform and snowfall precipitation. The strong sensitivity of the 90 and 150 GHz window frequencies is employed to recognize those pixels where the scattering signal can be reasonably associated with the presence of snow cover. The snow cover mask based on the window channels is further improved by exploiting the opaque channel at 190 GHz that receives the signal closer to the surface when land ice packs are formed.

The detection of snowfall is based on a range of thresholds where different combinations of the AMSU-B channels are applied only over rainy regions. The channel sensitivities at 186 and 190 GHz are combined with those of other frequencies to identify snowfall areas in the precipitating cores. NEXRAD data have been used to evaluate the sensitivity of the AMSU-B channels and to assess a series of threshold values to discriminate the attenuation due to falling snowflakes.

The first results presented hereafter refer to two severe blizzards over the Eastern part of the United States. Comparisons with radar images have highlighted the capabilities of the algorithm to delineate snowfall thus encouraging further investigations on the use of a probabilistic approach as an alternative to the fixed threshold tests. Uncertainties arise when the retrieval is done over frozen soils where snowfall signatures are drastically masked by scattering from snow-covered terrain.

INTRODUCTION

The quantification of the water components on the planet Earth is one of the most important challenges for hydrology and climatology. The quantitative assessment is important one hand for the biosphere and its delicate mechanisms and is also central to improve the knowledge of the hydrological cycle processes and of the possible impacts of the anthropogenic activities on the environment. Remote sensing from satellite has a key role in measuring and monitoring the water resources including snow. Moreover, note that snow is the predominant component of total precipitation amount in polar and sub-polar latitudes and its evaluation in terms of snowfall intensity from space is still ambiguous and affected by large errors (e.g., Levizzani et al., 2011). Many different satellite methods, mostly based on passive microwave sensors, have been developed to identify solid precipitation specifically connected to snowflakes. Pioneering investigations of Wilheit et al. (1982) tested the sensitivity of various microwave frequencies for ice cloud detection. Successively, Evans and Stephens (1995a,b) and more recently Bennartz and Petty (2001) and Bennartz and Bauer (2003) focused their attention on the scattering properties of the ice particles at high microwave frequencies. These studies have revealed the high sensitivity of frequencies at 89, 150 and 190 GHz to ice hydrometeors. In particular, the response to snow and graupel was found to increase with frequency. The 190 GHz frequency in drier conditions responds positively to the presence of snow-producing clouds since in these cases the peak of the weighting function is located at cloud height.

Two new modules of the 183-WSL retrieval method are proposed to detect snowy pixels. In particular, the first results of the tests on two severe blizzards over the US (D'Aurizio, 2010) and of a daily snow cover mask applied during the month of January over the Baltic Regions will be presented.

THE 183-WSL RETRIEVAL METHOD

The 183-WSL retrieval method estimates the rain rate intensity on the basis of the signal from the water vapor absorption frequencies in the 183.31 GHz band. Physically, the method exploits the absorbed radiation at 184, 186 and 190 GHz of the Advanced Microwave Sounding Unit-B (AMSU-B) on board the polar satellites of the National Oceanic and Atmospheric Administration (NOAA) to retrieve precipitation amounts. The scattering index values are also evaluated based on the difference between 89 and 150 GHz to distinguish rain/no-rain regions and to classify stratiform and convective precipitation types.

The 183-WSL retrieval scheme (Laviola and Levizzani, 2011a) is based on a series of linear equations that identify rainfall rates over various surfaces. The algorithm is schematically described in Fig. 1. The first step is dedicated to the ingestion and processing of the satellite data stream; here all relevant information, namely brightness temperature (T_B), surface type (land/sea/mixed), satellite local zenith angles, and topography, are separated from the overall data stream and arranged as input into the 183-WSL processing chain. At this stage the signal from all pixels over land are scrutinized by the snow cover processor. If $snwc=1$ the pixels are considered snow-

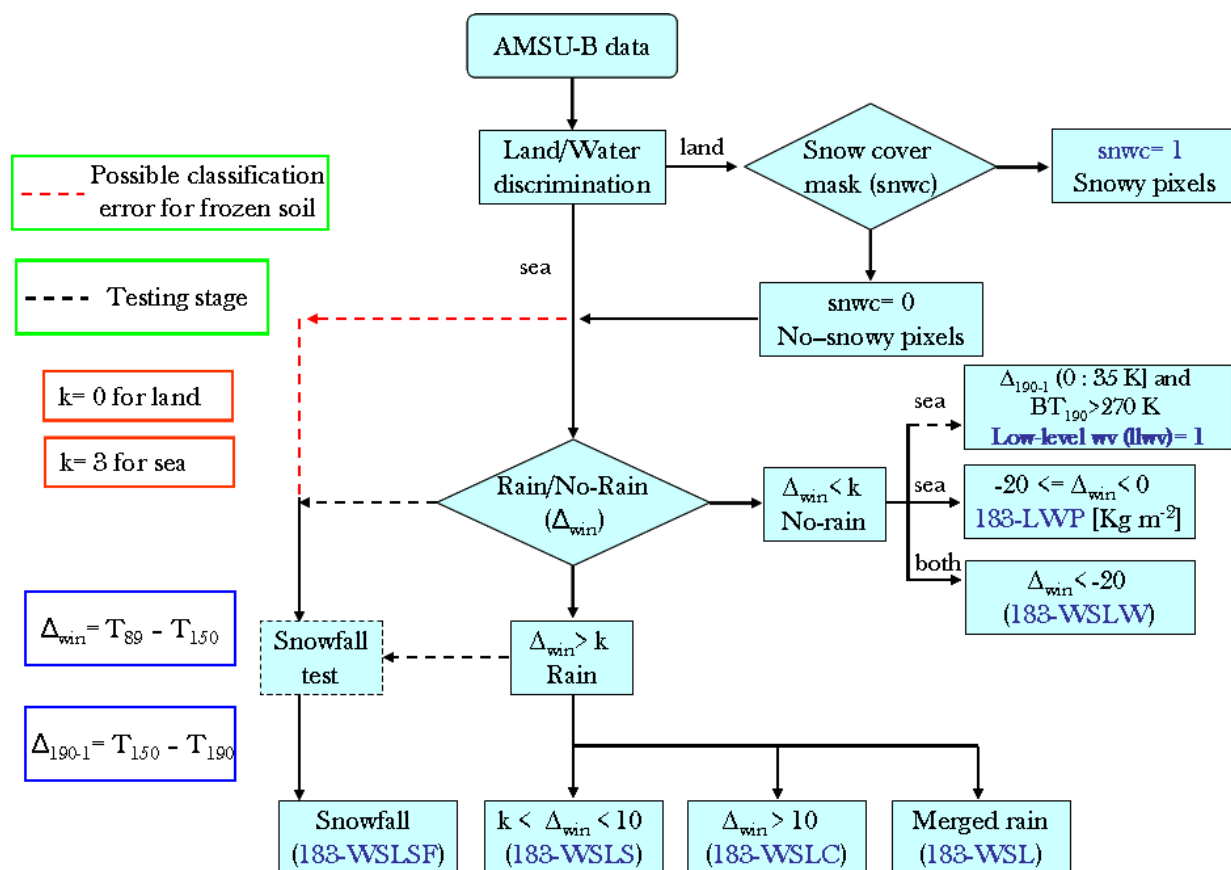


Figure1. The 183-WSL retrieval scheme. On the basis of the Δ_{win} threshold land/sea pixels are classified as rainy/non-rainy. Over land the value of variable *snwc* is previously evaluated in order to weigh up the presence of snow cover: if *snwc*= 0 the pixels are sent to the second decisional step where rain/no-rain data are separated. Similarly, over the sea rain data are cleared from no-rain ones; for the latter, cloud liquid water (183-LWP), cloud droplets/water vapor absorption (183-WSLW) and Low Layer Water Vapor (183-LLWV) are computed. The final rain product is specialized on the basis of the Δ_{win} values and snowfall cascade tests in four specific products.

covered and then rejected by the computation, otherwise they are considered snow-free. For pixels evaluated as precipitating the relationship $\Delta_{win}=(T_{89} - T_{150})>k$ holds and two distinct equations are applied over land and over sea. Other cascade tests are applied to categorize the selected rainy regions as stratiform (183-WLS module), convective (183-WSLC module) or snowfall precipitation (183-WLSF module). Furthermore, a detection is carried out on the discarded pixels ($\Delta_{win}<k$): cloud droplets and water vapor absorption (183-WSLW module), cloud liquid water in terms of Liquid Water Path (183-LWP module), and Low-Level Water Vapor (LLWV module) over water surfaces.

Many experiments have revealed that the method is highly sensitive to light/moderate rainfall as from stratiform formations and also compares very well with results of other retrieval algorithms in the convective cases. Laviola and Levizzani (2008) have compared the 183-WSL rain products with the Infra-Red (IR) and Visible (VIS)

Precipitation Index (PI), based on Meteosat Second Generation (MSG) Spinning Enhanced Visible and Infrared Imager (SEVIRI), and with the Scattering Index (SI) derived from the AMSU-B measurements. The results show that the 183-WSL precipitation type classification agree differently with the two techniques. Specifically, convective rainfall (183-WSLC) highly correlates with the SI outcomes, being this method specifically developed for this kind of precipitation type. On the other hand, light/moderate precipitation retrieved by the 183-WSLS, usually associated with fewer amounts of ice hydrometeors, compares well with PI rainy areas. Note that the SEVIRI technique largely overestimates the spatial extension of the rain systems especially during nighttime when the VIS channel contributions are not available.

Cattani et al. (2009) have in turn compared the 183-WSL performances with the cloud characterization products of the Advanced Very High Resolution Radiometer (AVHRR) on board the same platform of the AMSU-B. The statistical analysis shows that the 183-WSL method correctly detects rain clouds filtering out ambiguous or non precipitating clouds. Furthermore, the algorithm filters out thick water clouds frequently responsible of false alarms due to the large absorption of radiation around the 90 GHz frequency. Nevertheless, poorer performances of the algorithm were shown in the warm rain cases. The combination of the absence of ice hydrometeors and of the large absorption of water vapor surrounding the clouds masks the emission signal from liquid drops determining a substantial deviation between the AVHRR cloud classification and the 183-WSL rain products. The application of the 183-WSL method over warm rain regions will be subject of future studies.

THE 183-WSL SNOW COVER MASK

The new processor of the 183-WSL method for the assessment of snow cover is based on a series of tests. The physical approach exploits the strong scattering at 90, 150 and 190 GHz due to the ice crystals over frozen soils. Although the threshold $\Delta_{win} = (T_{89} - T_{150}) > 3$ K is used in the 183-WSL retrieval scheme to discern rain/no-rain, in presence of snow-covered terrains it assumes similar values giving rise to largely overestimated rainrates. To mitigate this effect the 190 GHz AMSU-B channel is used. By considering local dry conditions within the atmospheric surface layer over ice-covered terrain, the weighting function of this channel, that normally sounds the water vapor absorption around 2 km, peaks closer to the surface. A series of thresholds was developed based on a combination of the above frequencies with the scope to improve snow cover pixel detection and reduce false rain signals.

The images in Fig. 2 illustrate the impact of the snow covered surface on the frequencies at 89 and 150 GHz. As previously noted, the scattered signals from the snow cover impacts the Δ_{win} threshold in a similar way of rain clouds with values > 3 K. The application of the snow cover processor based on frequencies at 89, 150 and 190 GHz filters snowy pixels and classifies such areas as wet and dry snowpack.

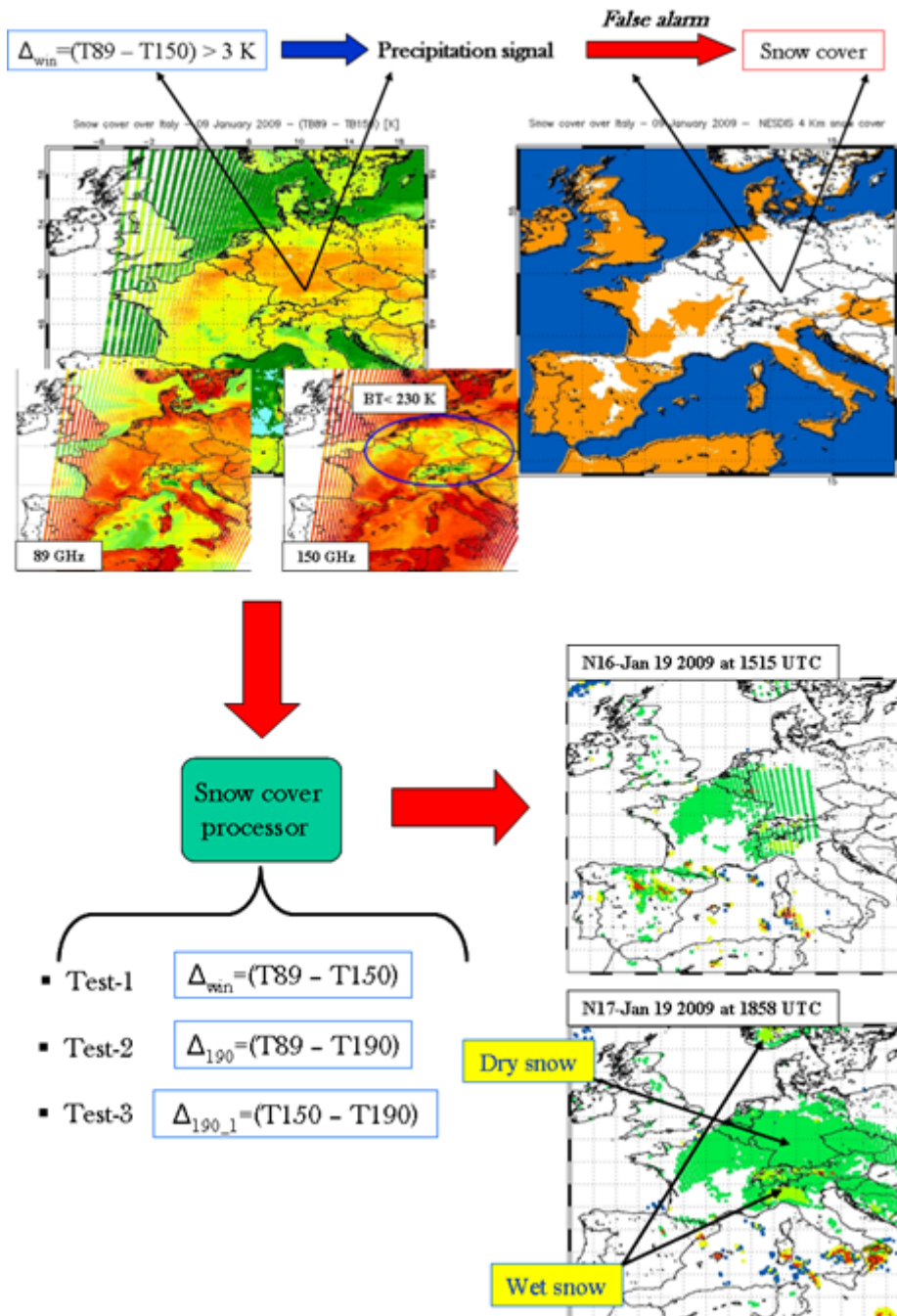


Figure 2. The 183-WSL snow cover mask processor. The snow cover signature is recognized by cascade of threshold tests based on the differences between 89, 150 and 190 GHz and potential false alarms for the rain intensity retrieval are filtered out. The final snow map is well correlated with the Northern Hemisphere map of NOAA's Interactive Multisensor Snow and Ice Mapping System (IMS).

A daily snow cover mask over the Baltic Regions

The severe winter conditions on January 2010 over the Baltic Regions offered the possibility to validate the new snow cover mask of the 183-WSL retrieval method. The daily products retrieved by the method were compared with the daily snow/ice cover maps for the Northern Hemisphere of the NOAA Interactive Multisensor Snow and Ice Mapping System (IMS), considered as ground “truth”. Figure 3 describes the daily percentages of snow pixel detection of the 183-WSL (3-a), IMS (3-b) and the daily discrepancies of two datasets. Note the increasing slope both in 3-a and b, which demonstrates that the 183-WSL snow mask is in general extremely sensitive to the accumulation of the snow mantle. However, due to the complexity of the scene the algorithm misclassifies some pixels. Discrepancies tend to decrease up to an almost perfect match on 23 January 2010 (see Fig. 4). The 183-WSL algorithm discriminates wet from dry snow as seen in the left image of Fig. 4 (green and dark green, respectively). The classification of the hydration status of the snowflakes is mainly based on the sensitivity of the $\Delta_{190} = (T_{89} - T_{190})$ threshold.

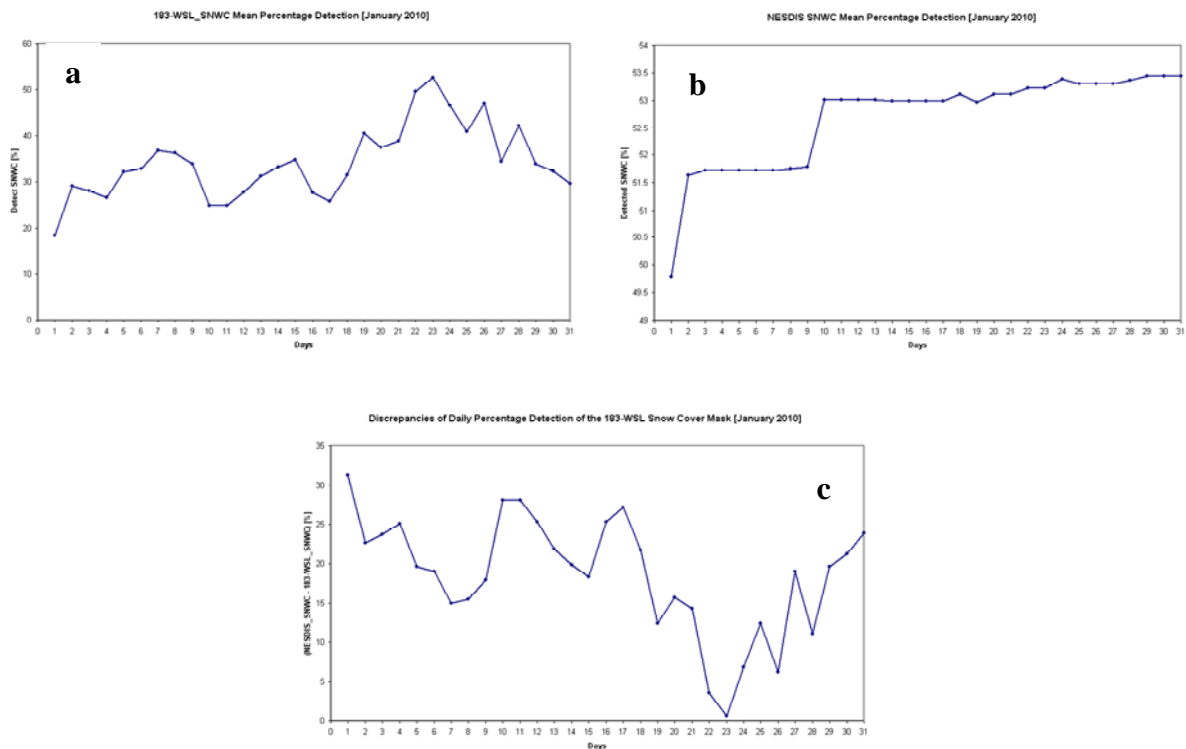


Figure 3. Daily percentages of snow pixel detection for January 2010 over the Baltic regions. The 183-WSL snow cover retrievals (a) show an irregular trend with respect to the regularity of the IMS product (b). This is due to possible misclassifications and to the presence of ice clouds that scatter the upwelling radiation masking snow signals from the surface below.

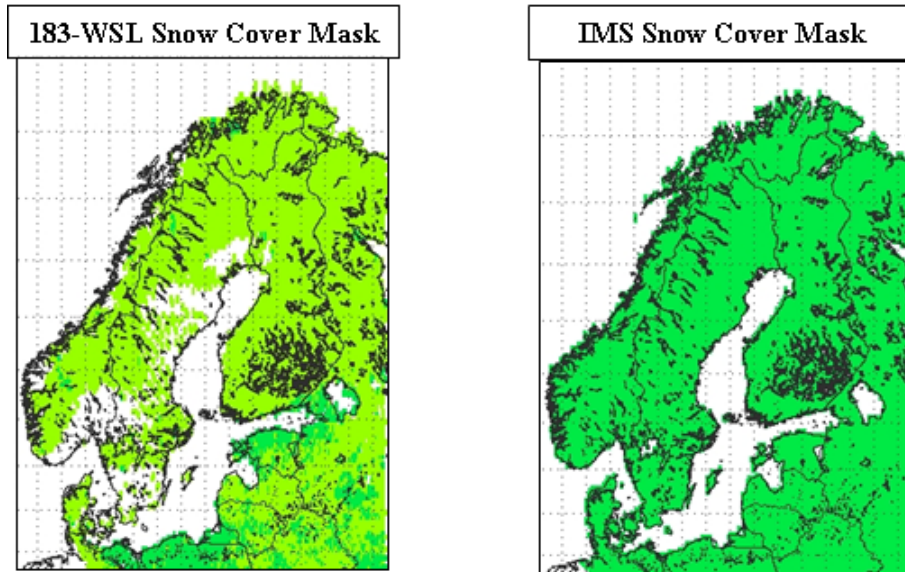


Figure 4. Daily snow cover mask on 23 January 2010. The 183-WSL snow cover classification (left) categorizes snowy pixels in wet (green) and dry (dark) on the basis of the estimated hydration amount. The evident misclassifications, i.e. the white holes in the left image with respect to the IMS map (right) considered as “truth”, is attributed to the presence of ice clouds that are classified in a different way by the 183-WSL computational scheme.

THE 183-WSL SNOWFALL MODULE

The detection of snowfall is based on a range of thresholds where different combinations of the AMSU-B channels are applied only over precipitating regions as detected by the 183-WSL. By considering as limit of snowfall formation the rainy clouds located from a few hundred meters to 5-6 km, the channel sensitivities at 90 and 190 GHz are combined to identify snowfall areas in the precipitating cores. NEXRAD data are used to evaluate the sensitivity of the different AMSU-B channels and to assess a series of threshold values that differentiate snowflake attenuation from other hydrometeor contributions.

Two cases of blizzard over the US are used to test the new 183-WSLSF module. The snowfall detection algorithm, still in testing stage, is developed on the basis of the analysis briefly reported in Fig. 5. More details can be found in D’Aurizio (2010).

The AMSU-B channels respond differently to the various hydrometeor types. Window channels clearly sense the scattering by ice crystals aloft but are also strongly affected by the emissivity of frozen surfaces (Fig. 5-top). Opaque frequencies, on the contrary, show high sensitivity to solid precipitation for clouds located in the low-and-middle atmosphere (190 and 186 GHz described by black and green dots, respectively, in fig.5-

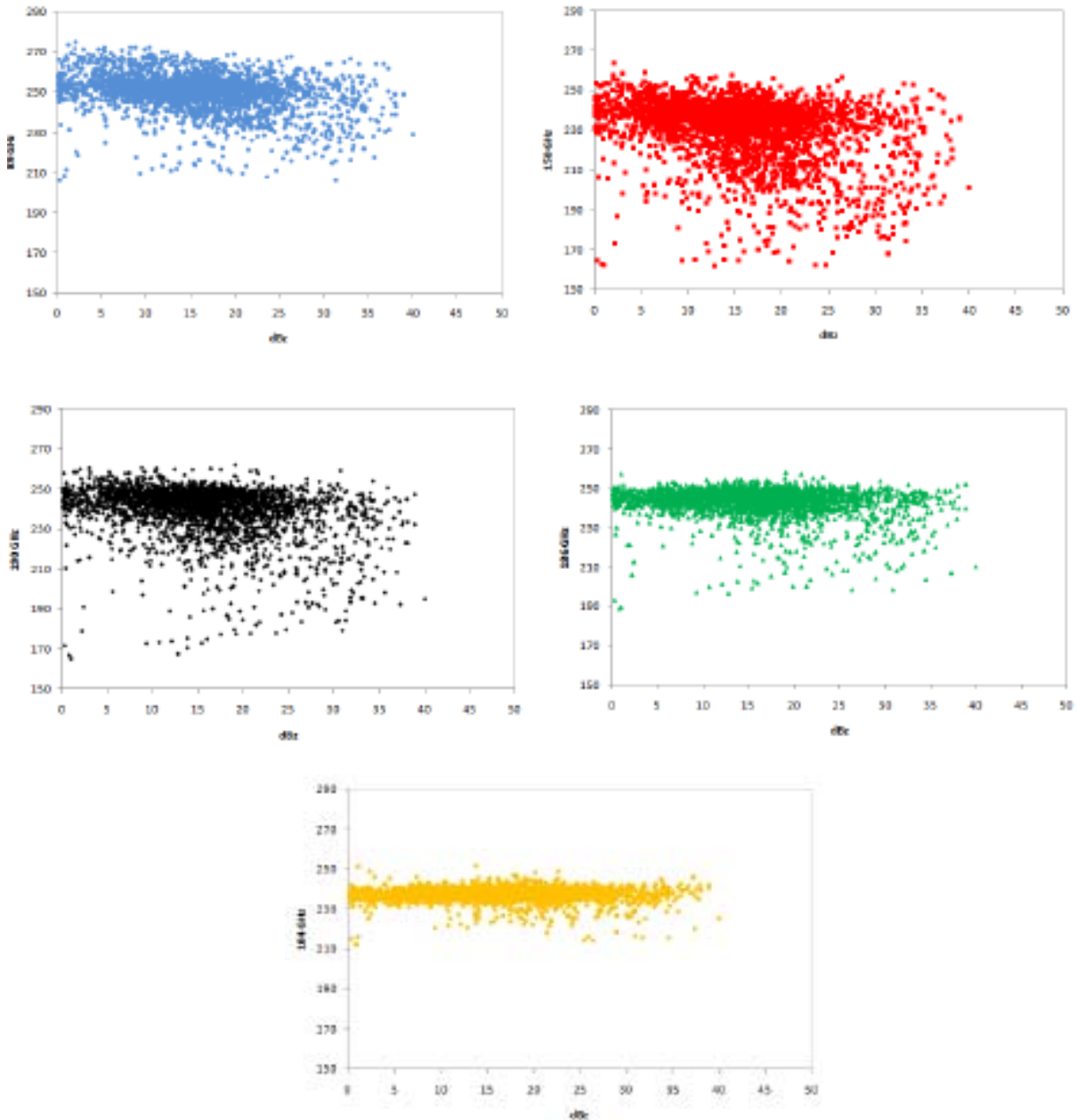


Figure 5. AMSU-B channel response vs NEXRAD co-located data. Window frequencies (top) sense the presence of snowflakes typically attributed to the reflectivity range between 10 and 35 dBz. In a similar way as the 150 GHz frequency, the 190 GHz channel (black dots) responds to the snow particles while the sounding of floating ice crystals at the 186 GHz channel (green dots), having a weighting function located around 6 km, is less effective. The 184 GHz channel (yellow dots) peaks too high to observe clouds where snowfall is forming.

bottom). No perturbation is revealed in the channel at 184 GHz (yellow dots). To roughly isolate the snowflake signature three are the major approximations:

- snowfall formation is substantially constrained to the first 5-6 km of the atmosphere;
- during both events all the precipitation bulk was formed by snowflakes;
- all snowfall deposits on the ground.

Two case of North-Eastern USA blizzard

The new 183-WSL snowfall module was applied to two case studies of severe winter

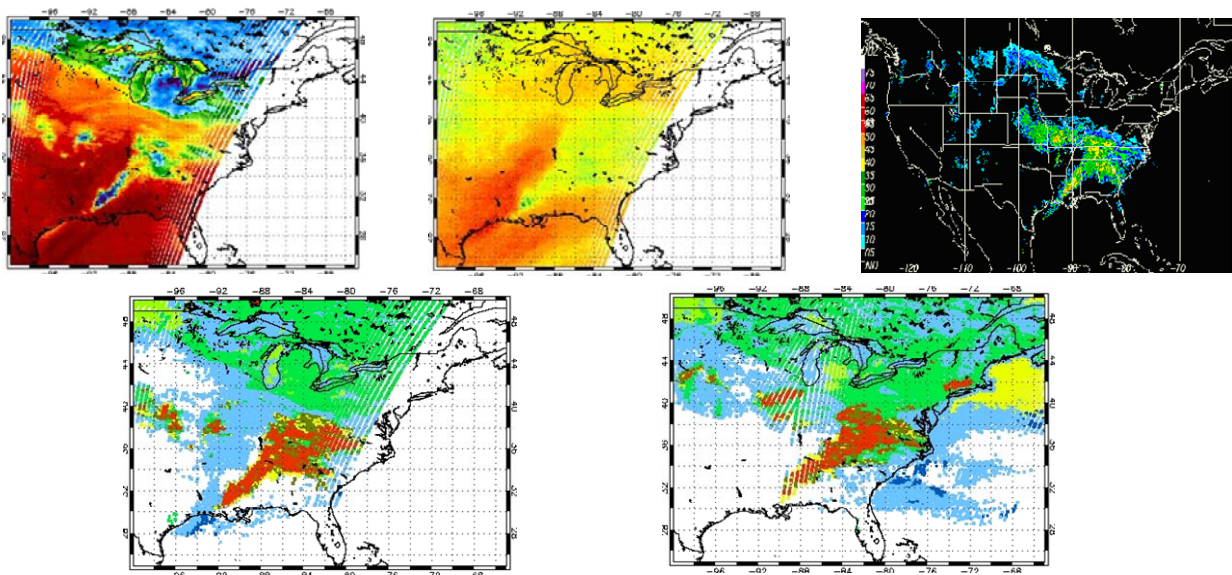


Figure 6. 25 January, 2004. AMSU-B T_{150} and T_{184} (top-left) on board N-15 at 1309 UTC and NEXRAD reflectivity (top-right). The images below describe the 183-WSL products where green, clear and dark green are dry and wet snow cover and snowfall pixels, respectively. Red, yellow and blue indicate convective rain, stratiform rain and cloud liquid water, respectively. Note that the detected snowfall corresponds to radar reflectivities in the 10-20 dBZ range while other pixels are flagged as convective.

storms over the US.

During the event described in Fig. 6 a V-shaped precipitating system formed over the South-Eastern part of the US. The AMSU-B channel at 150 GHz (top-left) highlights the intense scattering structures in the midst of the system where most intense rains were retrieved. Nevertheless, in agreement with the radar measurements (top-right) and following the conclusions reported by Ferraro et al. (2005) the terminal part of the “V” is associated with convective rain (higher reflectivity) while only on the top of the main system (lower reflectivity) the snowfall was identified. The 183-WSL results (bottom)

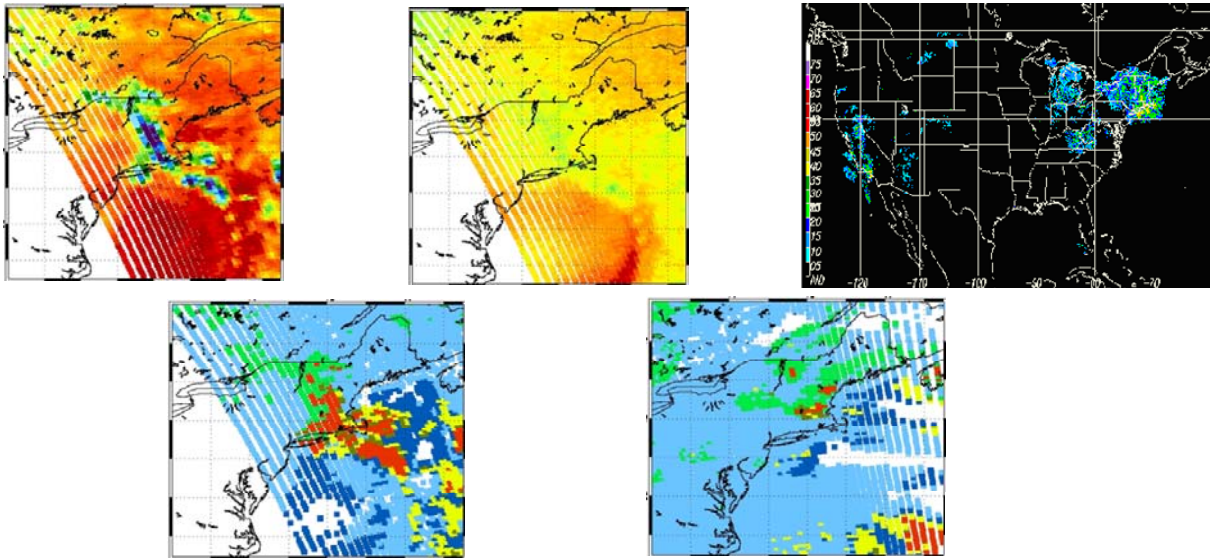


Figure 7. 5 March, 2001. AMSU-B T_{150} and T_{184} GHz (top-left) on board N-15 at 2302 UTC and NEXRAD reflectivity (top-right). The images below describe the 183-WSL products as in Fig. 6. Note that the X-shape is partially retrieved as convective rain and snowfall is confined to the borders.

show that snowfall features are attributed to the pixels located on top and central parts of the structure while the rest of them is classified as a mixture of convective and stratiform precipitation.

The second snow storm (Fig. 7) was characterized by a X-shaped system mainly affecting the New England where 75 cm of snow were deposited in Burlington. A physical model developed by Kim et al. (2003) quantified the snowfall rates in a few mm h^{-1} , roughly consistent with radar data measurements. Conversely, the 183-WSL overestimates both in the quantification of precipitation rates and in the extension of snowfall areas. In fact, although the scattering signatures from frozen hydrometeors strongly depress the T_{150} , the 183-WSL snowfall module classifies the precipitating areas as convective. The possible causes of the misclassification can be reasonably attributed to the relatively small dataset on which the algorithmic coefficients were calculated. In other words, the substantially different situation with respect to the previous case study drastically reduced the algorithm capabilities to discern snowfalls from other type of precipitation.

CONCLUSIONS AND FUTURE DEVELOPMENTS

The results of the new 183-WSL retrieval scheme suggest two fundamental considerations. First, the selection of frequencies directly involved in the estimation of snow with particular reference to the snow cover is accurate and consistent with the results of the retrievals. As to the snow cover mask, the different sensitivities of the 89,

150 and 190 GHz frequencies added to the different peaks of their weighting functions allow for a skilful mapping of frozen soils and of the degree of hydration of snow. The use of the 190 GHz opaque frequency is justified on the basis of several investigations of radiosonde humidity profiles over frozen soils. During a severe winter storms with a large snow deposit local dry conditions can establish in the first atmospheric layers close to the surface. Therefore, the 190 GHz frequency, which normally sounds the absorption of water vapor around 2 km, can sense effects closer to the surface. In this situation, commonly observed in polar regions, the scattering effects by frozen soils at this frequency is strictly comparable with the extinction at 150 GHz, which is normally used as a main detector for ice particles. Moreover, the use of the 190 GHz frequency is needed to modulate the scattering effect from snow surfaces that is quite similar to the extinction induced by rain on the Δ_{win} threshold.

Snow cover mask validation by considering the IMS snow data for the Northern Hemisphere over the Baltic Regions as “ground-truth” reveals high skills in detecting the snow mantle coverage. The current outcomes suggest to carry on the investigations with the focus to expand the validation dataset now limited to January, improve the classification of the snow status as wet and dry phases, and quantify the amount of snow in terms of equivalent water.

In the case of snowfall detection, where the 186 GHz frequency must be added to the existing suite, the experimental version of the algorithm shows some weaknesses most probably due to the rather small database used to calculate the threshold values. As a testbed, two severe blizzards over the Eastern part of United States were selected. Comparisons with radar images have highlighted the skills of the algorithm in delineating snowfall and have encouraged further investigations specifically in the refinement of the technique by using a probabilistic approach as an alternative to the fixed threshold tests. Uncertainties arise when the retrieval is done over frozen soils where snowfall signatures are drastically masked by the scattering from snow-covered terrain.

Acknowledgements

These results were partially improved at the Swedish Meteorological and Hydrological Institute during a Visiting Scientist Activity in the framework of EUMETSAT’s Satellite Application Facility on Support to Nowcasting and Very Short-Range Forecasting. Support from EUMETSAT’s Satellite Application Facility on support to Hydrology and Operational Water Management and from the Department of Civil Protection of the Italian Government is gratefully acknowledged.

REFERENCES

Bennartz, R., and G. W. Petty, 2001: The sensitivity of microwave remote sensing observations of precipitation to ice particle size distributions. *J. Appl. Meteor.*, **40**, 345-364.

- Bennartz, R., and P. Bauer, 2003: Sensitivity of microwave radiances at 85-183 GHz to precipitating ice particles. *Radio Sci.*, **38**, 8075, doi:10.1029/2002RS002626.
- Cattani, E., F. Torricella, S. Laviola, and V. Levizzani 2009: On the statistical relationship between cloud optical and microphysical characteristics from AVHRR and rainfall intensity derived from a new AMSU rain algorithm. *Nat. Hazards Earth Syst. Sci.*, **9**, 2135-2142.
- D'Aurizio, S., 2010: *Sviluppo di un algoritmo per la stima della precipitazione nevosa nelle microonde ad alta frequenza da satellite*. Thesis, Master in Physics, Dept. of Physics, Univ. of Bologna, p. 71.
- Evans, K. F., and G. L. Stephens, 1995a: Microwave radiative transfer through clouds composed of realistically shaped ice crystals. Part I: Single scattering properties. *J. Atmos. Sci.*, **52**, 2041-2057.
- Evans, K. F., and G. L. Stephens, 1995b: Microwave radiative transfer through clouds composed of realistically shaped ice crystals. Part II: Remote sensing of ice clouds. *J. Atmos. Sci.*, **52**, 2058-2072.
- Ferraro, R. R., F. Weng, N. C. Grody, L. Zhao, H. Meng, C. Kongoli, P. Pellegrino, S. Qiu, and C. Dean, 2005: NOAA operational hydrological products derived from the Advanced Microwave Sounding Unit. *IEEE Trans. Geosci. Remote Sens.*, **43**, 1036-1049.
- Kim, M.-J., G. Skofronick-Jackson, J. A. Weinman, and D.-E. Chang, 2003: Spaceborne passive microwave measurement of snowfall over land. *IEEE Int. Geosci. Rem. Sens. Symp.*, **5**, 3163-3165.
- Laviola, S., and V. Levizzani, 2008: Rain retrieval using the 183 GHz absorption lines. *IEEE Proc. MicroRad 2008*, doi:10.1109/MICRAD.2008.4579505.
- Laviola, S., and V. Levizzani, 2009: Observing precipitation by means of water vapor absorption lines; a new approach to retrieve rain rates from satellite. *Italian J. Rem. Sensing*, **41(3)**, 39-49.
- Laviola, S., and V. Levizzani, 2011a: The 183-WSL fast rain rate retrieval algorithm. Part I: Retrieval design. *Atmos. Res.*, in press.
- Laviola, S., A. Moscatello, M. M. Miglietta, and V. Levizzani, 2011b: Satellite and numerical model investigation of two heavy rain events over the Central Mediterranean. *J. Hydrometeor.*, in press.
- Levizzani, V., S. Laviola, and E. Cattani, 2011: Detection and measurement of snowfall from space. *Remote Sensing*, **3(1)**, 145-166.
- Wilheit, T. T., A. T. C. Chang, J. L. King, E. B. Rodgers, R. A. Nieman, B. M. Krupp, A. S. Milman, J. S. Stratigos, and H. Siddalingaiah, 1982: Microwave radiometric observations near 19.35, 92 and 183 GHz of precipitation in Tropical Storm Cora. *J. Appl. Meteor.*, **21**, 1137-1145.

GLOBAL PRECIPITATION DATA ACCESS, VALUE-ADDED SERVICES AND SCIENTIFIC EXPLORATION TOOLS AT NASA GES DISC

Zhong Liu^{1,2}, Dana Ostrenga^{1,3}, Gregory Leptoukh¹, and Steven Kempler¹

¹Goddard Earth Sciences Data and Information Services Center (GES DISC)
NASA Goddard Space Flight Center, Code 610.2, Greenbelt, MD, 20771, USA

²Center for Spatial Information Science and Systems (CSISS), George Mason
University, USA

³ADNET Systems, Inc., USA

e-mail: zhong.liu-1@nasa.gov

ABSTRACT

The Precipitation Data and Information Services Center (PDISC, <http://disc.gsfc.nasa.gov/precipitation>) is home of the Tropical Rainfall Measuring Mission (TRMM) data archive. For over 12 years, the NASA Goddard Earth Sciences Data and Information Services Center (GES DISC, <http://disc.gsfc.nasa.gov/>) has served not only TRMM, but also other space-based, airborne-based, field campaign and ground-based precipitation data products to the precipitation community and other disciplinary communities as well.

To facilitate data searching, ordering and downloading, the GES DISC has developed Mirador (<http://mirador.gsfc.nasa.gov/>). Mirador is a search and order web interface developed in response to the search habits of data users. It has a drastically simplified, clean interface and employs the Google mini appliance for metadata keyword searches. Other features include quick response, data file hit estimator, Gazetteer (geographic search by feature name capability), and an interactive shopping cart. Value-added services include data format conversions and spatial subsetting for limited products.

To enable scientific exploration of Earth science data products without going through complicated and often time-consuming processes, such as data downloading, data processing, etc., the GES DISC has developed the TRMM Online Visualization and Analysis System (TOVAS, <http://disc2.nascom.nasa.gov/Giovanni/tovas/>) in consultation with members of the user community, requesting quick search, subset, analysis and display capabilities for their specific data of interest.

Additional PDISC tool and service capabilities are: An on-line PDISC Portal (includes user guide, etc.); Data ingest, processing, distribution; Electronic distribution, Subscriptions; Uses semantic technology to help manage large amounts of multi-sensor data and their relationships; Data drill down and search capabilities; Data access through various web services, i.e., OPeNDAP, GDS, WMS, WCS; Conversion into various formats, e.g., netCDF, HDF, KML, ASCII; Visualization and analysis of Level-2 data profiles and maps; Generation of derived products, such as, daily products; Parameter and spatial subsetting; Time and temporal aggregation; Regridding; Data version control and provenance; Data Stewardship - Continuous archive verification; Documentation; Science support help desk for proper data usage; Monitoring services for applications; Expertise in data related standards and interoperability.

1. INTRODUCTION

Precipitation is an important atmospheric variable affecting our daily lives. Each year floods and droughts happen around the world, causing heavy property damages and human casualties. Traditionally rain gauge measured precipitation is the main source for weather forecast and research. However, satellite remote sensing has increasingly become important in providing precipitation information. In particular, the Tropical Rainfall Measuring Mission (TRMM) is a joint U.S.-Japan satellite mission to monitor tropical and subtropical (40° S - 40° N) precipitation and to estimate its associated latent heating (TRMM special issue 2000). TRMM provides the first detailed and comprehensive dataset on the four dimensional distribution of rainfall and latent heating over vastly under-sampled tropical and subtropical oceans and continents. TRMM was launched on November 27, 1997 and its data are archived at and distributed by the NASA Goddard Earth Sciences Data and Information Services Center (GES DISC).

Although a single satellite (e.g. TRMM) can provide importation information on precipitation, it suffers the lack of spatial coverage and temporal resolution. Combining with other satellites (e.g. microwave and geostationary satellites), TRMM products can be greatly improved in terms of their temporal resolution and spatial coverage (Huffman et al. 1995; Huffman et al. 1997; Huffman et al. 2001; Huffman et al. 2007), such as, the 3-hourly TRMM multi-satellite precipitation analysis (TMPA).

Accessing precipitation products can be a challenging task for many, especially for those in developing countries and non data experts (Liu et al. 2007). At the GES DISC, we have developed data services and tools to facilitate users from diverse backgrounds and with different computing skills.

2. PRECIPITATION DATA ACCESS AND SERVICES AT GES DISC

2.1 SEARCH AND ORDER PRECIPITATION DATA THROUGH MIRADOR

To facilitate data searching, ordering and downloading, the GES DISC has developed Mirador (<http://mirador.gsfc.nasa.gov/>). Mirador (Figs. 1 and 2) is a search and order web interface developed in response to the search habits of data users. It has a drastically simplified, clean interface and employs the Google mini appliance for metadata keyword searches. Other features include quick response, data file hit estimator, Gazetteer (geographic search by feature name capability), and an interactive shopping cart. Value-added services include data format conversions and spatial subsetting for limited products.



Figure 1. Mirador is a search and order web interface supporting metadata keyword searches and many other features.

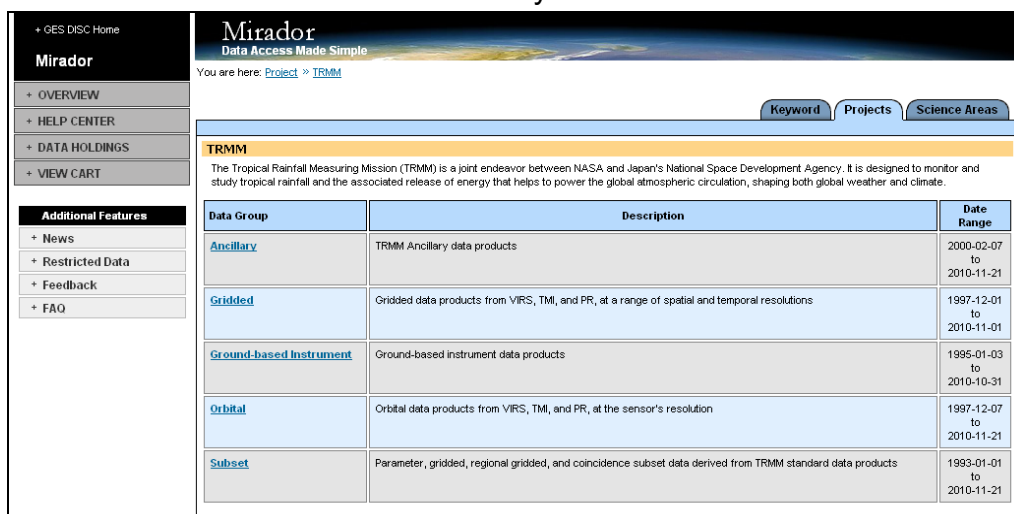


Figure 2. In Mirador, TRMM data are organized based on data types and science focus areas.

2.2 SCIENTIFIC EXPLORATION TOOLS

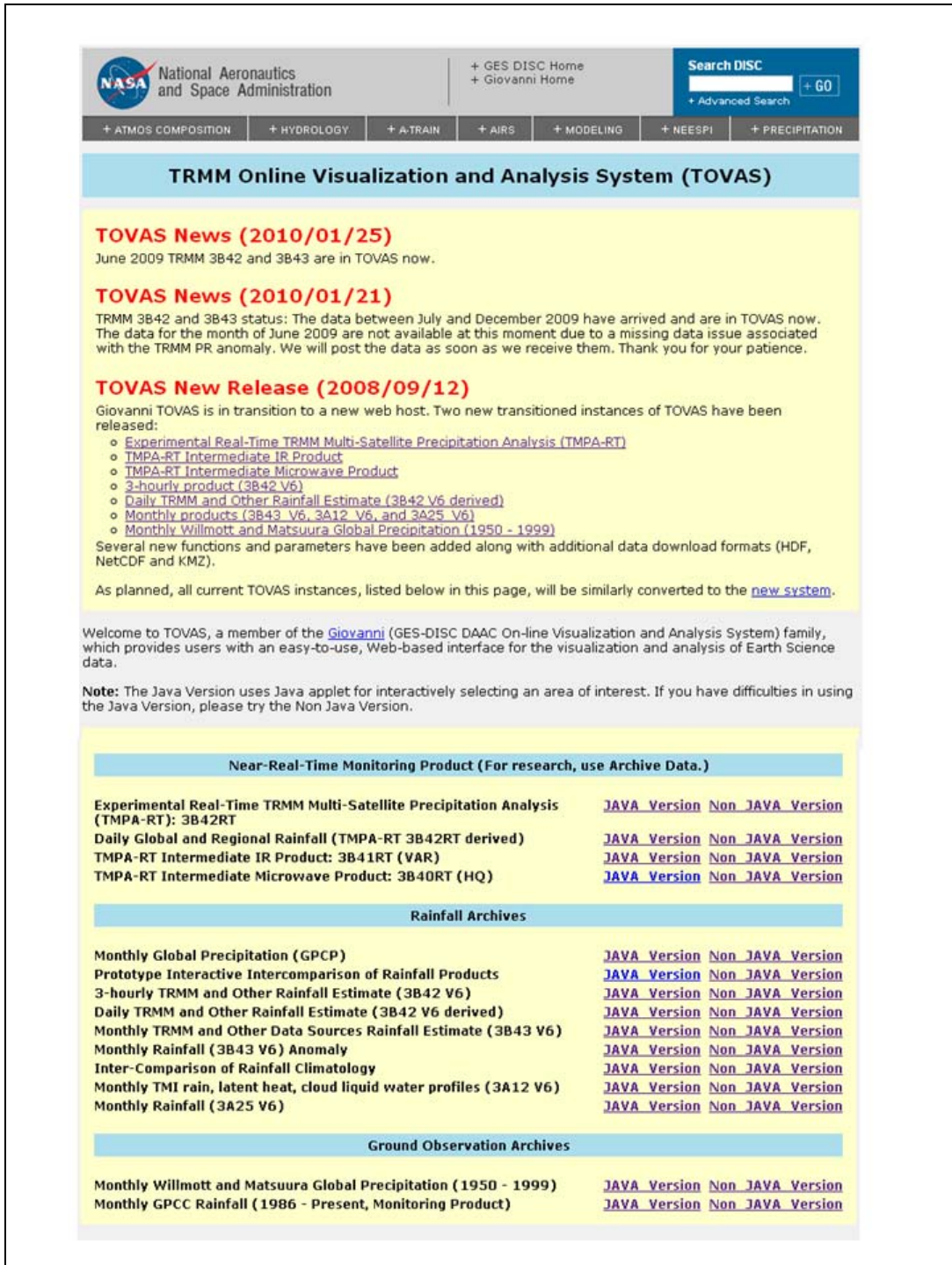
Despite the simple and easy-to-use Mirador, accessing precipitation data can still be a challenge. For example, to generate a global or regional precipitation map, users will have to first locate and download a file from a data archive center, set up a computing environment, learn data format and write their own software for data processing and display if it is not provided. All these could be a burden to them, especially for non-professional users and those in developing countries. To facilitate data access, the GES DISC has developed the TRMM Online Visualization and Analysis System (TOVAS; URL: <http://disc2.nascom.nasa.gov/tovas/>). With a web browser and few mouse clicks, an individual can obtain precipitation data visualization and analyses without downloading data and software (Liu et al. 2007). Tables 1 and 2 list TOVAS precipitation products and functions, respectively. Figure 3 shows the landing page of TOVAS, from where users can access different precipitation products. Plots in Fig. 4 are examples of TOVAS outputs.

Temporal Resolution	Products
3-hourly	3B43RT (near-real-time), 3B42
daily	3B42RT (derived), 3B42 (derived)
Monthly	3B43 (satellite-gauge combined), 3A12 (TRMM microwave imager), 3A25 (TRMM precipitation radar), GPCP (satellite-gauge combined), GPCC (gauges), Willmott (gauges)

Table 1. List of TOVAS global precipitation products.

Function	Description
Area Plot	Area plot averaged or accumulated over any available data period within any rectangular area
Time Plot	Time series averaged over any rectangular area
Hovmöller Plots	Longitude-time and latitude-time plots
Anomaly and Normalized Anomaly Plots	Area plot averaged over any available data period within any rectangular area. Normalized anomaly is defined as (rainfall – climatology)/climatology
Animations	Animations available for area plots
ASCII Output	ASCII output available for all plot types, suitable feeding GIS or other applications

Table 2. Functions supported by TOVAS.



NASA National Aeronautics and Space Administration

+ GES DISC Home
+ Giovanni Home

Search DISC
+ Advanced Search + GO

+ ATMOS COMPOSITION + HYDROLOGY + A-TRAIN + AIRS + MODELING + NEESPI + PRECIPITATION

TRMM Online Visualization and Analysis System (TOVAS)

TOVAS News (2010/01/25)
June 2009 TRMM 3B42 and 3B43 are in TOVAS now.

TOVAS News (2010/01/21)
TRMM 3B42 and 3B43 status: The data between July and December 2009 have arrived and are in TOVAS now. The data for the month of June 2009 are not available at this moment due to a missing data issue associated with the TRMM PR anomaly. We will post the data as soon as we receive them. Thank you for your patience.

TOVAS New Release (2008/09/12)
Giovanni TOVAS is in transition to a new web host. Two new transitioned instances of TOVAS have been released:

- Experimental Real-Time TRMM Multi-Satellite Precipitation Analysis (TMPA-RT)
- TMPA-RT Intermediate IR Product
- TMPA-RT Intermediate Microwave Product
- 3-hourly product (3B42 V6)
- Daily TRMM and Other Rainfall Estimate (3B42 V6 derived)
- Monthly products (3B43 V6, 3A12 V6, and 3A25 V6)
- Monthly Willmott and Matsuura Global Precipitation (1950 - 1999)

Several new functions and parameters have been added along with additional data download formats (HDF, NetCDF and KMZ).

As planned, all current TOVAS instances, listed below in this page, will be similarly converted to the [new system](#).

Welcome to TOVAS, a member of the [Giovanni](#) (GES-DISC DAAC On-line Visualization and Analysis System) family, which provides users with an easy-to-use, Web-based interface for the visualization and analysis of Earth Science data.

Note: The Java Version uses Java applet for interactively selecting an area of interest. If you have difficulties in using the Java Version, please try the Non Java Version.

Near-Real-Time Monitoring Product (For research, use Archive Data.)

Experimental Real-Time TRMM Multi-Satellite Precipitation Analysis (TMPA-RT): 3B42RT	JAVA Version	Non JAVA Version
Daily Global and Regional Rainfall (TMPA-RT 3B42RT derived)	JAVA Version	Non JAVA Version
TMPA-RT Intermediate IR Product: 3B41RT (VAR)	JAVA Version	Non JAVA Version
TMPA-RT Intermediate Microwave Product: 3B40RT (HQ)	JAVA Version	Non JAVA Version

Rainfall Archives

Monthly Global Precipitation (GPCP)	JAVA Version	Non JAVA Version
Prototype Interactive Intercomparison of Rainfall Products	JAVA Version	Non JAVA Version
3-hourly TRMM and Other Rainfall Estimate (3B42 V6)	JAVA Version	Non JAVA Version
Daily TRMM and Other Rainfall Estimate (3B42 V6 derived)	JAVA Version	Non JAVA Version
Monthly TRMM and Other Data Sources Rainfall Estimate (3B43 V6)	JAVA Version	Non JAVA Version
Monthly Rainfall (3B43 V6) Anomaly	JAVA Version	Non JAVA Version
Inter-Comparison of Rainfall Climatology	JAVA Version	Non JAVA Version
Monthly TMI rain, latent heat, cloud liquid water profiles (3A12 V6)	JAVA Version	Non JAVA Version
Monthly Rainfall (3A25 V6)	JAVA Version	Non JAVA Version

Ground Observation Archives

Monthly Willmott and Matsuura Global Precipitation (1950 - 1999)	JAVA Version	Non JAVA Version
Monthly GPCP Rainfall (1986 - Present, Monitoring Product)	JAVA Version	Non JAVA Version

Figure 3. TOVAS web landing page (<http://disc2.nascom.nasa.gov/tovas/>) consisting of product and development news and links to different precipitation products and services.

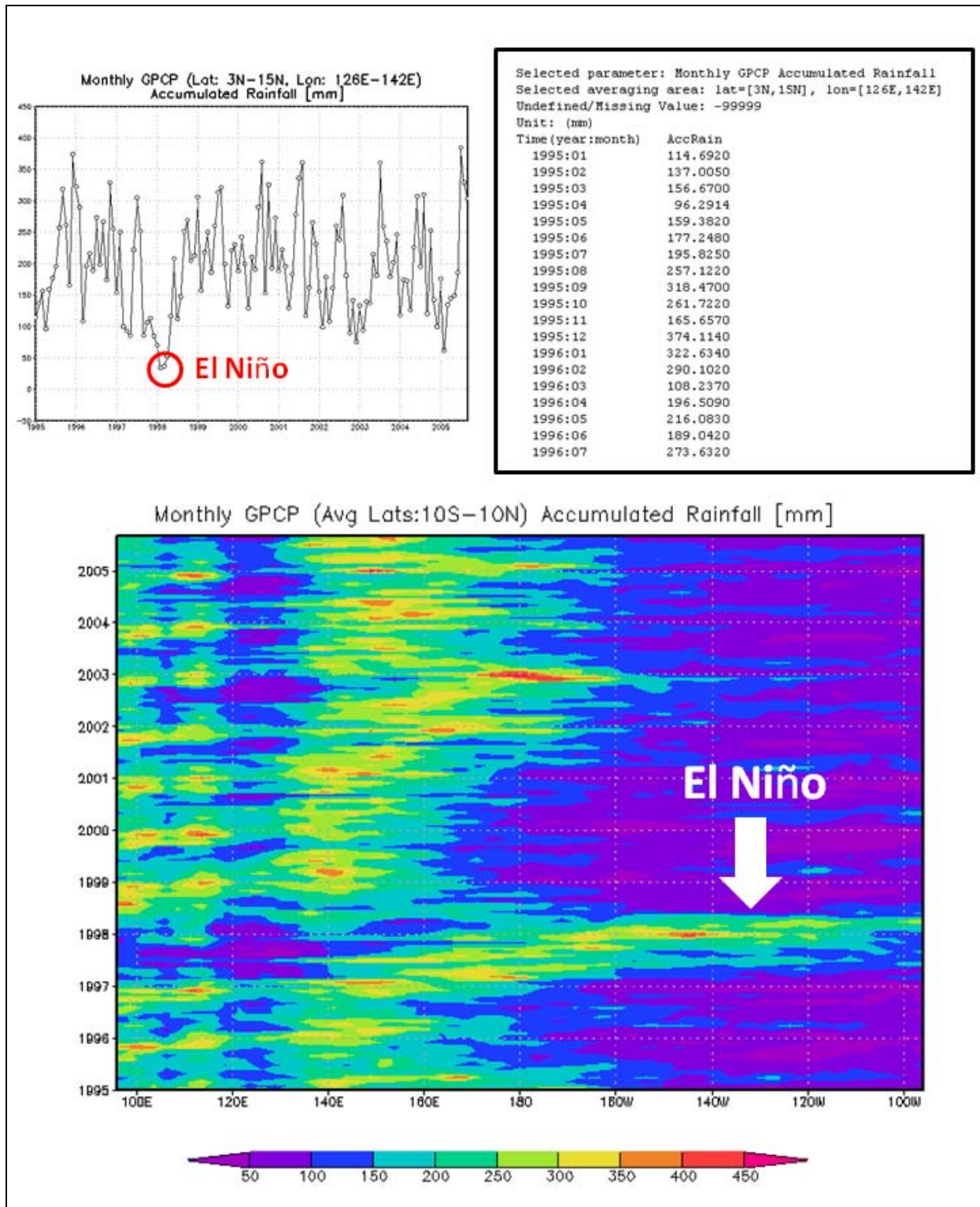


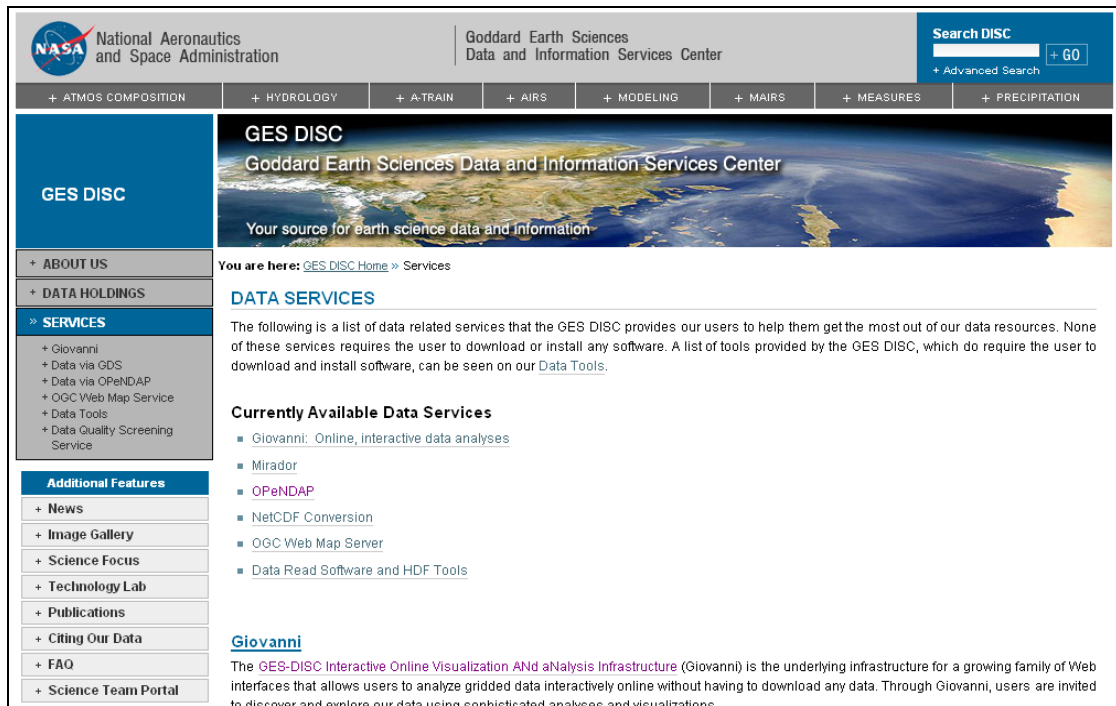
Figure 4. Examples of TOVAS outputs. Top left: A GPCP time-series plot; Top right: The ASCII data output for the time series; Bottom: A Hovmöller diagram.

2.3 VALUE ADDED SERVICES

Additional PDISC tools and services are: An on-line PDISC Portal (includes user guide, etc., see Fig. 5); Data ingest, processing, distribution; Electronic distribution, Subscriptions; Uses semantic technology to help manage large amounts of multi-sensor data and their relationships; Data drill down and search capabilities; Data access through various web services, i.e., OPeNDAP, GDS, WMS, WCS (Figs. 6 and 7); Conversion into various formats, e.g., netCDF, HDF, KML, ASCII; Visualization and analysis of Level-2 data profiles and maps; Generation of derived products, such as, daily products; Parameter and spatial subsetting; Time and temporal aggregation; Regridding; Data version control and provenance; Data Stewardship - Continuous archive verification; Documentation; Science support help desk for proper data usage; Monitoring services for applications; Expertise in data related standards and interoperability.

The screenshot displays the PDISC Portal interface. At the top, it features the NASA logo and the text 'National Aeronautics and Space Administration' on the left, and 'Goddard Earth Sciences Data and Information Services Center' on the right. A search bar labeled 'Search DISC' with a '+ GO' button is located in the top right corner. Below the header is a navigation menu with tabs for '+ ATMOS COMPOSITION', '+ HYDROLOGY', '+ A-TRAIN', '+ AIRS', '+ MODELING', '+ MAIRS', '+ MEASURES', and '+ PRECIPITATION'. The 'PRECIPITATION' tab is selected, leading to a page with a large image of clouds and the title 'Precipitation'. A red sidebar on the left contains a 'Precipitation' header and a list of menu items: '> OVERVIEW', '+ DATA HOLDINGS', '+ DOCUMENTATION', 'Additional Features', '+ News', '+ Tools', '+ Science Focus', '+ Applications', '+ Instruments', '+ Links', and '+ FAQ'. The main content area includes a breadcrumb trail 'You are here: GES DISC Home > Precipitation', a heading 'Precipitation: OVERVIEW', a welcome message, and several sections: 'Search for Precipitation Data' (mentioning the 'Mirador' search interface), 'Explore Precipitation Data with Giovanni' (mentioning the 'Giovanni TOVAS' visualization system), 'PDISC Guide for New Users' (offering a 'getting started guide'), and 'Precipitation Data Services at the DISC' (listing services like data access and cross-disciplinary research).

Figure 5. An on-line PDISC Portal containing precipitation related information.



GES DISC
Goddard Earth Sciences Data and Information Services Center
Your source for earth science data and information

DATA SERVICES

The following is a list of data related services that the GES DISC provides our users to help them get the most out of our data resources. None of these services requires the user to download or install any software. A list of tools provided by the GES DISC, which do require the user to download and install software, can be seen on our [Data Tools](#).

Currently Available Data Services

- Giovanni: Online, interactive data analyses
- Mirador
- OPeNDAP
- NetCDF Conversion
- OGC Web Map Server
- Data Read Software and HDF Tools

Giovanni
The [GES-DISC Interactive Online Visualization And aNalysis Infrastructure](#) (Giovanni) is the underlying infrastructure for a growing family of Web interfaces that allows users to analyze gridded data interactively online without having to download any data. Through Giovanni, users are invited to discover and explore our data using sophisticated analyses and visualizations.

Figure 6. Other value-added services (<http://disc.sci.gsfc.nasa.gov/services>) at GES DISC.



GES DISC
Goddard Earth Sciences Data and Information Services Center

TROPICAL RAINFALL MEASURING MISSION (TRMM) GRIDDED RAINFALL DATA

The information on this page is provided to the Open Source Project for Network Data Access Protocol (OPeNDAP) users. Assuming the users have some knowledge of the OPeNDAP client/server software, the information shown here will direct you to the locations where OPeNDAP enabled data are stored.

Data Products Available	Description	Document	Image
3A11: Monthly 5° x 5° Oceanic Rainfall	Rain rate, conditional rain rate, rain frequency, and freezing height for a latitude band from 40 degree N to 40 degree S, from TM	Readme	View
3A12: Monthly 0.5° x 0.5° mean 2A12 profile, and surface rainfall	0.5 x 0.5 degree gridded monthly product comprised of mean 2A12 data and calculated vertical hydrometeor profiles as well as mean surface rainfall	Readme	
3A25: Monthly 5°x5° and .5°x.5° Spaceborne Radar Rainfall	Total and conditional rain rate, radar reflectivity, path-integrated attenuation at 2, 4, 6, 10, 15 km for convective and stratiform rain, storm, freezing, and bright band heights, and snow-ice layer depth for a latitude band from 40°N to 40°S, from PR	Readme	View
3A26: Monthly 5° x 5° Surface Rain Total	Rain rate probability distribution at surface, 2 km, and 4 km for a latitude band from 40°N to 40°S, from PR	Readme	View
3A46: Monthly 1° x 1° SSM/I Rain	Global rain rate from SSM/I	Readme	
3B31: Monthly 5° x 5° Combined Rainfall	Rain rate, cloud liquid water, rain water, cloud ice, grauples at 14 levels for a latitude band from 40 degree N to 40 degree S, from PR and TM	Readme	View
3B42: 3-Hour 0.25° x 0.25° TRMM and Other-GPI Calibration Rainfall	Calibrated geosynchronous IR rain rate using TRMM estimates .	Readme	View
3B43: Monthly 0.25° x 0.25° TRMM and Other Sources Rainfall	Merged rain rate from TRMM, geosynchronous IR, SSM/I , rain gauges	Readme	View
CSH: Monthly 0.5° x 0.5° Convective/Stratiform Heating	TRMM Monthly 0.5° x 0.5° Convective/Stratiform Heating	Readme	

Figure 7. TRMM data via OPeNDAP (<http://disc.sci.gsfc.nasa.gov/services/opendap/TRMM/trmm.shtml>).

3. CONCLUSION AND FUTURE PLANS

We have described global precipitation data access, value-added services and scientific exploration tools at NASA GES DISC. Future plans include continuous improvements and new additions of data services, documentation, data application case studies and user services based on user feedback and future mission requirements. Emphasis will be on merging, integration, and inter-comparison of multi-satellite, multi-mission and multi-sensor data.

4. REFERENCES

Huffman, G.J., R.F. Adler, B. Rudolph, U. Schneider, and P. Keehn, 1995: Global Precipitation Estimates Based on a Technique for Combining Satellite-Based Estimates, Rain Gauge Analysis, and NWP Model Precipitation Information, *J. Clim.*, 8, 1284-1295.

Huffman, G.J., R.F. Adler, P. Arkin, A. Chang, R. Ferraro, A. Gruber, J. Janowiak, A. McNab, B. Rudolph, and U. Schneider, 1997: The Global Precipitation Climatology Project (GPCP) Combined Precipitation Dataset, *Bul. Amer. Meteor. Soc.*, 78, 5-20.

Huffman, G.J., R.F. Adler, D.T. Bolvin, G. Gu, E.J. Nelkin, K.P. Bowman, Y. Hong, E.F. Stocker, D.B. Wolff, 2007: The TRMM Multi-satellite Precipitation Analysis: Quasi-Global, Multi-Year, Combined-Sensor Precipitation Estimates at Fine Scale. *J. Hydrometeor.*, 8(1), 38-55.

Huffman, G.J., R.F. Adler, M. Morrissey, D.T. Bolvin, S. Curtis, R. Joyce, B McGavock, J. Susskind, 2001: Global Precipitation at One-Degree Daily Resolution from Multi-Satellite Observations. *J. Hydrometeor.*, 2(1), 36-50.

Liu, Z., H. Rui, W. Teng, L. Chiu, G. Leptoukh, and G. Vicente, 2007, Online visualization and analysis: A new avenue to use satellite data for weather, climate and interdisciplinary research and applications. *Measuring Precipitation from Space - EURAINSAT and the future, Advances in Global Change Research*, 28, 549-558.

Special Issue on the Tropical Rainfall Measuring Mission (TRMM), combined publication of the December 2000 *Journal of Climate* and Part 1 of the December 2000 *Journal of Applied Meteorology*, American Meteorological Society, Boston, MA.

COMBINING PRECIPITATION AND SOIL MOISTURE OBSERVATIONS: A WAY FOR IMPROVED ESTIMATES OF LAND SURFACE WATER FLUXES?

Alexander Löw

Max Planck Institute for Meteorology, KlimaCampus, Hamburg, Germany

e-mail: alexander.loew@zmaw.de

Simulations of the Earth water and energy fluxes are highly dependent on the reliability of model input data. Uncertainties of simulations of terrestrial water fluxes are hereby directly related to the accuracy of available precipitation data. As precipitation is characterized by small temporal and spatial correlation lengths, the uncertainties in precipitation data increase with decreasing density of available precipitation gauges.

Active and passive satellite sensor systems allow for the derivation of quantitative precipitation information from space. However, these precipitation estimates are prone to large uncertainties, especially over land, as the measured signal is also influenced by the underlying land surface.

However, as soil moisture directly depends on precipitation dynamics, its variation is likely to be used as a proxy for precipitation variability. Remote sensing techniques have been proven to allow for the monitoring of surface soil moisture dynamics at different spatio-temporal scales. Especially low frequency microwave data are most sensitive to soil moisture dynamics.

The present paper investigates the potential of combining microwave soil moisture information with (uncertain) precipitation estimates to partly compensate for uncertainties in precipitation data sets. The combined use of soil moisture and precipitation information within a data assimilation framework should therefore be favourable for an estimation of surface water fluxes.

The present paper investigates the general potential of a such combined approach by integrating L-band (1-2 GHz) microwave radiometer data into a simple model for soil wetness to compensate for uncertainties in a priori information of precipitation. A high correlation between the microwave signature and surface soil moisture was found which is consistent with previous findings. An analytical data assimilation scheme for the integration of that information into a soil wetness model, based on an antecedent precipitation index (API), was developed.

The results reveal that the data assimilation filter adds or removes an amount of water partially compensating for the actual precipitation error. The correlation coefficient between the filter update and actual precipitation error was found to be $0.6 < r < 0.8$ and the model simulations did show a better coincidence with in situ soil moisture records, by integrating the microwave data. The results indicate a high potential to use L-band microwave data to compensate for uncertainties in precipitation measurements in the absence of detailed ground based measurements.

TARCAT - TAMSAT AFRICAN RAINFALL CLIMATOLOGY AND TIME SERIES

Ross Maidment¹, Elena Tarnavsky¹, David Grimes¹, Richard Allan¹

¹TAMSAT, Department of Meteorology, University of Reading, Reading, UK

e-mail: ross.maidment@pgr.reading.ac.uk

1. BACKGROUND

The majority of the African population is dependent on rainfed agriculture. Thus, changes in future rainfall climate can have serious consequences - both from humanitarian and economic viewpoints. Good predictions of future climate depend on sound knowledge of present climate, this is poorly understood due to the inadequacy of ground-based observations. Operational radar measurements are virtually non-existent in Africa and rain gauge data are sparse and unevenly distributed (Washington et al. 2007).

The only feasible way of filling the gap in rainfall measurements is to use satellite data. However, in terms of producing a homogeneous time series suitable for analysis of long-term trends, there are deficiencies in the products available. Existing global rainfall time series using satellite data are either too short (<10 years) or temporally inhomogeneous (different sensors and different proportions of gauge data included at different times). Examples of short time series include the Climate Prediction Center (CPC) MORPHing technique (CMORPH) (Joyce et al. 2004) and PERSIANN (Precipitation Estimation from Remotely Sensed Information using Artificial Neural Networks) (Sorooshian et al. 2007). Examples of inhomogeneous time series include the Global Precipitation Climatology Project (GPCP) dataset (Adler et al. 2003) and the CPC Rainfall Estimate (CPC-RFE), an amalgam of rainfall estimates derived from thermal infra-red (TIR) satellite imagery and gauge data from synoptic stations in the Global Telecommunications System (GTS) network based on the approach described in Xie and Arkin (1996).

2. THE TAMSAT ALGORITHM

In contrast to the methods mentioned above, the TAMSAT algorithm (Thorne et al. 2003) developed at the University of Reading is temporally homogeneous and relatively long term. This is because it is derived entirely from a single data stream - TIR imagery from the Meteosat satellite which is available back to 1983. Comparison with local rain gauge data is used to determine a threshold temperature T_t which identifies rainy

cloud. Calibration against the same local gauges is used to derive a relationship between rainfall amount and number of hours colder than threshold temperature (Cold Cloud Duration or CCD). The standard TAMSAT product is dekadal (~10 day) totals at 0.0375° spatial resolution. Although the algorithm is only reliable for convective rainfall, it is appropriate for use in Africa because most African rainfall is convective.

3. VALIDATION

The quality of the TAMSAT rainfall estimates has been investigated in several validation experiments. An example is the study carried out in Uganda with the collaboration of the European Commission Joint Research Centre and the Ugandan Met Service. The study compared 3 sets of satellite-based estimates (TAMSAT, CPC-RFE, GPCP) and two climate model re-analysis products ERA-40 and ERA-Interim produced by the European Centre for Medium Range Weather Forecasting. The estimates were evaluated by comparison with gauge data provided by the Ugandan Meteorology Service. All data were averaged over a regular 0.5° x 0.5° latitude-longitude grid. The averaging for the gauge data was carried out using kriging. Rainfall amounts were compared at dekadal time scale. Only grid squares containing at least one gauge were used as indicated in Figure 1. Validation covered the long rainy season (Feb-Jun) 2001-2005. Each point in the scatter plots in Figure 2 corresponds to one dekad averaged over all grid squares for the various estimation methods. Statistical comparisons are given in Table 1. It can be seen that all satellite methods have similar quality and outperform the model outputs. Similar validation experiments have been carried out in Ethiopia (Dinku et al. 2007), West Africa (Jobard et al. 2007) and southern Africa (Thorne et al. 2001). Because of the local calibration, the TAMSAT estimates have a consistent quality over all of these regions. Other algorithms based on global calibrations do not exhibit this consistency. For example, the CMORPH algorithm performs well over Ethiopia but not in west Africa, while the reverse is true of CPC-RFE.

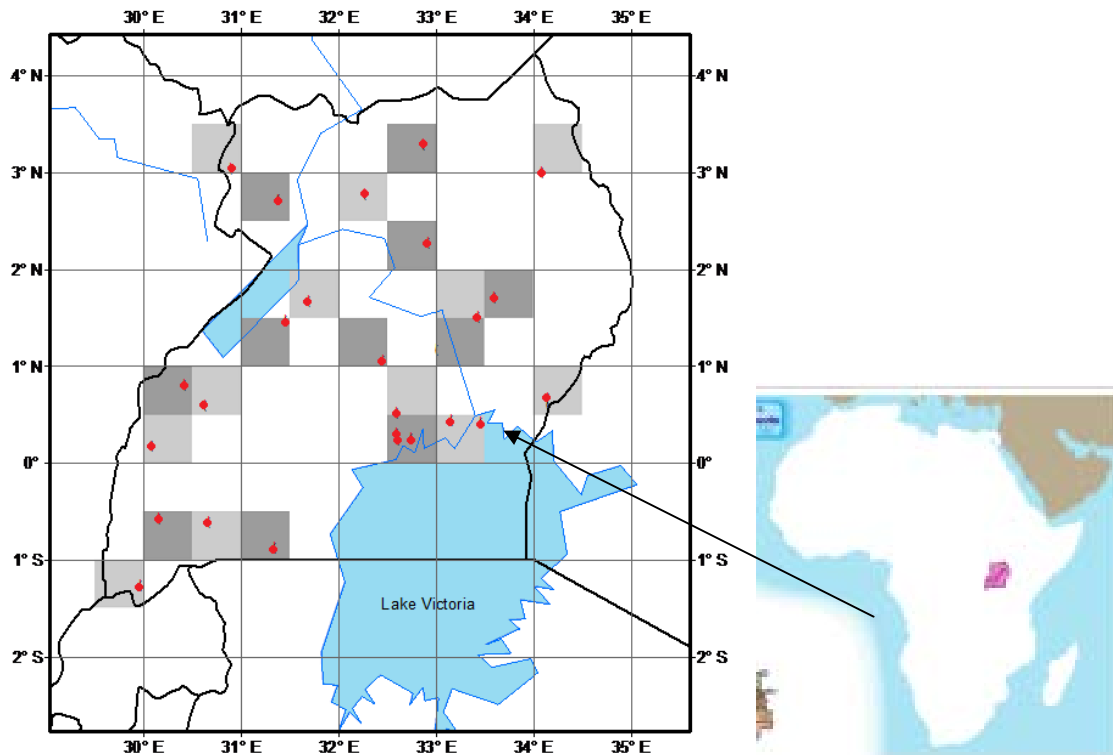


Figure 1. Ugandan validation experiment. Gauge locations are shown by red dots. Grey shading indicates grid squares used in the validation. Heavy black lines indicate national borders.

Table 1. Statistical comparison of estimation methods. Best results in each category are in red.

Product	Bias/mm	RMSD/mm	R²
ERA-40	-9.86	18.09	0.41
ERA-Interim	14.06	26.55	0.39
TAMSAT	-1.01	10.41	0.72
RFE 2.0	-1.73	11.00	0.74
GPCP	0.16	11.56	0.72

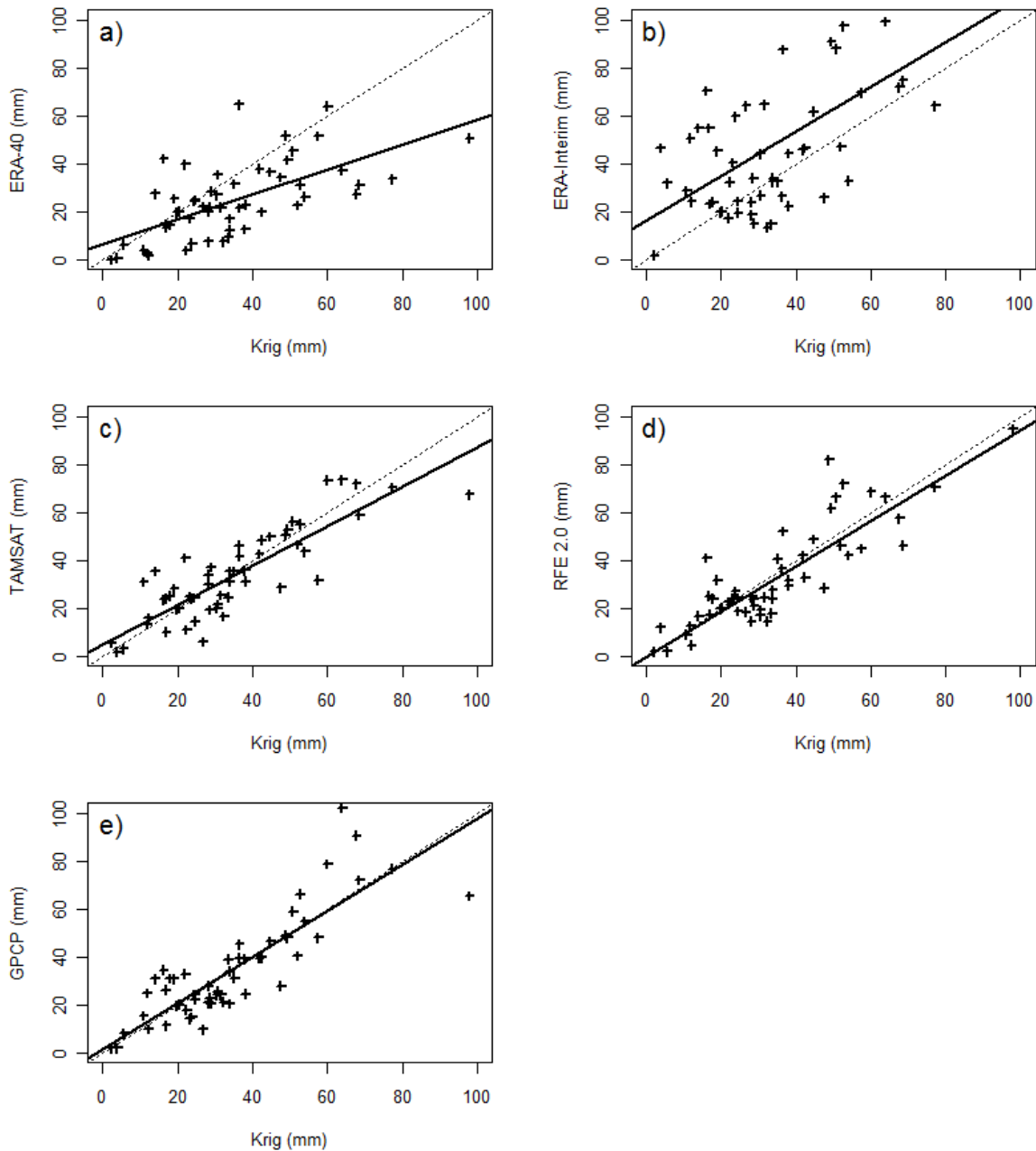


Figure 2. Comparison of mean dekadal grid estimates against kriged gauge data for all methods.

4. THE TARCAT TIME SERIES

Based on these encouraging results, all available Meteosat TIR data have been obtained from Eumetsat and quality controlled to remove corrupt images and overcome calibration errors. Figure 3 gives an overview of data availability. Blue dekads are complete; yellow and green will be recoverable with some interpolation. Red dekads are probably non-recoverable. It can be seen that there are sufficient data available to generate an almost complete dekadal time series from 1982 to the present. As a pilot

project, a 29-year rainfall time series has been generated for Ethiopia in collaboration with Columbia University IRI (USA) and the Ethiopian National Met Agency. The TARCAT time series compared with ERA Interim and GPCP at a monthly time step averaged over all Ethiopia is shown in Figure 4a. Six month and 12 month running means are shown in Figure 4b. The three time series show broad agreement in terms of the overall pattern. However, as with the Uganda validation experiment in Figure 2, the model values are significantly higher and their variability is greater than the satellite estimates. It appears that ERA-Interim strongly overestimates dry season rainfall. GPCP and TAMSAT agree fairly closely from 1988 to the present but there is a decreasing trend in GPCP pre-1987 which is not present in TAMSAT. The different agreement before and after 1987 could be related to the change in the GPCP algorithm in this year (Adler et al. 2003).

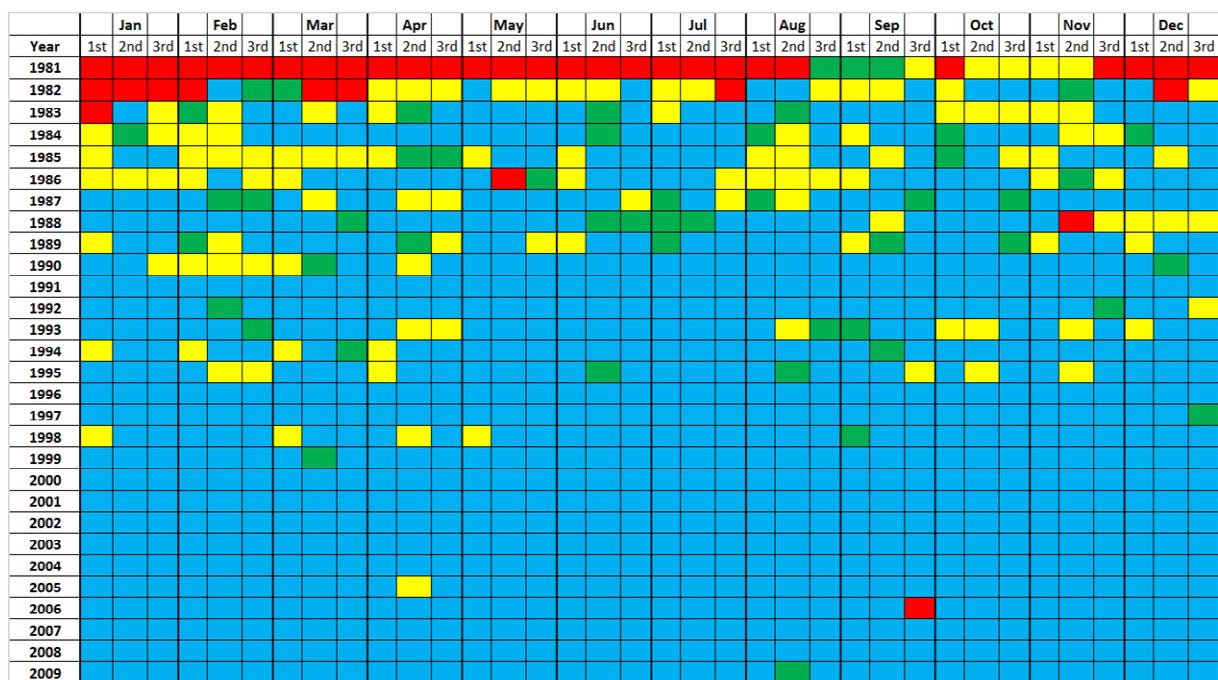


Figure 3. TIR data availability for all dekads from 1981 to present. Each cell is one dekad. Colour indicates number of missing hours in the dekad: blue < 3; 3 < green < 5; 5 < yellow <30; red > 30.

5. CONCLUSION AND FUTURE WORK

Analysis of rainfall climate in Africa requires a temporally homogeneous rainfall time series so that long-term trends can be evaluated and model performance in predicting future trends can be assessed. Currently available time series are either too short or temporally inhomogeneous. Because the TAMSAT algorithm is temporally homogeneous and requires only TIR data from the Meteosat satellite, it is being used to generate a rainfall time series for Africa (TARCAT) from 1982 to the present. Although the algorithm is very simple, validation experiments in different parts of Africa indicate that it is as good as other, more complex algorithms and is more consistent than these algorithms over different regions.

We expect to produce a preliminary version of the rainfall data set for the whole of Africa from 1982 to the present by the end of 2011. Tests on the long-term stability of the rainfall calibration will be carried out using currently available gauge data from the TAMSAT archive. We intend to carry out further detailed calibration and validation experiments in collaboration with African NMAs. One such workshop was held in Ethiopia in December 2010, a second for East Africa will be held in Uganda 2011. We are currently seeking funding for other workshops.

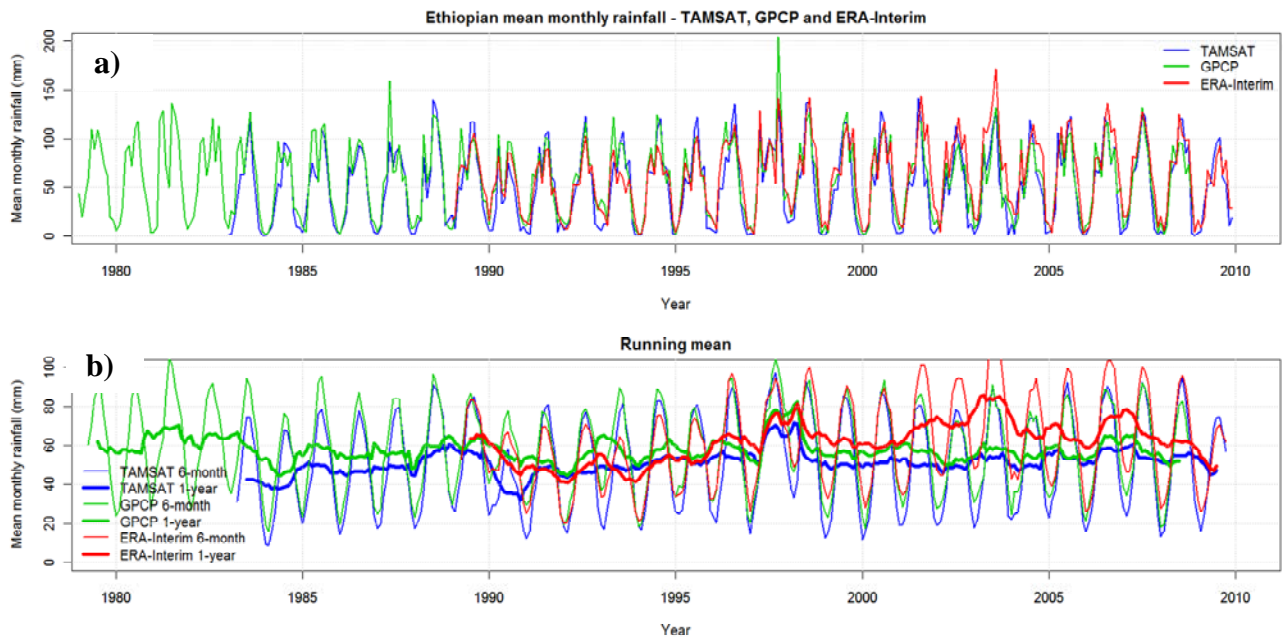


Figure 4. a) Time series of monthly rainfall for Ethiopia. b) Time series for 6 and 12 month running means.

Acknowledgements

The authors are grateful to the National Meteorological Services of Ethiopia and Uganda and the International Research Institute at Columbia University for their collaboration and provision of raingauge data for this study.

The European Commission JRC funded the Ugandan validation. The Ethiopian calibration workshop was funded by Google.org. The 2011 Ugandan workshop will be funded by the UK Natural Environmental Research Council

References

Adler, R.F., Huffman, G.J., Chang, A., Ferraro, R., Ping-Ping, X., Janowiak, J., Rudolf R., Schneider, U., Curtis, S., Bolvin, D., Gruber, A., Susskind J., Arkin P., Nelkin, E., 2003: The version-2 global precipitation climatology project (GPCP) monthly precipitation analysis (1979-present). *Journal of Hydrometeorology* Volume: 4 Issue: 6, 1147-1167.

Dinku, T, Ceccato, P, Grover-Kopec, E.; Lemma, M., Connor. S.J.; Ropelewsk C.F., 2007: Validation of satellite rainfall products over East Africa's complex topography. *Int. J. Rem. Sensing*, 28(7), 1503-1526.

Jobard, I.M., Chopin, F., Berges, J.C., Ali, A., Lebel, T., Desbois, M., 2007: Presentation of the EPSAT-SG method and comparison with other satellite precipitation estimations in the frame of Precip-AMMA *EGU Vienna 15-20 April 2007*.

Joyce, R.J., Janowiak, J.E., Arkin, P.A., Xie, P., 2004: CMORPH: A method that produces Global Precipitation Estimates from Passive Microwave and Intra-Red Sorooshian, S., Hsu, K-L., Gao, X., Gupta, H.V., Imam, B. and Braithwaite, D.: 2000, Evaluation of PERSIANN System Satellite-based Estimates of Tropical Rain. *Bull. Am. Met. Soc*, Vol 81, No 9, 2035-2046.

Thorne, V., Coakley, P., Grimes, D.I.F. & Dugdale, G., 2001: Comparison of TAMSAT and CPC rainfall estimates with rainfall, for southern Africa. *Int. J.Remote Sensing*, 2001, Vol 22, No.10, pp1951-1974.

Washington R., Harrison M., Conway D., Black E.C.L., Challinor A.J., Grimes D.I.F., Jones R., Morse A., Todd M., 2006: African Climate -taking the shorter route. *Bull. Amer. Met. Soc.* 87, 10, 1355-1366.

Xie, P. Arkin, P.A., 1996: Analysis of global monthly precipitation using gauge observations, satellite estimates and numerical model predictions. *Journal of Climate*, 9: 840-858.

PERFORMANCE OF TRMM LEVEL 2 AND 3 RAINFALL RETRIEVALS IN THE COMPLEX TERRAIN OF SOUTH ASIA

Stephen W. Nesbitt and Kimberly A. Reed

Department of Atmospheric Sciences. University of Illinois at Urbana-
Champaign, USA

e-mail: snesebitt@illinois.edu

With an eye towards Global Precipitation Mission algorithm improvement, we will examine the performance of the Tropical Rainfall Measuring Mission (TRMM) level 2 and level 3 algorithms in the complex terrain of South Asia. In this region, a diverse set of precipitation systems occurs, from winter cyclones near the Himalayas, to summer monsoon shallow and deep convection and stratiform rain near and apart from terrain over the Himalayas and coastal and interior ranges from India into southeast Asia. The precipitation radar aboard TRMM offers a unique perspective as to the vertical structure of the precipitation (apart from its own retrieval issues, several of which we have identified) that can put microwave-based retrievals in context with instantaneous and climatological measurements from rain gauges. We have established a 16-site rain gauge network in the Western Ghats, with data beginning in mid-2008; in this presentation comparisons of instantaneous rain rate measurements from radar and passive microwave sensors will be compared with results from our network. We will also statistically compare level 2 and 3 monthly and longer time scale measurements from the high-resolution APHRODITE 0.05° product developed by the Japanese Research Institute for Humanity and Nature (RIHN) and the Meteorological Research Institute of Japan Meteorological Agency (MRI/JMA) to examine the bias and random error characteristics of TRMM level 2 and 3 algorithms. Preliminary results show, somewhat unsurprisingly, that microwave sensors severely underestimate precipitation over sloped terrain, which is only adjusted for in level 3 algorithms by occasional PR overpasses and the gauge adjustment procedure in TRMM 3B42 v6. This leads to biases in daily rainfall that may lead to problematic inputs to land surface and hydrological models; a possible solution to this problem will be proposed.

ACTIVITY ON SATELLITE BASED PRECIPITATION IN KMA: CURRENT STATUS AND PLAN

Mi-Lim Ou¹, Ji-Hye Kim¹, Dohyeong Kim² and Jun-Dong Park²

¹ National Institute of Meteorological Research, KMA, Seoul, Republic of Korea

² National Meteorological Satellite Center, KMA, Jincheon, Republic of Korea

e-mail: milim@kma.go.kr

ABSTRACT

Precipitation measurements using passive and active microwave sensors provide vital environmental information for both scientific and societal applications. It has given emphasizing to use space-borne microwave remote sensors to improve the monitoring severe weather and precipitation forecast. Followed by success of the Tropical Rainfall Measurement Mission (TRMM), core satellite of the Global Precipitation Measurement (GPM) is scheduled to launch in July 2013 with follow-on constellation satellite afterward to improve prediction of weather and climate through accurate, precise, and frequent measurement of precipitation over the globe.

Korea Meteorological Administration (KMA) retains dense surface observation network including surface rain gauges, ground-based radars, and intensive observation sites. It will give an excellent environment for GPM ground validation (GV) over Korean peninsula.

During the GPM pre-launch stage, GV prototypes will be used to develop and test the GPM precipitation retrieval algorithms by using TRMM data. KMA collaborates with GPM Measuring Mission (PMM) Office in NASA/GSFC, USA on research of GPM GV using TRMM and ground-based observations. It starts with direct reflectivity comparisons between TRMM Precipitation Radar (PR) and ground-based S-band radars over Korea. To perform the comparisons, four ground-based S-band radars that are overlapped with the TRMM overpasses have been selected during August 2006 to May 2008.

In June 2010, the first geostationary satellite with a meteorological mission, called COMS was launched. The meteorological mission for COMS is for continuous monitoring of weather phenomena and utilizing for climate change and atmospheric environment monitoring over the East Asia and Western Pacific regions as a component of Global Observing System (GOS) by WMO. In this study, some information is briefly described for current status of COMS and plan for L2 and L3 products.

1. COMMUNICATION, OCEAN, AND METEOROLOGICAL SATELLITE (COMS)

1.1 Overview

The COMS is the first geostationary satellite in Korea with three payloads. The basic information for COMS is listed in Table 1.

Table 1: Overview of COMS

Information	
Orbital Location	128.2 E
Lifetime	7 Years
Spacecraft Stabilization	3-axis
Station-keeping Accuracy	± 0.05 in Lon/Lat
Payloads	Meteorological Imager (MI, 5 channel) Geostationary Ocean Color Imager (GOCI, 8 channel, VIS & NIR) Communication
Data Distribution	HRIT/LRIT

There are three missions for COMS such as meteorological observation by MI, ocean monitoring by GOCI, and in-orbit verification of the communication payload. KMA is responsible for MI operation and user services.

The COMS has been launched on 27 June 2010 at Kourou, French Guiana and will be in operation during the 2nd quarter in 2011.

1.2 COMS Products for Meteorological Applications

There are 16 baseline products developed as level 2 data for COMS. The products were previously tested with MTSAT-1R data, and will be tuned after in-orbit test with the COMS observation data. Then, the final day-1 products will be determined for user service. Figure 1 shows the flow of the COMS products. The 16 products are processed in an integrated system which includes pre-processing, product retrievals, post-processing, and validation, called COMS Data Processing System (CMDPS). COMS is one component of the space-based global observation system by WMO as a backup satellite over Asia-Pacific region and 2.2 billion potential users of 30 countries are expected for the region.

The National Meteorological Satellite Center (NMSC) which is responsible for the MI operation on COMS has a plan to produce satellite based precipitation information. The overall plan is described in Figure 2. The automated satellite processing system at NMSC consists of a rapidly developing thunderstorm detection system (RDT) based on the nowcasting software package from the NWC SAF of EUMETSAT, a convective rain rate retrieval system (CRR), and 3-hr rain rate estimation based on the hydro-estimator

of NOAA/NESDIS. The system will be upgraded by merging the COMS data with other satellite data such as MTSAT, Terra, Aqua and in-situ observations. The COMS L2/L3 products will be officially distributed during 1st half of 2011.

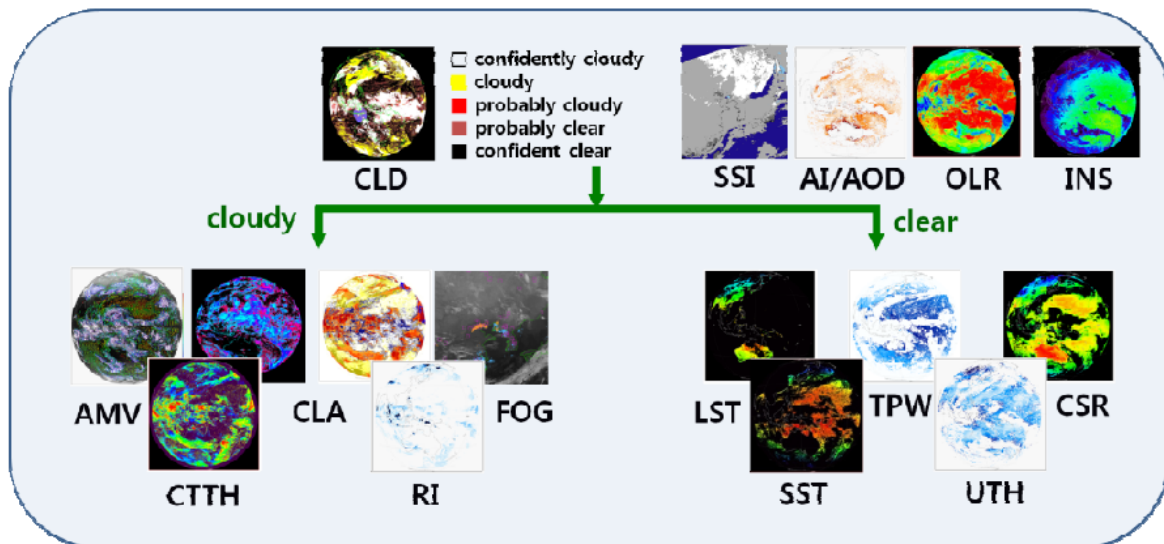


Figure 1: The 16 baseline products for COMS

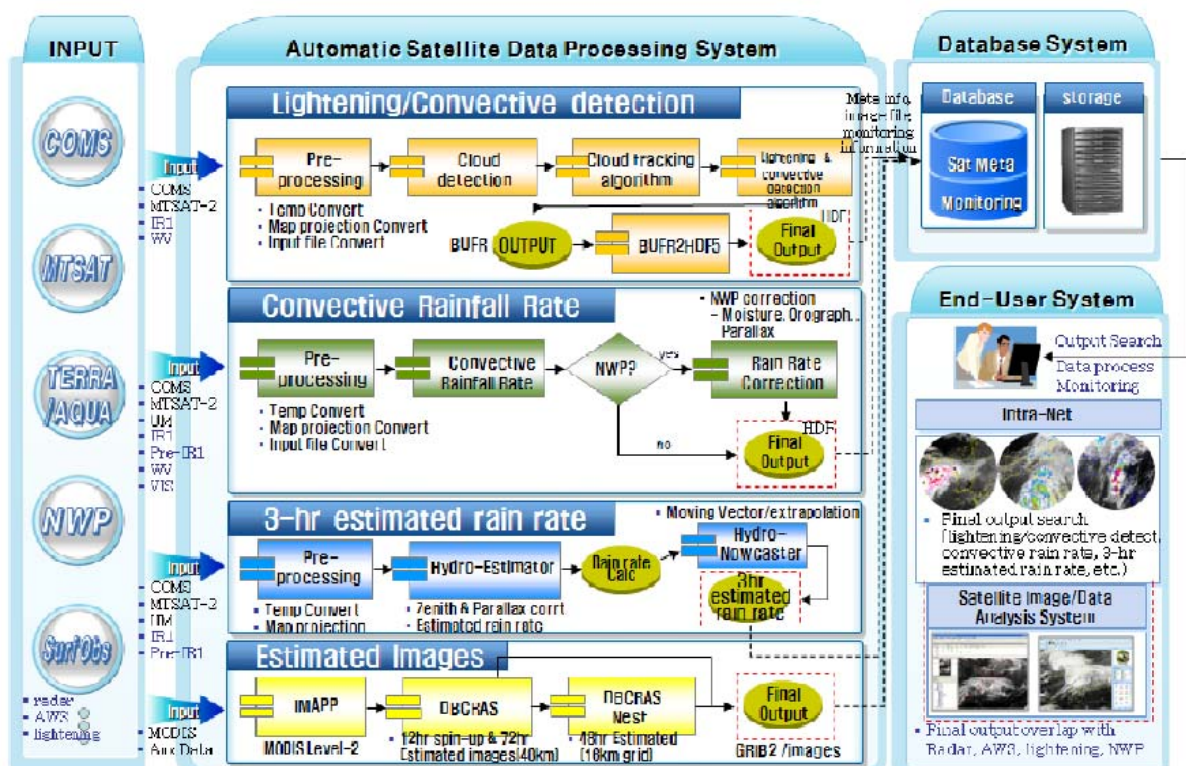


Figure 2: Automated satellite data processing system in NMSC, KMA

2. GPM ACTIVITIES IN KOREA

2.1 Background

KMA retains dense surface observation networks including surface rain gauges, ground based radars, and intensive observation sites, which give an excellent environment for GPM ground validation (GV) over Korean peninsula. Starting with preliminary study in 2003 regarding “Feasibility Study on Maximizing the Benefits from GPM Project”, KMA has officially participated in the GPM program with “NASA GPM/PMM Joint Research for Algorithm Development, Calibration/Validation, and Scientific Research” in 2009. The recent research activities include the reflectivity comparisons for 4 KMA S-band radars with TRMM/PR, the rain rate comparisons among radar, AWS, TRMM PR and TMI data.

2.2 Direct Validation over Korean Peninsula

KMA S-band radars located at Gosan (RGSN), Sungsan (RSSP), Jindo (RJNI), and Pusan (RPSN) are used for GPM direct validation over Korea peninsula. TRMM PR and S-band radar data have been re-sampled to 4 km horizontal grid on 3-dimensional uniform Cartesian grid for 100 x 100 km area centered on radar site and 1.5 km vertical grid from 1.5 to 19.5 km altitude. Each event has been selected by satisfying the criteria over 100 grid-points confirmed rain within the overlapped area for 100 km radius from each radar site. During August 2006 to May 2008, 60 to 110 events have been selected. PR reflectivity data of 18 dBZ or greater and ground-based radar reflectivity data of 15 dBz or greater were used. Figure 3 shows the location of the 4-KMA S-band radars within TRMM overpasses used for this study.

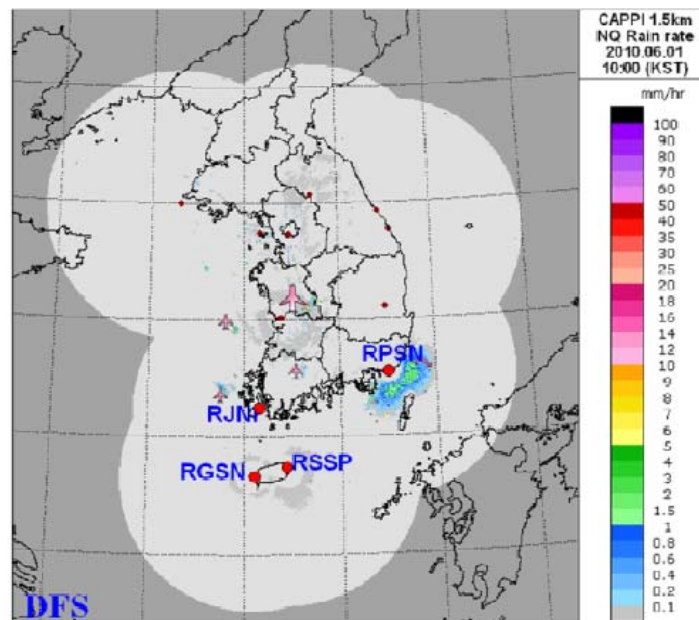


Figure 3. KMA S-band radars within TRMM overpasses for Jindo(RJNI), Pusan(RPSN), Gosan(RGSN), and Sungsanpo(RSSP).

Figure 4 shows the layer-averaged reflectivity between TRMM/PR and ground based S-band radars for 4 sites. In this figure, the S-band radar reflectivity shows low biases compared to the PR for about two year period except for Jindo site. The vertical structures of the layer-mean reflectivity are different according to the sites. Some of the reasons for the difference may be the calibration status of the ground based radars and number of sampling for each layer.

Figure 5 shows the mean dBZ difference for each site. The comparison has been performed for stratiform rain for the pixels within and above bright band height. The mean differences shows within ± 2 dBZ averaging for whole period, indicating that 4 S-band radars have been operated in good condition on calibration. It means that the KMA S-band radars can be considered as GPM GV radars. However, the reason for the peaks higher than 5 dBZ especially for Pusan and Jindo needs to be investigated further.

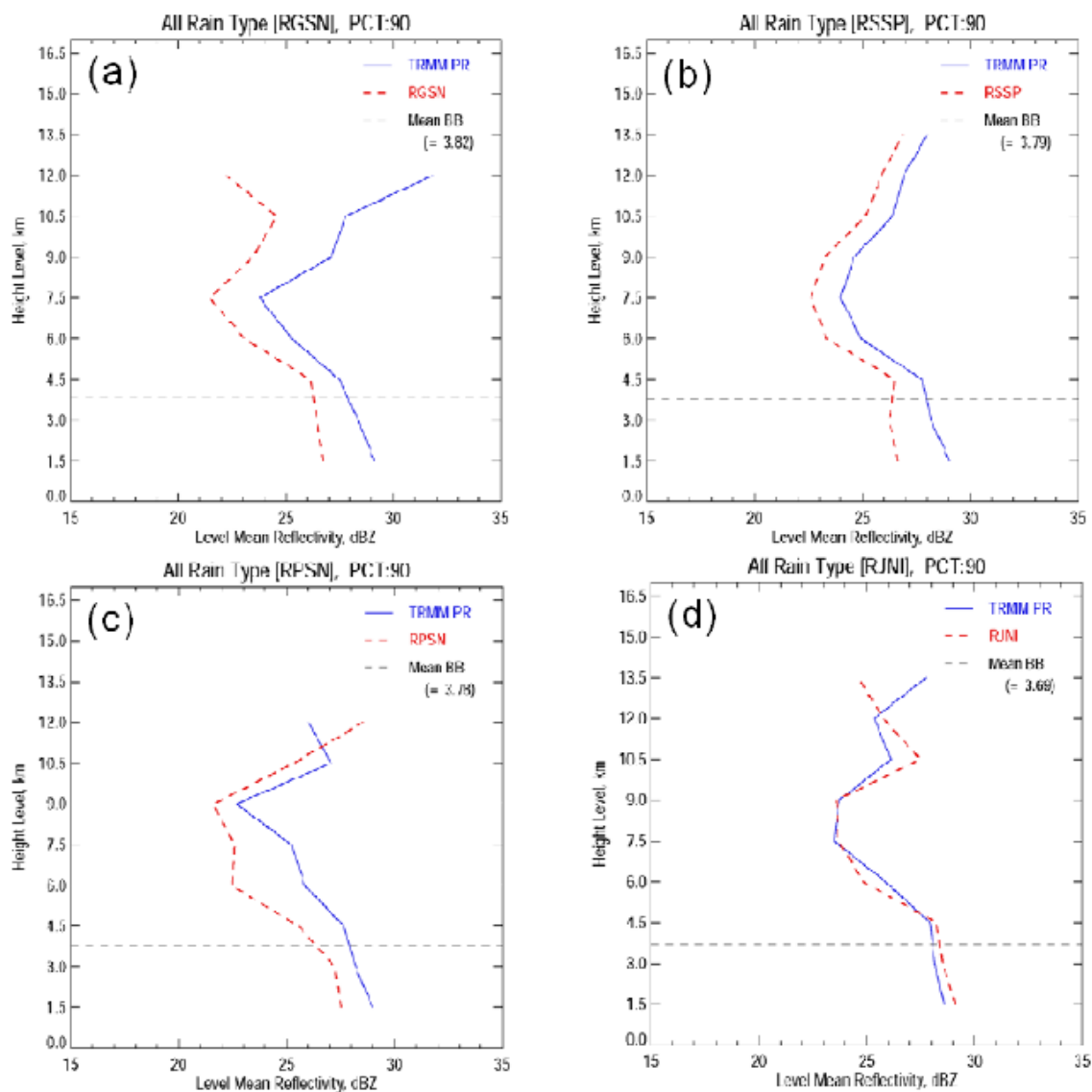


Figure 4. Layer-averaged reflectivity Gosan, (b) Sungsanpo, (c) Pusan, and (d) Jindo sites between KMA S-band radar and TRMM PR, for August 2006 to May 2008 of (a) 2008.

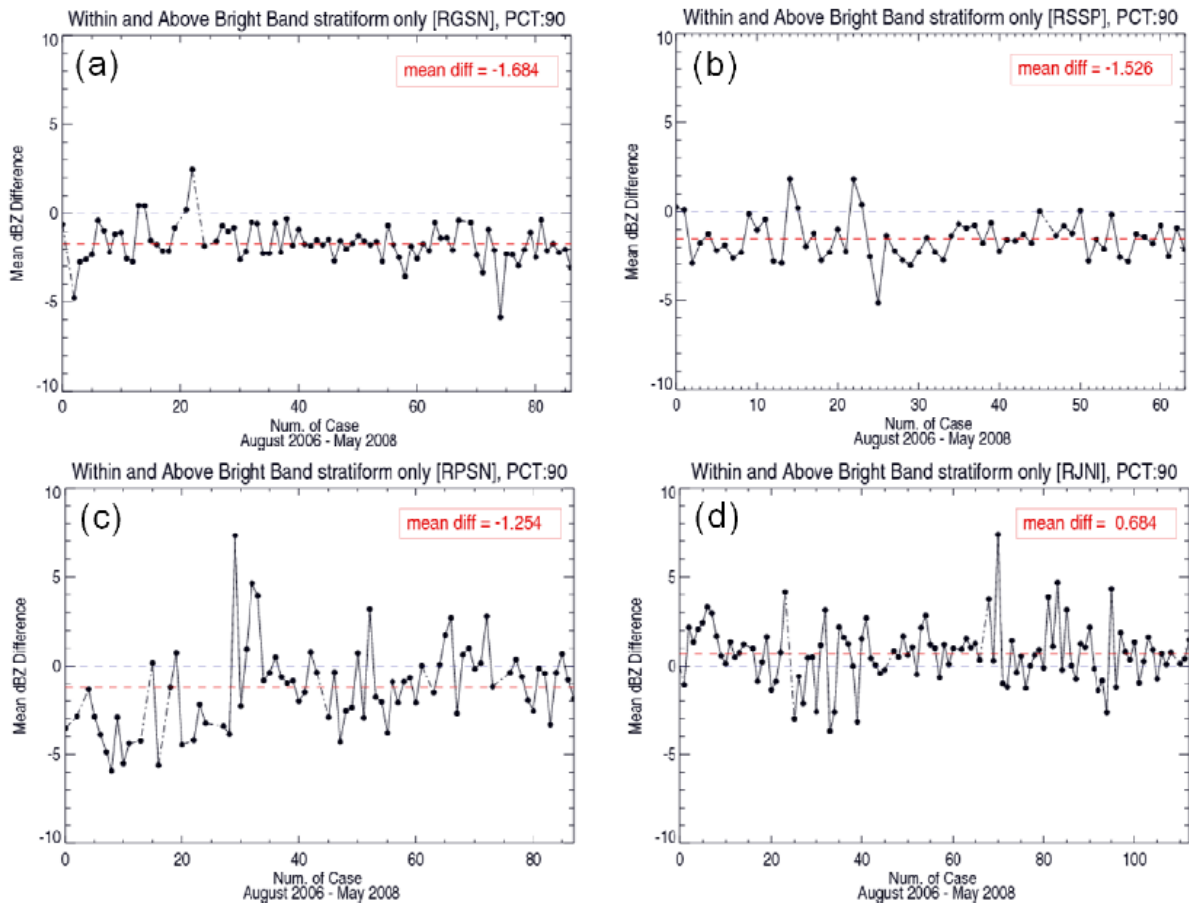


Figure 5: Same as Figure 4 except for mean dBZ differences.

2.3 Future Plan

KMA has cooperated with universities on GPM in the framework of Korean GPM Working Group (KGPM WG) initiated in Sep. 2010. The KGPM WG focuses on microwave rainfall algorithm, investigating regional characteristics of precipitating systems including snowfall over Korean peninsula, and microwave sensors, too. Before the GPM core satellite's launch, KMA will continue the direct validation by cooperating with various in-situ observations such as Micro Rain Radars, disdrometers, etc. And some important works will be performed to understand precipitation processes over Korean peninsula. KMA keeps working on the GPM ground validation activity as well as researches in the area of microwave sensor applications over Korean peninsula including satellite precipitation.

ACKNOWLEDGEMENT

This study was supported by "Research for the Meteorological Observation Technology and Its Application" of National Institute of Meteorological Research (NIMR) at KMA.

THE PRECIPITATION PRODUCT VALIDATION SERVICE DEFINED DURING THE DEVELOPMENT PHASE OF THE HYDROLOGICAL SAF

Silvia Puca¹, Eszter Labo², Bocena Lapeta³, Ján Kanák⁴, Thomas Maurer⁵, Ahmet Öztopal⁶, Federico Porcu⁷, Emmanuel Roulin⁸, Ibrahim Sonmez⁹

¹Italian Civil Protection Department

²Országos Meteorológiai Szolgálat-Távérzékelési Osztály-
Műholdmeteorológiai Kutató

³Satellite Research Department, Institute of Meteorology and Water
Management,

⁴Slovak Hydrometeorological Institute,

⁵Federal Institute of Hydrology (BfG),

⁶Istanbul Technical University, Meteorology Department,

⁷Universita' di Ferrara - Dipartimento di Fisica,

⁸Risk Analysis and Sustainable Development Section-Meteorological
Research and Development,

⁹Turkish State Meteorological Service

email: silvia.puca@protezionecivile.it

The development phase (2005- 2010) of the Hydrological Satellite Application Facilities (H-SAF) was closed the 31st of August of this year. Several precipitation products with different time and spatial resolution have been developed into the H-SAF project. The precipitation retrieval methods developed into the project use geostationary and polar satellite data with different instruments as AMSU-MHS, SSM/I-SSMIS and SEVIRI. During the development phase a Precipitation Product Validation (PPV) Service has been realized in order to give support to end-users and precipitation product developers. The H-SAF PPV group is composed by experts from the National Meteorological and Hydrological Institutes of Belgium, Germany, Hungary, Italy, Poland, Slovakia and Turkey. Hydrologists, meteorologists and radar and rain gauge experts are involved in this activity. The validation activity consists of a common methodology and case studies analysis. The common validation methodology is based on comparison of satellite product with rain gauges and radar data. The error is calculated on multi categorical and continuous statistics evaluated on daily and seasonal bases. Coast/ sea/ land classification is considered in the validation exercises. The precipitation classes of the multi categorical statistics were defined following the hydrologist experiences. Each Institute in addition to the common validation methodology has developed a specific validation methodology for case studies only, based on its own knowledge and experience. The Institutes have decided whether to introduce also the use of lightning data, numerical weather prediction and nowcasting products for the analysis of specific case studies. The results obtained were discussed inside the validation group and with product developers by email and annual meeting, reported in the project documents and published in the H-SAF web page section dedicated to the validation.

The structure and the results of validation service defined during these 5 years of activities by the PPV group, will be here presented.

THE GLOBAL PRECIPITATION CLIMATOLOGY CENTRE (GPCC) HAS RELEASED IN DECEMBER 2010 ITS FULL DATA REANALYSIS VERSION 5, SERVING THE HYDRO-CLIMATOLOGY COMMUNITY

**Bruno Rudolf, Andreas Becker, Udo Schneider, Anja Meyer-Christoffer, Markus
Ziese**

Global Precipitation Climatology Centre

e-mail: gpcc.dwd.de

1. INTRODUCTION

Since 1989, the Global Precipitation Climatology Centre (GPCC) performs analyses of the global land-surface precipitation distribution. Meanwhile, the related data set has continuously grown in terms of its temporal coverage and the scope of data sources exploited. Moreover the analysis methodology has successively advanced. The GPCC constitutes a German contribution to the World Climate Research Programme (WCRP) and the Global Climate Observing System (GCOS) of the World Meteorological Organization (WMO). Plenty of use cases from customers of the GPCC data have been documented and published (Rubel and Kottek, 2010; Yatagai et al., 2009; Dinku et al., 2008; Gruber and Levizzani, 2008; Kaspar and Cubasch, 2008, Wild et al., 2008; Kottek and Rubel, 2007, Rajeevan et al., 2005).

Core source of the GPCC analysis are the observed data from networks operated by the national meteorological Services worldwide. Due to the high geo-temporal variability of precipitation events, even their global analysis requires a high density of the measurement data. The data set yielded is supposed to address a broad spectrum of requirements from manifold kinds of users. Therefore different products, tailored for each kind of user, have been designed, developed and implemented at the GPCC. In doing so, two products ('First Guess' and 'Monitoring Product') are delivered comparatively fast based on the limited data set of those measurements reported in near-real time mode, whereas other gridded analysis products are later derived from a much more comprehensive data set covering also a longer temporal range. For the latter products there is a trade off decision between data availability and temporal range to be taken. Usually the ultimate purpose of the product factors into this decision.

Since the ensemble of available observation data has substantially grown compared to the previous re-analysis issued in year 2008, the GPCC has put intensive efforts to accomplish the next update of the precipitation analysis and gridded data sets. Following an intense test phase and four iterations of gridding and outlier evaluation the new gridded data sets "GPCC Climatology 2010" (mean monthly precipitation) and "GPCC Full Data Reanalysis Version 5" (time series 1901-2009) were put out in December 2010.

2. FEATURES OF THE NEW RELEASE

The available data of all stations featuring at least an observation period of 10 years are taken into account for the new 'Full Data Reanalysis'. Therefore its data availability (Figure 1) is not only time dependent but varies also for each grid cell in order to provide for the best possible area precipitation, serving an optimum basis for regional climate mapping or hydrological budget studies.

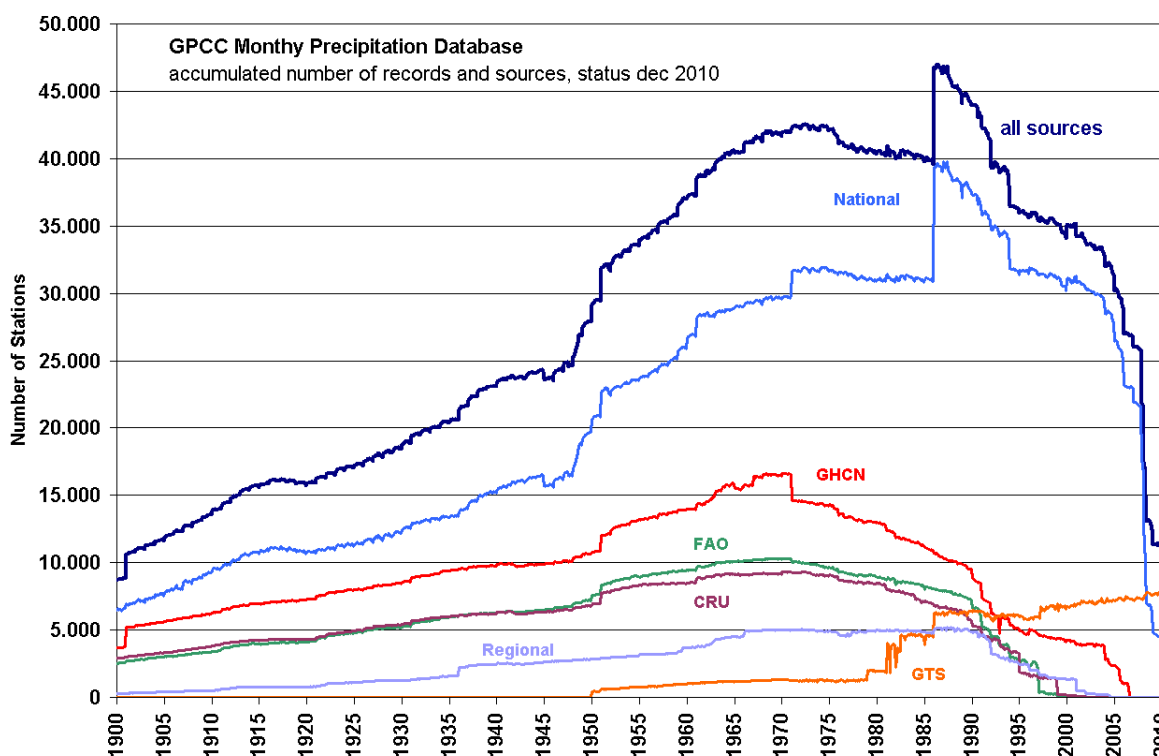


Figure 1. Temporal course of precipitation data availability for the different data sources and the resulting total ensemble (assigned 'GPCC Full Data' in the plot).

Meanwhile the GPCC data set comprises observed monthly totals from more than 80,000 stations worldwide, but only 64,400 stations (see Figure 2 for their global distribution) satisfy the above mentioned 10 years limit so their data series are long enough to derive temporal averages and climate parameters, respectively, and to produce charts of gridded averages. For the monthly analysis of the gridded precipitation anomalies these maps of the 'GPCC Climatology 2010' provide for the background values, during the monthly analysis of the gridded precipitation anomalies.

With access to a GPCC product of any single month, the user is automatically provided with grid cell specific information in addition to the precipitation values alike the number of stations and additional parameters suitable to access the reliability of the gridded precipitation data.

For the aforementioned reasons the 'Full Data Reanalysis' does not comply with the requirements on temporal data homogeneity as applicable for trend analysis studies. Therefore this product is not foreseen to serve climate change studies. To serve for this important use case a new accordingly homogenised product is in preparation at the GPCC. It shall be published in the near future and will cover a new period of more than

50 years from 1951 to 2005. To generate this homogenised data set, the full data ensemble is reviewed to identify those stations with long data series. These series are subsequently subdued to a rigorous test for homogeneity. Based on the data series passing the homogeneity test, parameters on the global distribution of the temporal change of precipitation are calculated. Methodology and results shall be published in a peer-reviewed journal and become part of the 5th IPCC report.

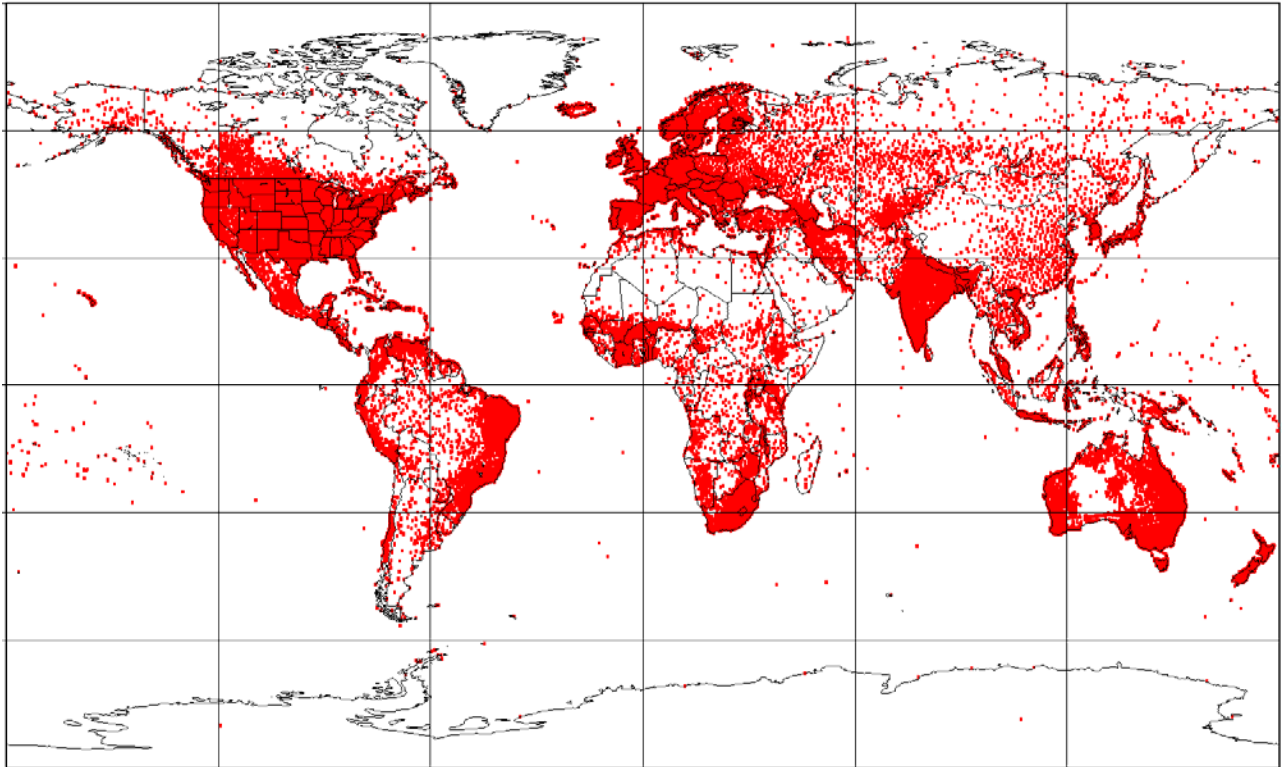


Figure 2. Locations of the globally distributed 64,400 stations featuring measurement periods longer than 10 years within the GPCC data base.

3. DATA SOURCES

The data supplies from the national weather services to the GPCC are regarded as primary data source. This data from 190 countries origins directly from the producer and constitutes the major compartment of the GPCC data base. Moreover the GPCC receives the daily SYNOP and the monthly climate (CLIMAT) messages while listening to the WMO GTS. To be comprehensive in its approach, the GPCC integrates also other global precipitation data collections from the Food and Agriculture Organisation (FAO), the Climate Research Unit (CRU) of the University of East Anglia, and the Global Historical Network (GHCN) as well as several regional data sets. As an example for the latter, the important data set from Nicholson (1979) was integrated recently to still become part of the new products. In total of these efforts the GPCC owns the worldwide largest and most comprehensive collection of precipitation data, which is continuously extended. However, it should be noted that in dependence of its source, data arrives sooner or later in comparison to its time reference.

4. DATA PROCESSING AND QUALITY CONTROL

The collected data are imported into a relational data base, where they are kept in separate source specific slots (Figure 3). This methodology allows for a source specific cross-comparison of the data. As none of the sources is error free, each source is allowed to provide for the reference information on a case-by-case basis. This is realized by a comparative analysis of data entries from different sources relevant for the same or neighbouring stations, the latter only in cases staying ambiguous if only the station itself is regarded. Typical errors identified during data import are factor 10, factor 2.54 or also factor 25.4 errors due to erroneous inch to mm conversions, shifts of the reference time, or geo-reference errors that had affected the data already before arrival at the GPCC. Any time new data is imported to the data base, an elaborated procedure is applied to compare the accompanying metadata of the belonging stations to the metadata already available for this station from the data base (Figure 4). In case of discrepancies (e.g. deviating coordinates), external geographical sources of information are utilized to decide whether a correction of the metadata information in the data base is required or not. Moreover the precipitation data to be imported is compared against a background statistic. Exceptional values are checked and either confirmed, if possible corrected, or excluded from the product. This approach requires a high level of human interaction, due to the complexity of the error analysis, which varies strongly from case to case in the absence of general valid screening criteria. Nevertheless, despite all corrections applied by the GPCC, a set of the original data is also kept, allowing backtracking of all corrections.

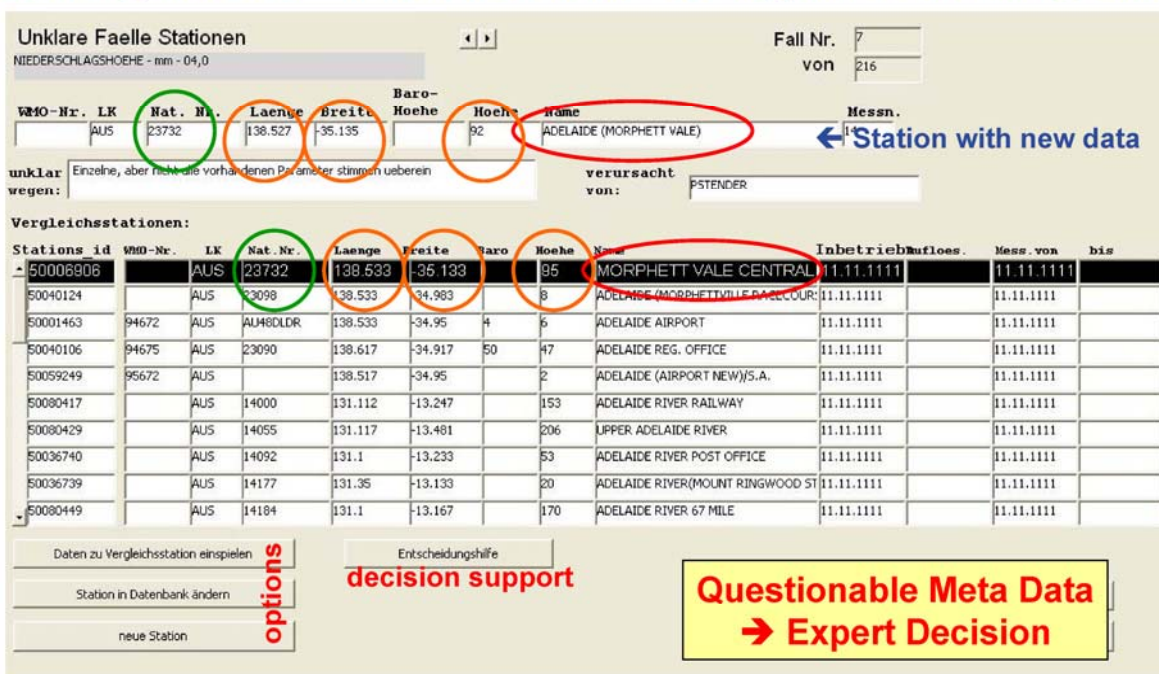
Data for analysis		Station - Meta Information						Precipitation Data separated for the data sources (Dec. 1995)							Dec.	
precip (mm)	selected source	GPCC ID	Name	Continent	long	lat	elev m NN	SYNOP (mm)	CLIMAT (mm)	CPC (mm)	Regio (mm)	National (mm)	CRU (mm)	GHCN (mm)	FAO (mm)	normals (mm)
9	National	50000100	Oslo-Blindern	Europe	10,717	59,950	96		9			9	9	9	9	54
28	National	50000092	Turku	Europe	22,267	60,517	59	30	28	29		28	28	28	28	64
60	SYNOP	50002750	Orleans	Europe	1,783	47,983	125	60		62						54
34	National	50000516	Alicante	Europe	5,333	35,333	460	37	34	13		34	34	34	34	34
73	National	50000406	Pescara	Europe	14,200	42,433	11	71				73				77
20	National	50000193	Poznan	Europe	16,850	52,417	92	21	20	21		20	20	20	20	38
21	National	50000477	Sivas	Europe	37,017	39,750	1285	23	21	22		21	21	21	21	47
6	SYNOP	50002287	Odense	Europe	10,333	55,467	17	6		8						
25	National	50002508	Sumy	Europe	34,783	50,850	181	26		24	25	25				53
156	National	50000365	Sarajevo	Europe	18,433	43,867	638					156		156		85
51	National	50000492	Cagliari	Europe	9,067	39,250	5	53	49	48		51		49	49	55
72	National	50002788	Kufstein	Europe	12,164	47,575	493	74		71		72				
103	National	50030955	Basel	Europe	7,593	47,533	317	104				103				54
71	National	50002770	Satu Mare	Europe	22,883	47,800	124	74		69		71				49
73	National	50000355	Bucuresti	Europe	26,100	44,417	83					73				46
55	National	50003217	Bari	Europe	16,783	41,133	49	58		55		55				65
66	National	50018829	Hull	Europe	-0,350	53,750	2					66	66	66		64
69	National	50002522	Beauvechain	Europe	4,767	50,750	127	69		60		69				
147	National	50025284	Kustendil	Europe	22,767	42,267	527					147				52
95	CLIMAT	50000548	Kalamata	Europe	22,017	37,067	8		95			117	95	95	95	154
64	CLIMAT	50035663	Bet Dagan	Europe	34,817	32,000	35		64				64	64	64	139
156	National	50019414	Kredarica	Europe	13,850	46,383	2515	169	156	155		156				120

Figure 3. Snapshot of the graphical user interface showing an example of source specific data import and archival.

5. SPATIAL INTERPOLATION

As was true for the 2008 data re-analysis ('Full Data Reanalysis Version 4'), also the new GPCC data gridding method applies the spatial interpolation on the gridded anomalies which are subsequently added to the gridded global background. For versions prior to Version 4, this methodology was not feasible, as there were too few stations with sufficiently long data series to form a reliable gridded global background. However, since the GPCC owns a sufficient number of stations providing climatic mean monthly precipitation totals, it is possible to interpolate them prior to the interpolation of the monthly data sets, to provide for the global background field. As before, we have applied the SPHEREMAP method for the interpolation (Wilmott et al., 1985). For comparison we have also applied the 'Ordinary Kriging' method (Krige, 1951).

Loading new data – check station meta data against the existing data



Unklare Faelle Stationen

NIEDERSCHLAGSHOEHE - mm - 04,0

Fall Nr. 7
von 216

WMO-Nr. LK Nat. Nr. Laenge Breite Baro-Hoehe Name Messn.

AUS 23732 138.527 -35.135 92 ADELAIDE (MORPHETT VALE) ← Station with new data

unklar wegen: Einzelne, aber nicht alle vorhandenen Parameter stimmen ueberein

verursacht von: PSTENDER

Vergleichsstationen:

Stations_id	WMO-Nr.	LK	Nat. Nr.	Laenge	Breite	Baro	Hoehe	Name	Inbetrieb	Abfloes.	Mess. von	bis
50006906		AUS	23732	138.533	-35.133		95	MORPHETT VALE CENTRAL	11.11.1111		11.11.1111	
50040124		AUS	23098	138.533	-34.963		8	ADELAIDE (MORPHETTVILLE BASE COUR	11.11.1111		11.11.1111	
50001463	94672	AUS	AUM8DLDR	138.533	-34.95	4	6	ADELAIDE AIRPORT	11.11.1111		11.11.1111	
50040106	94675	AUS	23090	138.617	-34.917	50	47	ADELAIDE REG. OFFICE	11.11.1111		11.11.1111	
50059249	95672	AUS		138.517	-34.95		2	ADELAIDE (AIRPORT NEW)/S.A.	11.11.1111		11.11.1111	
50080417		AUS	14000	131.112	-13.247		153	ADELAIDE RIVER RAILWAY	11.11.1111		11.11.1111	
50080429		AUS	14055	131.117	-13.481		206	UPPER ADELAIDE RIVER	11.11.1111		11.11.1111	
50036740		AUS	14092	131.1	-13.233		53	ADELAIDE RIVER POST OFFICE	11.11.1111		11.11.1111	
50036739		AUS	14177	131.35	-13.133		20	ADELAIDE RIVER(MOUNT RINGWOOD ST	11.11.1111		11.11.1111	
50080449		AUS	14184	131.1	-13.167		170	ADELAIDE RIVER 67 MILE	11.11.1111		11.11.1111	

stations in the data base

Daten zu Vergleichsstation einspielen

Station in Datenbank ändern

neue Station

options

Entscheidungshilfe

decision support

Questionable Meta Data
→ Expert Decision

Figure 4. Snapshot of the graphical user interface (GUI) covering the calibration of meta data from a new station (top line on GUI) against similar data already available in the GPCC data base. The meta data parameters checked in this example, are indicated.

6. SCHEDULED GPCC PRODUCTS

There are two scheduled GPCC products, the 'First Guess' and the 'Monitoring Product'.

The 'First Guess' product comprises an analysis of the monthly total precipitation at 1° - horizontal resolution. The data for this product is solely recruited from the SYNOP messages, that are available in 'near real-time', so it is available in due course for a comparatively fast (normally 3 to 5 days after the end of the observation period regarded) generation of the analysis. For this product only an automated quality control procedure is applied. If a temporal coverage of 70% of the month regarded is reached, the precipitation total is calculated and extrapolated to the total length of the month. For

this method approximately 6500 stations worldwide are available as data source. For these stations all information available from the SYNOP messages (temperature, humidity, wind, snow- and liquid water compartment of precipitation, level of systematic measurement error) are calculated according to a permanent schedule. All these parameters are also monthly aggregated and gridded. In the longer term it is planned to derive from the SYNOP data also daily global precipitation data sets and to provide them in a scheduled manner.

Compared to the 'First Guess' the data basis of the 'Monitoring Product' is extended by the climate messages (CLIMATs) and other data available reported at regular intervals through the GTS, so that 7-8 thousand stations are available for the analysis. The most recent monitoring products were based on more than 8100 stations. Moreover, there is a manual quality control performed by GPCC staff, on top of the automated quality control. With the supplementary data to the 'First Guess' product and the better quality of the data set yielded, the 'Monitoring Product' becomes available approximately two months after the end of the observation period regarded. The spatial resolution of this gridded data set is again 1°. For an example monthly monitoring product valid for February 2010, please refer to Figure 5.

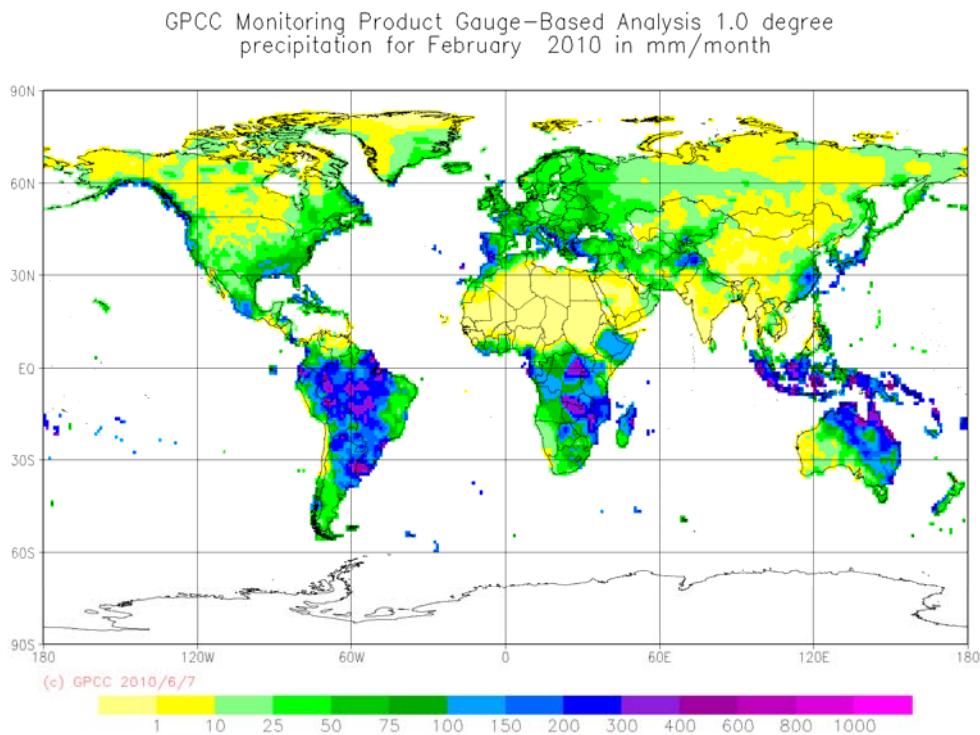


Figure 5. Example plot of a monthly gridded data product, as available from the GPCC web portal (<http://gpcc.dwd.de>)

7. POINTER TO THE GRIDDED GPCC DATA PRODUCTS

All GPCC gridded data products are available for download free of charge from the GPCC web portal (<http://gpcc.dwd.de>). Data has been made available in different spatial resolutions as described on the web page. It is also possible, to generate maps

of the data by means of the 'Visualizer' software, running also within the aforementioned web portal.

8. OUTLOOK

Along with the near future projects already described, the GPCC permanently aspires to extend its data basis. This is true for the continuously incoming new data but also with regard to the filling of gaps within the already existing data series. Moreover the quality control and analysis methodologies are developed further. Therefore, there will be new issues of the 'Full Data' and 'Precipitation Climatology' products released in intervals of two to three years. Figure 6 shows a true success story of the GPCC data base, namely its development in terms of the increasing number of precipitation gauge stations integrated until 2001 (Full Data Version 2), 2004 (Version 3), 2008 (Version 4) and 2010 (Version 5).

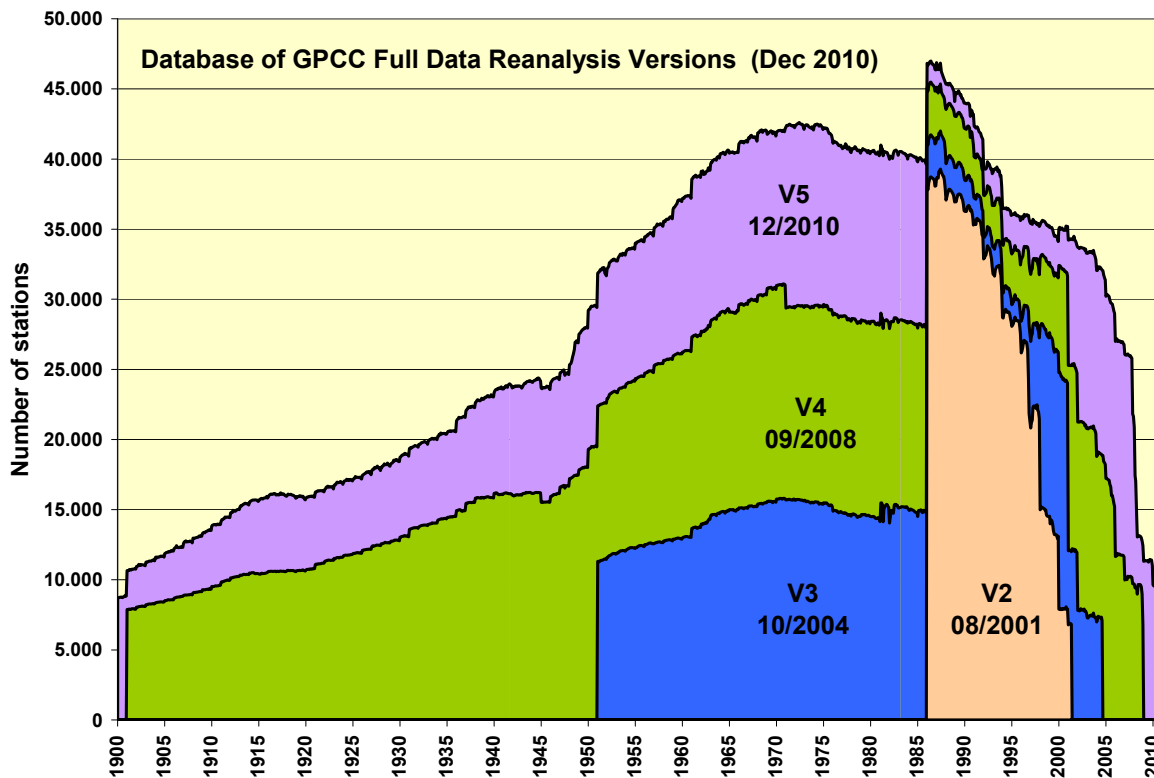


Figure 6. Development of the data base in terms of number of precipitation gauge stations integrated until 2001 (Version 2), 2004 (V3), 2008 (V4), and 2010 (V5).

9. GPCC Scientific Team

Udo Schneider, Anja Meyer-Christoffer, Markus Ziese, Andreas Becker, Bruno Rudolf

10. Acknowledgements

First of all we are most appreciative to the data suppliers that are to the largest extent the world wide spread National Meteorological and/or Hydrological Services but also some other institutes. Only their data puts GPCC into the position to provide the global precipitation analyses described in this document and we are looking forward to their further contributions that are crucial to maintain and enhance GPCCs level of products in terms of scope and quality.

We are grateful for the contribution of Dr. Hermann Österle, Potsdam Institute for Climate Impact (PIK), who has de facto served as beta tester of Versions 4 and 5 of the Full Data , while checking them for the existence of in-homogeneities. His work has substantially supported the quality control and improvement of the GPCC products.

11. References

- Dinku, T., S.J. Connor, P. Ceccato and C.F. Ropelewski, 2008: Comparison of global gridded precipitation products over a mountainous region of Africa, *Int. J. Climatol.* **28**, 1627–1638.
- Gruber, A. and V. Levizzani, 2008: *Assessment of Global Precipitation, A Project of the Global Energy and Water Cycle Experiment (GEWEX) Radiation Panel GEWEX, World Climate Research Program, WMO, WCRP Report, May 2008, WCRP-128, WMO/TD-No. 1430; p. 5*
- Nicholson, S.E., 1979: Revised rainfall series for the West African subtropics. *Mon. Wea. Rev.* **107**, 620-623.
- Kaspar, F. and U. Cubasch, 2008: Simulation of East African precipitation patterns. *Meteorol. Z.* **17**(4), 511-517.
- Kottek, M. and F. Rubel, 2007: Global daily precipitation field from bias-corrected rain gauge and satellite observations. Part I: Design and Development. *Meteorol. Z.* **16**(5), 525-539.
- Krige, D.G., 1951: A statistical approach to some basic mine valuation problems on the Witwatersrand. *J. of the Chem., Metal. and Mining Soc. of South Africa* **52**(6), 119–139.
- Rajeevan, M., J. Bhate, J.D. Kale, and B. Lal, 2005: *Development of a High Resolution Daily Gridded Rainfall Data for the Indian Region*. Met. Monograph Climatology No. 22/2005, 26pp., National Climate Centre, India Meteorological Department, Pune 411 005, India.
- Rubel and Kottek, 2010: Observed and projected climate shifts 1901-2100 depicted by world maps of the Köppen-Geiger climate classification. *Meteorol. Z.* **Fast Track**, DOI 10.1127/0941-2948-2010-0430
- Wild, M., J. Grieser, and C. Schär, 2008: Combined surface solar brightening and increasing greenhouse effect support recent intensification of the global land-based hydrological cycle, *Geophys. Res. Lett.* **35**, L17706.
- Willmott, C.J., C.M. Rowe and W.D. Philpot, 1985: Small-scale climate maps: A sensitivity analysis of some common assumptions associated with grid-point interpolation and contouring. *American Cartographer* **12**(1), 5-16.
- Yatagai, A., O. Arakawa, K. Kamiguchi, H. Kawamoto, M. I. Nodzu1 and A. Hamada. 2009: A 44-Year Daily Gridded Precipitation Dataset for Asia Based on a Dense Network of Rain Gauges, *SOLA* **5**, 137-140.

PERFORMANCE EVALUATION OF PRECIPITATION ESTIMATIONS OVER SOUTH-EASTERN SOUTH AMERICA CONSIDERING DIFFERENT CLIMATIC REGIONS

**Paola Salio^{1,2}, Daniel Vila³, Yanina Garcia Skabar^{4,5}, Maria Paula Houbouchian²
and Cynthia Matsudo⁴**

¹Department of Atmospheric and Oceanic Science, FCEN – UBA, Argentina

²Centre of Atmospheric and Oceanic Science, CONICET-UBA, Argentina

³Centro de Previsao de Tempo e Estudos Climáticos, INPE, Brazil

⁴National Weather Service, Argentina

⁵Cátedra de Fenología Agrícola, FA – UBA, Argentina

e-mail: salio@cima.fcen.uba.ar

Rain-producer systems are monitored from multiple precipitation platforms – radar and radiometers both from space and from the ground. From this information it is possible to obtain estimates of precipitation for various uses, agriculture, hydrology or the weather forecast, among others. A variety of sensors allowed obtaining reliable estimates of extreme precipitation on a monthly basis and mainly in inland areas considering that these estimations are calibrated with gauges observations. While there are important antecedents of the use of these calibration techniques on shorter time scales (daily precipitation, CoSch, Vila et al 2009, 3B42_V6, Huffman et al. 2007), the networks available for this calibration are very poor in the southeastern region of South America.

This paper evaluates the performance of the calibrated estimates of precipitation gauges (CoSch, 3B42_V6) and uncalibrated (CMORPH, 3B42_RT) on networks of high spatial resolution available in the area of southeastern South America during the period 2003-2009. These networks are not available in the Global Telecommunication System, so are not covered by any of the gauges calibrated estimates. Three networks are selected for this evaluation: RIAP, Salto Grande and San Luis. Each of them is related to a different climatic behavior. Salto Grande and RIAP have a mid-latitude temperate climate, but Salto Grande is strongly affected by mesoscale convective systems (MCSs) in its maximum rainfall phase, while the MCSs over RIAP are in their start-up without large amounts of precipitation. By contrast, San Luis is situated in a drier area with potential rainfall events but mainly to the presence of severe weather like hail. Although the networks are composed of several automatic stations, data are evaluated accumulating 24 hours.

Many statistics are calculated on the networks in order to evaluate the behavior of the precipitation estimates. BIAS score, FAD, POD and ETS, RMS and correlation coefficient, density probability functions are calculated for each of the seasons of year and during selected events of MCSs in order to understand the differences presented.

TOWARDS A CLIMATE DATA RECORD OF PRECIPITATION FROM SATELLITE MICROWAVE IMAGER DATA

Mathew R P Sapiano and Wesley Berg

Department of Atmospheric Science, Colorado State University, USA

e-mail: msapiano@atmos.colostate.edu

Existing long-term precipitation datasets such as the Global Precipitation Climatology Project (GPCP) rely heavily on satellite rainfall estimates from a constellation of microwave imagers that extend from the launch of the first Special Sensor Microwave/Imager (SSM/I) in July of 1987 up through the present. To develop a true long-term Climate Data Record (CDR) of precipitation, however, requires carefully intercalibrating the observed brightness temperatures, accounting for sensor differences by the retrieval algorithm in a physically consistent manner, and understanding uncertainties in the final products, particularly with regard to systematic errors. Differences between sensors, including channel frequencies, spatial resolution, viewing angle, and observation times, can lead to significant regional and/or time-dependent biases that can either mask or be mistaken for real climate variability or trends if not accounted for properly. Assumptions in the retrieval algorithm can similarly lead to systematic biases that can mimic or mask real climate signals. Recent activities associated with NASA's Global Precipitation Mission (GPM) and NOAA's efforts to create Climate Data Records of important geophysical parameters have led to significant improvements and insights related to both the intercalibration of satellite imager data as well as consistency in precipitation retrievals between sensors. Current activities include an effort funded by NOAA to create an intercalibrated fundamental CDR of brightness temperatures from SSM/I and SSMIS along with efforts by an intercalibration working group (i.e. XCAL) funded through NASA's Precipitation Measurement Missions (PMM). In addition, rainfall products from a major new release of the operational GPROF precipitation retrieval algorithm will be available shortly. This new retrieval algorithm was developed for GPM to provide more consistent precipitation estimates from the current and future constellations of microwave imagers. It uses a suite of sensor specific a-priori databases that were created using a combination of passive and active observations from the Tropical Rainfall Measuring Mission (TRMM) along with cloud resolving model (CRM) simulations. A summary of these activities along with their current status and ongoing challenges and issues related to the goal of creating a precipitation CDR will be discussed.

STATUS OF AND EARLY RESULTS FROM THE IPWG/WGNE MODEL PRECIPITATION INTERCOMPARISON

Mathew R P Sapiano

Colorado State University, Department of Atmospheric Science, Fort
Collins, CO, USA

e-mail: msapiano@atmos.colostate.edu

At the last IPWG meeting, a proposal was made to extend the Program to Evaluate High Resolution Precipitation Products (PEHRPP) to include short-range quantitative precipitation forecasts (QPFs) from numerical weather prediction (NWP) model forecasts, assimilations, and reanalyses. A collaboration between IPWG and the Working Group for Numerical Experimentation (WGNE) was established to provide access to these numerical precipitation estimates. I will give an update on progress and early results from this activity. I will also show preliminary results from my own validation of these operational model data. Previous work has shown that satellite and model estimates of precipitation have complimentary strengths and the aim of this work is to assess the information content of the models relative to satellite estimates with the goal of improving techniques for merging these data types. To that end, several QPFs have been compared to US radar data (Stage IV) and their relative skill in forecasting precipitation has been assessed. I will then look at the relationship with other model variables to see if these can be used to estimate the skill of the model at a particular time. Such relationships would be extremely useful for determining weights and errors of any merged products.

IMPROVEMENT OF GSMAP PASSIVE MICROWAVE IMAGER RAINFALL RETRIEVALS OVER THE MOUNTAINOUS AREA IN JAPAN

Shoichi Shige¹, Hiroki Ashiwake², Aina Taniguchi¹, Satoshi Kida¹, and Takuji Kubota³

¹Graduate School of Science, Kyoto University, Kyoto, Japan

²Department of Aerospace Engineering, Osaka Prefecture University,
Sakai, Japan

³Earth Observation Research Center, Japan Aerospace Exploration
Agency, Tsukuba, Japan

e-mail: shige@kugi.kyoto-u.ac.jp

Underestimation of passive microwave imager (MWI) algorithms has been found for orographic heavy rainfall over Japan. In this study, we improve the Global Satellite Mapping of Precipitation (GSMaP) MWI estimates over the mountain area in Japan. Shallow precipitation profiles observed by the Tropical Rainfall Measuring Mission (TRMM) precipitation radar for a case of orographic heavy rainfall are used to calculate look-up tables (LUTs). Then, the LUTs are applied for rain retrievals over areas with topographic forced upward motion and low-level moisture convergence, which are estimated from global analysis data with terrain height data. Revised estimates from TRMM microwave imager showed a better agreement with ground-based measurements and TRMM precipitation radar.

QUANTIFYING UNCERTAINTIES IN SATELLITE-BASED GLOBAL PRECIPITATION MEASUREMENTS

Y. Tian and C. D. Peters-Lidard

Earth System Science Interdisciplinary Center, University of Maryland,
College Park, Maryland, USA

Hydrological Sciences Branch, NASA Goddard Space Flight Center,
Greenbelt, Maryland, USA

e-mail: yudong.tian-1@nasa.gov

Determining the uncertainties in global precipitation measurements by satellite remote sensing is of fundamental importance to many applications. However, due to the lack of “ground-truth,” it is difficult to quantify the uncertainties in the satellite-based measurements on the global scale. In this work, we estimated these uncertainties by calculating the measurement spread from an ensemble of six different TRMM-era precipitation products (3B42, 3B42RT, CMORPH, PERSIANN, NRL and GSMaP). A global map of measurement uncertainties was thus produced. The map yields a global view of the error characteristics and their regional and seasonal variations, and reveals many undocumented error features over areas with no validation data available. The uncertainties are relatively small (40-60%) over the oceans, especially in the tropics, and over the lower-latitude South America. There are large uncertainties (100-140%) over high latitude (> 40-degree N/S), especially during the cold season. High uncertainties also persisted through the seasons over complex terrains, including the Tibetan Plateau, the Rockies and the Andes. Coastlines and water bodies also posed considerable challenges. The global uncertainties also exhibited systematic seasonal, regional as well as rain-rate dependencies, with lowest uncertainties over tropical oceanic regions with strong, convective precipitation, and highest ones over wintery, complex land surfaces with light precipitation. In particular, the southeastern U. S. also enjoys lower uncertainties. However, large uncertainties (100-140%) exist over high latitude (> 30N) land surfaces, especially during the cold season. Such areas include the northern U. S., most of Europe, and the Tibetan Plateau. The high uncertainties over the Tibetan Plateau also persist through the Northern Hemisphere warm season. In addition, high uncertainties (> 100%) are also associated with the Andes Mountains through all seasons.

VERTICAL PROFILING OF SNOW USING CLOUDSAT AND C-BAND GROUND RADAR

F. Joseph Turk¹, Kyungwon Park¹, Ziad Haddad¹, Peter Rodriguez², Dave Hudak²

¹Jet Propulsion Laboratory, California Institute of Technology, Pasadena, CA 91109

²Environment Canada, Toronto, Canada

e-mail: joseph.turk@jpl.nasa.gov

ABSTRACT

The CloudSat Precipitation Radar (CPR), launched in 2006, provides vertical profiles of W-band (94 GHz) reflectivity and is sensitive to falling snow through all but the most intense precipitating cloud structures. Precipitation retrievals of falling snow are affected by a wide diversity of factors describing the medium, such as snow particle shape, size and composition, which in turn are controlled by ambient factors including the environmental temperature and humidity. Information on snow particle medium gained from CloudSat or other radar observations can be used to model passive microwave signatures of snow events, which in the absence of radar can be estimated from radiometers such as the Advanced Microwave Humidity Sounder (AMSU) and the Special Sensor Microwave Imager Sounder (SSMIS). We examine the vertical structure of winter precipitation events from overpasses of CloudSat (94 GHz W-band radar) coordinated with the C-band (5 GHz) polarization-agile King City radar (WKR) operated by Environment Canada. These C/W-band dual-frequency radar observations are used to examine the radar and radiometric signatures of several winter storms. 2-D video disdrometer observations are used constrain the range of retrieved snow particle mass-weighted drop size distribution (DSD) parameters and associated water content. The constrained database produces snow profiles that replicate the observed radar reflectivity profiles and smoothly transition between the single and dual-frequency regions.

1. INTRODUCTION

The CloudSat Precipitation Radar (CPR), launched in April 2006, provides vertical profiles of the W-band (94 GHz) reflectivity through all but the most intense precipitating cloud structures (Liu, 2008a; Tanelli et. al, 2008). Recent investigations have examined various methods to estimate snowfall rates from passive microwave (PMW) observations between 89-190 GHz from the 5-channel Microwave Humidity Sounder (MHS) and the Special Sensor Microwave Imager Sounder (SSMIS) instruments (Noh

¹ This work was performed at the Jet Propulsion Laboratory, California Institute of Technology, under contract with the National Aeronautics and Space Administration. © 2011. All rights reserved.

et al., 2006; Skofronick-Jackson et al., 2004). In the future, the 65-degree orbit inclination of the Global Precipitation Mission (GPM) core satellite will provide dual-frequency (Ku/Ka band) radar observations of cold season precipitation, coincident with radiometric observations between 10-190 GHz. Combined algorithms utilize information from the inner-swath radar and radiometric observations to extend to the radiometer-only outer-swath region (Marzano et al., 2002). Typically, precipitation algorithms use a-priori databases to inform inversion algorithms about the characteristics of the physical medium, e.g., shapes of the particle types, composition and their size distribution. We examine several snowfall events which were well-sampled by multiple active/passive microwave and ground-based observations, to benefit the development of physically meaningful a-priori hydrometeor databases.

During winter months, the C-band (5 GHz) polarization-agile King City radar (WKR) operated by Environment Canada (EC) near Toronto provides coverage of falling snow events over portions of three of the Great Lakes (Huron, Erie and Ontario), and partially frozen lakes and snow cover, which are among the most challenging surfaces for passive microwave snowfall retrievals. In particular, Lake Erie is much shallower than Lake Ontario and therefore more likely to freeze over in winter than Lake Ontario, which typically freezes over near shorelines and bays. In the winter months, prevailing cold winds often produce long lasting lake effect snowstorms near and inland from their southern shorelines. The WKR radar was operated continuously during the Canadian CloudSat CALIPSO Validation Project (C3VP) (Peterson et al., 2007) which took place near Toronto, Canada between December 2006 and February 2007, and has since been continuously collecting data synchronized to CloudSat overpass times. CloudSat's 16-day repeat track provides coverage of precipitation events within the range of the EC radar network covering these Great Lakes areas (Figure 1). Hudak et al. (2008) used the EC C-band radar network to develop a CloudSat beam-matching technique for validation of the CloudSat precipitation occurrence (2B-CLDCLASS) product. With close enough time and space alignment, the WKR/CloudSat radar data form a unique set of dual frequency observations (C/W band), which provide a different range of sensitivity to frozen precipitation than W/Ka-band (Matrosov, 2007), or Ku/Ka-band observations (Greco et al., 2008). It is therefore relevant to examine dual-frequency snowfall retrievals from these C/W-band observations. Also, since the GPM core satellite will make frequent revisits within the EC radar scanning area, the triple-frequency (C/Ku/Ka) set of observations will be potentially useful for physical validation of GPM precipitation products.

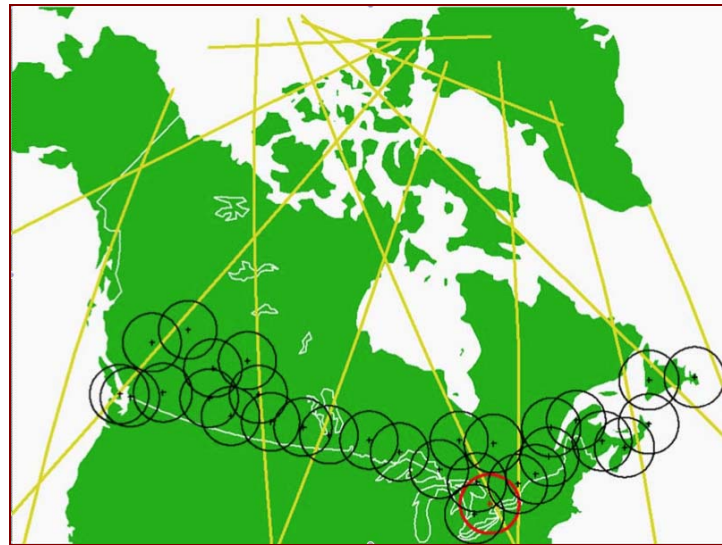


Figure 1. Location and 150-km range of the WKR radar (red circle) and other radars within Canada (black circles). Typical one-day overpass ground tracks of the CloudSat spacecraft are shown in yellow lines. Figure adapted from Hudak et al. (2008).

2. DATA COLLECTION

In order to facilitate the analysis methods described in the previous section, it was first necessary to locate time and space coordinated observations within the WKR scan coverage area. The times of all CloudSat overpasses passing within 100-km of the location of the WKR radar during the months of December, January and February (each year 2006 through 2010) were identified. We also coordinated the CloudSat overpasses with NOAA-18 overpasses, to examine the passive microwave signatures from MHS of these winter storms (not shown in this article). For each of these cases, a one-minute data segment (375 CloudSat profiles) centered upon the CloudSat overpass time was extracted from the ECMWF-AUX and 2B-GEOPROF products (available from the CloudSat Data Processing Center). Non-precipitating cases were discarded, identified when the 2B-GEOPROF cloud mask flag never exceeded a value of 20. Lastly, in order to filter melting snow events, precipitating cases where the vertical temperature profile exceeded -2 C (any level in the profile) were discarded. Since the overpasses of Aqua are within one minute of CloudSat, various products from AMSR-E, MODIS, and AIRS are available.

Figure 2 depicts the radar data from case 1. In Figure 2a, the reflectivity from the WKR CONVOL scan at 0740 UTC on 14 February 2007 (Case 1) is shown, which occurred during the C3VP experiment. Range rings at 40, 80, 120, 160, 200 and 240 km are overlaid in white. The white line indicates the CloudSat track near 0740 UTC (night time descending). For a large scale view, Figure 2b provides the associated MODIS channel 31 ($11 \mu\text{m}$) imagery. Widespread snow is evident with the main snow bands located to the south of WKR, oriented along Lake Erie, Lake Ontario, with lake effect snow in western New York state. In this case, CloudSat passed west of WKR,

over a portion of Georgian Bay, intersecting the strongest snow band just north of Lake Erie.

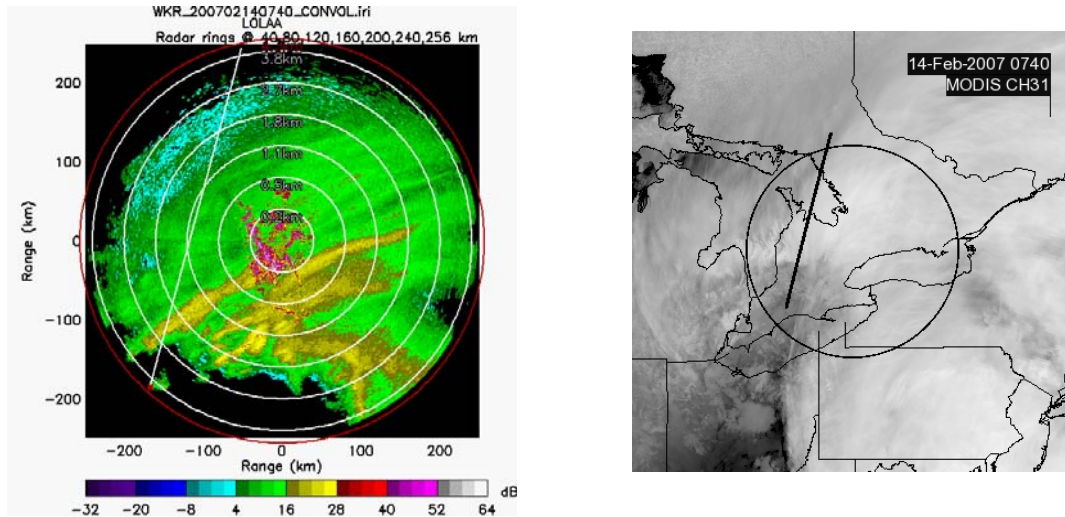


Figure 2. (a): Reflectivity from the WKR CONVOL scan at 0740 UTC on 14 February 2007 (Case 1). Range rings at 40, 80, 120, 160, 200 and 240 km are overlaid in white. The 0740 UTC CloudSat descending track is shown with the white line. (b): Associated MODIS channel 31 (longwave infrared) image.

3. RETRIEVAL FRAMEWORK

In order to invert the observed CloudSat radar profile into profiles of snow content and radar and radiative parameters, a multi-dimensional lookup table of candidate DSD solutions were generated offline using the database of ice crystal scattering properties developed by Liu (2008b). This database has been used by other studies (Skofronick-Jackson et al., 2011) and is briefly summarized here. This database provides electromagnetic properties needed for radar and plane-parallel radiative transfer modeling including backscatter, extinction and scattering cross sections ($\sigma_B, \sigma_{ext}, \sigma_{sca}$, respectively), the asymmetry factor g , and the phase function tabulated every five degrees in scattering angle, for eleven different snow crystal types. The crystal types used in this work are limited to dendrites, which best approximate the complex aggregates commonly noted in near-surface winter precipitation (Brandes et al., 2007). For a wide range of variability of a gamma drop size distribution (DSD),

$$N(D) = N_0 D^\mu \exp(-\Lambda D) \quad \text{mm}^{-1} \cdot \text{m}^{-3} \quad (1)$$

the reflectivity factor Z , and extinction, scattering and asymmetry factors (k_{ext}, k_{sca}, g , respectively) were computed and tabulated in lookup tables (LUT). Alternatively, the slope of the DSD is expressed by the mean diameter D_m , where $D_m = (\mu + 4) / \Lambda$ (Ulbrich, 1983). Rather than express the lookup tables in terms of (N_0, Λ, μ) , each with

an associated $(q_s, Z, k_{ext}, k_{sca}, g)$, we varied the two parameters (D_m, μ) and tabulated each of the mass-weighted parameters as a function of snow water content q_s where

$$q_s = \frac{\pi \cdot 10^6}{6} \int \rho(D) D^3 N(D) dD \quad g \cdot m^{-3} \quad (2)$$

where $\rho(D)$ is the snow particle density in $g \cdot cm^{-3}$ as a function of the equivalent spherical particle diameter.

The retrieval methodology is a top-down attenuation correction approach, similar to other recent investigations (Noh et al., 2006). The observed CloudSat reflectivity profile (240-m bins extending to 20-km altitude), denoted by $Z_{94}^{obs}(z)$ at a given vertical level z , is attenuation-corrected bin by bin from the top down to the surface due to total accumulated 2-way path attenuation due to extinction from gases, cloud water and snow,

$$Z_{94}(z) = Z_{94}^{obs}(z) + 2 \int_{z+1}^{z_{top}} (k_{ext,g} + k_{ext,c} + k_{ext,s}) dz \quad mm^6 \cdot m^{-3} \quad (3)$$

At W-band, cloud liquid water scatters very little but can contribute to the overall path attenuation. It is known that frozen precipitation can be accompanied by the presence of supercooled cloud liquid water (Molthan et al., 2010; Shi et al., 2010), but there is no way to separate cloud and precipitation liquid from the single CloudSat measurement. Model studies suggest that supercooled water is most likely where $T > -15$ C, above this temperature supercooled water is depleted by a higher ice crystal concentration. The retrieval has an option to insert cloud water within individual CloudSat bins based upon a unitless cloud fraction f , defined as $f \equiv q_c / (q_s + q_c)$, where the total $q \equiv q_c + q_s$. For these cases, the expected amount of supercooled liquid water was expected to be minimal, therefore we left $f=0$ at all levels. In the discussion to follow, we will simply use q to denote snow equivalent water content, and k_{ext} to denote the extinction coefficient due to snow, unless otherwise noted.

In general, with only one frequency there are many candidates for (μ, D_m, q) , since there are many simulated values of Z_{94} that lie close to the (attenuation corrected) observed Z_{94} . Adding a second frequency places an additional constraint on the number of possible candidate solutions. However, this formulation weights candidate solutions by proximity in reflectivity space, and does not take into account any possible relationships that may exist amongst the DSD parameters themselves. However, in general for snow we have little a-priori knowledge of how to narrow down the combinations of expected DSD solutions. Aircraft-based dual-frequency snow retrievals at Ku/Ka-band (Grecu et al., 2008) use mesoscale cloud model simulations of winter storms to provide a wide set of candidate DSD profiles. This approach relies upon the reality of the cloud model simulation and its parameterizations of the hydrometeor size distributions. Molthan et al. (2010) examined assumptions and physical relationships for the snow category within the Goddard six-class, single-moment microphysics scheme implemented within

the Weather Research and Forecasting (WRF) model. Using spiral aircraft observations thru C3VP winter storms, they found that use of a fixed distribution intercept (N_0) in WRF did not represent the observed increase in N_0 with height, with a mean snow crystal size smaller than observed below 3-km (near -15 C) altitude.

4. ANALYSIS FROM 14 FEBRUARY 2007

The event on 14 February 2007 (case 1) is discussed since there are associated ground observations for comparison and subsequent analysis. The leftmost top panel (a) of Figure 3 depicts the vertical profile of the observed CloudSat 94 GHz reflectivity (2B-GEOPROF) associated with the overpass tracks in Figure 2, a one-minute (375 CloudSat beams) profile between 073932 to 074032 UTC on 14 February 2007. The overpass intersects the southern end of the main precipitation band near the end of this transect. Cloud tops are near 7-8 km. Figure 3b shows the associated 5-GHz WKR profile aligned with the CloudSat reflectivity curtain, constructed from the 0740 UTC plan position indicator (PPI) volume scan sequence (Hudak et al., 2008). Owing to the lowest radar elevation angle, the lower altitudes are not well covered the further from the radar, but the volume scan does capture much of the cloud top midway along the CloudSat transect. The nearest-neighbor alignment between the two radar beams leaves some artifacts, notably occasional missing 5-GHz profiles. However, as will be demonstrated below, for the purposes of this work it is not necessary to have the two radar observations for all beams and vertical levels.

a) *Unconstrained dual-frequency retrieval*

The dual-frequency retrieval algorithm described above was applied to the reflectivity profiles (Figures 3a and 3b) along the CloudSat overpass. In this section, we show only the Bayesian estimates of the DSD parameters, and not the associated range of variability (standard deviation). We assumed no prior information about the DSD, and the retrieval described above defaults to a single-frequency mode (94 GHz only) outside of intersecting WKR scan coverage. By design, the retrieval will give increasingly larger weights to the (μ, D_m, q) entries whose associated (Z_{94}, Z_5) lie closest in reflectivity space to the (2-way path attenuation corrected) observed (Z_{94}, Z_5) . Figure 3c and 3d show the values of \hat{Z}_{94} and \hat{Z}_5 , respectively. The observed and simulated 94 GHz reflectivity profiles match up in the single frequency area (first part of the transect) and lie within 2 dB of each other near the surface in the regions of heaviest precipitation. However, the retrieved 5 GHz profile is often 10 dB or more higher. For CloudSat beams where there is a missing 5-GHz profile the retrieval falls back to a single-frequency mode, however in these regions the retrieved 5-GHz reflectivity \hat{Z}_5 exhibits unrealistic abrupt discontinuities with adjacent profiles. Profiles of the equivalent water content q , mass-weighted mean diameter D_m , and gamma shape factor μ are shown in panels 6e, 6f, and 6g, respectively. q is unreasonably large (often $> 2 \text{ g m}^{-3}$) given these observed reflectivity values.

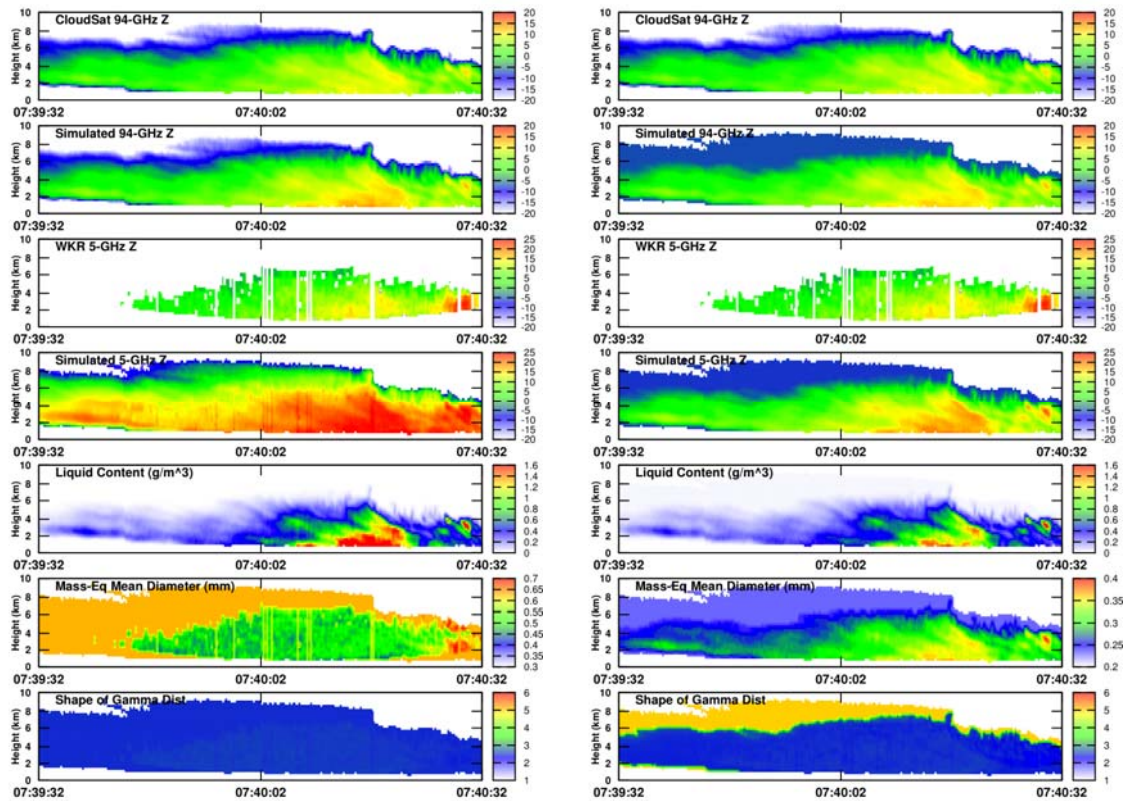


Figure 3. One-minute time-height cross section from the Case 1 CloudSat descending overpass on 14 February 2007 near 0740 UTC. **(Left panels)** From top to bottom: (a) Observed 94 GHz CloudSat reflectivity. (b) Observed WKR 5-GHz reflectivity profile reconstructed along the CloudSat curtain. Panels (c)-(g) show retrieved results from the unconstrained database. (c) Retrieved 94 GHz reflectivity profile. (d) Retrieved 5-GHz reflectivity profile. (e) Retrieved profile of equivalent liquid water content q_s in g m^{-3} . (f) Retrieved profile of mass-weighted mean particle diameter D_m in mm. (g) Retrieved profile of gamma distribution shape parameter μ in Eq. (1). **(Right panels)** Same as left side, but for retrievals done using the constrained database. The scale of D_m and q has been modified.

Typically, in winter storms snowflakes fall faster with higher bulk density as the particle size grows due to aggregation. Here the vertical profile of D_m exhibits unrealistic behavior, remaining vertically constant in the single-frequency region, and with a larger value (near 0.65 mm) at the top of the cloud than nearer to the surface (near 0.45 mm) in the dual frequency regions. The profile of μ remains constant throughout, near a value of 2.5. It is therefore worthwhile to examine whether some means to limit or omit possible candidate DSD solutions could be applied in order to bring observed and simulated reflectivity profiles into better agreement.

b) 2DVD observations from C3VP

Huang et. al. (2010) derived equivalent radar reflectivity factor-liquid equivalent snow rate (Z_e -SR) power-law relations using WKR radar data and coincident 2DVD

observations from C3VP. The 2DVD was located at the Center for Atmospheric Research Experiments (CARE) site situated approximately 30-km northwest of the WKR radar, where data were collected during C3VP for seven winter storms between 6 December 2006 and 14 February 2007. The 2DVD consists of two orthogonal line-scan imaging cameras separated vertically, which allows two views of the particle shape falling through a common measuring area, as well as the fall speed. The sampling frequency is fast enough to infer the DSD (Kruger and Krajewski, 2002), from which the mass-weighted mean diameter and mass content can be calculated using density-diameter relations (Huang et al., 2010). Figure 4a displays the time series of the drop size distribution from Case 1 (14 February 2007). The corresponding best-fit gamma distribution for the D_m, μ, N_0 parameters and associated q is shown in Figures 4b and 4c. While this is not a particularly strong snow event, there is a high variability in the retrieved DSD parameters as a function of snowfall intensity. In general μ varies between 1 and 4, and N_0 between 10^6 and 10^3 , with the smaller values occurring for larger values of q . Similar behavior was noted by Brandes et. al (2007) in a study of Colorado snowstorms sampled by a 2DVD between 2003 and 2005. Molthan et. al. (2010) also inferred a similar range and vertical profile of N_0 from spiral aircraft descents taken during the C3VP 22 January 2007 storm.

In Figure 5a, the scatterplot of $\log_{10}(D_m)$ versus $\log_{10}(q)$ is shown where each color indicates 2DVD data from seven different snow events between December 2006 and February 2007. These two quantities are highly correlated for all events with a slope of approximately 0.21, suggesting that D_m and q are not independent of each other. Figure 5b is similar to Figure 5a, except the vertical coordinate is now $D' = \log(D_m) + a \log(q)$, where $a = -0.21$. The values of D' range between $0.2 < D' < 1.3$, regardless of the value of q . This shows that there range of D' that can be specified independently of q , or more importantly, a range of D' that can be effectively disregarded in the retrieval process. In the next section, we repeat the profile retrievals of Section 4a using constraints on the values of D' found in the database. It should be noted that this result was derived from surface observations and that the range of D' may be different for higher levels within the cloud.

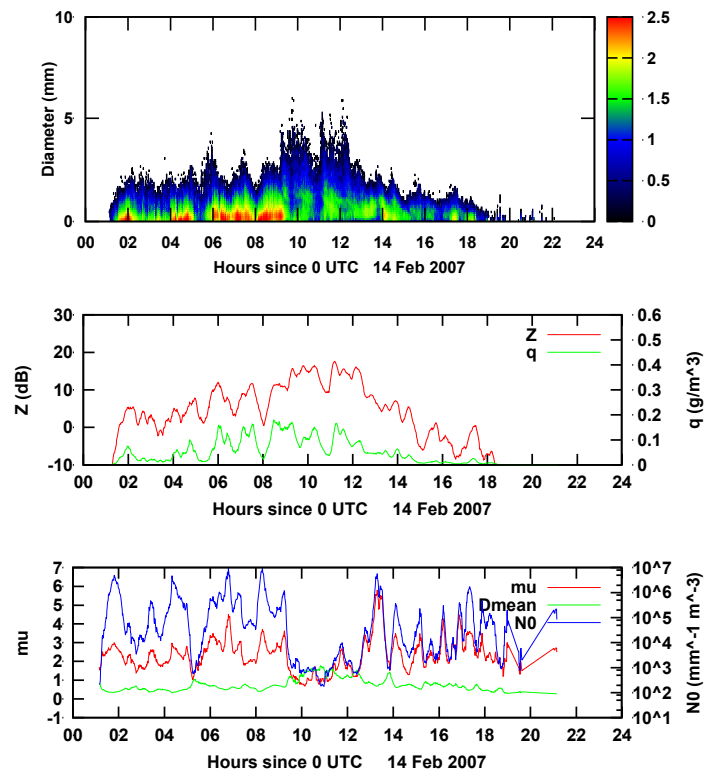


Figure 4. (a, top) Time history of the snow particle DSD obtained from 2DVD observations on 14 February 2007 during C3VP. Each point represents a one-minute average. The colors indicate the frequency of occurrence in each size bin, scaled in logarithmic units. The descending (night time) CloudSat overpass occurred near 0730 UTC, approximately 50 km southeast of the 2DVD location. **(b, middle)** Associated equivalent liquid water content q in g m^{-3} and equivalent radar reflectivity Z (dBZ). **(c, lower)** Associated best-fit gamma DSD parameters (μ , D_m and N_0).

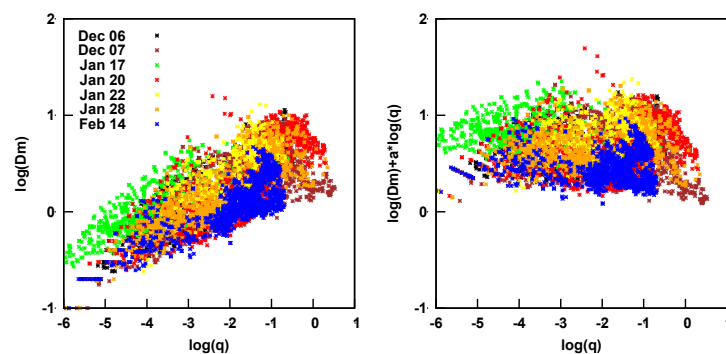


Figure 5. (a, left) Scatterplot of $\log_{10}(D_m)$ versus $\log_{10}(q)$ extracted from analysis of 2DVD data from seven winter storm cases (each color representing a different date during C3VP), where D_m is the mass-weighted mean particle diameter in mm, and q refers to the equivalent liquid water content in g m^{-3} . **(b, right)** Same data as (a), but now plotted with $\log_{10}(D_m) + a \cdot \log_{10}(q)$ on the vertical axis, where $a = -0.21$ is the slope of the best fit to the points in (a).

c) Constrained dual-frequency retrieval

The rightmost panels of Figure 3 displays the identical panels to the leftmost panels, the only difference being the range of the color scale, which was adapted to fit the values for D_m and q . In these rightmost panels of Figure 3, candidate profiles were included in the retrieval process when the associated value of D' was within the range $-1.0 < D' < -0.3$ (i.e, database constrained). Since there were no in-cloud observations of the snow particle properties, this threshold was determined by trial and error by noting the best match between the observed and retrieved 5 GHz profiles. However, a similar range for D' was found for case 5 and case 6 storms (not shown). The retrieved 5-GHz profile now transitions seamlessly between the single and dual-frequency regions. For these constrained retrievals, the profile of q shows more reasonable values, exceeding 1 g m^{-3} only for the largest 5 GHz reflectivity values. The profile of D_m (compare panels f) shows more realistic behavior compared to what was obtained in Section 4a, now increasing with decreasing altitude to a maximum of near 0.35 mm near the surface. The profile of the gamma shape factor μ is near 6 in the upper cloud, transitioning to near 2.5 once the 5 GHz reflectivity exceeds $\approx 0 \text{ dB}$. This is somewhat larger than noticed in Brandes et al. (2007) 2DVD observations, which showed that snow distribution μ was exponentially distributed between 0 and 10 in snow, with the majority of values less than 1. However, larger values of μ were noted to occur at the beginning and ending of storms when small numbers of small particles are observed, whereas the more intense precipitation was characterized by a broader DSD with small values of μ . μ was found to decrease with decreasing Λ (increasing D_m), consistent with our snow retrievals.

While the observed and simulated reflectivity profiles in the constrained (rightmost panels of Figures 3) are in much better agreement than in the unconstrained (leftmost panels of Figure 3), there is up to a 5 dB disagreement in various places. In addition to observed beam matching errors, another reason for this is the overly simplistic treatment of particle shape and the assumption of no supercooled liquid water. We emphasize that our cases are from snowstorms within a cold environment (pre-screened to eliminate melting conditions anywhere in the column), and our assumption of a dendritic shape for the snow particle modeling is an oversimplification of the complex profile of particle shape.

5. CONCLUSIONS

We have demonstrated the synergistic use of a ground radar network in conjunction with satellite-based radar overpasses to provide multi-frequency radar observations of wintertime precipitation scenes. These radar observations at C/W bands provide a different range of sensitivity to typical winter storms compared to more closely spaced Ku/Ka-band radar observations. 2-D video disdrometer measurements were used to analyze the particle size distribution within winter storms sampled during the C3VP field experiment. We avoided comparison of snowfall rates between 2DVD and retrievals, rather using these 2DVD data to narrow down the validity of various combinations of

parameters (μ, D_m, q) , which are equivalent to specifying the three parameters (N_0, Λ, μ) of a gamma drop size distribution (DSD). In particular, the parameter $D' = \log(D_m) + a \log(q)$ was demonstrated for placing physical constraints the DSD parameter combinations used by a dual-frequency Bayesian-based retrieval of snow water content. Comparisons of the 5 GHz radar profile between the observations and modeled profiles (performed using the unconstrained and constrained database) exhibited much closer alignment for the constrained database, and a more realistic profile of the mass-weighted mean particle diameter. The results suggest that there are dependencies between the DSD parameters that can be exploited to further constrain a-priori assumptions that go into snow retrieval algorithms (Haddad et al., 1996; Haddad et al., 2006). Findings from previous studies of combined radar-radiometric precipitation retrievals (Munchak et. al, 2011; Masunaga and Kummerow, 2005; Viltard et. al 2000) also concluded that inconsistencies between modeled and simulated T_B from TMI could be reduced with further refinement of the a-priori rain profile database.

These comparisons of observed and simulated forward observations have focused upon one radar within the greater C-band EC radar network. Despite the measurement uncertainty that is introduced when matching ground and space radar (Anagnostou et al., 2001), there is currently no other way to gather the relatively non-attenuating, longer wavelength (e.g., S- or C-band) radar observations together with space-based radar data. In recent years, many physical models have started to include simulated radar and T_B fields within the model output fields. For example, mesoscale model simulations of now routinely include simulated radar and radiometric output fields for model diagnostics and comparison with satellite and aircraft observations gathered during field campaigns (Shi et al., 2010), and for examination of appropriate microphysical packages (Thompson et al., 2004).

The dual-frequency Ku/Ka-band GPM radar will provide the opportunity for triple frequency observations during overpasses of ground radar networks. Such a three-frequency set of radar observations can further constrain the allowable set of candidate DSD compared to dual frequency, and will provide a means to further discern differences in the DSD and its natural variability embedded within different types of precipitation. These data will be useful to observational programs directed towards physical ground validation useful to precipitation algorithms, such as the follow-on to C3VP, the GPM Cold-season Precipitation Experiment (GCPEX). GCPEX will be conducted in cooperation with Environment Canada and NASA's CloudSat mission during the winter 2011-2012 in the CARE region.

Acknowledgements

We acknowledge support from NASA's CloudSat mission through Dr. Hal Maring, and from NASA's Precipitation Measurement Missions through Dr. Ramesh Kakar. We are grateful to Dr. Gwo-Jong Huang from Colorado State University for his assistance with analyses of the 2DVD data. CloudSat dataset processing was greatly facilitated through the efforts of the CloudSat Data Processing Center (DPC) managed by the Cooperative Institute for Research in the Atmosphere (CIRA) at Colorado State

University. This work was performed at the Jet Propulsion Laboratory, California Institute of Technology, under contract with the National Aeronautics and Space Administration.

References

- Anagnostou, E., C.A. Morales, T. Dinku, 2001: The use of TRMM precipitation radar observations in determining ground radar calibration biases. *J. Atmos. Ocean. Tech.*, **18**, 616-628.
- Brandes, E.A., Ikeda, K., Zhang, G., Schönhuber, M. and Rasmussen, R.M., 2007: A statistical and physical description of hydrometeor distributions in Colorado snowstorms using a video disdrometer. *J. Appl. Meteor. Clim.*, **46**, 634-650.
- Greco, M., and W. S. Olson, 2008: Precipitating snow retrievals from combined airborne cloud radar and millimeter-wave radiometer observations. *J. Appl. Meteor. Climatol.*, **47**, 1634–1650. doi: 10.1175/2007JAMC1728.1
- Haddad, Z. S., J.P. Meagher, S.L. Durden, E.A. Smith, and E. Im, 2006: Drop size ambiguities in the retrieval of precipitation profiles from dual-frequency radar measurements. *J. Atmos. Sci.*, **63**, 204–217. doi: 10.1175/JAS3589.1
- Haddad, Z. S., S.L. Durden, and E. Im, 1996: Parameterizing the raindrop size distribution. *J. Appl. Meteor.*, **35**, 3–13.
- Huang, G.J., V. N. Bringi, R. Cifelli, D. Hudak, and W. A. Petersen, 2010: A methodology to derive radar reflectivity–liquid equivalent snow rate relations Using C-band radar and a 2D video disdrometer. *J. Atmos. Oceanic Technol.*, **27**, 637–651. doi: 10.1175/2009JTECHA1284.1
- Hudak, D., P. Rodriguez, and N. Donaldson, 2008: Validation of the CloudSat precipitation occurrence algorithm using the Canadian C-band radar network. *J. Geophys. Res.*, **113**, D00A07, doi:10.1029/2008JD009992.
- Kruger, A., and Krajewski, W.F., 2002: Two-dimensional video disdrometer: A description. *J. Atmos. Oceanic Tech.*, **19**, 602-617.
- Liu, G., 2008a: Deriving snow cloud characteristics from CloudSat observations. *J. Geophys. Res.*, **113**, D00A09, doi:10.1029/2007JD009766.
- Liu, G., 2008b: A database of microwave single-scattering properties for nonspherical ice particles. *Bull. Am. Met. Soc.*, **89**, 1563-1570.
- Marzano, F. S., A. Mugnai, G. Panegrossi, N. Pierdicca, E. A. Smith, and J. Turk, 1999: Bayesian estimation of precipitating cloud parameters from combined measurements of spaceborne microwave radiometer and radar. *IEEE Trans. Geosci. Remote Sens.*, **37**:596–613

Masunaga, H. and C. D. Kummerow, 2005: Combined radar and radiometer analysis of precipitation profiles for a parametric retrieval algorithm. *J. Atmos. Oceanic Tech.*, **22**, 909-929.

Matrosov, Sergey Y., 2007: Modeling backscatter properties of snowfall at millimeter wavelengths. *J. Atmos. Sci.*, **64**, 1727-1736. doi: 10.1175/JAS3904.1

Molthan, A.L., W. Peterson, S. Nesbitt, D. Hudak, 2010: Evaluating the snow crystal size Distribution and density assumptions within a single-moment microphysics scheme. *Month. Weath. Rev.*, **138**, 4254-4267.

Munchak, S. J., and C. D. Kummerow, 2011: A modular optimal estimation method for combined radar-radiometer precipitation profiling. *J. Appl. Meteor. Climatol.*, **50**, 433-448. doi: 10.1175/2010JAMC2535.1.

Noh, Y.-J., G. Liu, E.-K. Seo, J.R. Wang, K. Aonashi, 2006: Development of a snowfall retrieval algorithm at high microwave frequencies. *J. Geophys. Res.*, **111**, D22216, doi: 10.1029/2005JD006826.

Peterson, W.A., and coauthors, 2007: NASA GPM/PMM participation in the Canadian CloudSat/CALIPSO validation project C3VP: Physical processes in snow. Preprints, *33rd Int. Conf. on Radar Meteorology*, Cairns, Australia, Amer. Meteor. Soc., 1-7.

Shi, J.J., and co-authors, 2010: WRF simulations of the 20-22 January 2007 snow events over eastern Canada: Comparison with in-situ and satellite observations. *J. Appl. Meteor. Clim.*, **49**, 2246-2266.

Skofronick-Jackson, G., M.J. Kim, J. Weinman, and D. Chang, 2004: A physical model to determine snowfall over land by microwave radiometry. *IEEE Trans. Geoscience Rem. Sens.*, **42**,5, 1047-1058.

Skofronick-Jackson, G., and B. T. Johnson, 2011: Surface and atmospheric contributions to passive microwave brightness temperatures. *J. Geophys. Res.*, **116**, D02213, doi:10.1029/2010JD014438.

Tanelli, S.; Durden, S.L.; Im, E.; Pak, K.S.; Reinke, D.G.; Partain, P.; Haynes, J.M.; Marchand, R.T., 2008: CloudSat's Cloud Profiling Radar after two years in orbit: Performance, calibration, and processing. *Geoscience and Remote Sensing, IEEE Transactions on*, vol.46, no.11, pp.3560-3573. doi: 10.1109/TGRS.2008.2002030.

Thompson, G., Rasmussen, R. M., and Manning, 2004: K.: Explicit forecasts of winter precipitation using an improved bulk microphysics scheme. Part I: Description and sensitivity analysis. *Mon. Weather Rev.*, **132**, 519-542.

Ulbrich, C.W., 1983: Natural variations in the analytical form of the raindrop size distribution. *J. Clim. Appl. Meteor.*, **22**:10, 1764-1775.

**Fifth Workshop of the
International Precipitation Working Group
11-15 October 2010, Hamburg, Germany**



Viltard, N., C. Kummerow, W.S. Olson, Y. Hong, 2000: Combined Use of the Radar and Radiometer of TRMM to Estimate the Influence of Drop Size Distribution on Rain Retrievals. *J. Appl. Meteor.*, **39**, 2103-2114.

IMPLEMENTATION OF A METHODOLOGY TO CALIBRATE GROUND RADARS USING TRMM-PR OVER ARGENTINA

Luciano Vidal^{1,2}, Paola Salio^{2,3} and Carlos A. Morales⁴

¹CONICET/Servicio Meteorológico Nacional, Buenos Aires, Argentina

²Departamento de Ciencias de la Atmósfera y los Océanos, FCEyN, UBA

³Centro de Investigaciones del Mar y la Atmósfera (CIMA/CONICET)

⁴Departamento de Ciências Atmosféricas, Univ. de São Paulo, Brazil

e-mail: lvidal@smn.gov.ar

ABSTRACT

This research uses a methodology to evaluate ground weather radar (GR) calibration biases from coincident Tropical Rainfall Measuring Mission (TRMM) Precipitation Radar (PR) observations. The method matches GR and PR observations in a common earth parallel three-dimensional Cartesian grid following Anagnostou et al. (2001). The data matching is performed in a way that minimizes uncertainties associated with the type of weather seen by the radars, grid resolution, attenuation and differences in radar sensitivities, sampling volumes, viewing angles, and radar frequencies. The present paper show an application of the method to the C-band Doppler Radar in Ezeiza, Argentina. Reflectivity difference statistics derived from the matched GR-PR data reveal systematic differences around 6 dB, which is attributed to GR calibration bias. The proposed scheme can be a useful tool to radar engineers for the systematic monitoring of their radar system calibration.

1. INTRODUCTION

Since the TRMM (Tropical Rainfall Measuring Mission) satellite was launched it has provided valuable information allowing to study the global distribution of the convection, mainly in tropical areas. In order to use the existing network of radars available in the world, many authors contrast the values of ground-based weather radar reflectivity with values obtained by the algorithms associated with TRMM Precipitation Radar (PR). Measurement error in the field of PR reflectivity is about ± 0.8 dB, while it has an observation threshold of 17 dBZ, the data are highly reliable due to the strong consistency. These arguments make this source of information a valuable tool when calibrating the reflectivity values observed by ground-based radars and its subsequent use in order to obtain a possible estimate of the values of precipitation near the surface for more accurate moderate to strong events.

The main objective of this study is to analyze the behavior of the ground radar (GR) reflectivity data located in Ezeiza (Argentina) from the analysis of BIAS and Cumulative

Distribution Functions (CDFs) to identify systematic errors and obtain a calibration curve to adjust the same from PR observations. Only show results of Ezeiza but the research includes extending the analysis and the methodology to other Argentine radars (Paraná, Pergamino and Anguil) with the final goal of having a rainfall map composite of all ground radars.

2. DATA AND METHODOLOGY

In this study, attenuation-corrected PR reflectivities derived from hybrid method (TRMM 2A-25, Iguchi and Meneghini 1994) have been used. The precipitation radar on board TRMM has a 13.8-GHz frequency (2.2-cm wavelength), an approximately 4.5-km spatial resolution at near nadir, and a 250-m vertical resolution, information from this sensor is available from 1998 to the present.

Ground-based radar operated by National Weather Service is deployed at Ezeiza – Argentina (34.49°S 58.32°W, 20m ASL) (Fig.1). This radar is an Enterprise DWSR-2500C with 5.36-cm wavelength (C-band), 1° beam width, 0.5-km range resolution and volume scan sampling frequency every ~10 min. Each volume scan consists of approximately 16 sweeps, with elevation angles ranging from 0.5° (base scan) to 34°. The available period runs from January 2004 to December 2009.

An analysis of the coincident PR orbits with Ezeiza GR was conducted considering an area less than 200 km and a 10-min time window [$-5 \text{ min} \leq \text{Time}_{\text{PR}} - \text{Time}_{\text{GR}} \leq 5 \text{ min}$]. This results in 64 orbits.

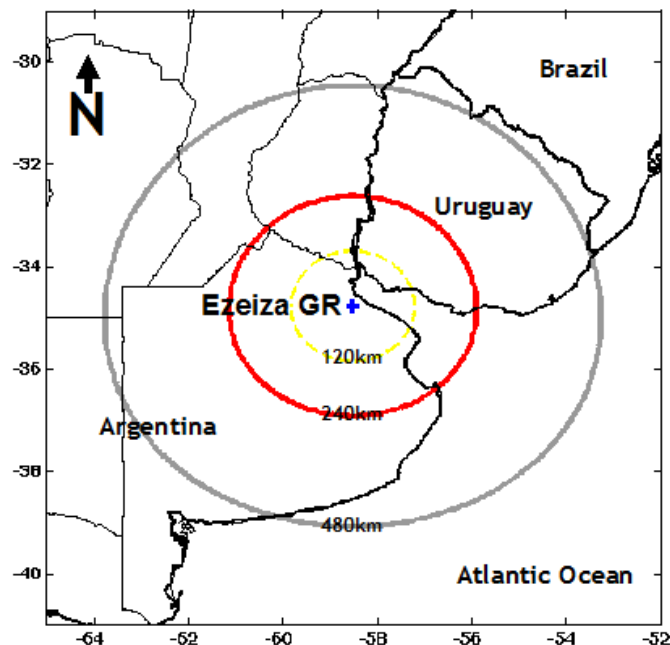


Figure 1. Ezeiza ground radar site

In order to compare both samples, a similar methodology proposed by Anagnostou et al. (2001) for the correct spatial arrangement of both sources of information has been followed. The method is based on a scheme that interpolates

ground and space radar volume scans into a fixed grid and on a data selection that minimizes uncertainties associated with the type of weather seen by the radars, grid resolution, and differences in radar sensitivities, sampling volumes, viewing angles, and radar frequencies. Instantaneous PR and ground radar reflectivity volume scans that are within a time lag at a maximum of 10 min are projected into a common earth parallel three-dimensional Cartesian grid with 5×5 km horizontal and 2 km vertical resolution. The 3D-box pixel dimensions are selected to be consistent with both the ground radar's low vertical resolution (~ 2 km at 100-km range for 1° beam-width) and the PR's field-of-view resolution ($\sim 4.5 \times 4.5$ km). The 3D-box is centered at Ezeiza ground radar site with a horizontal extend of ± 200 km and vertical levels ranging from a minimum of 4 km to a maximum of 14 km.

The study of the systematic difference between the PR and GR data is evaluated considering the statistics (BIAS and RMSE) and a method based on the histogram matching technique, e.g., Hamill (1999), which is based on the comparison of the CDFs between GR data and PR data (Fig. 2a). The main goal of this algorithm is find a calibration curve that adjust the CDF of the ground radar so it matches as close as possible the CDF of the PR. The idea in considering this methodology is to remove the bias of the ground radar information related to PR. Given the individual CDF for each sample, each value of the uncalibrated dataset is matched with the value of the reference dataset corresponding to the same probability values. Figure 2a shows an example of this methodology, Z_1 is the uncalibrated reflectivity value and Z_2 is the reference data, $P\%$ represents the probability level for both samples. A scatter-plot considering all pair (Z_1 and Z_2) of probability levels between 5% to 95% is built for the analyzed period (2004-2009) and it is shown in Figure 2b. The calibration curve is defined, in the present paper, as the linear interpolation between two successive probability intervals (e.g. 5% and 10%).

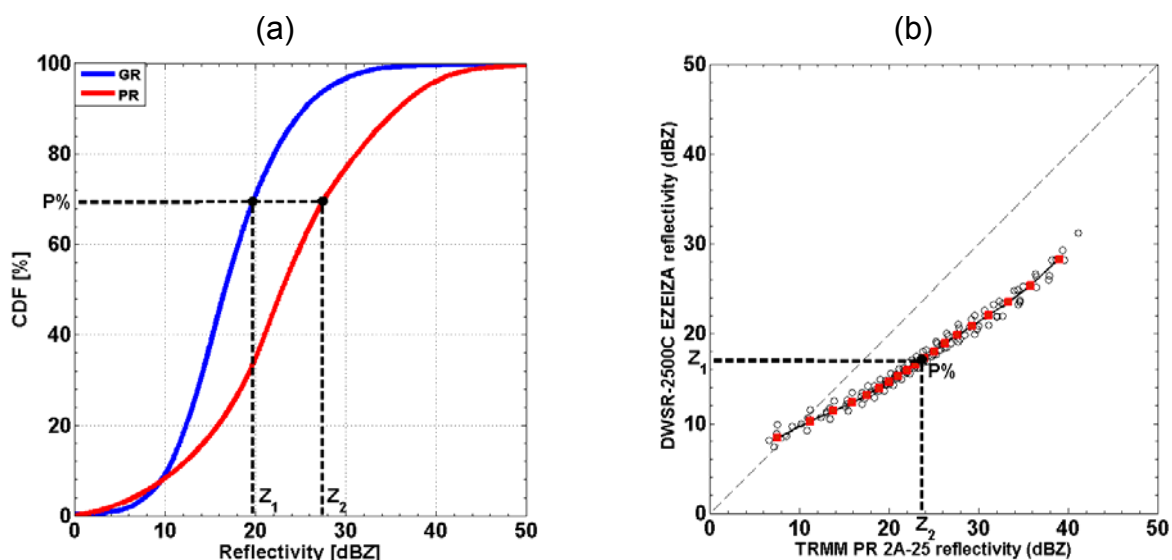


Figure 2. (a) Scheme of the histogram matching function. (b) Definition of calibration curve.

3. Results

3.1 Statistical analysis

This section present quantitative comparisons between PR and Ezeiza GR observations for the data period described in section 2. The data used in this analysis are the 5 X 5 X 2 km 3D-box interpolated reflectivity values selected according to the procedure described in our methodology. We first present (see Fig. 3) PR, GR and GR-PR reflectivity difference histograms. A first observation extracted from Fig. 3 is that the reflectivity difference histogram have shapes close to Gaussian distribution. The standard deviation is 7 dB. This variability is attributed to random effects associated with the hydrometeors size distribution variability, residual attenuation correction errors, incomplete knowledge of the ground radar beam propagation, ground radar interpolation errors due to gaps in their elevation sweeps, and temporal lags between PR and GR measurements. Nevertheless, one can clearly distinguish the significant systematic difference between the two sensor measurements. Figure 4 shows PR reflectivity versus reflectivity difference values of the matched 3D-box data. It is apparent that there is an obvious dependence of the difference on the reflectivity magnitude, where differences are positive below 14 dBZ and negative above this threshold. Largest differences are observed for large values of reflectivity. Finally, the Figure 5 shows time series of the Ezeiza GR bias (in dB) estimated using our proposed methodology. The horizontal axis of this panel shows the years of the matched datasets used in the bias estimates. The horizontal line correspond to the overall bias estimates derived from our method. It is shown that the temporal fluctuation of the bias is less than 1 dB, which is within the calibration accuracy of the PR system.

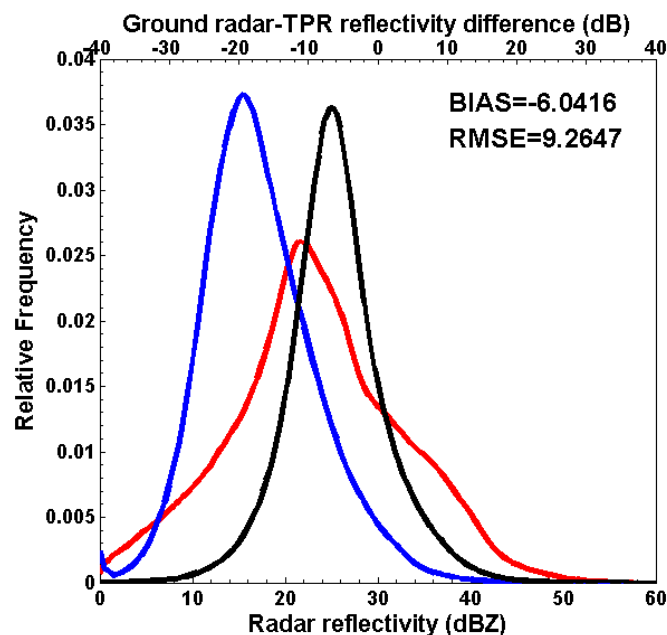


Figure 3. Histograms of GR reflectivity (blue line), PR reflectivity (red line) and difference between both (black line). The BIAS and RMSE shows in the figure.

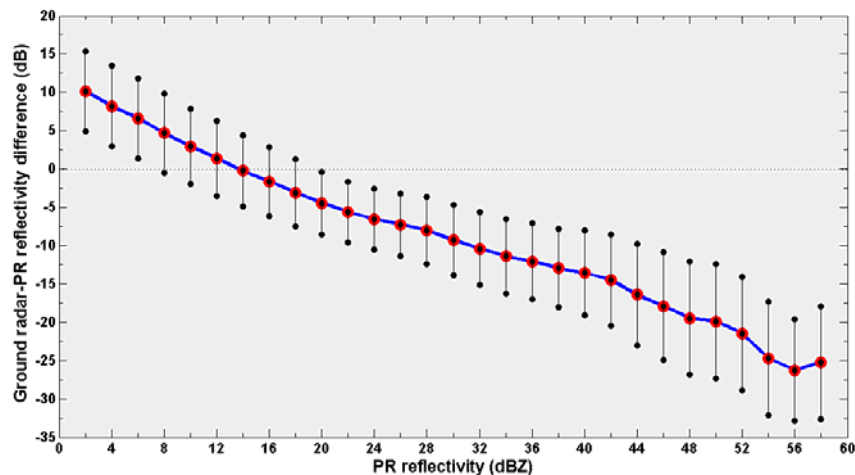


Figure 4. GR-PR difference versus PR reflectivity value considering 2-14 km CAPPI volumes.

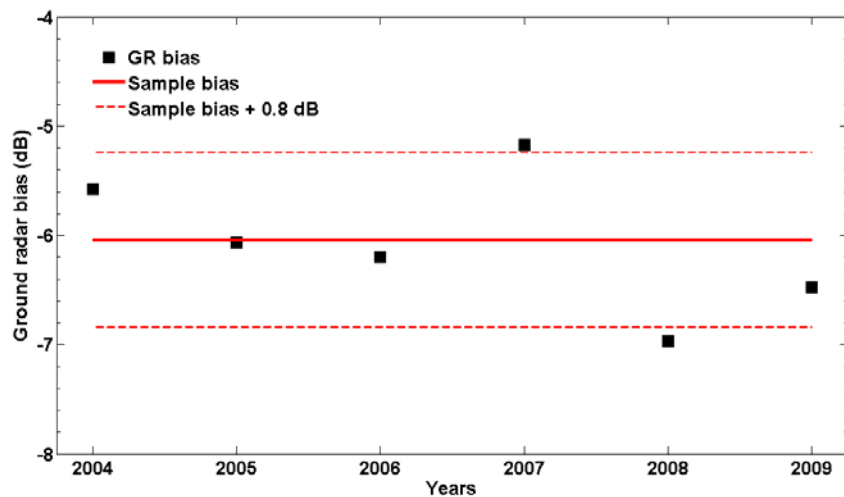


Figure 5. Time series of GR bias.

3.2 Calibration examples

Some cases associated with different weather conditions has been selected to test the calibration during 2010 (Fig. 6). These cases are not part of the training set with which the calibration curve has been calculated. Case 1 and 2 have a convective behavior, while case 3 presents a stratiform precipitation, and case 4 shows squall line. Calibration curve derived from the histogram matching of Ezeiza GR and PR reflectivities for the entire sample of data (Fig. 2b) has been applied for each event to obtined calibrated images (Fig. 6, right column). First, we can note that although the patterns and positioning of the systems are the same for both radars there is significant difference in the relative magnitude of their corresponding values. Calibration in case 4 fits properly, during convective cases a underestimation is still present. Stratiform case denotes a reflectivity overestimation. This result is coincident with observational information at surface for this radar observed by Salio et al (2010). This bias ranging between -8.2 dB and -5.2 dB, considering extreme values during convective cases (Fig.

7). In all cases histograms shows that the maximum frequency for GR is located between 15 and 20 dBZ, with a skew towards higher reflectivity values but never exceeding 40 dBZ. For the PR, the maximum frequency is located between 25 and 30 dBZ for all cases.

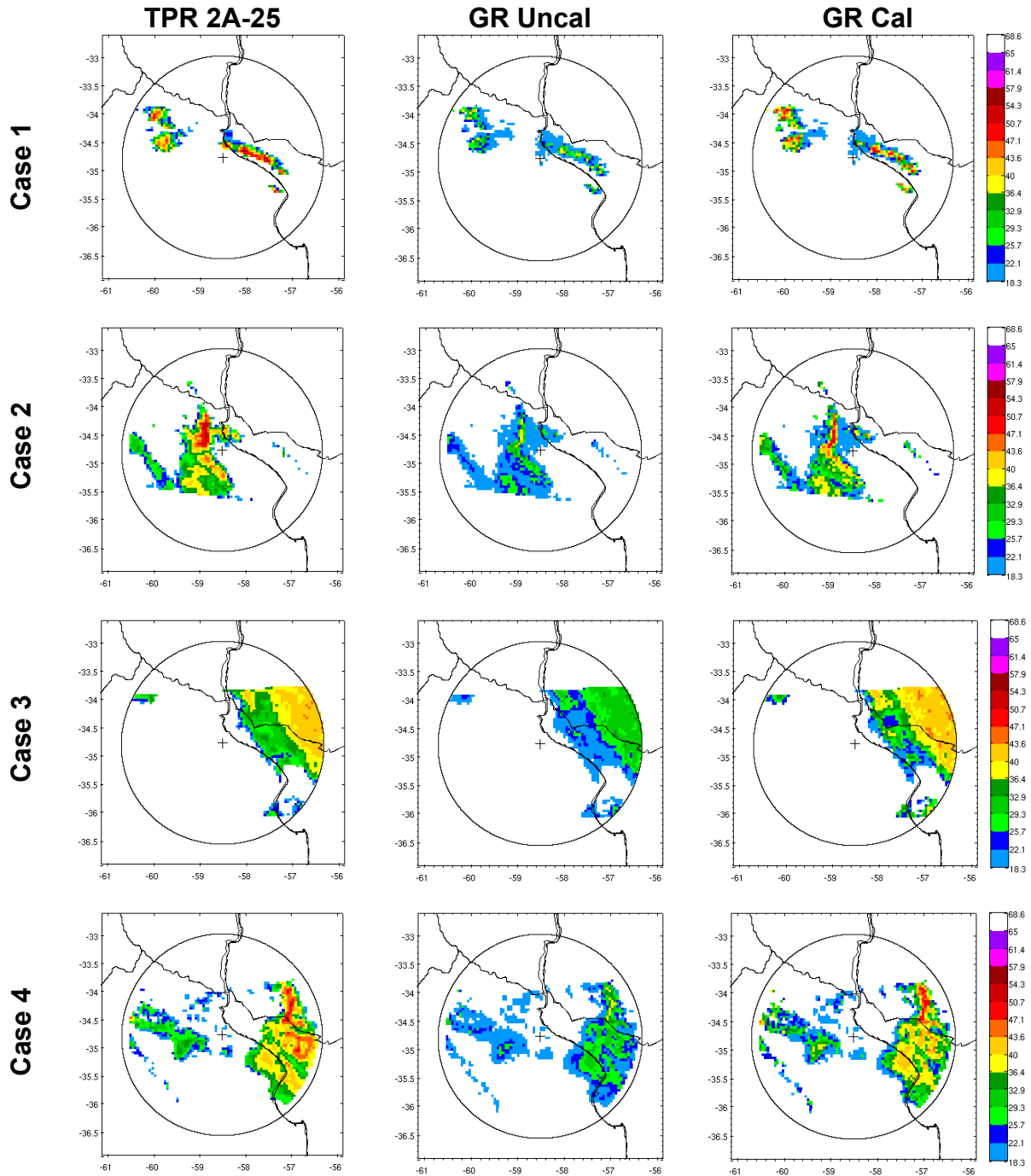


Figure 6. PR reflectivity field (3-km CAPPI) (left panels), GR uncalibrated reflectivity field (3-km CAPPI) (central panels), and GR calibrated reflectivity field (3-km CAPPI) (right panels). The radar circles shown in the figure have 200-km radius.

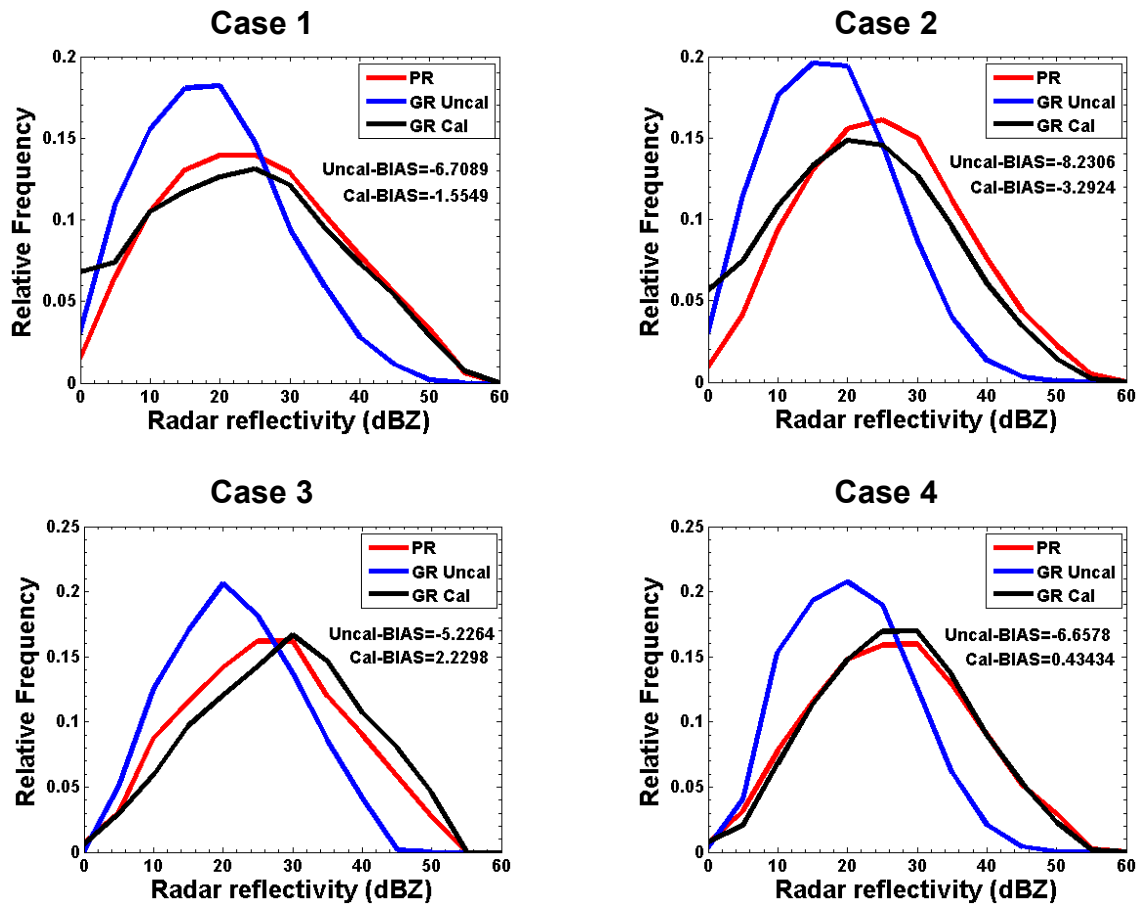


Figure 7. Histograms of GR uncalibrated (blue), GR calibrated (black) and PR (red) for each calibration example.

4. CONCLUSIONS

A methodology that matches PR and GR measurements in a common earth parallel three-dimensional grid porpuse by Anagnostou et al. (2001) was applied in this study to evaluate the calibration bias of an C-band weather radar located in Ezeiza, Argentina. We demonstrated good matching between GR and PR reflectivity patterns. Evaluation of the difference statistics revealed significant systematic difference (-6 dB), which is attributed mainly to GR calibration bias. The temporal fluctuation of the radar bias was not significant (< 1dB). We are expanding the applications of this method to several radar sites in Argentina.

5. REFERENCES

Anagnostou, E. N., C. A. Morales, and T. Dinku, 2001: The use of Precipitation Radar observations in determining ground radar calibrations biases. *J. Atmos. Oceanic Technol.*, **18**, 616-628.

- Bolen, S. M., and V. Chandrasekar, 2000: Quantitative cross validation of space-based and ground-based radar observations. *J. Appl. Meteor.*, **39**, 2071-2079.
- Hamill, T., 1999: Hypothesis Tests for Evaluating Numerical Precipitation Forecasts. *Wea. Forecasting*, **14**, 155-167.
- Iguchi, T., and R. Meneghini, 1994: Intercomparison of single-frequency methods for retriving a vertical rain profile from airborne or spaceborne radar data. *J. Atmos. Oceanic Technol.*, **11**, 1507-1516.
- Kozu, T., and Coauthors, 2001: Development of precipitation radar on board the Tropical Rainfall Measuring Mission (TRMM) satellite. *IEEE Trans. Geosci. Remote Sens.*, **39**, 102-116.
- Salio, P. V., and Coauthors, 2010: Calibration of C-band radar in Argentina. *6th European Conference on Radar in Meteorology and Hidrology*, Sibiu, Romania.
- Wang J., and D. B. Wolff, 2009: Comparisons of Reflectivities from the TRMM Precipitation Radar and Ground-Based Radars. *Journal of Atmospheric and Oceanic Technology*, **26**, 857-875.

Acknowledgment

This work was partly funded by the projects: ANPCyT PICT 2007-355, ANPCyT PICT 2008-215, UBACyT X633, CONITEC PIP Nicolini. The first author would like to special thank CONICET for a PhD scholarship fund that allows such research, to the National Weather Service for Ezeiza ground radar data and Erich Stocker for proving TRMM data over South America.

SSM/I ASSESSMENT FOR RAINFALL RETRIEVAL: PRELIMINARY RESULTS

Daniel Vila^{1,2}, Robert Joyce³, Ralph Ferraro^{2,4}, Carlos F. De Angelis¹

¹ Centro de Previsão de Tempo e Estudos Climáticos - Rodovia Presidente Dutra, Km 40, SP-RJ, 12630-000, Cachoeira Paulista, SP, Brasil, e-mail: daniel.vila@cptec.inpe.br

² Cooperative Institute of Climate Studies (CICS/ESSIC/UMD), College Park, MD

³ CPC/NCEP/NOAA, Camp Spring, MD

⁴ STAR/NESDIS/NOAA, Camp Springs, MD

e-mail: daniel.vila@cptec.inpe.br

ABSTRACT

Global rainfall estimates have been produced from 1987 to present using measurements from the Defense Meteorological Satellite Program (DMSP) series of Special Sensor Microwave Imager (SSM/I). The aim of this presentation is to introduce recent efforts that are necessary to extend the 21-year climate records of this valuable product. Since the DMSP F16, F17 and F18 satellites were successfully launched carrying onboard the Special Sensor Microwave Imager/Sounder (SSM/I), the objective is focused on the application of SSM/I channels to evaluate the performance of rainfall estimates using the heritage of existing algorithms for SSM/I.

Preliminary results show that a larger bias on monthly retrievals is observed when F17 is compared with F13 due to the fact that F17 is around one hour before F13 and closer to the pick of the convective activity while when instantaneous retrievals (SSM/I F16 & 17 vs. TMI) are compared a slight positive bias is observed (below 2 mm/day)

1. INTRODUCTION

Global rainfall estimates and other hydrological products have been produced from 1987 to present using measurements from the Defense Meteorological Satellite Program (DMSP) series of Special Sensor Microwave Imager (SSM/I). Since the DMSP F16, F17 and F18 satellites were successfully launched carrying onboard the Special Sensor Microwave Imager/Sounder (SSM/I), those satellites are replacing the old SSM/I series that are being decommissioned along the time due to their age. One of the main objectives of this research is the continuation in monitoring and retrieving of atmospheric and surface parameters such as precipitation using SSM/I measurements. The SSM/I sensor is the first operational microwave satellite radiometer for profiling temperature and humidity using a conical scanning sensor, so that the viewing area and slant path remains constant as it scans the Earth. SSM/I imaging channels maintain similar resolution and spectral frequency to the SSM/I except 91.655 GHz on SSM/I vs.

85.5 GHz on SSM/I. Additionally, the SSMI/S added a new 150 GHz channel plus three humidity profiling channels, which consists of pairs of narrow passbands on either side of the H₂O absorption line center at 183.3 GHz similar to those on the Advanced Microwave Sounding Unit-B/ Microwave Humidity Sounder (AMSU-B/MHS) instruments. A wider swath, approximately 1700 km for SSMI/S compared with only 1400 km for SSM/I, is also a new characteristic of this instrument.

These products, combined with those derived from other passive microwave sensors such as the AMSU, offer the scientific community an excellent source of global hydrological products. The high temporal frequency of rainfall retrievals and other hydrological products will also help to better understand the diurnal cycle for different climate regimes around the world (Vila et al., 2007).

The aim of this paper is in the application of SSMI/S channels to evaluate the performance of several rainfall products using the heritage of existing algorithms for SSM/I.

2. DATA AND ALGORITHMS

For this particular project, SSM/I and SSMI/S Temperature Data Record (TDR) files from Comprehensive Large Array-data Stewardship System (CLASS) were used. CLASS is a web-based data archive and distribution system for NOAA's environmental data. TDRs contain calibrated and earth-located data prior to irreversible antenna pattern correction (antenna temperature, TA hereafter).

Two passive microwave-based algorithms were used to evaluate the performance of the proposed intercalibration methodology between SSM/I and SSMI/S sensors: The Goddard Profiling Algorithm (GPROF, Kummerow et al., 2001) were used to assess instantaneous retrievals when compared against high-quality TMI retrievals while a scattering-based rainfall algorithm described in Ferraro (1997, appendix A) was used for monthly scale assessments.

In the new SSMI/S sensor, the highest SSM/I frequency (85.5 GHz V & H) was moved to 91.655 GHz (V & H). In this case, scattering is larger for the new frequency (colder temperatures), so the rainfall retrievals based on scattering could be affected.

The intercalibration methodology, fully described in Vila et al. (2008), is based on simultaneous observations between two satellites. A Simultaneous Conical Overpass (SCO) (Yan and Weng, 2008) is defined as the data pair generated when two polar-orbiting satellites cross the same area at similar local times. The frequency of occurrence of SCO events depends on the criteria of simultaneity. After the spatial remapping of all SSM/I and SSMI/S channels, we define a temporal match-up when for a given grid-point time window between SSM/I and SSMI/S samples is below 7 minutes. The methodology to evaluate the performance of SSMI/S-based retrievals is based on a direct linear mapping between SSMI/S and the corresponding SSM/I as follows:

$$TA_{SSMI/S} = \alpha_{chan, sfctype, rain} + \beta_{chan, sfctype, rain} * TA_{SSMI} \quad (1)$$

where $\alpha_{chan, sfctype, rain}$ and $\beta_{chan, sfctype, rain}$ denote the offset and slope, respectively, and both of them are produced by using SCO observation between SSM/I and SSMI/S. This procedure is performed for each SSM/I channel, for two different surface types: land and ocean (coastline, snow and sea ice were excluded) and two extreme situations:

clear sky and rainy pixels (based on SSM/I estimates). Note that this empirical approach also transforms SSM/I/S 91.655 GHz as SSM/I 85.5 GHz. Table I shows the coefficients for all channels under different environmental conditions for F15 (SSM/I) and F16 (SSM/S). A similar set of coefficients were developed for the F14-F17 pair.

Table I: Offset (α) and slope (β) values used for linearly remapping F16 to F15-like channels under different environmental conditions.

Frequency (GHz)		rain		clear sky	
		α	β	α	β
19.35 (V)	ocean	-4.3056	1.0154	-3.7588	1.0081
19.35 (H)		-0.1004	1.0000	-0.5628	0.9941
19.35 (V)	land	-2.5415	1.0116	-3.0527	1.0139
19.35 (H)		1.2867	1.0001	1.3982	1.0000
22.235 (V)	ocean	-4.7092	1.0064	-5.6801	1.0059
22.235 (V)	land	1.0261	0.9879	0.0261	0.9879
37.0 (V)	ocean	15.9657	0.9279	-2.5349	0.9950
37.0 (H)		18.9355	0.9165	0.4925	0.9900
37.0 (V)	land	2.3171	0.9825	-8.1856	1.0206
37.0 (H)		1.6337	0.9875	1.0819	0.9905
91.655 (V) - 85.5 (V)	ocean	30.1409	0.8985	-9.1453	1.0463
91.655 (H) - 85.5 (H)		30.8093	0.8947	-3.2688	1.0066
91.655 (V) - 85.5 (V)	land	29.9904	0.8980	1.0681	1.0090
91.655 (H) - 85.5 (H)		28.0057	0.9067	0.8296	1.0111

3. RESULTS

Figure 1 shows the bias between F17 and F13 retrieval for January 2009 (upper panel) and July 2009 (lower panel). In the upper panel, the larger positive bias (F17 > F13) is observed around the tropical region in the southern hemisphere (mainly over the Amazonian region and Africa), while over the northern hemisphere (winter season) the bias is very close to zero over land. This behavior can be explained by the fact that F17 is around 1 hour before F13 and closer to the pick of the convective activity (Nesbitt, 2003) during the ascending passes of both satellites. During the winter season over southern hemisphere (bottom panel), this particular behavior is smoothed, while the positive bias is now observed over the northern hemisphere where the convective activity is enhanced due to the displacement of ITCZ.

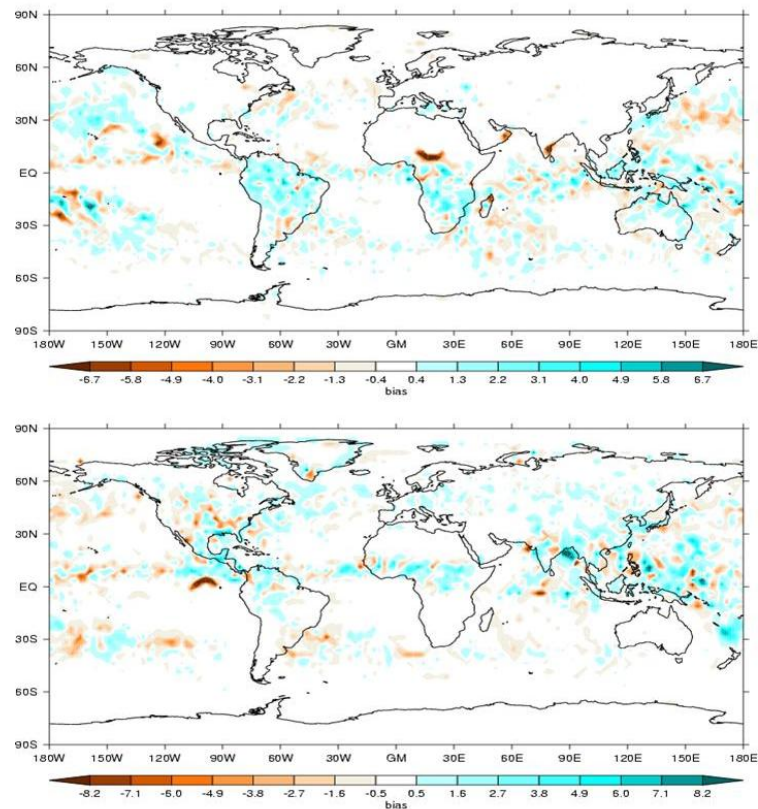


Figure 1: Upper Panel: F17-F13 rainfall retrieval bias for January 2009. Lower panel: idem for July 2009.

The second assessment was done for instantaneous retrievals using a modified version of GPROF algorithm for SSMI/S (using the linear remapping technique presented in the previous section) and TMI retrievals. In this case, the matchups were performed between TMI and SSMI/S retrievals for the period 23 January – 21 February 2010 using a common 0.25-degree grid and a 30-minute time window. Figure 2 shows the results for South America. The upper left panel shows the main rainfall for those scenes of F16 and F17 within 30 minutes of TMI, while the upper right panel is the same procedure for TMI scenes. The lower left panel shows the bias, while the zonal mean profile for both estimates (and the difference) is presented in the lower right panel. The observed bias is slightly positive (below 2 mm/day), while the spatial distribution agrees very well between both retrievals. Similar results are observed over the ocean (not shown). These preliminary results are very encouraging for including SSMI/S retrievals in many blended techniques (i.e., CMORPH, TMPA, etc.) because the order of magnitude of the observed bias is very similar to that obtained for SSMI/I retrievals.

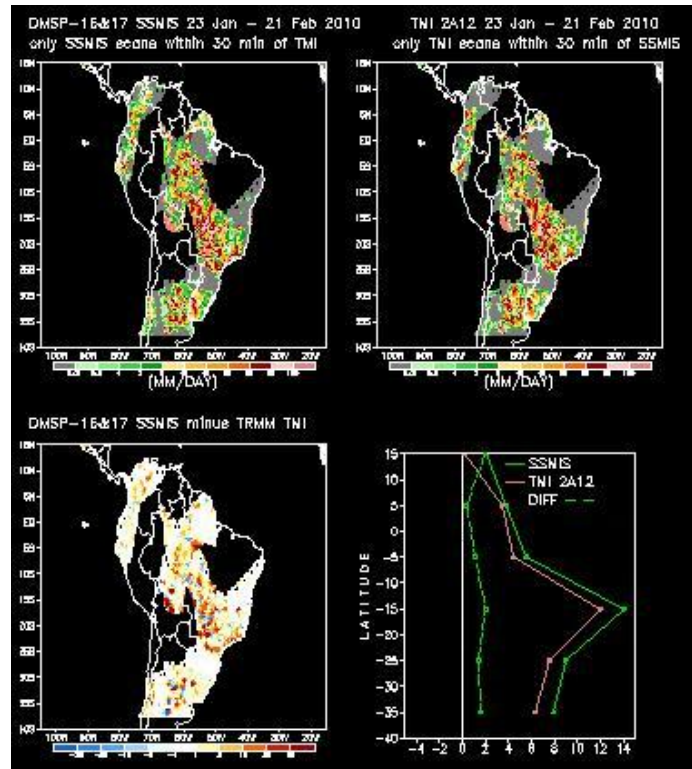


Figure 2: Upper panel: Left: rainfall retrieval for DMSP F16 & F17. Right: Idem for TMI 2A12 product. Lower panel: Left: SSMI/S – TMI bias. Right: zonal mean for both retrievals. The dashed line represents the difference.

4. REFERENCES

- FERRARO R., 1997: Special sensor microwave imager derived global rainfall estimates for climatological applications. *J. Geophys. Res.*, 102 (D14), 16715-16735.
- KUMMEROW C., Y. HONG, W. S. OLSON, S. YANG, R. F. ADLER, J. MCCOLLUM, R. FERRARO, G. PETTY, D-B. SHIN, T. T. WILHEIT, 2001: The Evolution of the Goddard Profiling Algorithm (GPROF) for Rainfall Estimation from Passive Microwave Sensors. *Journal of Applied Meteorology* 40:11, 1801-1820.
- NESBITT S. W., E. ZIPSER, 2003: The Diurnal Cycle of Rainfall and Convective Intensity according to Three Years of TRMM Measurements. *Journal of Climate* 16:10, 1456-1475
- VILA, D., FERRARO R., JOYCE R., 2007: Evaluation and Improvement of AMSU Precipitation Retrievals. *J. Geophys. Res.*, 112, D20119, doi:10.1029/2007JD008617.
- VILA D., 2008, An SSM/I - SSMI/S Application for Climate Research: the Extension of Hydrological Products Climate Records – 4th Workshop of the International Precipitation Working Group – Beijing, China - October 2008.
- WENG, F., AND N. C. GRODY, 1994, Retrieval of cloud liquid water using the special sensor microwave imager (SSM/I), *J. Geophys. Res.*, 99(D12), 25,535–25,551.

**Fifth Workshop of the
International Precipitation Working Group
11-15 October 2010, Hamburg, Germany**



YAN B. AND F. WENG, 2008, Intercalibration Between Special Sensor Microwave Imager/Sounder and Special Sensor Microwave Imager, *IEEE Trans. Geo. Remote Sensing*, 46 (4), 1-14.

MEGHA-TROPIQUES: MISSION AND ALGORITHMS STATUS

Nicholas Viltard

LATMOS-IPSL CNRS-UVSQ

e-mail: nicholas.viltard@latmos.ipsl.fr

Megha-Tropiques is a French-Indian project aimed at studying the energy and water budget in relation to tropical convection. The mission will carry a set of three instruments: a conical scanning-passive microwave imager (MADRAS), a cross-track scanning-passive microwave sounder and a cross-track scanning radiative budget instrument. The main products that will be generated from the data collected by the satellite are: surface rain and rain profiles, water vapor profiles and TOA fluxes. During the presentation, the mission's goals and design will be briefly detailed, emphasizing on the rain retrieval aspects. An update on the mission and products status will also be given. In addition, a field campaign meant to characterize the relationship between ice microphysics and surface rain over continental West Africa took place in Niamey in August 2010. Ground and airborne radar were deployed in addition to in-situ microphysics measurements collected with the French F20. A short summary of the campaign will also be presented.

DEVELOPING WINTER PRECIPITATION ALGORITHM OVER LAND FROM SATELLITE MICROWAVE AND C3VP FIELD CAMPAIGN OBSERVATIONS

Nai-Yu Wang¹, Kaushik Gopalan¹, Ralph Ferraro²

¹University of Maryland, Earth System Science Interdisciplinary Center
(ESSIC), USA

²NOAA/NESDIS/Center for Satellite Research and Applications (STAR),
USA

e-mail: nai-yu.wang@noaa.gov

As we move from the TRMM to GPM era, more emphasis will be placed on precipitation in mid- and high-latitudes. In these areas, a large and highly variable portion of the total annual precipitation is snow. During the winter of 2006-2007, NASA GPM Ground Validation program joined a field campaign designed to measure winter precipitation for the Canadian Cloudsat/CALIPSO validation program (C3VP). GPM's participation was aimed at improving satellite-based snowfall detection and retrieval algorithms. Intensive observations of snowfall using airborne and ground-based instrumentation were conducted centered on the Centre of Atmospheric Research Experiments (CARE) site near Egber, Ontario, Canada (about 80km north of Toronto). Emphasis was placed on intensive ground-radar sampling of snow by the scanning King City C-band radar (WKR), coordinated aircraft flight patterns through clouds, and coincident passive microwave satellite overpasses. In this paper, we will present the progress towards developing a winter precipitation algorithm over land using satellite data from microwave radiometer and cloud radar and C3VP field campaign data including aircraft microphysics, radiosonde, and ground station measurements.

PRECIPITATION ESTIMATION FOR TYPHOON USING SATELLITE MICROWAVE DATA

Nan-Ching Yeh¹, Wann-Jin Chen², Jian-Liang Wang³, Jen-Chi Hu⁴, Gin-Rong Liu⁵,
Ming-Da Tsai³

¹ School of defense science, Chung Cheng Institute of Technology, National Defense
University, Taoyuan, Taiwan

² Department of Electronic Engineering, Ta Hwa Institute of Technology, Hsinchu,
Taiwan

³ Department of Environmental Information and Engineering, Chung Cheng Institute of
Technology, National Defense University, Taoyuan, Taiwan

⁴ Armed Weather Center, Ministry of National Defense, Taipei, Taiwan

⁵ Center for Space and Remote Sensing Research, National Central University,
Taoyuan, Taiwan.

e-mail: jim912104@gmail.com

ABSTRACT

On 8 August 2009, torrential rainfall during the landfall of Typhoon Morakot had broken the record of past decades in Taiwan. The extreme rainfall has caused severe landslides, floods and heavy disasters in Taiwan. The major reason for these disasters is the huge amounts of rain falling in a very short period. Usually people need information of rainfall in time to prepare for disasters and then can significantly reduce the damage and loss of lives and properties. It is the aim of this study to provide accurate rainfall estimations quantitatively for severe weather systems.

The Bayesian approach was accepted in this study. At first a prior probability distribution was obtained by model simulations, then a conditional probability distribution was derived by microwave radiative transfer models (RTM), finally a posterior probability distribution of rainfall was calculated by combining a prior probability distribution and conditional probability distribution. The brightness temperatures of microwave channels are calculated by RTM and the required vertical hydrometeors input to the model are from the Weather Research and Forecast model.

In addition, one brightness temperature threshold for non-raining case was obtained by using a lot of 2A15 TRMM/PR rainfall products at non-raining conditions. An attenuation index representing the degree of rain was accepted in this study. And the retrieved rainfalls are validated with the standard PR rainfall products. Results show that the

coefficient correlation between Bayesian rainfall retrievals and the standard PR rainfall products is larger than 0.6 and that the rainfall retrievals are overestimated to weak weather systems but underestimated to severe weather systems.

1. INTRODUCTION

The time span, spatial distribution, and the amount of precipitation have always been deeply concerned with human life. It is also closely relative to global energy transportation, atmosphere circulation, and climate change. However, the rainfall data provided by the traditional weather observation station cannot satisfy the need of weather operation units and people's livelihood in aspects of both time and space. The precipitation estimation from satellite remote observation recovers the shortage in space. In the early time, satellite infrared and visible channels were used to estimate precipitation, but both of them just can receive the signals from the top of clouds and no any information from the underlying clouds. Therefore the estimated rainfall is often overestimated when there is high cirrus or anvil clouds in the field of observation. In addition, the visible channel is not available at night. The satellite microwave observations are now widely used to retrieve surface rain rate, because the microwave is not influenced by clouds (Adler et al. 2001).

In 1997, the Tropical Rainfall Measuring Mission (TRMM) satellite was launched. The observations of the TRMM Microwave Imager (TMI) are dual-polarization frequencies ranging from 10 to 85 GHz, and the frequency of the Precipitation Radar (PR) is at 13.8 GHz (Kummerow et al. 1998). There are many exertions in both development and validation of retrieval methods from TMI and PR data (Benedetti et al. 2005).

The Bayesian approach for rain rate retrievals from TMI observations was used in this study. It is our aim in this study to provide an accurate rainfall retrieval algorithm for typhoon weather system in order to reduce the damage to livelihood and economy caused by heavy rainfall brought by severe weather systems like typhoon Morakot (2009).

2. SATELLITE OBSERVATIONS

2.1 TRMM/Microwave Imager (TMI)

The frequencies of the TMI are 10.65, 19.35, 21.3, 37.0, and 85.5 GHz, and all of them have dual-polarized brightness temperatures (TB), except 21.3 GHz only has vertical polarization. The field-of-view of TMI depends on frequency, so there are different from all of TRMM's frequencies. For the purpose of development and validation of our retrieval method, all brightness temperatures of TRMM channels are interpolated to 10 x 10 km grid points.

2.2 TRMM/Precipitation Radar (PR)

The observations of TRMM/PR are 3 dimensional precipitation distributions over both land and ocean surfaces (Kummerow et al. 1998). The PR scans from 0° to 17°,

and each scan interval is 0.35° . The swath was 215 km before August 2001, and it was become 247 km after boosting in August 2001.

The horizontal resolution at nadir is from 4.3 km (original) to 5 km (after-boost), and the vertical resolution is 250 m. The minimum threshold of PR reflectivity detection is about 17 dBZ, corresponding to a rain rate of $0.5 - 0.7 \text{ mm hr}^{-1}$. The one standard product (2A25) of TRMM/PR includes vertical profiles of rain rate retrieved through the Z-R relations (Iguchi et al. 2000). In this study, we used near-surface rain rate from 2A25 and interpolated them to $10 \times 10 \text{ km}$ grid points in order to match TMI data.

3. THEORY FOUNDATION AND RESEARCH METHODS

A lot of rain rate retrieval methods were developed based on the Bayes' theorem methods (Evans et al. 1995; Olson et al. 1996; Marzano et al. 2002; Di Michele et al. 2005; Chiu and Petty 2006; Grecu and Olson 2006). At first a prior probability distribution ($f(R)$) was obtained by observations, then a conditional probability distribution ($f(P|R)$) was derived by microwave radiative transfer models (RTM), finally a posterior probability distribution of rainfall ($f(R|P)$) was calculated by combining a prior probability distribution and conditional probability distribution. The relationship among three distributions shows the following formula

$$f(R|P) \propto f(P|R)f(R)$$

Where R means the rain rate to be retrieved, P represents passive microwave observation, and $f(R|P)$ is the posterior PDF describing rain rate probability at given observations.

Due to the saturation of brightness temperature of channels, microwave brightness temperature shows non-monotonic dependency on rain rate. In 1994, Petty brought up a suggestion that attenuation index P as the observed variable to reduce retrieval ambiguity. The P index is defined as

$$P \equiv \frac{T_V - T_H}{T_{V,0} - T_{H,0}}$$

Where T_V and T_H are vertical and horizontal polarization of TB; $T_{V,0}$ and $T_{H,0}$ are the TB observations in the clear condition. For simulations, back-ground brightness temperatures can be calculated by simply setting all hydrometeors to be zero. Figure 1 is the flowchart of this research method.

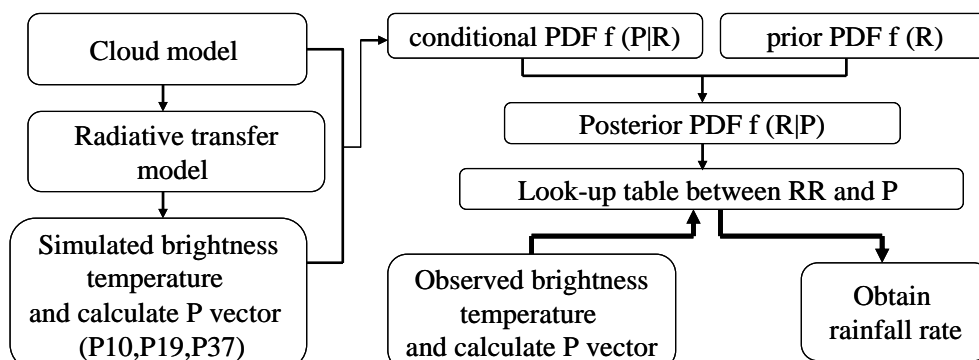


Figure 1. The flowchart of the Bayesian method

4. RESULTS AND DISCUSSION

Retrieved rain rate is validated both in qualitative and quantitative aspects. First, we present qualitative comparison of horizontal structures from one overpass of Typhoon Morakot. This comparison was conducted mainly against PR-retrieved rain rate. Second, we present quantitative comparisons against PR-retrieved rain rate for three overpasses of typhoon Morakot (Figure 2)

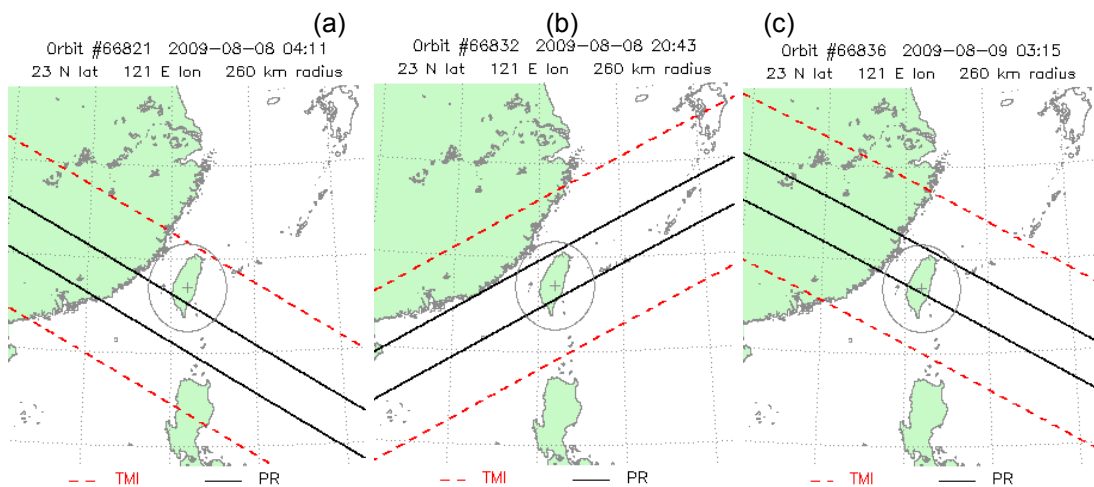


Figure 2. The swath of TRMM/TMI (red dash line) and of TRMM/PR (black solid line). (a) 2009/08/08 0411UTC; (b) 2009/08/08 2043UTC; (c) 2009/08/09 0315UTC.

Figure 3 and Figure 4 show retrieved rain rate distribution of Typhoon Morakot from PR, and from the retrieval method of Bayesian approach respectively. In Fig. 3 of the PR rain map, the main heavy rain area is seen between the south of the Taiwan Straits (21°N, 118°E) and Bashi Channel (21°N, 120°E). Fig. 4 shows that the retrieved precipitation distributions are similar to PR rain map, although the retrieval rainfalls underestimate for the most heavy rain area.

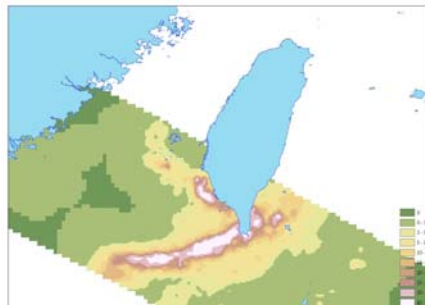


Figure 3. The rain rate of Typhoon Morakot retrieved from PR at 0411 on 08 August 2009.

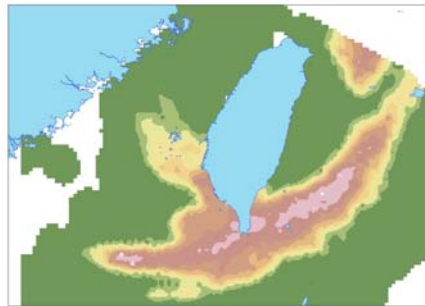


Figure 4. The rain rate of Typhoon Morakot retrieved from Bayesian approach at 0411 on 08 August 2009.

Three passes of Typhoon Morakot were used in our quantitative validations. After excluding land contamination, and there are 2860 match-up pixels are left in our comparisons. Figure 5 and Figure 6 show scatter plots of retrieved rain rate versus PR measurements. The coefficients of determination and total samples are also listed for two different lookup tables. Comparing Figure 5 with Figure 6, we have found that the lookup table made from GCE model and RTM has a little better performance than that from WRF model and RTM. The maximum of rain rate from lookup table from GCE model (Figure 5) have more heavy than it from WRF (Figure 6).

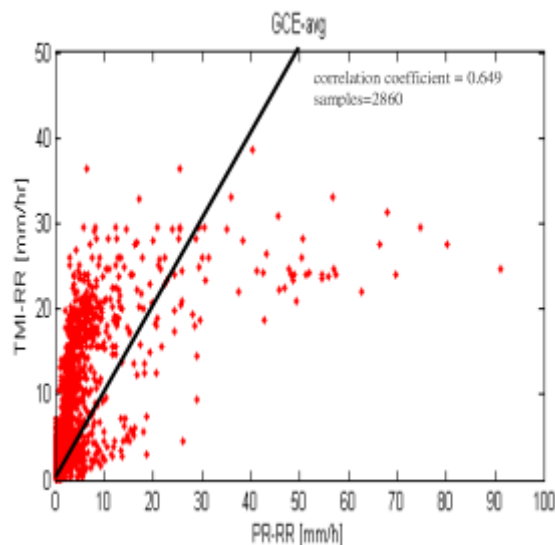


Figure 5. Scatter plots of retrieved rain rate versus PR measurements. Rain rate is retrieved using lookup table from GCE model. Coefficients of determination and total samples of three passes are also shown here.

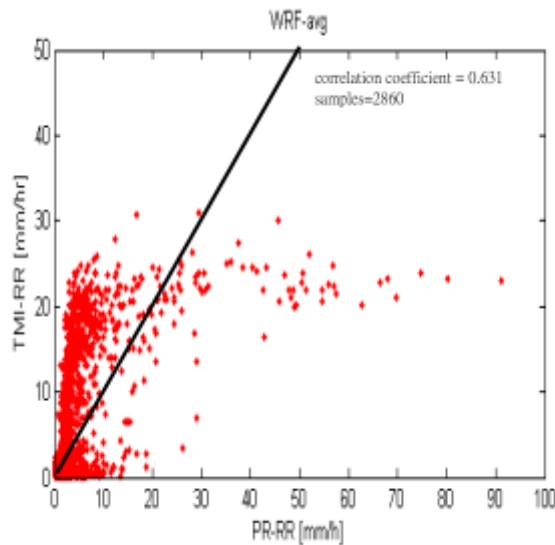


Fig. 6 the same with Fig. 5, but the rain rate is retrieved using lookup table from WRF model.

In addition, both of the two methods tend to overestimate in light rain rate regimes and underestimate in heavy rain rate regimes, as is a typical drawback for a linear statistical retrieval method.

5. CONCLUSION

The Bayesian approach was accepted in this study to retrieve rain rate over ocean using TRMM/TMI microwave brightness temperatures, with an emphasis on typhoon Morakot. In addition, an attenuation index as the observed variable was used in our method, because it has a monotonic relationship with rain rate, and is less influenced to water vapor, wind speed and sea surface temperature and so on.

There are three overpasses of TRMM satellite for Typhoon Morakot as case studies. The results show that the Bayesian retrievals and PR rain rate show significant similarity in horizontal distribution of precipitation, and the correlation coefficient between them is above 0.6.

6. REFERENCES

1. Adler, R. F., C. Kidd, G. Petty, M. Morrissey, and H. M. Goodman, 2001: Intercomparison of global precipitation products: The Third Precipitation Intercomparison Project (PIP-3). *Bull. Amer. Meteor. Soc.*, 82, 1377-1396.
2. Chiu, J. C. and G. W. Petty, 2006: Bayesian retrieval of complete posterior PDFs of oceanic rain rate from microwave observations. *J. Appl. Meteorol. Climatol.*, 45, 1073-1095.
3. Grecu, M. and W. S. Olson, 2006: Bayesian estimation of precipitation from satellite passive microwave observations using combined radar-radiometer retrievals. *J. Appl. Meteorol. Climatol.*, 45, 416-433.
4. Di Michele, S., A. Tassa, A. Mugnai, F. S. Marzano, P. Bauer, and J. P. V. P. Baptista, 2005: Bayesian algorithm for microwave-based precipitation retrieval:

- Description and application to TMI measurements over ocean. *IEEE Trans. Geosci. Remote Sensing*, 43, 778-791.
5. Evans, K. F., J. Turk, T. Wong, and G. L. Stephens, 1995: A Bayesian approach to microwave precipitation profile retrieval. *J. Appl. Meteorol.*, 34, 260-279.
 6. Kummerow, C., 1998: Beam-filling errors in passive microwave rain fall retrievals. *J. Appl. Meteorol.*, 37, 356-370.
 7. Marzano, F. S., E. Fionda, P. Ciotti, and A. Martellucci, 2002: Ground-based multi frequency microwave radiometry for rainfall remote sensing. *IEEE Trans. Geosci. Remote Sens.*, 40, 742-759.
 8. Benedetti, A., P. Lopez, E. Moreau, P. Bauer, and V. Venugopal, 2005: Verification of TMI-adjusted rainfall analyses of tropical cyclones at ECMWF using TRMM precipitation radar. *J. Appl. Meteorol.*, 44, 1677-1690.
 9. Olson, W. S., C. D. Kummerow, G. M. Heymsfield, and L. Giglio, 1996: A method for combined passive-active microwave retrievals of cloud and precipitation profiles. *J. Appl. Meteorol.*, 35, 1763-1789.
 10. Petty, G. W., 1994: Physical retrievals of over-ocean rain rate from multi channel microwave imagery. Part I: Theoretical characteristics of normalized polarization and scattering indices. *Meteorol. Atmos. Phys.*, 54, 79-99,

CORRECTING THE CMORPH BIAS USING A DAILY GAUGE ANALYSIS

Soo-Hyun Yoo and Pingping Xie

NOAA Climate Prediction Center

e-mail: soo-hyun.yoo@noaa.gov

ABSTRACT

A new technique is developed to correct the bias in the high-resolution CMORPH satellite estimates using gauge observations on a 0.25° lat/lon grid over the global land areas. The correction is by matching the PDF of the CMORPH estimates with the CPC unified global daily gauge analysis. The PDF matching is first carried out for each grid box and for each calendar day using co-located CMORPH and gauge data over a spatial domain centering at the target grid box and over a 31-day period centering at the target calendar day for a 10-year period from 2000 to the present. This practice ensures reasonable correction of the seasonally and regionally changing bias over the entire global land. Bias remaining in the CMORPH caused by year-to-year variations of observing instruments and precipitation systems is then removed through PDF matching using recent data over a 30-day period ending at the target date. Examinations demonstrated stable performance of this procedure in removing CMORPH bias over regions with different gauge network configurations and precipitation patterns.

1. INTRODUCTION

Over the past 10 years or so, several new techniques have been developed to integrate passive microwave (PMW) observations from low earth orbit (LEO) satellites and infrared (IR) observations from geostationary platforms (GEO) into satellite-based global precipitation estimates with the best time / space resolution and quantitative accuracy (Hsu et al. 1997; Turk et al. 2004; Huffman et al. 2004, 2007; Joyce et al. 2004; Ushio et al. 2009). Examinations studies showed reasonable skills of the products of these techniques in representing the spatial patterns and temporal variations of global precipitation with refined time / space scales compared to products of previous generations (Xie et al 2007; Ebert et al. 2007; Shen et al. 2009).

One major problem in the current version of the high-resolution satellite precipitation products is the bias passed through from the PMW rainfall retrievals used as primary inputs to the integrating procedures. These biases may cause problems in applications where accurate representation of absolute precipitation magnitude is required (Tian et al. 2007).

In this paper, we describe a new technique developed recently at NOAA Climate Prediction Center (CPC) to remove the bias in the high-resolution satellite precipitation estimates over the global land through calibration against an gauge-based analysis. The technique is developed for the global precipitation fields generated by the CPC Morphing technique (CMORPH, Joyce et al. 2004), but it should be applicable to the adjustment of satellite precipitation estimates from other techniques which present similar bias structures.

2. CMORPH AND GAUGE DATA

CPC Morphing (CMORPH) technique is developed to generate high-quality, high resolution global precipitation estimates through integrating information from all available satellite observations from both geostationary (GEO) and low earth orbit (LEO) platforms (Joyce et al. 2004). First, instantaneous rain rates retrieved from various passive microwave (PMW) sensors are calibrated against a common reference, retrievals from the Tropical Rainfall Measurement Mission (TRMM) Microwave Imager (TMI), to ensure quantitative consistency among the various PMW inputs. Advection vectors of the cloud / precipitation systems are then computed from the infrared (IR) images observed by GEO satellites in 30-min intervals. Calibrated PMW retrievals from individual LEO satellites are finally propagated from their observation times to the analysis time to get the integrated estimates of global precipitation. As of December 2010, the CMORPH satellite precipitation estimates are produced on an 8kmx8km resolution over the globe from 60°S to 60°N and in a time interval of 30-min for a 13-year period from August 1998 to the present. In this study, the CMORPH estimates at their original resolution are integrated into hourly precipitation estimates on a 0.25°lat/lon grid over the globe.

The gauge-based analysis of daily precipitation used in this study to calibrate the CMORPH satellite estimates is the CPC Unified Global Daily Gauge Analysis (Xie et al. 2010). The analysis is constructed by interpolating quality controlled gauge reports of daily precipitation from over 30,000 stations over the global land. Available for a 32-year period from 1979, the daily gauge analysis is originally created on a 0.125°lat/lon grid over the globe and integrated into a 0.25°lat/lon grid for use in this work.

Ending time of a daily report differs from country to country. To ensure complete match, daily precipitation for CMORPH satellite estimates are assembled from the hourly fields with daily ending time consistent with that of the local gauge reports.

3. CMORPH BIAS

First, structures of the CMORPH biases are examined through comparisons against the daily gauge analysis for a 10-year period from 2000 to 2009. Only pairs of CMORPH and gauge analysis data at grid boxes with at least one reporting station are included in the calculation to ensure quantitative accuracy.

CMORPH bias presents large seasonal variations, with an over-/under-estimation of ~1mm/day during summer / winter for daily rainfall averaged over the entire contiguous United States (CONUS) (Fig.1,top). In addition, the CMORPH also contains substantial bias of sub-monthly (Fig.1, middle) and inter-annual time scales (Fig.1, bottom). The CMORPH also presents range-dependent bias, with over- and under-estimation for weak and strong precipitation events, respectively (Fig. 2).

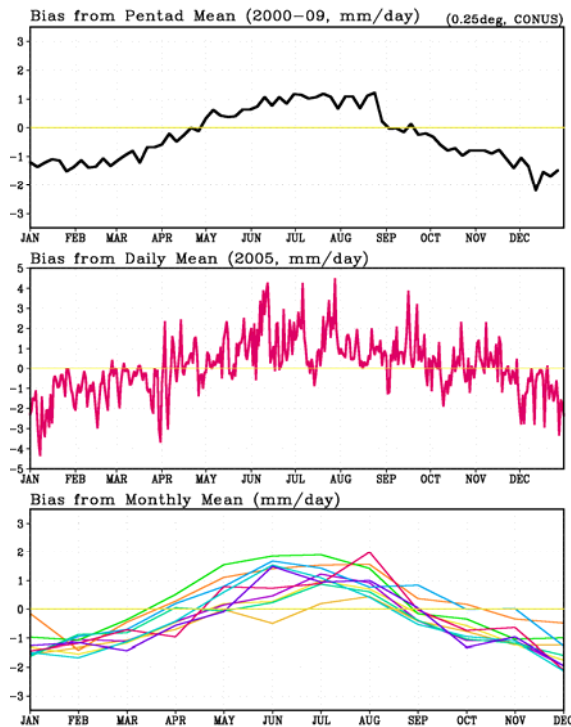


Figure 1. Time series of CONUS mean CMORPH bias (mm/day) a) averaged over 2000-1009 (top); b) for 2005 (middle); and c) for the 10 individual years (bottom). Bias for the individual years plotted in the bottom panel is smoothed to monthly scale.

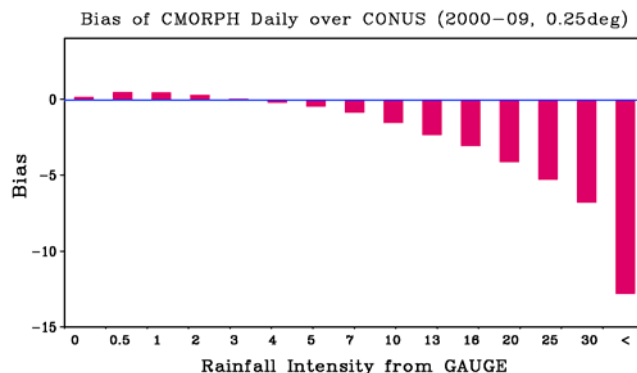


Figure 2. CMORPH bias (mm/day) as a function of rainfall intensity measured from daily gauge analysis. The bias is computed by comparison with co-located daily gauge analysis over the CONUS for a 10-year period from 2000 to 2009.

4. BIAS CORRECTION AGAINST DAILY GAUGE DATA

The range dependency and substantial magnitude of sub-monthly time scales of the CMORPH biases suggest that the bias in the high-resolution satellite estimates needs to be calibrated against daily gauge observations through non-linear processing. To this end, Xiong et al. (2008) developed a conceptual model to calibrate the bias in the CMORPH by matching the accumulated probability density function (PDF) for the CMORPH with that for the daily gauge analysis of Xie et al. (2010) over China. The PDF tables are created for each 1.0° lat/lon grid box for each target day using co-located CMORPH and gauge data collected over a spatial domain centering at the target grid box and for a 30-day period ending at the target day. Only data pairs over 0.25° lat/lon grid boxes with at least one reporting gauge are included. The spatial domain is expended until more than 500 data pairs are collected to ensure stable PDF tables.

The conceptual model described above works well over regions with reasonable gauge coverage. In applying the model to gauge sparse regions such as Africa, co-located data pairs have to be collected from a very extensive region. This degrades the spatial representativeness of the bias structure reflected in the resulting PDF tables. To solve this problem, we devised a strategy to perform the PDF bias correction in two steps.

First, bias in the CMORPH satellite estimates are corrected using PDF tables defined from historical data. PDF tables for the original CMORPH and gauge observations are constructed for each 1.0° lat/lon grid box and for each calendar day using co-located satellite and gauge data collected over a spatial domain centering at the target grid box and for a 31-day sliding window centering at the target calendar day over the 10-year period from 2000 to 2009. The spatial domain is expended from 1° lat/lon until 500 pairs of data are secured.

Use of historical data ensures the collection of sufficient number of data pairs from a relatively small domain. This greatly improves the spatial representativeness and the statistical robustness of the PDF tables upon which the bias correction is performed. The PDF correction based on the historical data, however, is unable to remove the year-to-year variations of the CMORPH bias as shown in the bottom panel of Fig. 1. To this end, a second step is incorporated to conduct the bias correction for the historical data corrected CMORPH using PDF tables from real-time data for a 30-day period ending at the target date.

We applied the procedures described above to correct the bias in the original CMORPH for a 10-year period from 2000 to 2009. As shown in Fig. 3, the CMORPH high-resolution precipitation analysis is capable of capturing the spatial distribution patterns of global precipitation very well, while it tends to over- and under-estimate the precipitation over tropical and mid-latitude land areas, respectively. The bias corrected CMORPH (Fig.3; bottom) exhibits magnitude very close to that of the gauge analysis. Differences between the bias-corrected CMORPH and the gauge data are mainly observed over gauge sparse regions (e.g. Africa) and present in small scales, a combined effect of the larger spatial domain required to define the PDF tables and the error in the gauge analysis over the regions. After the bias correction, the correlation

with the daily gauge analysis is improved from 0.600 to 0.695, while the bias is reduced from -0.311 to -0.137 mm/day.

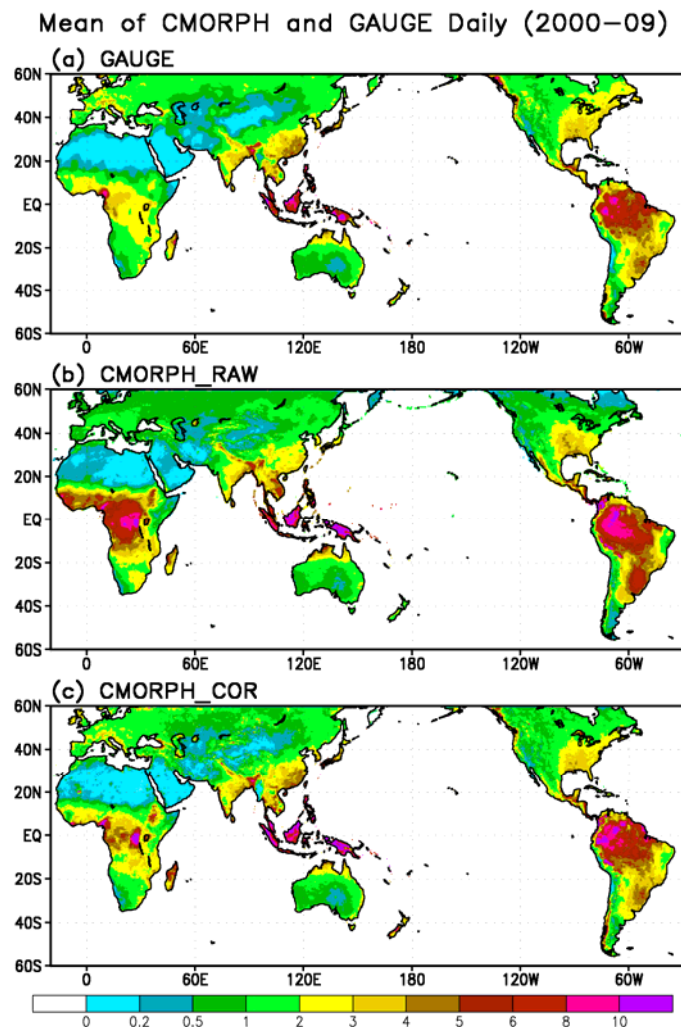


Figure 3. Distribution of 2000-2009 annual mean precipitation (mm/day) derived from the CPC daily gauge analysis (top), the original CMORPH (middle), and the bias-corrected CMORPH (bottom).

	Correlation	Bias
CMORPH_RAW	0.600	- 0.311
CMORPH_COR	0.695	- 0.137

Table 1: Comparison results between the daily gauge analysis and the original and bias-corrected CMORPH over the global land from 2000 to 2009.

To further understand the performance of our new gauge bias correction algorithm, we compared the CMOPRH satellite estimates with gauge data over two important regions: the CONUS and the Africa.

Pattern correlation is improved consistently throughout the annual cycle and for both regions examined here. Bias in the original CMORPH is reduced substantially. The gauge-adjusted CMORPH presents slightly negative bias, especially during cold seasons over CONUS. A preliminary inspection found that this is caused mainly by cases when the PMW retrievals are unable to detect rain.

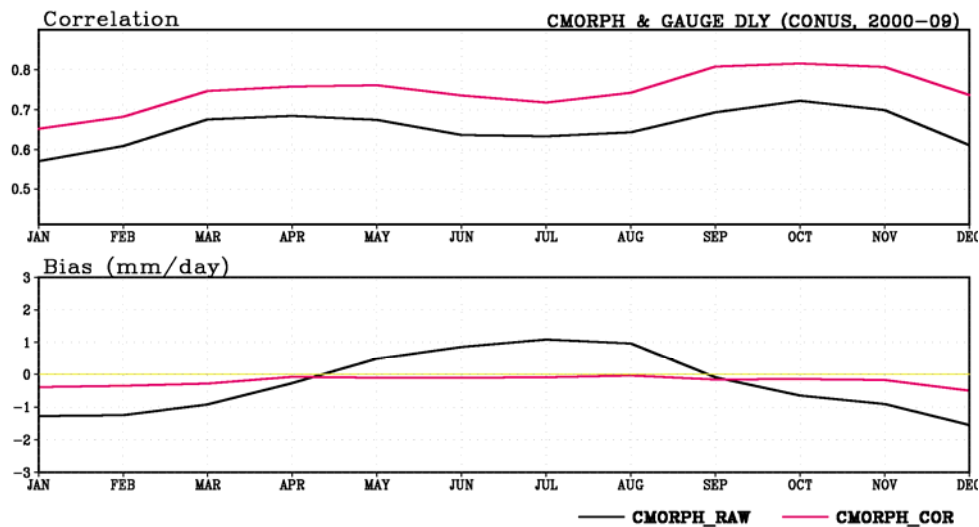


Figure 4. Mean annual cycle of (top) correlation and (bottom) bias (mm/day) between the original (black) / Bias-corrected CMORPH and the daily gauge data over CONUS.

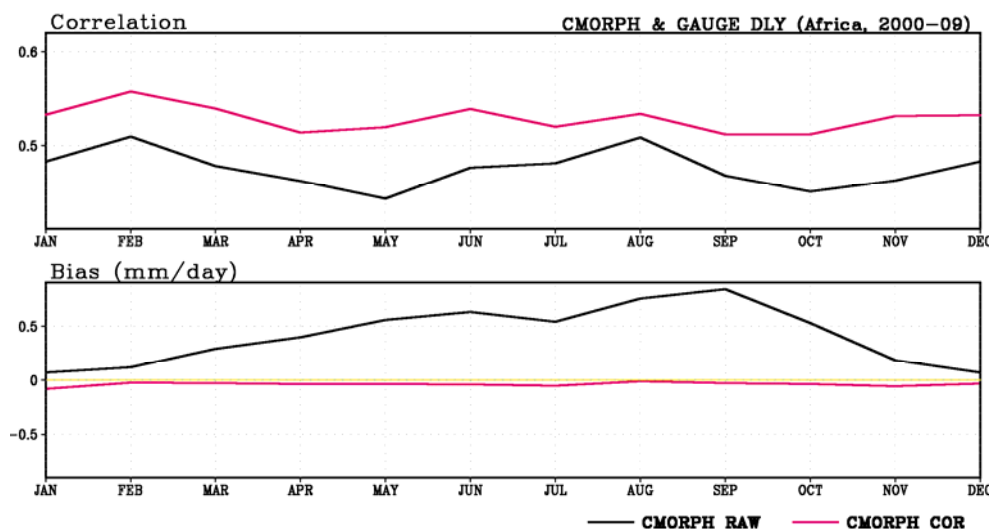


Figure 5. The same as in Fig. 4, except for comparisons over Africa.

5. SUMMARY

High-resolution satellite precipitation estimates such as those of CMORPH present temporally changing and spatially varying bias with range dependency. To remove the bias, we developed a technique to adjust the CMORPH through matching the cumulated probability density function (PDF) of the satellite estimates against that of the daily gauge analysis in two successive steps using historical and real-time data, respectively.

Preliminary examinations showed effective removing of the bias over most of the global land areas and for most time especially during the warm seasons. A prototype operational system has been developed to perform the bias correction on a real-time basis using the algorithm described in this paper.

Further work is under way to perform cross-validations for the algorithms and to develop bias correction algorithms for high-resolution satellite precipitation estimates over oceans.

REFERENCES

- Ebert, E. E., J. E. Janowiak, and C. Kidd, 2007: Comparison of Near Real Time Precipitation Estimates from Satellite Observations and Numerical Models. *Bull. Amer. Meteor. Soc.*, DOI:10.1175/BAMS-88-1-47.
- Hsu, K-L, X. Gao, S. Sorooshian, and V. Gupta, 1997: Precipitation estimation from remotely sensed information using artificial neural networks. *J. Appl. Meteor.*, **36**, 1176 – 1190.
- Huffman, G. J., R. F. Adler, E. F. Stoker, D. T. Bolvin, and E. J. Nelkin, 2004: Analyses of TRMM 3-hourly multi-satellite precipitation estimates computed in both real and post-real time. *AMS 12th Conf. on Satellite Meteorology & Oceanography*. 11-15 January, 2004, Seattle, WA.
- Huffman, G. J., R. F. Adler, D. T. Bolvin, G. Gu, E. J. Nelkin, K. P. Bowman, E. F. Stoker, D.B. Wolff, 2007: The TRMM Multi-satellite Precipitation Analysis: Quasi-Global, Multi-Year, Combined-Sensor Precipitation Estimates at Fine Scale. *J. Hydrometeor.*, **8**, 38-55.
- Joyce, R. J., J. E. Janowiak, P. A. Arkin, and P. Xie, 2004: CMORPH: A method that produces global precipitation estimates from passive microwave and infrared data at high spatial and temporal resolution. *J. Hydrometeor.*, **5**, 487 – 503.
- Shen, Y., A.-Y. Xiong, Y. Wang, and P. Xie, 2009: Performance of high-resolution satellite precipitation products over China. *J. Geophys. Res.*, **115**, D02114, doi:10.1029/2009JD012097.
- Tian, Y., C. D. Peters-Lidard, B. Choudhury, and M. Garcia, 2007: Multitemporal analysis of TRMM-based satellite precipitation products for land data assimilation applications. *J. Hydrometeor.*, **8**, 1165-1183.
- Turk, F. J., E. E. Ebert, B.-J. Sohn, H.-J. Oh, V. Levizzani, E. A. Smith, and R. Ferraro, 2004: Validation of an operational global precipitation analysis at short time scales. *12thAMS Conf. on Satellite Meteorology and Oceanography*, 11-15 January, 2004, Seattle, WA.

- Ushio, T., K. Sasashige, T. Kubota, S. Shige, K. Okamoto, K. Aonashi, T. Inoue, N. Takahashi, T. Iguchi, M. Kachi, R. Oki, T. Morimoto and Z. Kawasaki, 2009: A Kalman Filter Approach to the Global Satellite Mapping of Precipitation (GSMaP) from Combined Passive Microwave and Infrared Radiometric Data. *J. Meteor. Soc. Japan*, **87A**, 137-151.
- Xie, P., M. Chen, A. Yatagai, T. Hayasaka, Y. Fukushima, and S. Yang, 2007: A gauge-based analysis of daily precipitation over East Asia. *J. Hydrometeor.*, **8**, 607 – 626.
- Xie, P., M. Chen, and W. Shi, 2010: CPC unified gauge-based analysis of global daily precipitation. *AMS 24th Conf. on Hydrology*. Jan.18 -21, 2010, Atlanta, GA.
- Xiong, A., P. Xie, J. Liang, Y. Shen, J. Joyce, J. E. Janowiak, and P. A. Arkin, 2008: Merging gauge observations and satellite estimates of daily precipitation over China. *4th International Precipitation Working Group (IPWG) Workshop*. 13-17 October, 2008. Beijing, CHINA.

INVESTIGATION OF TRENDS IN THE MOISTURE BUDGET OF THE TROPICAL ATMOSPHERE

Matthias Zahn¹ and Richard P. Allan²

¹ Environmental Systems Science Centre, University of Reading, 3 Earley Gate,
Reading, Berkshire, RG6 6AL, UK.

² Department of Meteorology, University of Reading, Earley Gate, PO Box 243,
Reading, RG6 6BB, UK

e-mail: m.zahn@reading.ac.uk

ABSTRACT

Recent studies have found contradicting results regarding the tropical atmospheric circulation (TAC) has intensified or weakened in the recent past. We here conduct a preliminary study to investigate changes in TAC and in tropical moisture transports. We divided the tropics between $\pm 30^\circ$ latitude into regions with upward and downward vertical wind motion, representing the ascending (ASC) and descending (DESC) branches of TAC. Typically moisture is advected from DESC into ASC at the lower levels of the atmosphere and from ASC into DESC at the upper levels. The moisture budget of ASC has been calculated in terms of the difference between precipitation and evaporation (P-E) and in terms of moisture fluxes along the boundary separating ASC and DESC.

In addition to mean values often used for calculating moisture transports we here also used instantaneous moisture values and wind vectors. Between both ways of calculating the moisture budget we found large discrepancies not only in the total water budget, but also in the annual cycle and in the vertical profiles highlighting the importance of using instantaneous values instead of mean values over time.

1 INTRODUCTION

The tropical atmospheric circulation (TAC) carries huge amounts of moisture and thus constitutes an important component of the Global Water Cycle. Some elements of the TAC, such as the Hadley Cell, can even extend to the extra-tropics. Changes in the intensity of TAC can affect the tropical moisture transports and can impact the characteristics of precipitation inside as well as outside the tropics.

TAC patterns are typically characterised by regions of rising air, e.g. due to more pronounced surface heating. The supply of continuously rising air causes horizontal divergence of air at upper levels. While being moved away this air cools again and sinks some distance from the region of rising. Low level flow is typically directed towards the region of rising. The most prominent example of such a pattern is the Hadley Circulation, extending over the tropical region of the whole globe.

Different answers, whether TAC has intensified or weakened in the past are given in literature, with e.g. Vecchi et al. [2006] finding a weakening, but Sohn and Park [2010] finding a strengthening. We here reinvestigate recent trends in the TAC applying mean as well as instantaneous values by means of the moisture transport. So far we have not distinguished between changes in atmospheric moisture amounts and changes in wind strength.

2 DATA AND METHOD

To investigate moisture fluxes of the TAC we applied global reanalysis data from ERA-interim [Simmons et al., 2007] developed at the European Centre for Medium-Range Weather Forecast (ECMWF). From ERA-interim horizontal and vertical wind vectors (U, V and ω), specific humidity (Q) and vertical pressure information were used for the period 1989-2008 and between $\pm 30^\circ$ latitude, representing the tropics. Calculations were restricted to the lowest 30 model levels (representing the atmosphere up to an altitude of $\approx 200\text{hPa}$), which contain almost all of the atmospheric moisture. Additionally, precipitation (P) and evaporation (E) were used as a reference to confirm the resulting moisture budgets. The change of TAC in our study is characterized by means of changing transports along a boundary separating regions of upward (ASC) and downward (DESC) vertical wind motion in the tropics. Accordingly our calculations were subdivided into two steps:

- first, the boundary along the ASC regions has to be defined,
- then, the transport of water vapour over this boundary is calculated.

2.1 DEFINITION OF BOUNDARY SEPARATING ASCENDING AND DESCENDING BRANCH OF THE TROPICAL CIRCULATION

The regions of upward and downward vertical wind motion (ascending (ASC) and descending (DESC) regions), and thus the branches of the Hadley cell, vary over time. Although ASC and DESC are highly variable even on the six hourly timescale of ERA-interim, we in this first study used monthly mean ω for their identification. To distinguish between ASC and DESC ω at 500hPa level has previously been used [Allan and Soden, 2007]. Here vertically averaged monthly mean ω was calculated for each grid box, weighting ω by the thickness of each layer, respectively. Whenever we find different directions of this averaged ω in two neighbouring grid boxes, a boundary segment is defined between these two boxes. Two resulting examples of the computed boundary are given in Fig. 1 for northern and for December 1995 and Jun 1996.

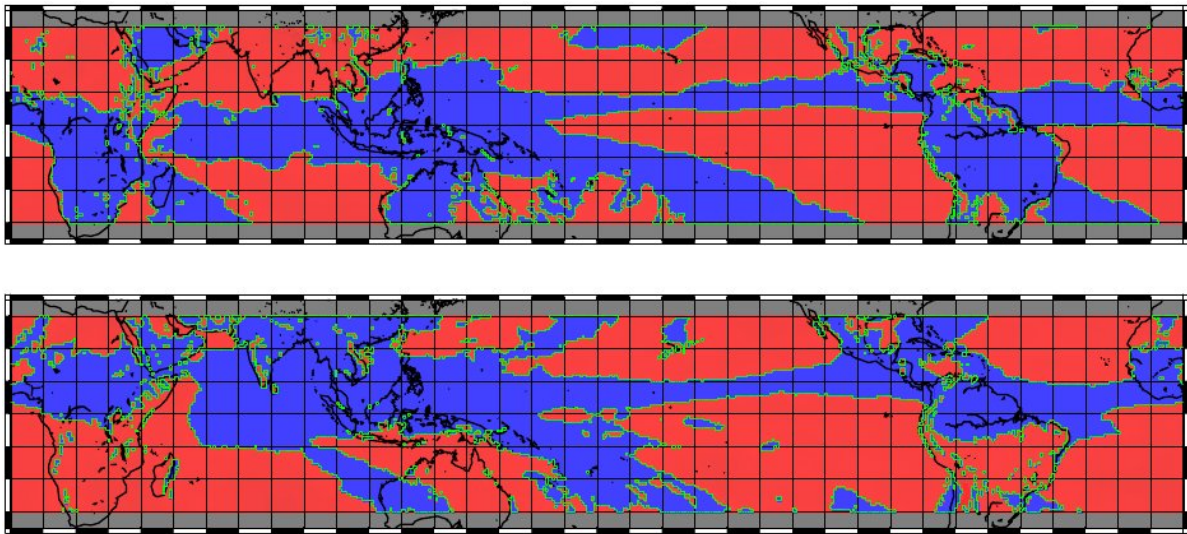


Figure 1. Direction of vertically averaged monthly mean ω per grid box in Dec 1995 (a) and Jun 1996(b). Regions with ascending (blue) and descending (red) vertical motions in the tropics and boundary (green line) separating both.

2.2. ESTIMATION OF THE MOISTURE BUDGET

To estimate the moisture budget, the moisture flux (MF) is calculated along all the n_b boundary segments b between ASC and DESC (green line in Fig. 1) each month. Therefore the perpendicular wind vector (WP) and the precipitable water content (PWC) are estimated along each boundary segment on each of the n_l model levels l . For each segment on each level, MF then is the product of WP and PWC. The total moisture budget at time t then is the sum of MF at each segment on each level:

$$MF_t = \sum_b^{n_b} \sum_l^{n_l} WP_{bl} * PWC_{bl} \quad (1)$$

This total moisture budget is calculated based on monthly average values for Q and U and V (MFmm) as well as based on (6-hourly) instantaneous values (MFhr). Additionally, precipitation and evaporation are used for all ASC grid boxes and the moisture budget is estimated from P-E.

3 RESULTS

Fig.2 shows the yearly time series and the yearly cycle of the moisture budget. Calculations are based on instantaneous (MFhr) wind and humidity on the one hand and based on monthly means (MFmm) on the other. Also given is the moisture budget estimated from precipitation minus evaporation as a reference.

There is a large offset between MFhr and MFmm. The influx into ASC is $\approx 25\%$ higher when mean values are applied. However, the yearly time series of MFhr and MFmm take a similar course: years of peak or minimum influx are usually the same, no matter if

mean or instantaneous values are applied. This situation is different in the yearly cycle. While in MFhr there are two peaks in the respective hemispheres' summers, in December/January and July/August, there is only one distinct peak found in MFmm, in southern summer. In other words: there is a relatively high correlation coefficient $r = 0.94$ between the yearly time series, but a considerably lower one of $r = 0.50$ in the yearly cycle.

Also shown in Fig.2 are the yearly time series and the yearly cycle of the moisture budget calculated from P-E. There is a similar mean budget in P-E and MFhr (323 and 320 km) and also the respective yearly and monthly values differ little. Differences may just be related to numerical reasons or to changing atmospheric moisture content (AMC). Note, that MF may either affect P-E or the total AMC over a given region, as

$$MF = P - E + \Delta AMC \quad (2)$$

The budgets from P-E and MFhr share the large offset compared to MFmm.

We calculated trends for all the three data sets based on the least squares method:

- P-E : $0.27 \frac{\text{km}^3}{\text{day} \cdot \text{year}}$
- MFhr : $0.24 \frac{\text{km}^3}{\text{day} \cdot \text{year}}$
- MFmm : $0.51 \frac{\text{km}^3}{\text{day} \cdot \text{year}}$

All the trends are positive, but none of them is significantly (according to a t-test based on the yearly values) different from 0. We found the trend in MFhr and P-E to be of a similar strength, whereas the trend in MFmm is approximately twice as large.

To find out the reason for the large discrepancies between MFmm and MFhr/P-E, we investigated closer the vertical profile of moisture fluxes along the boundary. A plot of the mean MFmm and MFhr over the whole time period is shown in Fig.3. In accordance to the lower level convergent flow (trade winds) of the Hadley Circulation, both data sets reflect the equator ward motions, indicated by inward fluxes of moisture into ASC. At the medium height and uppermost levels, fluxes are directed poleward in also accordance to the Hadley Cell's upper level divergence.

There is one substantial difference between the vertical profiles: while the lower level influx is of similar magnitude for both, MFhr and MFmm, there is a much lower outflow at the upper levels in MFmm. This lower outflow probably is the reason for the higher values in the moisture budget in MFmm. So far, we can only speculate about the reasons for this difference. We suggest, that largest upper level outward fluxes of moisture occur, when high amounts of PWC and high wind speeds directed outwards occur at the same time. This coincidence of high wind speeds and moisture are 'averaged out', when only monthly values are applied. Recall, that despite the relatively regular pattern of the Hadley Cell, wind speeds can be very variable and even directed inwards to the ASC at upper levels, thus reducing the average strength of the outward directed wind speed.

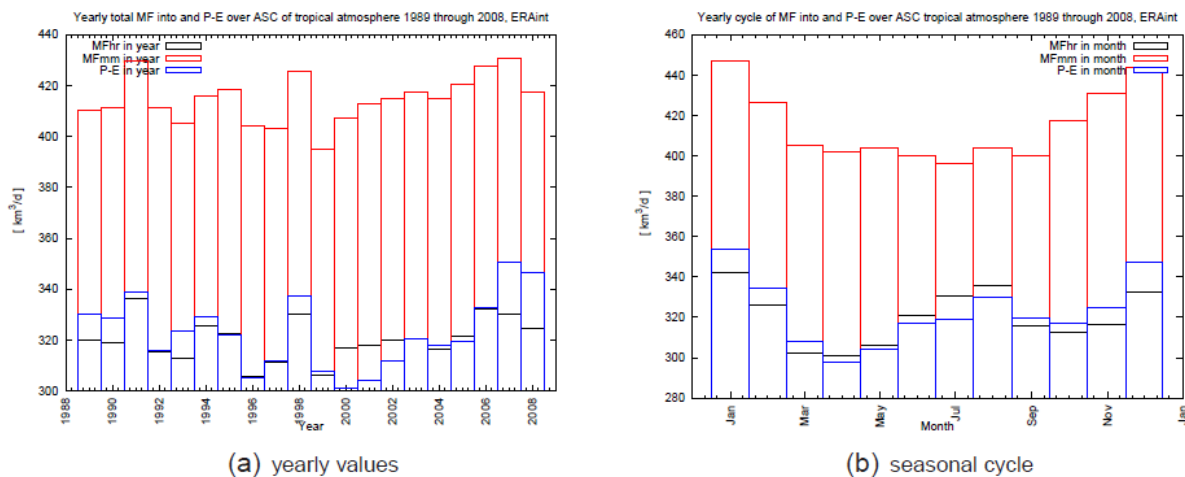


Figure 2. Yearly moisture budget calculated as atmospheric moisture transports based on instantaneous (MFhr) and monthly mean wind and humidity as well as on precipitation and evaporation. Time series (2(a)) and monthly mean values (2(b))

4 SUMMARY AND OUTLOOK

In our effort towards a reassessment of changes in the tropical moisture budget and changes in the tropical circulation, we have calculated the moisture transports using wind vectors and atmospheric humidity from ERA-interim. For the moisture flux calculations, we applied monthly mean values on the one hand, and 6 hourly instantaneous values on the other. We found a large offset in the calculations based on the monthly values as compared to those based on 6 hourly values. Unlike the budget from the monthly values, that of the 6 hourly values is close to a reference budget derived from the difference of precipitation and evaporation. We conclude, that there is a systematic error in the moisture budget calculated from the monthly mean values, which originates from badly represented fluxes in the upper model levels. This error does not only influence the amount of the budgets, but also leads to an inaccurate annual cycle of the budget as well as to an overestimated trend.

We conclude for our further investigations, that mean values are inadequate for the moisture budget calculations. For the sake of simplicity we in this study have applied a mask for regions of rising and sinking motion which is based on monthly mean vertical winds. To what extent the usage of mean values for the definition of regions and the boundary line over which the moisture transports are calculated remains to be investigated.

Further future tasks will be to compare moisture fluxes in ERA-interim with satellite data for validation purposes. Changes in moisture transports can be due to changing wind patterns or changes in atmospheric moisture content. Thus, another branch of investigations will be to relate changes to either of these options.

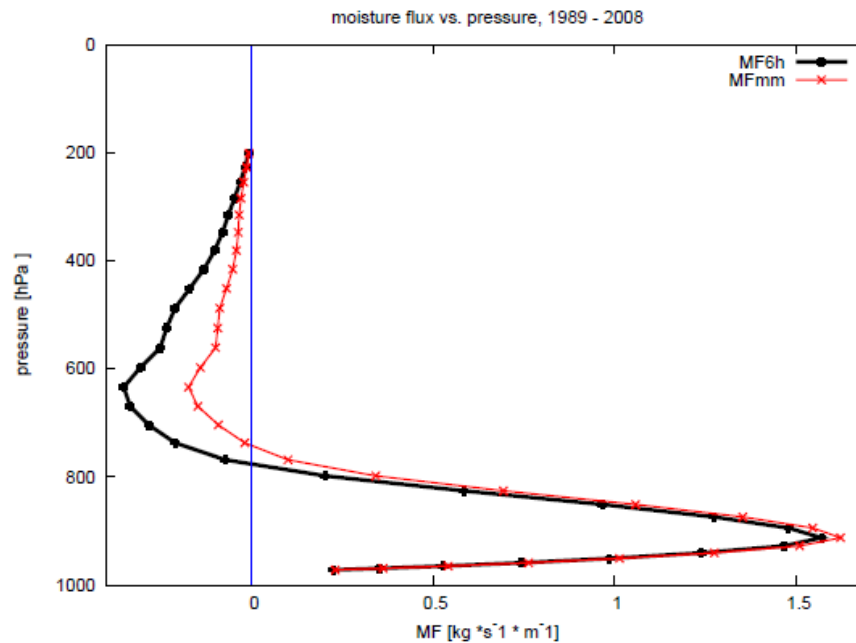


Figure 3. Average vertical profile of moisture transport (moisture transport against pressure) into ascending regions of the tropics calculated based on instantaneous (black) as well as on monthly mean (red) values.

References

Allan, R. P., and B. J. Soden, Large discrepancy between observed and simulated precipitation trends in the ascending and descending branches of the tropical circulation, *Geophys. Res. Lett.*, 34, 2007.

Simmons, A., S. U. J., D. Dee, and S. Kobayashi, Era-Interim: New ECMWF reanalysis products from 1989 onwards, *Newsletter 110*, ECMWF, 2007.

Sohn, B. J., and S.-C. Park, Strengthened tropical circulations in past three decades inferred from water vapor transport, *J. Geophys. Res.*, 11, 2010.

Vecchi, G. A., B. J. Soden, A. T. Wittenberg, I. M. Held, A. Leetmaa, and M. J. Harrison, Weakening of tropical Pacific atmospheric circulation due to anthropogenic forcing, *Nature*, 441, 73–76, 2006.

WORKING GROUP REPORTS

RESEARCH AND NEW TECHNOLOGIES WORKING GROUP

Chair: Nai-Yu Wang
Rapporteur: Joe Turk

e-mail: nai-yu.wang@noaa.gov

Participants: Robert Adler, K. Aonashi, Axel Andersson, Ali Behrangi, Sid Boukabara, Ralph Ferraro, Robert Joyce, Misako Kachi, Takuji Kubota, Vincenzo Levizzani, Riko Oki, Mario Mech, Mi-Lin Ou, Shoichi Shige, Yudong Tian, Joe Turk, Nan-Ching Yeh, Soo-Hyun Yoo, Nai-Yu Wang,

FROM PREVIOUS MEETING SUMMARY

RECOMMENDATIONS

IPWG website- currently has links to different datasets, but don't often get updated with changes to products, descriptions, etc. First action is to update the product lists on IPWG, action to each dataset provider or new datasets. (Algorithms and datasets)- suggest an online form that VL would provide passwd to.

Merged algorithm datasets- suggestion was to advertise to the various satellite simulator development (Matsui, Tanelli etc) the development of multi satellite datasets. Currently being done- these simulators can already do radars/radiometers, VIS/MW, etc.

Recommendations for support of incorporation of model products into precipitation products- CloudSat/PMM starting to do this in their science efforts, not so much in Europe which has not yet approved a precip mission. Suggest more synergy between related missions, eg SMAP, SMOS (soil moisture).

Recommendation- developers focus on light precip rates, such as level of ambiguous detectability threshold. Algorithm developers to specify detectability level in their product descriptions. Better methods and evaluations to determine how much light rain is being missed. 1 mm/day is the best we can do. Accumulation are often too large unless minimum detectability of Level-2 product is taken into account.

Recommendation: synergy of orbits to allow synergy (ie, A-Train). Noted that JAXA GCOM-W to fly in the A-Train orbit, allowing comparison with AMSR-E.

Recommendation- agencies to support HF channels for rain over land/ocean. AMSR3 will be on GCOM-W2, will include 150/190 GHz on AMSR3. Continue recommendation,

noting that conically scanning imager/sounder are being used (SSMIS) in model DA, so modelers are getting used to these data also.

Recommendation- should snowfall workshops be continued? Better coordination with other communities, eg hydrology, sea ice. Need more diverse representation at the snowfall meetings. Hydrologists always want the highest resolution- incorporate more input from hydrological model groups (not sure how this is different from current recommendation). More participation from the NWP DA community since there is much overlap between the DA/precip groups (fwd models, sensor characterization). Better timing between specialty (snowfall) workshop and IPWG workshop

Recommendation- data sharing between international agencies (eg, AMSR2, MADRAS), etc. Second ground station for M-T has already been done.

Recommendation for space radar measurements able to sense within 100-200 m of the surface with sensitivity near -20 to -30 dB. Need to update status for new recommendations.

STATEMENTS

Band protection and maintenance of specific bands. Keep as a statement for future CGMS requests.

Support for future missions with highest resolution imager or sounder (rather than saying imagers or sounders) HF channels relevant to light precip (conically scanning preferred). Discuss more in the plenary session.

Continue recommending support for geostationary microwave measurements – based on superior time sampling of the precip process. Having the precipitation even in a course scale (FOV of ~50km) is extremely useful since it can be combined with coincident GOES multi-spectral to get fine scale rain rate.

Stress the need for continued free and open access to data- fundamental to CGMS- realtime as much as possible. Russian satellite (METEOR-M) access? (also FY-3A, M-T MADRAS, etc) - Suggest having this as action for CGMS rapporteur.

(End of review from previous meeting)

RESEARCH

ALGORITHMS AND RETRIEVALS

1. Status/direction of high latitude, light rain/snowfall- over ocean, over land? Define what we mean by light precipitation.

HF (150/183) microwave methods can pick up stratiform precip when ice is present; if no ice not detected. Temperature sounding channels for detection of warm rain over both land and ocean. Combined CloudSat/MODIS/AMSRE data combinations to use train AMSU-only retrievals. Explore use of LPVEx (and future field expt) data to study more use of these channels with ground validation datasets to verify. Nature of error better understood today better than two years ago. Suggest more regional development of these techniques rather than trying to run it globally. Ongoing LSWG analysis to assist HF techniques with better surface emissivities. Connection with ITWG subgroup on the emissivity issue through the ITWG speciality meetings (3rd workshop in NY in June 2011). (Nai-Yu Wang, Mario Mech).

2. Further advanced in multispectral/multisensor techniques, eg ill-posed retrievals such as sfc emissivity, 3-D radtran, beamfilling, tracking/morphing, bin microphysics in CRM's, info on particle shape, size etc.

Continue exploitation cloud phase/property information from SEVIRI-like imagers (Bob Kuligowski, Ali Behrangi) to adapt to future geostationary imagers. Currently vis/WV/IR are most useful since all geosats have them. Multispectral sampling from microwave also has not been very well exploited. Do we need to develop and construct multi-geo composites of more than just longwave channel data (vis, near-IR, etc). The rising popularity of distributed hydrologic and land-surface modeling and recent enhancements of atmospheric models' resolution have contributed to the increasing demands for accurate high resolution precipitation data.

3. Leveraging non-precip specific missions eg SMAP, Aquarius, SMOS, humidity sounders, lightning, aerosol, hydrology records, etc. (Also scatterometers, GRACE, GPS, MODIS).

Information from these missions are useful to components of the precipitation retrieval problem. Encourage interaction amongst these programs at the program management level rather than only at the science level. Soil moisture retrievals to better derive surface emissivity. More representation from soil moisture community in particular (Joe Turk, Ralph Ferraro).

4. Leverage ground-based methods (radars, gauges etc) to complement space based retrievals, vertical profiles, etc.

GPM-GV program as a template of how this is to be done (GV data, algorithm and model communities come together). Exploitation of ground radar profile at the time of the satellite overpass (ground radar is at a lower frequency that is not attainable from space). Need to expand high latitude gauge data collection. Integration and incorporation of ground data to modelers and for continuous observation of surface emissivity. Ask Paul Kucera to report on ground data availability from NCAR repositories. Parameters that assist deep snow emissivity modeling (density profile).

CLIMATE PRODUCTS (AND DATA ISSUES)

1. Methods to keep track of SSMI and SSMIS data records (UPP-CP, Scope-CM, NCDC/CSU, EUMETSAT CM-SAF, RSS).

Bring up to plenary on Thursday- suggest Matt Sapiano/Wes Berg as POC, Karsten Fenning at CM-SAF. Suggest UPP-CP and CSU coordinate efforts. Exploit overlap period between SSMI/SSMIS to extend data reprocessing back to 2003 and into the future.

Ongoing thru GSICS, Scope-CM, etc. Example is the NCDC stewardship effort. Ongoing progress in this area in the creation of fundamental climate records.

Encourage better coordination of overpass times between satellite operators. Early afternoon gap is particularly vulnerable. A-Train samples at 1330 and often the NOAA satellites drift in time to slots that are not ideal for precip. Consider overpass times for NOAA/JPSS that are coordinated to drift to revisit gap periods. Maintenance of backup satellites to fill revisit time gaps as long as possible (action for operational satellite group). Currently miss late afternoon if NOAA-15 is unavailable.

Representation from the ocean fluxes community (was done this time) is a good idea and to encourage more synergy between ocean heat flux and precip communities- use of similar data, etc. And in future with ocean salinity community (eg, Aquarius). (Axel Andersson)

Common data formats- precipitation data to keep advised of changes to formats used by data providers.

DATA ASSIMILATION

1. Assimilation of Cloud/Rain affected radiances
2. Recent May 2010 meeting at ECMWF on this topic (George Ohring and Peter Bauer have report). Include their recommendations into this report. Did not have much discussion from this topic at this meeting, should encourage operational agencies to send people. However, assimilation of precipitation products directly are used by other areas (non-NWP) and there are research studies ongoing to use these products in a realtime mode. (Sid Boukabara)
3. Timely release of Level-1 data (radiances) from new sensors to NWP agencies for Cal/Val testing, to reduce the latency time from launch-to-operations.

NEW SENSORS AND TECHNOLOGY

1. Geo-MW. Encourage model simulation studies showing benefit of rapid microwave for severe weather forecasting.
2. Continue further studies for further microwave spectral measurements, eg 118, 220, 340 GHz, etc. in the context of NWP applications and storm intensity/track predictions. Ralph Ferraro to explore.
3. Status of space based radar techniques? CloudSat/ATrain studies on cloud properties ongoing since 2006. Cloud radars finding use for precip studies. Amount of light rain that is being “missed” by passive microwave. Adaptation of community models (CRTM) to simulate active radar/lidar directly (Sid as POC). Lidar/CloudSat synergy useful for precip-aerosol studies. Studies ongoing as CloudSat and PR still operating.
4. Long-term continuity of cloud/precip space radars. Cloud radar has shown potential for precipitation, keeps focus on new missions eg ACE, PPM.
5. Improved precip radar, eg 14/35/94 GHz, addition of Doppler, polarimetric measurements, with swath capability. Promote radar technologies that are able to probe closer to the surface than current PR is able to.
6. Lightning mapper. GOES-R, MTG, FY-4 already slated. Also support a LEO lightning mapper (GPM will not have) for finer resolution. Continue support for studies to fuse lightning data into retrievals, model assimilation, etc. Emerging science.
7. Encourage the maintenance of conically scanning microwave series. Low-inclination orbits are preferred. Prefer GPM-constellation at 40-degree latitude to maintain TRMM climate continuity. Continuity for SSMIS is crucial (DWSS sensor) and AMSR2/GCOM-W for climate records and operational users. Will need at least the 10 GHz on DWSS microwave to use for cross calibration with other sensors, also for soil moisture retrieval.

SPECIFIC NEW TECHNOLOGY RECOMMENDATIONS TO CGMS:

1. Need for geostationary microwave.
2. Longterm continuity of space-based radars
3. Longterm continuity of conically-scanning microwave imagers on operational missions
4. Coordination of satellite overpass times.

APPLICATIONS WORKING GROUP

Chair: Thomas Heinemann
Rapporteur: Steve Nesbitt

e-mail: thomas.heinemann@eumetsat.int .

Participants: Stephan Bakan, Daniel Barrera, Tufa Dinku, Kevin Garrett, George Huffman, Misako Kachi, Zhong Liu, Elena Tarnavsky, Soo-Hyun Yoo, Markus Ziese

1. EXPANSION OF USE OF PRECIPITATION PRODUCTS; TRAINING

IPWG recommendation to CGMS:

The IPWG recommends that CGMS endorse developing an initiative or tasking an existing initiative to interface between providers and users.

- IPWG recommends that CGMS ask WMO to identify and alleviate barriers in integrating satellite-derived precipitation products in operational activities in close cooperation with the IPWG. The co-chairs of IPWG will act as a point of contact for this initiative.
- IPWG recommends that CGMS encourages the WMO Space Program to advertise, organize, and provide information on existing relevant training events and online resources in organizations worldwide for training in the use of satellite precipitation products in NMHS and other applications. IPWG will provide assistance in technical content and lectures for such training activities.

Action (IPWG members): Actively participate in developing training materials and volunteering to make presentations at training venues, and if possible become proactive in developing training materials.

Action (IPWG members): Provide links to training materials to IPWG webmaster, make sure current links work

Action (Co-Chairs): Act as a point of contact for incoming requests for experts providing training materials and presentations to the user community

2. TIMELY DISSEMINATION OF RAIN GAUGE DATA

The IPWG has identified the lack of availability of rain gauge data sets in near real time to the precipitation research community as a major barrier in progress in developing and evaluating precipitation products.

IPWG recommendation to CGMS:

IPWG recommends that CGMS encourages WMO to facilitate the access to rain gauge data from NMHS and intensify data sharing activities from data sparse regions like

Africa, South America, and Asia. For example, we see projects like the WIFA initiative in Africa could be useful for satellite precipitation community.

3. GLOBALLY-MERGED IR DATASETS

The availability of the globally merged IR-brightness temperature data sets from geostationary satellites, as they are generated by NOAA-CPC, is essential for the generation of many precipitation products. Currently data can only be provided with a delay of 3 days due to a limitation by the EUMETSAT data policy. New satellite algorithms require these data sets in near real time.

Action (Thomas Heinemann): EUMETSAT will work with CPC to check availability of full resolution IR data in near real time for this data set.

4.1 WEB PAGE CONTENT

Various problems concerning the web page content were identified. In particular, there are inconsistencies between the lists of products and algorithms on the IPWG page. We should:

- a. update the product list to be current,
- b. add metadata to the product list, part of this can be taken from the algorithm inventory, and
- c. present product information in a table format for easier perusal by the users.

Action (TBD): Provide a template for products which can be based on template for algorithms (consult existing algorithm template, streamline ISO guidance), including definition of keywords (such as biosphere, agriculture, nowcasting).

Action (IPWG members): Product generators should update the current list of their products to the IPWG.

Action (IPWG webmaster): Create a table of products and corresponding metadata.

4.2 WEB PAGE VISIBILITY

The IPWG web page is difficult to find with search engines even if the keyword "IPWG" is known. Users searching for information on precipitation remote sensing in general will hardly find the IPWG web-page at all. An increased visibility of our web page is highly desirable.

Action (TBD): Investigate ways to make our web presence more visible. Add HTML tags to move link up on search engines. Shorten domain name by obtaining an org.int domain name.

Action (IPWG webmaster): Clean up data section. Main page should be made more user-friendly, information about IPWG should be on a separate page.

Action (Zhong Liu): Add 'frequently asked questions' section.

Action (Steve Nesbitt): Create links from Wikipedia to IPWG web page. First create IPWG Wikipedia page template in English, then provide it for translation in other languages.

5. USER REQUIREMENTS LIST

Operational agencies and some algorithm developers have collected requirements of various user communities. This information should be made available to all algorithm developers and product providers to help them to address the right user communities with their products or to improve the algorithm in the right direction.

Action (Thomas Heinemann): Create a user requirements list.

Action (IPWG members): Provide list of existing user requirements of various user groups to Thomas.Heinemann@eumetsat.int .

Action (IPWG webmaster): Include user requirements list on the IPWG web page.

6. DATA ARCHIVING AND REPROCESSING

IPWG recognizes the utility of homogeneous satellite precipitation datasets in the creation of climate data records.

IPWG recommendation to CGMS:

The IPWG recommends that CGMS members support reprocessing activities of all available satellite product archives as advances in algorithms or user requirements are made in order to maintain homogeneity in data records. These activities should cover both, current operational, and decommissioned L1 and L2 data products. The former would include primary operational GEO and LEO satellites (e.g., POES, MetOP, JPSS, etc.) and research satellites (e.g., EOS, TRMM, etc.) while the latter would include heritage data sets that span several satellites (e.g., MSU/AMSU, AVHRR, HIRS, etc.). When reprocessing occurs, we recommend that the existing archive of the prior version is kept available for at least 2 years for version intercomparison.

VALIDATION WORKING GROUP REPORT

Chair: Paul Kucera and Matt Sapiano
Rapporteur: Emad Habib

e-mail: p.kucera@ncar.edu

Participants: Bob Adler, Sagar Bajracharya, Andreas Becker, Karl Bumke, Karsten Fennig, David Grimes, Rafal Iwanski, Chris Kidd, Christian Klepp, Bob Kuligowski, Bozena Lapeta, Silvia Puca, Paola Salio, Shoichi Shige, Daniel Vila.

SUMMARY

The validation working group reviewed the previous 14 actions and found that progress on some recommendations was good, but poor on others. It was felt that it would be beneficial to have a narrower set of objectives with clear actions on each of the recommendations. The following 7 recommendations/actions were accepted by the Validation Working Group:

1. IPWG high resolution precipitation intercomparison
2. Validation of satellite data in hydrological models
3. Listing of data available for validation
4. Make collection of code to convert datasets to ASCII for validation.
5. Validation techniques
6. Encourage validation activities over Africa
7. Improve collection of validation data over data sparse areas of the oceans.

The validation working group had no recommendations/actions for CGMS or the wider IPWG group.

1. OVERVIEW

The group spent the first session going over old business from the last IPWG meeting, reviewing all 14 previous recommendations. Progress on many was encouraging although no progress had been made on some of the recommendations. It was felt that some of the previous recommendations that had not been achieved did not have sufficient merit to continue or had been achieved by other means. Based on the discussion, the Validation Working Group developed a list of seven recommendations. The list was reduced by half in an effort to provide more focused, achievable recommendations. The next section provides an overview the 2010 recommendation. The following section presents notes from the Validation Working Group general discussion. The final section provides a summary of the discussion of the 2008 Validation Working Group Recommendations.

2. RECOMMENDATIONS

1. IPWG high resolution precipitation inter-comparison

Conduct a global validation project drawing on international expertise of the Validation WG and the IPWG at large. The results of this inter-comparison should guide users to appropriate products given a particular situation. The study should focus on trying to understand where products are good/bad and why these differences exist (we need to use "local" expertise of the wider group to assess this). This activity should engage validation experts and algorithm developers from IPWG. The utilization of gauges from GTS and from GPCC should be explored as well as other possible databases.

Action: Adler/Sapiano

Develop a plan of how to proceed including science questions and scope of study. Take lead on obtaining and collating validation work.

Timeline: Circulate plan by January 2011; Expect preliminary results by IPWG6

2. Validation of satellite data in hydrological models

There is a need to assess the suitability of satellite products for hydrological models. We need to understand the conditions under which satellite precipitation estimates are useful for hydrological models, and at what time/space scales and geographic locations the estimates can be useful for this purpose. In particular, we seek information to inform recommendations to users that might wish to use high-resolution precipitation estimates from satellites in areas where radar or gauge data is sparse.

Action: Sylvia Puca for H-SAF; Bob Kuligowski for Hydrometeorological Testbed; Yudong Tian/Bob Adler GPM-GV; Emad Habib for Nile Forecasting system.

Encourage organizations listed to include high-resolution satellite datasets (e.g., CMORPH, TMPA, PERSIANN, GSMaP, etc.) in their validation studies. These contacts will provide relevant validation statistics and results once available.

Timeline: Contacts report on progress by end of 2010

3. Listing of data available for validation

This will be somewhat similar to the IPWG satellite products description webpage, but with information on datasets that can be used for validation. Include mechanisms for user feedback on validation data and tips from experts who have used these datasets (e.g., tips on how to read the data, data quality, etc.). Include high latitudes and data sparse regions where possible. Identify datasets that should be available but are not for various reasons (e.g., unnecessarily embargoed data).

Action: Bob Kuligowski

Request input on data sources from validation WG; collate and make webpage. Bob has developed a Ground Validation Data Links Webpage:

<http://www.star.nesdis.noaa.gov/smcd/emb/bobk/links.html>

Timeline: Summer 2011

4. Make collection of code to convert datasets to ASCII for validation.

It was noted that some users (e.g., hydrologists, others) would be more likely to include (high resolution) precipitation products in their research if such products were in a common format. We accept that IPWG should avoid hosting data that are freely

provided by data centers. Therefore, it is recommended that code be developed/collected and maintained centrally by IPWG to read common satellite datasets and write them into a simple format (e.g., ASCII).

Action: *Chris Kidd*

Work with Validation WG to obtain code. Put this code on the IPWG website. Include instructions to run code on various operating systems (e.g. Windows, Linux, etc.).

Timeline: *Summer 2011*

5. Validation techniques

Build on currently available information on Beth Ebert's website by extending this to include more techniques (e.g., geospatial statistics; sparse data methods, any other techniques used by IPWG members (e.g., Helen Greatrex at Reading: rainfall kriging package). As part of this effort, make validation software available (include software from IPWG members where appropriate).

Action: *Paul Kucera*

Develop an outline of the document/website and circulate around Validation WG for ideas.

Timeline: *Outline circulates by end of 2010; first draft by summer 2011*

6. Encourage validation activities over Africa

Precipitation estimates need particular improvement over Africa, but it is usually not possible to directly obtain validation data (gauge networks, etc.). One model that has been successful is to help national level entities in Africa to do the validation themselves (e.g., as done by TAMSAT; organized workshops at individual Met Services in Africa to compare local observations with satellite precipitation estimates).

Action: *David Grimes*

Develop ideas on best ways to establish validation activities in collaboration with African nations. Need help from CGMS/WMO (also EUMETSAT via Gartner; Nile Basin Initiative via Emad Habib; GPCC via Becker) to make connections with national institutions and to help secure funding for such activities (specific actions for CGMS/WMO should be identified). Identify issues and barriers to completion based on TAMSAT and others' (e.g., AMMA) experience.

Timeline: *Disseminate ideas via email to validation WG by end 2010*

7. Improve collection of validation data over data sparse areas of the oceans.

Survey the IPWG community for contacts who might be able to secure space on ships in remote parts of the oceans where disdrometers (and potentially other instruments) can be deployed. These data are essential for improving our estimates of precipitation over the oceans.

Action: *Christian Klepp*

Timeline: *By end of 2011*

3. GENERAL DISCUSSION NOTES

The following list provides a summary of several notes from the validation WG discussion that did not warrant specific recommendations.

- A. Obtain status report from Mekonnen Gebremichael regarding white paper on new validation techniques [*Action: Christian Klepp*].
- B. Several SSMIS datasets are being produced. The WG should consider a comparison of SSMIS datasets in the future.
- C. Matt Sapiano will liaise with Phil Arkin to see if it is possible to extend the ECMWF data agreement to get full globe ECMWF precipitation estimates for IPWG/WGNE intercomparison.

4. REVIEW OF 2008 (IPWG4) RECOMMENDATIONS

The session of the working group was dedicated to reviewing the recommendations from IPWG4. For reference, each of the 14 recommendations from IPWG4 is provided in italics. Each recommendation was discussed to determine if it had been resolved. If not, the WG discussed if it should be brought forward with the 2010 recommends or removed if was no longer relevant to the WG. The following provides a summary of the discussion of each of the 14 recommendations:

1. *The creation of a subcommittee on validation for PEHRPP (Program to Evaluate High Resolution Precipitation Products; <http://essic.umd.edu/~msapiano/PEHRPP/>).*
There was much discussion on whether or not PEHRPP should continue. We heard that PEHRPP had a finite structure that had been partly achieved, but the group felt that the remaining goals were of diminished interest. It was decided that the subcommittee should be dissolved, which was agreed upon by the committee and the group.
2. *Implementation of an inter-comparison project (similar to the Precipitation Intercomparison Project (PIP), and the Algorithm Intercomparison Project (AIP) for the evaluation of HRPP.*
This recommendation was thought to be a good concept, but it was felt that the science questions needed to be better developed. This has been partly transformed into 2010 Recommendation 1.
3. *Support of the proposal for Joint Precipitation Intercomparison Activities between International Precipitation Working Group (IPWG) and the Working Group on Numerical Experimentation (WGNE).*
The committee heard that this recommendation had been achieved and was going well. There were no strong feelings about how this should evolve, although there was agreement that the current plan of implementation at IPWG sites was a sufficient use of the data. No further recommendation was thought to be necessary.
4. *Development of a list with links on the IPWG web page of existing high quality reference data to enable improved validation of satellite rainfall estimates.*
This recommendation was thought to still be a useful idea. It has been transformed into 2010 Recommendation 3.

5. *Encourage providers of validation observations to provide some type of quality index (e.g., 1 = poor, 10 = excellent).*
This recommendation was thought to be a difficult goal to achieve, and was not explicitly carried forward. The group agreed that the recommendation required no further action since this was a recommendation to the CGMS. However, we felt that this could be partly achieved through 2010 Recommendation 3 by including some user feedback on data quality on the validation data information page.
6. *Development of a website to provide feedback for validation product developers.*
The issues around this recommendation were discussed. There was not a strong feeling from the group that such a survey should be conducted and so this was not pursued further.
7. *Encourage the production/availability of quantitative precipitation estimates (QPE) products from new sensors (e.g., SSMIS, FY-03) for validation purposes.*
Whilst this recommendation was considered an important topic, it was felt that this was more in the realm of the New Technologies or Research WGs. The Chair passed these comments along during the plenary session.
8. *Encourage the use of existing HRPP in hydrological impact studies, such as the EUMETSAT H-SAF and HydroMet test beds in the US, to assess the usefulness of the HRPP products in hydrological models.*
The group felt this recommendation to be a good idea, but one that was difficult to achieve. Discussions on this topic lead to the formation of 2010 Recommendation 2.
9. *Encourage that the meteorological modeling community actively (make available) provides model outputs (e.g. precipitation fields, 700mb winds) to the satellite precipitation development and validation communities.*
To some extent, this was felt to include the IPWG/WGNE collaboration that had led to the capture of operational model precipitation forecasts. It was noted that such fields are available from several reanalysis datasets and from the NCEP GFS operational model and this was sufficient to meet the requirement.
10. *Encourage that investigators should evaluate the usefulness of other validation tools and encourage the development of methods to address the issue of validation in regions of sparse surface data.*
The WG felt that this recommendation would be useful, although the status was not clear. An action was assigned to Christian Klepp to request a status update from Mekonnen Gebremichael regarding this white paper. This was not kept as a recommendation.
11. *Recommend that guidelines are established for the standardization of product formats and filename conventions (grid format, units, etc.) with the goal of making the data more easily usable among the validation community.*
The difficulties surrounding this concept were discussed, and some examples of potential convergence in formats and filenames were given. The group felt that this recommendation would be very hard to fully achieve, but that some progress had been made. This was considered in specifying 2010 Recommendation 4.
12. *Recommend that a discussion at a higher level, maybe WMO, concerning the distribution of HRPP through networks such as GEONETCast, should be made to maximize the utility of such products.*

This recommendation was felt to be useful, but as something for the Applications WG to consider. This action was passed to that group.

13. *Recommend that the use or development of high-latitude validation sites such as the BALTEX, LOFZY follow up 5 years Nordic Seas, high latitude maritime radar sites, Alaskan WSR-88D radars, and/or the Canadian sites.*

This was considered to be of ongoing importance and is now achieved by 2010 Recommendations 3 and 7.

14. *Recommend that countries or weather institutions with high quality ground validation dataset actively participate in IPWG sponsored validation activities.*

This recommendation was thought to be too vague to make an impact and was essentially dropped as a recommendation. However, this concept is continued in 2010 Recommendation 6.

